Carbon and Sulfur Isotopic Constraints on Ediacaran Biogeochemical Processes, Huqf Supergroup, Sultanate of Oman

by

David Andrew Fike

B.S. Engineering Physics
B.S. Astronomy
B.S. Geology
University of Illinois, Urbana-Champgain, 2001

M. Phil. Polar Studies
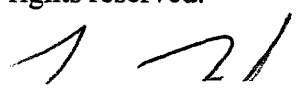Churchill College, University of Cambridge, UK, 2002

SUBMITTED TO THE DEPARTMENT OF EARTH, ATMOSPHERIC &
PLANETARY SCIENCES IN PARTIAL FULFILLMENT OF THE REQUIREMENTS
FOR THE DEGREE OF

DOCTOR OF PHILOSOPHY IN GEOCHEMISTRY
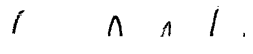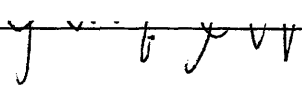AT THE
MASSACHUSETTS INSTITUTE OF TECHNOLOGY

AUGUST 2007
[September 2007]

Signature of author: _____
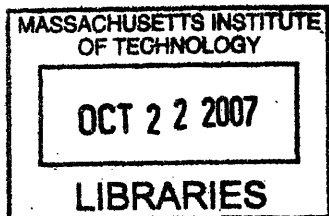Department of Earth, Atmospheric, & Planetary Sciences
August 6, 2007

Certified by: _____
Professor John Grotzinger
Thesis Supervisor

Accepted by: _____
Maria T. Zuber
E.A. Griswold Professor of Geophysics
Head, Department of Earth, Atmospheric & Planetary Sciences

Carbon and Sulfur Isotopic Constraints on Ediacaran Biogeochemical Processes, Huqf Supergroup, Sultanate of Oman

by

David Andrew Fike

Submitted to the Department of Earth, Atmospheric, & Planetary Sciences
on August 6, 2007 in Partial Fulfillment of the Requirements
for the Degree of Doctor of Philosophy

ABSTRACT

The link between environmental and evolutionary change is investigated in the Ediacaran Period ($\sim$ 635 – 541 million years ago (Ma), an interval where we see the emergence of macroscopic animals along with large perturbations to the carbon and sulfur cycles. Paleoenvironmental reconstruction used the carbon and sulfur isotopic composition of sedimentary minerals and organic matter, supplemented by geochemical and molecular biomarker proxies, of strata from the Huqf Supergroup, Sultanate of Oman.

Within Ediacaran strata, three successive stages of geochemical oxidation are observed and correlated to episodes of biological evolution. The second stage corresponds to the large Shuram $\delta^{13}C_{carb}$ excursion and is identified with the oxidation of an organic carbon reservoir. An extreme enrichment in sulfur isotopes occurs in the overlying strata spanning the Ediacaran-Cambrian (E-C) boundary. This interval is characterized using paired sulfate and pyrite sulfur isotopes to quantify pyrite burial and the isotopic composition of sulfur entering the ocean, which leads to a reinterpretation of existing Phanerozoic data. These strata contain sulfates in two forms (carbonate-associated sulfate: CAS, and anhydrite), providing an opportunity to investigate isotopic offsets reported between these seawater sulfate proxies. The results indicate that changing basin restriction can significantly alter the isotopic composition of gypsum/anhydrite and suggest that CAS is the most reliable proxy for the reconstruction of the marine sulfur cycle. A combination of geochemical and biomarker proxies were used to investigate the biological and environmental changes across the Ediacaran-Cambrian boundary. In the Huqf strata, a crash in the photic zone primary production is observed immediately before the geochemical evidence for anoxia that is typically associated with the extinction of the Ediacaran organisms at the E-C boundary.

All of these studies rely on interpretations made from geochemical data, which depend on how representative of depositional conditions (local, regional, or global) a given dataset is. Carbon and sulfur isotopes are characterized from replicate sections of the Huqf Supergroup strata to assess the basin-scale ($\sim$1,000km) reproducibility of these signals. The trends in the sulfur isotopic record were reproducible across the basin and serve to correlate sections lacking distinctive carbon isotopes or lithologies.

Thesis Supervisor: John Grotzinger
Title: Professor of Geology

ACKNOWLEDGMENTS

This thesis has come together over the course of five years through a combination of hard work, helpful discussions with my colleagues and advisors, the oft-called-upon support of friends and family, and a healthy dose of good luck. I first and foremost want to acknowledge the unflagging support (moral, mental, and fiscal) from my advisor John Grotzinger. When John became my advisor in the fall of 2002, he found himself with a student possessed by a chronic need to switch disciplines and learn something about everything. Under his guidance, I was moulded into a scientist capable of the detailed focus required for a Ph.D., and more importantly, John kindled the desire to distil problems to their essence that will serve me well for the rest of my career. Despite carefully shepherding my research focus, John exposed me to a variety of different experiences that profoundly changed my life. Two weeks in the Namibian wilderness during the summer before I officially began at MIT introduced me to Ediacaran-age rocks, which would later become the focus of my Ph.D. In my second year of grad school, I had the opportunity to work with John on NASA's MER mission and help Opportunity explore Meridiani Planum. I will cherish the experiences from this mission for the rest of my life. When John left MIT during the start of my fourth year, my last two years of grad school were split between Caltech and MIT. I am grateful for the warm welcome I received during my temporary stay at Caltech, particularly from Victoria Orphan, John Eiler, and Alex Sessions as well as the entire GPS Division. In addition, friendships and discussions with Joannah, Amy, Crystal, Justin, and Shana have made my life (and this thesis) better. Since moving out to Caltech, I have been grateful for the presence of Tim Lyons and his group at UC-Riverside, where I have often found a second (third?) home and good friends.

My continued sanity during the frequent trips between MIT and Caltech is due in no small part to Roger Summons. Roger had essentially been a co-advisor from the start of my time at MIT, giving me full access to his lab and his time. Roger's generosity continued after my departure and he provided both the necessary lab space and welcome lodging during my return visits. I am profoundly indebted to his generosity (and that of his wife Elizabeth!). Within Roger's lab, I have greatly enjoyed the interactions and

Table of Contents

INTRODUCTION

One of the longstanding goals in the study of biogeochemical cycling is to understand the evolutionary history of the Earth's surface environment – ocean, atmosphere, and biosphere. The motivating interest behind this dissertation was the desire to reconstruct environmental conditions across a time span that has been of significant recent paleobiological interest: the Ediacaran Period ($\sim$ 635 – 541 million years ago (Ma)) of Earth history (KNOLL et al., 2004). The Ediacaran Period begins in the wake of the Marinoan glaciation, in which ice sheets are believed to have extended to very low latitudes, possibly covering the Earth – with profound consequences for biological and geochemical evolution on Earth (HOFFMAN et al., 1998). The first appearance of macroscopic organisms, the Ediacaran fauna (NARBONNE, 2005), appear in successive stages throughout the later Ediacaran and appear to go extinct at the Ediacaran-Cambrian boundary (AMTHOR et al., 2003), making way for the ancestors of all modern animals in the subsequent evolutionary radiation known as the Cambrian explosion. The unanswered question that remains is how these evolutionary changes are related (if at all) to environmental changes, such as the oxygenation of the ocean (MARSHALL, 2006). The mid-Ediacaran records an extreme perturbation, the Shuram excursion (BURNS and MATTER, 1993), to the global carbon cycle, as measured by the carbon isotopic composition of marine carbonate minerals ($\delta^{13}C_{carb}$). The end-Ediacaran is known to contain strata characterized by anomalously enriched sulfur isotopes in marine sulfates ($\delta^{34}S_{SO4}$) (THODE and MONSTER, 1965). These two events stand out as the most extreme perturbations to their respective (carbon and sulfur) biogeochemical

cycles. The timing of their occurrence, the sulfur anomaly beginning at the end of the carbon excursion, and its relationship to stages of animal evolution suggest that there are strong environmental controls on the evolutionary events of the Ediacaran Period. Thus the goal behind the present study has been to characterize environmental change throughout the Ediacaran period, understand its cause, and relate it to evolutionary development.

To this end, I have undertaken a study of biogeochemical cycling in Ediacaran – earliest Cambrian (~635 – 540 Ma) strata of the Huqf Supergroup, Sultanate of Oman, using the carbon and sulfur isotopic composition of marine sedimentary minerals and organic matter. In Chapter 1 (Oxidation of the Ediacaran Ocean), the record of carbon isotopes in carbonates and organic matter and sulfur isotopes in sulfate and pyrite is examined from a section that spans the majority of the Ediacaran Period (~ 635 – 548 Ma). Here, three successive stages of geochemical oxidation are observed, and correlated to stages of biological evolution. In Chapter 2 (A paired sulfate-pyrite $\delta^{34}S$ approach to understanding the evolution of the Ediacaran-Cambrian sulfur cycle), the dynamics of the sulfur cycle are examined across the extreme enrichment in sulfur isotopes in strata spanning the Ediacaran-Cambrian boundary (~ 548 – 540 Ma) using paired sulfate and pyrite sulfur isotopes. Using a new approach, we are able for the first time to quantify parameters of sulfur cycling (f_{pyr}: pyrite burial; $\delta^{34}S_{in}$: the isotopic composition of sulfur entering the ocean) and reinterpret existing data from the Phanerozoic (~541 Ma – present) to cast new light on the long-term operation of the sulfur cycle. In Chapter 3 (Detection of variable basin restriction using sulfate $\delta^{34}S$ in carbonate-evaporite strata: An example from the Ediacaran-Cambrian Ara Group, Sultanate of Oman), a high-

resolution study of carbonate-evaporite strata was undertaken to understand reported offsets between sulfur isotopes in two different proxies for seawater sulfate (CAS: carbonate-associated sulfate and gypsum/anhydrite). The results indicate that changing basin restriction can significantly alter, and in particular enrich, the isotopic composition of gypsum/anhydrite and suggest that CAS is the most reliable proxy for the reconstruction of the marine sulfur cycle. In Chapter 4 (The Ediacaran-Cambrian boundary: a two-stage record of ecological and geochemical change), a combination of geochemical proxies (carbon and nitrogen isotopes, and trace element enrichments) and molecular biomarkers (a suite of phylogeny- and metabolism-specific organic molecules) are used to investigate the biological and environmental changes across the Ediacaran-Cambrian boundary. In the Huqf strata, a crash in the photic zone primary production is observed immediately before the geochemical evidence for anoxia that is typically associated with the extinction of the Ediacaran organism.

All of these studies rely on interpretations made from geochemical data. The utility, in terms of the paleoenvironmental information that can be extracted and the potential as a tool for correlation, of these biogeochemical proxies depends to a large degree in the confidence one has about how representative of depositional conditions (local, regional, or global) a given dataset is. This is investigated in Chapter 5 (Basin-wide sulfur isotope chemostratigraphy of the Ediacaran-Cambrian strata of the Huqf Supergroup, Sultanate of Oman: a synthesis of subsurface and outcrop data), where the sulfur and carbon isotopes are characterized from replicate sections of the Ediacaran Huqf Supergroup strata in Oman to assess the basin-scale (~1,000km) reproducibility of these signals.

References:

Amthor, J. E., Grotzinger, J. P., Schroder, S., Bowring, S. A., Ramezani, J., Martin, M. W., and Matter, A., 2003. Extinction of Cloudina and Namacalathus at the Precambrian-Cambrian boundary in Oman. *Geology* **31**, 431-434.

Burns, S. J. and Matter, A., 1993. Carbon isotopic record of the latest Proterozoic from Oman. *Eclogae Geologicae Helvetiae* **86**, 595-607.

Hoffman, P. F., Kaufman, A. J., Halverson, G. P., and Schrag, D. P., 1998. A Neoproterozoic snowball earth. *Science* **281**, 1342-1346.

Knoll, A. H., Walter, M. R., Narbonne, G. M., and Christie-Blick, N., 2004. A new period for the geologic time scale. *Science* **305**, 621-622.

Marshall, C. R., 2006. Explaining the Cambrian "explosion" of animals. *Annual Review of Earth and Planetary Sciences* **34**.

Narbonne, G. M., 2005. The Ediacara Biota: Neoproterozoic Origin of Animals and Their Ecosystems. *Annu. Rev. Earth Planet. Sci.* **33**, 1 - 22.

Thode, H. D. and Monster, J., 1965. Sulfur-isotope geochemistry of petroleum, evaporites, and ancient seas, *Fluids in Subsurfaces Environments, Memoir 4*. American Association of Petroleum Geologists, Tulsa, OK.

CHAPTER 1
Oxidation of the Ediacaran Ocean

D. A. Fike[1*], J. P. Grotzinger[1†], L. M. Pratt[2], and R. E. Summons[1]

[1]Department of Earth, Atmospheric, & Planetary Sciences, Massachusetts Institute of Technology, Cambridge, MA 02139, USA

[2]Department of Geological Sciences, Indiana University, Bloomington, IN 47405, USA

[†]present address: Division of Geological and Planetary Sciences, California Institute of Technology, Pasadena, CA 91125, USA

ABSTRACT

Oxygenation of the Earth is increasingly regarded to have occurred in two steps. The first step, which occurred ~2,300 million years ago (Myr) ago, involved a significant increase in atmospheric oxygen concentrations and oxygenation of the surface ocean (BEKKER et al., 2004; HOLLAND, 1984). A further increase in atmospheric oxygen appears to have taken place during the late Neoproterozoic period (CANFIELD and TESKE, 1996; DES MARAIS et al., 1992) (~800–542 Myr ago). This increase may have stimulated the evolution of macroscopic multicellular animals and the subsequent radiation of calcified invertebrates (DES MARAIS et al., 1992; KNOLL and CARROLL, 1999), and may have led to oxygenation of the deep ocean (ROTHMAN et al., 2003). However, the nature and timing of Neoproterozoic oxidation remain uncertain. Here we present high-resolution carbon and sulphur isotope records from the Huqf Supergroup, Sultanate of Oman, that cover the majority of the Ediacaran periood (~635 – 548 Myr ago). These records indicate that the ocean became increasingly oxygenated after the end of the Marinoan glaciation, and they allow us to identify three distinct stages of oxidation. When considered in the context of other records from this period (BOWRING et al., 2007; CALVER, 2000; CONDON et al., 2005; CORSETTI and KAUFMAN, 2003; GREY, 2005; GROTZINGER et al., 1995; MARTIN et al., 2000; NARBONNE, 2005; WORKMAN et al., 2002), our data indicate that certain groups of eukaryotic organisms appeared and diversified during the second and third stages of oxygenation. The second stage corresponds with the Shuram excursion in the carbon isotope record (BURNS and MATTER, 1993) and seems to have involved the oxidation of a large reservoir of organic carbon suspended in the deep ocean (ROTHMAN et al., 2003), indicating that this event may have had a key role in the evolution of eukaryotic organisms. Our data thus provide new insights into the oxygenation of the Ediacaran ocean and the stepwise restructuring of the carbon (BURNS and MATTER, 1993; LOGAN et al., 1995; ROTHMAN et al., 2003) and sulphur cycles (CANFIELD, 2004; CANFIELD and TESKE, 1996; HURTGEN et al., 2006) that occurred during this significant period of Earth's history.

The Huqf Supergroup (~635 – 540 Myr) provides one of the best preserved, most

continuous sections of Ediacaran-age strata(AMTHOR et al., 2003) (Figure 1). The Abu

Mahara Group contains Marinoan-equivalent glacial deposits (Fiq Formation and

associated Hadash cap carbonate) that overlie ~800-Myr-old crystalline basement

(BOWRING et al., 2007). Nafun Group sediments were deposited in a regionally extensive

sag basin under open, shallow marine conditions, and each formation can be traced

laterally for several hundred km (McCARRON, 2000). Nafun strata (see Supplementary

Information for a detailed discussion of lithostratigraphy) comprise two clastic-to-

carbonate shallowing-upward successions (Masirah Bay Formation–Khufai Formation;

Shuram Formation – Buah Formation) with an unconformity across the Khufai-Shuram

boundary that probably includes the interval of Gaskiers glaciation at ~ 580 Myr

(BOWRING et al., 2002). Global correlation of $\delta^{13}C_{carb}$ (carbonate carbon, see

Supplementary Information for carbon and sulphur isotope nomenclature) anomalies

provides two age constraints for the Buah Formation (Figure 1): ~550 Myr for the mid-

Buah (correlation with Doushantuo Formation, China (BOWRING et al., 2007; CONDON et

al., 2005)); and ~548 Myr for the upper Buah (correlation with Nama Group, Namibia

(BOWRING et al., 2007; GROTZINGER et al., 1995)). These ages are supported by multiple

ages spanning 541 – 547 Myr ago obtained from the overlying Ara Group.

Here we present carbon and sulphur isotope data from the Huqf Supergroup (Figure

1; see Supplementary Information for detailed discussion of the data). All data from the

Nafun Group were collected from cuttings in the Miqrat-1 well (Supplementary Figure

S1), previously established as one of the most representative subsurface sections of Huqf

strata (BURNS and MATTER, 1993). The Shuram Formation preserves a >15‰ negative

excursion in $\delta^{13}C_{carb}$, reaching a minimum of ~ -12‰. The excursion spans ~500m of stratigraphic section (BURNS and MATTER, 1993) and is the largest known perturbation to the global carbon cycle in Earth history.
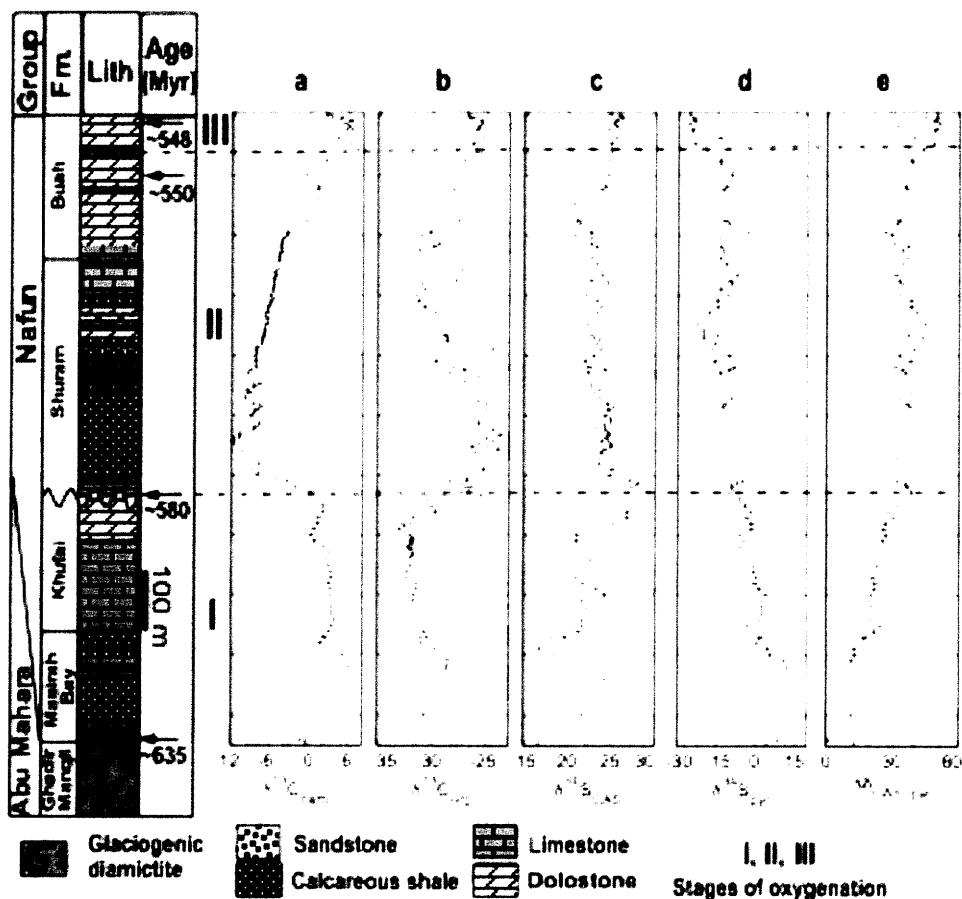
Figure 1: Huqf Supergroup showing geochronologic, paleobiological, and chemostratigraphic contraints. The Hadash cap carbonate lies immediately above the Ghadir Manqil glacial diamictite and conformably below the Masirah Bay Formation. Geochronologic data are from correlation to other sections containing U-Pb zircon ages on ash beds (BOWRING et al., 2002; CONDON et al., 2005; GROTZINGER et al., 1995). Data plotted are as follows: $\delta^{13}C_{carb}$ (a), $\delta^{13}C_{org}$ (TOC) (b), $\delta^{34}S_{SO4}$(c), $\delta^{34}S_{pyr}$ (d), and $\Delta\delta^{34}S = \delta^{34}S_{SO4} - \delta^{34}S_{pyr}$ (e). The dashed line at 46‰ indicates the maximum fractionation associated with BSR. The 2σ error bars for isotopic measurements, based on replicate analyses of standards and samples, are $\delta^{13}C_{carb} = \delta^{34}S_{SO4} \leq 0.15‰$; $\delta^{13}C_{org} = \delta^{34}S_{pyr} \leq 0.4‰$).

The Shuram excursion is fundamentally different from all known $\delta^{13}C_{carb}$ excursions (for example the Marinoan cap carbonate, the Ediacaran/Cambrian boundary, and the Permian/Triassic boundary), in that $\delta^{13}C_{carb}$ reaches well below the mantle value of about -6‰. Because $\delta^{13}C_{carb}$ values extend below -6‰, and cannot readily be explained by changes in organic carbon burial or isotope fractionation during carbon fixation (DES MARAIS et al., 1992), the Shuram excursion was initially attributed to diagenetic alteration of the $\delta^{13}C_{carb}$ signal (BURNS and MATTER, 1993; MCCARRON, 2000). However, standard methods of assessing diagenesis (see Supplementary Figure S2a,b and discussion in Supplementary Information) indicate these samples retain primary $\delta^{13}C_{carb}$ values. Furthermore, the Shuram excursion is now documented in over 30 sections in Oman, covering a region in excess of 10^5 km^2 with little variation in either the magnitude or duration (AMTHOR et al., 2003; BURNS and MATTER, 1993; LE GUERROUE et al., 2006a). Additionally, potentially correlative excursions have been found across the globe: the Doushantuo Formation, China (CONDON et al., 2005); the Wonoka Formation, Australia (CALVER, 2000); the Johnnie Formation, USA (CORSETTI and KAUFMAN, 2003); and the Nama Group, Namibia (WORKMAN et al., 2002) (Figure 2). Together, these argue that the Shuram excursion is a primary record of an unprecedented perturbation to the global carbon cycle.

Unlike younger carbon isotopic anomalies that are expressed by $\delta^{13}C_{carb}$ in carbonate sections and $\delta^{13}C_{org}$ (organic carbon) in siliciclastic sections, the Shuram excursion has been identified only in carbonate sections(BURNS and MATTER, 1993; CALVER, 2000; CONDON et al., 2005; CORSETTI and KAUFMAN, 2003; MELEZHIK et al., 2005; WORKMAN et al., 2002). Given the absence of covariation in $\delta^{13}C_{org}$ with $\delta^{13}C_{carb}$ during the Shuram

excursion reported here and from the Wonoka Formation in Australia(CALVER, 2000), the excursion would be undetectable in Shuram-equivalent siliciclastic strata, which are reliant on $\delta^{13}C_{org}$ for chemostratigraphy. This may explain why the Shuram excursion has not been found in more Ediacaran sections (e.g., Windemere Supergroup, Canada).

The data presented here point to a progressive oxidation of the Ediacaran ocean in three stages following the end of Marinoan glaciation. These successive stages occur well after the last of the extreme Neoproterozoic glaciations (CONDON et al., 2005) and before the extinction and subsequent evolutionary radiation across the Ediacaran-Cambrian boundary (AMTHOR et al., 2003). The first stage of oxidation occurs in the Khufai and Masirah Bay formations above the Marinoan-equivalent Hadash cap carbonate. In the Hadash cap, $\Delta\delta^{34}S$, the difference between coeval $\delta^{34}S_{SO4}$ (carbonate-associated sulphate) and $\delta^{34}S_{pyr}$ (pyrite) (Figure 1e), ranges from 1‰ to 12‰. These low values, consistent with those found above the coeval Marinoan in Namibia (HURTGEN et al., 2006), indicate marine sulphate concentrations ([SO$_4$]) of less than 200 μM (HABICHT et al., 2002), which prevents the expression of significant isotopic fractionation during bacterial sulphate reduction (BSR). Throughout the Masirah Bay and Khufai formations above the cap carbonate, $\Delta\delta^{34}S$ rises gradually to ~35‰, recording a rise to [SO$_4$] > 200μM and the unlimited expression of BSR fractionation. Although it is difficult to gauge the magnitude of the increase in [SO$_4$], reports (CANFIELD, 2004; HURTGEN et al., 2006) of Ediacaran and early Cambrian enrichment and variability in $\delta^{34}S_{SO4}$, suggest that [SO$_4$] did not exceed ~5 mM (KAH et al., 2004), which is appreciably lower than the modern value of 28 mM. Two key fluxes for regulating [SO$_4$] are riverine sulphate derived from pyrite oxidation (source) and marine reduction of sulphate to sulphide

(sink). Because these fluxes both depend directly on oxygen concentrations, increased [SO_4] probably correlates with increased oxygen availability. It is likely that the increase in [SO_4] above the cap carbonate is in part the recovery from a glacially induced drawdown of sulphate concentrations (HURTGEN et al., 2006). However, on the basis of ~610-Myr-old detrital zircons in the upper Khufai (BOWRING et al., 2007; LE GUERROUE et al., 2006b) the minimum time represented by the increase in $\Delta\delta^{34}S$ in stage I strata overlying the ~635-Myr-old Marinoan cap carbonate is ~25 Myr and therefore probably records an increase in atmospheric oxygen in addition to any effects associated with deglaciation. This increase in $\Delta\delta^{34}S$ constitutes the first stage (Figure 1, stage I) of Ediacaran oxidation observed in the Huqf sediments. Throughout stage I strata, $\delta^{13}C_{carb}$ and $\delta^{13}C_{org}$ were not coupled.

The second stage (Figure 1, stage II) of Ediacaran oxidation corresponds to the duration of the Shuram excursion and encompasses the Shuram and lower Buah formations. Although these strata lie immediately above the Khufai, the likely presence of a significant unconformity prevents meaningful comparison between data from the base of the Shuram and those from the top of the Khufai. The absence of a parallel negative excursion in $\delta^{13}C_{org}$ suggests that pools of organic carbon and dissolved inorganic carbon in the Ediacaran ocean were effectively decoupled, such that excursions in $\delta^{13}C_{carb}$, which reflects the dissolved inorganic carbon pool – the source for carbon fixation of coeval organic matter – were not recorded in $\delta^{13}C_{org}$ of syndepositional sediments (ROTHMAN et al., 2003). Our trends agree with the observation (ROTHMAN et al., 2003) of an overall absence of covariation between $\delta^{13}C_{org}$ and $\delta^{13}C_{carb}$ in a global compilation of Neoproterozoic data from ~ 730 – 555 Myr ago. With decoupled carbon

reservoirs, negative excursions in $\delta^{13}C_{carb}$ can result from the oxidation of part of a much larger DOC reservoir represented by the deep ocean, and their amplitude is limited by $\delta^{13}C_{org}$ (~ -30‰) rather than mantle composition (about -6‰) as in a steady-state model. (Here and throughout the text, the term DOC is used to refer to a large reservoir of organic carbon (not the result of coeval primary production) suspended in the deep ocean; use of the term DOC is not intended to distinguish between truly 'dissolved' organic carbon and suspended colloidal or fine particulate organic carbon.) This vast DOC reservoir would effectively buffer coexisting $\delta^{13}C_{org}$ through adsorption on siliciclastic particles and/or during carbonate precipitation in significant excess of the influx of detritus from primary production. At the initiation of the Shuram excursion, this adsorption would have to contribute ≥90% of TOC to mask the signal of δ^{13}C-depleted primary organic matter. However, because the organic reservoir is depleted through progressive oxidation, the relative contribution of coeval δ^{13}C-depleted primary production to $\delta^{13}C_{org}$ increases; this is observed (Figure 1b) in the upper portion of stage II as $\delta^{13}C_{org}$ decreases from about -26‰ to about -31‰. As the organic reservoir is finally oxidized, the onset of covariation in $\delta^{13}C_{carb}$ and $\delta^{13}C_{org}$ (r^2 = 0.72 for the upper ~ 200m of section) becomes apparent. Further evidence supporting oxidation during stage II is given in Supplementary Information.

The constancy of $\Delta\delta^{34}S$ during the Shuram excursion indicates that, despite these changes, BSR under sulphate-replete conditions remained the dominant pathway for sulphur cycling in the ocean. However, in the upper Buah, an increase in $\Delta\delta^{34}S$ to ~ 50‰ indicates a change in the metabolisms involved in marine sulphur cycling. The maximum fractionation observed (Canfield and Teske, 1996) in both laboratory and field studies

during BSR is 46‰; typical fractionations are often much smaller (DETMERS et al., 2001). However, communities characterized by BSR coupled with bacterial sulphur disproportionation (BSD), a pathway (CANFIELD and TESKE, 1996) in which intermediate valence sulphur species (for example S^0 and $S_2O_3^{2-}$) are split into ^{34}S-enriched sulphate and ^{34}S-depleted hydrogen sulphide, have fractionations that can approach 70‰. There is evidence from paired $\delta^{33}S$-$\delta^{34}S$ data for the evolution of BSD as early as the Mesoproterozoic (JOHNSTON et al., 2005); however, there have been no reports of coeval $\Delta\delta^{34}S$ >46‰ in any Proterozoic sample (Hurtgen et al., 2005). Because BSD requires the presence of intermediate valence S species, the oxidative sulphur cycle must have been active. Evidence for BSD therefore demonstrates additional oxidation of the Ediacaran ocean immediately after the Shuram recovery and constitutes the third stage (Figure 1, stage III) of Ediacaran oxidation preserved in the Huqf sediments.

The data presented in this paper provide a record of multi-stage oxidation of Earth's surficial environment during Ediacaran time. We now place this record into a global paleobiological context by integrating coeval records of both plankton (acanthomorph acritarchs) and benthic Ediacaran soft-bodied animals into our chemostratigraphic context (Figure 2). Well-characterized palynological assemblages that record the evolution of the acanthomorph acritarchs (GREY, 2005) are preserved in two chemostratigraphically-constrained sections (China and Australia) potentially correlative to the Shuram excursion (Figure 2). In Australia, the appearance of acanthomorph acritarchs approximately coincides with the onset of the Shuram excursion (our stage II oxidation) in the Wonoka Formation, Adelaide Rift Complex (CALVER, 2000; GREY, 2005). The Acraman impact event has previously been postulated as the stimulus for the
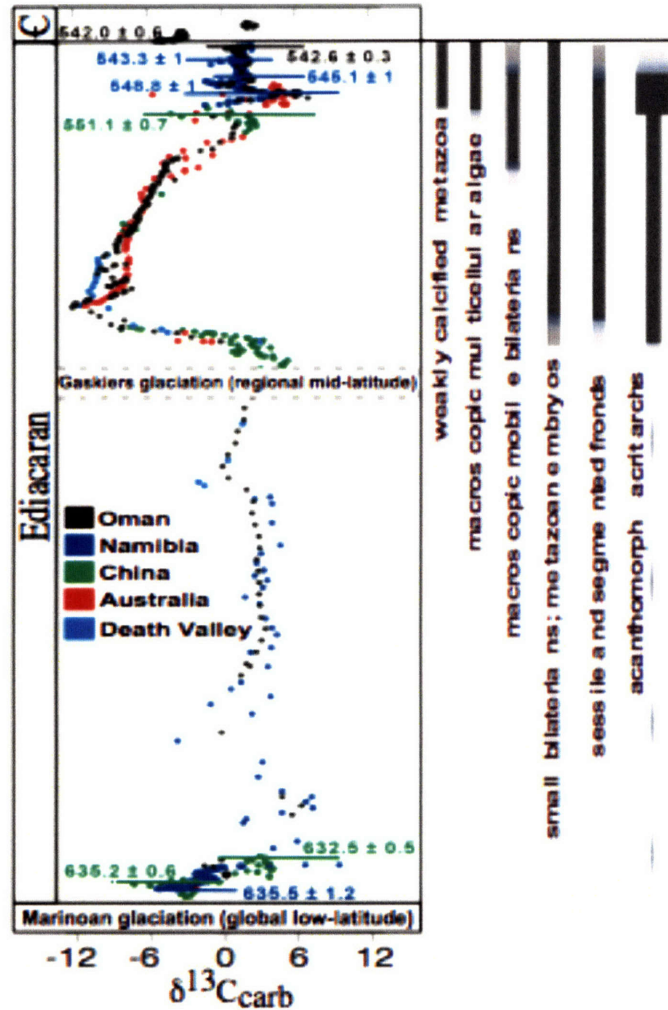
Figure 2: Compilation of Ediacaran $\delta^{13}C_{carb}$ from sections known to contain the Shuram excursion. The vertical axis is approximate time, with known geochronologic constraints plotted. On the right are plotted the known range of acanthomorph acritarchs and Ediacaran biota are plotted (shading indicates uncertainty relative to $\delta^{13}C$ chemostratigraphy). Points are coloured as follows: black, Oman; dark blue, Namibia; green, China; red, Australia; cyan, Death Valley. Full references for data, U/Pb zircon ages, biostratigraphic range, and the method for correlating sections are provided in Supplementary Information.

acanthomorph acritarch radiation (GREY, 2005). However, impact ejecta occur ~140m below strata marking both the radiation and the initiation of the Shuram excursion. We therefore propose alternatively that the acritarch radiation is temporally correlated with the increased oxidation of the ocean and subsequent ecological changes that occurred during the Shuram excursion. The most diverse assemblage of acritarchs occurs in (or

just below, see Appendices C,D) the Julie Formation, Amadeus Basin (GREY, 2005) during an excursion in $\delta^{13}C_{carb}$ of up to +5 (Figure 2), which we interpret as equivalent to the stage III oxidation event based on $\delta^{13}C_{carb}$ correlation to the upper Buah Formation in Oman and the lower Nama Group of Namibia, where the age of the correlative positive $\delta^{13}C_{carb}$ isotopic excursion is constrained to ~548 Myr (GROTZINGER et al., 1995). Although neither the carbonates of the Nama Group nor the Buah Formation have yielded well-preserved acritarch populations, acanthomorph acritarchs in the shale-rich Doushantuo Formation of China (GREY, 2005) appear at approximately the same stratigraphic position as the reported Shuram excursion (CONDON et al., 2005). The coincidence of the latter two stages of oxidation with the first appearance and subsequent diversification of acanthomorph acritarchs suggests that the oxidation of the ocean played a major role in the evolution of these planktic photosynthetic organisms.

It is not possible to confidently determine whether the first known appearance of the Ediacaran biota at ~575Ma (NARBONNE, 2005) predates or postdates the onset of the Shuram excursion, because of a lack of overlapping biostratigraphic and chemostratigraphic data. However, both the Shuram excursion and the first appearance of Ediacaran organisms postdate the Gaskiers glacial event at ~580 Myr (see Supplementary Information), yet predate the positive $\delta^{13}C_{carb}$ excursion at ~548 Myr ago. It is therefore possible that the second stage of oxygenation helped to stimulate radiation of the first Ediacaran organisms, which are interpreted to have been sessile frond-like animals (such as *Charnia*); while these organisms appear to have inhabited a variety of different paleoenvironments (MARTIN et al., 2000; NARBONNE, 2005), all evidence indicates they were likely confined to the oxygenated mixed layer of the ocean.

However, it is not until ~555 Myr (MARTIN et al., 2000), as the Shuram excursion drew to a close, that we see the appearance of the first motile, bilaterian organisms (for example, *Kimberella*) in a wider range of depositional facies. Finally, the first calcifying metazoa *Cloudina* and *Namacalathus*, well documented in both Oman and Namibia, appeared ~548 Myr ago, after the strong BSD signal. The coincidence of the latter two stages of oxidation identified in this study with the appearance of motile and calcifying Ediacarans, respectively, suggests that the events observed in Oman were global and affected the evolution of early metazoa.

Examination of the Huqf Supergroup, Sultanate of Oman reveals a three-stage oxidation of the Ediacaran ocean. The first stage corresponds to an increase in sulphate concentrations (>200μM) after the Marinoan glaciation, due in part to an increase in atmospheric oxygen. The second stage consists of the Shuram excursion and the oxidation of a deep-ocean DOC reservoir, probably the last major redox barrier to ocean oxygenation. This stage is coincident with the appearance of complex acanthomorph acritarchs and motile metazoa. The final stage of Ediacaran oxidation is based on strong signals of BSD and covariation in $\delta^{13}C_{carb}$ and $\delta^{13}C_{org}$, coincident with an increase in the diversity of acanthomorph acritarchs and the first appearance of the calcifying metazoa *Namacalthus* and *Cloudina*. Taken together, these data record the progressive oxygenation of the Ediacaran ocean, stimulating the evolution of both planktic and benthic groups of organisms.

References

Amthor, J. E., Grotzinger, J. P., Schroder, S., Bowring, S. A., Ramezani, J., Martin, M. W., and Matter, A., 2003. Extinction of Cloudina and Namacalathus at the Precambrian-Cambrian boundary in Oman. *Geology* **31**, 431-434.

Bekker, A., Holland, H. D., Wang, P. L., Rumble, D., Stein, H. J., Hannah, J. L., Coetzee, L. L., and Beukes, N. J., 2004. Dating the rise of atmospheric oxygen. *Nature* **427**, 117-120.

Bowring, S. A., Grotzinger, J. P., Condon, D. J., Ramezani, J., and Newall, M., 2007. Geochronologic constraints on the chronostratigraphic framework of the Neoproterozoic Huqf Supergroup, Sultanate of Oman. *American Journal of Science* **(in press)**.

Bowring, S. A., Myrow, P. M., Landing, E., and Ramezani, J., 2002. Geochronological contraints on terminal Neoproterozoic events and the rise of Metazoans. *Astrobiology* **2**, 457.

Burns, S. J. and Matter, A., 1993. Carbon isotopic record of the latest Proterozoic from Oman. *Eclogae Geologicae Helvetiae* **86**, 595-607.

Calver, C. R., 2000. Isotope stratigraphy of the Ediacarian (Neoproterozoic III) of the Adelaide Rift Complex, Australia, and the overprint of water column stratification. *Precambrian Research* **100**, 121-150.

Canfield, D. E., 2004. The evolution of the Earth surface sulfur reservoir. *American Journal of Science* **304**, 839-861.

Canfield, D. E. and Teske, A., 1996. Late Proterozoic rise in atmospheric oxygen concentration inferred from phylogenetic and sulphur-isotope studies. *Nature* **382**, 127-132.

Condon, D., Zhu, M., Bowring, S., Wang, W., Yang, A., and Jin, Y., 2005. U-Pb Ages from the Neoproterozoic Doushantuo Formation, China. *Science* **308**, 95 - 98.

Corsetti, F. A. and Kaufman, A. J., 2003. Stratigraphic investigations of carbon isotope anomalies and Neoproterozoic ice ages in Death Valley, California. *Geological Society of America Bulletin* **115**, 916-932.

Des Marais, D. J., Strauss, H., Summons, R. E., and Hayes, J. M., 1992. Carbon Isotope Evidence for the Stepwise Oxidation of the Proterozoic Environment. *Nature* **359**, 605-609.

Detmers, J., Bruchert, V., Habicht, K. S., and Kuever, J., 2001. Diversity of sulfur isotope fractionations by sulfate-reducing prokaryotes. *Applied and Environmental Microbiology* **67**, 888-894.

Grey, K., 2005. *Ediacaran palynology of Australia.* Association of Australasian Paleontologists.

Grotzinger, J. P., Bowring, S. A., Saylor, B. Z., and Kaufman, A. J., 1995. Biostratigraphic and Geochronological Constraints on Early Animal Evolution. *Science* **270**, 598-604.

Habicht, K. S., Gade, M., Thamdrup, B., Berg, P., and Canfield, D. E., 2002. Calibration of Sulfate Levels in the Archean Ocean. *Science* **298**, 2372-2374.

Holland, H. D., 1984. *The chemical evolution of the atmosphere and oceans.* Princeton University Press, Princeton, NJ.

Hurtgen, M. T., Arthur, M. A., and Halverson, G. P., 2005. Neoproterozoic sulfur isotopes, the evolution of microbial sulfur species, and the burial efficiency of sulfide as sedimentary pyrite. *Geology* **33**, 41-44.

Hurtgen, M. T., Halverson, G. P., Arthur, M. A., and Hoffman, P. F., 2006. Sulfur cycling in the aftermath of a 635-Ma snowball glaciation: Evidence for a syn-glacial sulfidic deep ocean. *Earth and Planetary Science Letters* **245**, 551-570.

Johnston, D. T., Wing, B. A., Farquhar, J., Kaufman, A. J., Strauss, H., Lyons, T. W., Kah, L. C., and Canfield, D. E., 2005. Active microbial sulfur disproportionation in the Mesoproterozoic. *Science* **310**, 1477-1479.

Kah, L. C., Lyons, T. W., and Frank, T. D., 2004. Low marine sulphate and protracted oxygenation of the proterozoic biosphere. *Nature* **431**, 834-838.

Knoll, A. H. and Carroll, S. B., 1999. Early animal evolution; emerging views from comparative biology and geology. *Science* **284**, 2129 - 2137.

Le Guerroue, E., Allen, P. A., and Cozzi, A., 2006a. Chemostratigraphic and sedimentological framework of the largest negative carbon isotopic excursion in Earth history: The Neoproterozoic Shuram Formation (Nafun Group, Oman). *Precambrian Research* **146**, 68 - 92.

Le Guerroue, E., Allen, P. A., Cozzi, A., Etienne, J. L., and Fanning, M., 2006b. 50 million year duration negative carbon isotope excursion in the Ediacaran ocean. *Terra Nova* **18**, 147 - 153.

Logan, G. A., Hayes, J. M., Hieshima, G. B., and Summons, R. E., 1995. Terminal Proterozoic Reorganization of Biogeochemical Cycles. *Nature* **376**, 53-56.

Martin, M. W., Grazhdankin, D. V., Bowring, S. A., Evans, D. A. n. D., Fedonkin, M. A., and Kirschvink, J. L., 2000. Age of Neoproterozoic Bilatarian Body and Trace Fossils, White Sea, Russia: Implications for Metazoan Evolution. *Science* **288**, 841-845.

McCarron, G., 2000. The sedimentology and chemostratigraphy of the Nafun Group, Huqf Supergroup,Oman. *PhD Thesis (Oxford University)*, 175.

Melezhik, V. A., Fallick, A. E., and Pokrovsky, B. G., 2005. Enigmatic nature of thick sedimentary carbonates depleted in 13C beyond the canonical mantle value: The challenges to our understanding of the terrestrial carbon cycle. *Precambrian Research* **137**, 131-165.

Narbonne, G. M., 2005. The Ediacara Biota: Neoproterozoic Origin of Animals and Their Ecosystems. *Annu. Rev. Earth Planet. Sci.* **33**, 1 - 22.

Rothman, D. H., Hayes, J. M., and Summons, R. E., 2003. Dynamics of the Neoproterozoic carbon cycle. *Proceedings of the National Academy of Sciences of the United States of America* **100**, 8124-8129.

Workman, R. K., Grotzinger, J. P., and Hart, S. R., 2002. Constraints on Neoproterozoic ocean chemistry from delta (super 13) C and delta (super 11) B analyses of carbonates from the Witvlei and Nama Groups, Namibia. *Geochimica Et Cosmochimica Acta* **66**, 847.

Acknowledgments

Appendix A: Supplementary Information
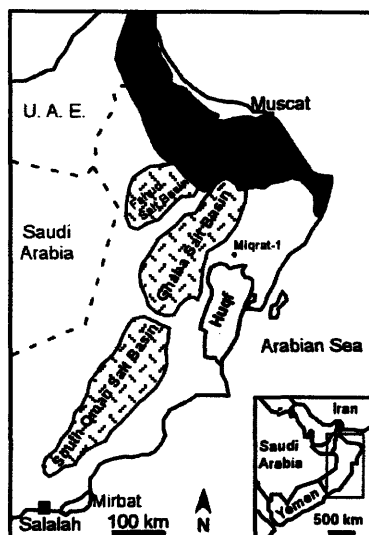
Figure S1: Map of the Sultanate of Oman. Neoproterozoic rocks crop out in the Oman Mountains in the north, in the Huqf area along the east-central coast, as well as near Mirbat in the south. Neoproterozoic deposits are also found throughout much of the subsurface in Oman, where they have not been exposed to oxidative weathering and alteration. Samples from this study are from the drill hole Miqrat-1, spanning a depth range from 3200 – 4244 m.

Huqf lithostratigraphy

The Nafun Group varies in composition and facies depending on paleogeographic position (McCARRON, 2000). The basal Masirah Bay consists of deeper-water black and grey shales that interfinger with post-glacial cap carbonates. These grade upward into siliciclastic shales that shallow upward and interfinger with tidal- and storm-emplaced sandstones and siltstones. The Masirah Bay passes conformably into the peritidal limestones and dolostones of the Khufai Formation which form a prograding shallow-marine ramp succession (McCARRON, 2000). Khufai carbonates are abruptly overlain by the Shuram Formation. The basal Shuram is comprised of outer shoreface calcareous sandstones and limestones which grade upward into red shales, while the upper Shuram contains interstratified carbonates that become more abundant into the basal Buah Formation. The Buah is a simple shallowing-upward carbonate succession that culminates in shallow subtidal stromatolitic and oolitic grainstone facies.

The Khufai-Shuram contact is at least locally unconformable (LE GUERROUE et al., 2006a) based on field observations and regional seismic data showing incised channels. This interpretation is supported by the locally variable profile of $\delta^{13}C_{carb}$ across the Khufai-Shuram boundary (LE GUERROUE et al., 2006a), indicating spatially variable erosion/deposition and by the presence of inflection points (Figure 1a,c-d) or jumps (Figure 1b) in carbon and sulphur isotopes across the contact, suggesting discontinuous deposition. The age of the topmost Khufai is constrained to be younger than ~600 – 620 Myr, based on U/Pb ages from detrital zircons (BOWRING et al., 2007; LE GUERROUE et al., 2006b). Based on sequence stratigraphic correlation, we interpret the unconformity to encompass the period of Gaskiers glaciation (~580 Myr (BOWRING et al., 2002)). However, see (LE GUERROUE et al., 2006b) for an alternative view

that suggests the basal Shuram is ~ 600 Myr. Our inference suggests the basal Shuram is younger than 580 Myr, consistent with an estimate (BOWRING et al., 2007) of ~560 - 570 Myr from models of sedimentation rates coupled to U/Pb ages from ash beds in overlying strata and from global chemostratigraphic correlation.

Overlying the Nafun Group is the Ara Group, a series of six carbonate-evaporite cycles (AMTHOR et al., 2003; SCHRÖDER et al., 2003). The contact between the Buah and overlying Ara Group is marked by a disconformable, karstic surface. Additional ages (AMTHOR et al., 2003; BOWRING et al., 2007) from overlying Ara carbonate units indicate ongoing deposition from ~ 547 through ~541 Myr. At the base of the fourth Ara carbonate unit the Ediacaran-Cambrian boundary has been identified (AMTHOR et al., 2003) based on a 7‰ negative excursion in carbonate $\delta^{13}C$ and the disappearance of Ediacaran *Namacalathus* and *Cloudina* fossil assemblages.

Detailed description of observed trends (Figure 1a-e)

Observation of $\delta^{13}C_{carb}$ provides a reference framework for interpreting other isotope proxies and for global correlations. Above Abu Mahara glacial strata, $\delta^{13}C_{carb}$ rises to ~6‰ and falls to 0‰ just prior to the Masirah Bay-Khufai boundary. $\delta^{13}C_{carb}$ then rises to +3‰ where it plateaus for most of the Khufai, except for a negative excursion to 0‰ near the limestone-dolostone transition from deeper to shallower water facies in the mid-Khufai. The uppermost Khufai is marked by $\delta^{13}C_{carb}$ = 2.6‰; whereas the base of the Shuram is characterized by $\delta^{13}C_{carb}$ = 0.0‰, decreasing to -12.0‰ at the nadir of the Shuram excursion. Above this level, $\delta^{13}C_{carb}$ rises gradually to -4.5‰ at the Shuram-Buah transition. $\delta^{13}C_{carb}$ rises throughout most of the Buah, hovering briefly around 0‰ before peaking at 6.5‰ in the upper Buah. $\delta^{13}C_{carb}$ decreases to 0‰ in the uppermost Buah.

In contrast, $\delta^{13}C_{org}$ in the form of total organic carbon (Figure 1b) reveals a very different pattern. Above Abu Mahara glacial strata, $\delta^{13}C_{org}$ = -31.1‰ and gradually increases to ~ -29‰ in the upper Masirah Bay. From the uppermost Masirah Bay there is a decrease in $\delta^{13}C_{org}$ to ~ -33‰ in the mid-Khufai, followed by an increase to -31‰ at the top Khufai. Beginning in the base of the Shuram, $\delta^{13}C_{org}$ increases slightly to -26‰ transitioning upward from the interbedded sandstones and limestone to the basal Shuram red shales, an interval over which $\delta^{13}C_{carb}$ plunges from 0 to -12‰ and then rises to ~ -8‰. Throughout the rest of the Shuram, $\delta^{13}C_{org}$ gradually decreases in magnitude to ~ -31‰ while $\delta^{13}C_{carb}$ rises to -4‰. The increased scatter in the data through this part of the section may be due to very low TOC levels (Figure S3), characteristic of the majority of the Shuram and Buah formations. In the lower Buah, $\delta^{13}C_{org}$ begins to show sympathetic covariation with $\delta^{13}C_{carb}$ in the uppermost Buah (r^2 = 0.72).

Examination of $\delta^{34}S_{SO4}$ (Figure 1c, in the form of carbonate-associated-sulphate) reveals significant variability in the basal section, with an increase in $\delta^{34}S_{CAS}$ from 9‰ above Abu Mahara glacial strata to 22‰ in the lower Masirah Bay. From this point through the upper Khufai, $\delta^{34}S_{CAS}$ generally follows the same trends as $\delta^{13}C_{carb}$. There is a 5‰ decrease in $\delta^{34}S_{CAS}$ in the upper Masirah Bay coincident with the 6‰ negative trend in $\delta^{13}C_{carb}$. Following this, $\delta^{34}S_{CAS}$ increases to ~21‰ at the Masirah Bay-Khufai boundary and remains approximately constant until the limestone-dolostone transition in the Khufai, coincident with the rebound and plateau in $\delta^{13}C_{carb}$. From the base of the Khufai dolostone, $\delta^{34}S_{CAS}$ increases linearly to ~29‰ at the top Khufai, while $\delta^{13}C$ rises from 0 to +3. The lowermost Shuram calcareous sandstones are characterized by $\delta^{34}S_{CAS}$ = 28.0‰. This decreases to ~ 24‰ in the basal red shales as $\delta^{13}C_{carb}$ plunges to ~ -12‰. Here, the covariance with $\delta^{13}C_{carb}$ ends as $\delta^{34}S_{CAS}$ decreases gradually to

~21‰ in the mid-Buah while $\delta^{13}C_{carb}$ recovers from the Shuram excursion. The upper Buah is marked by an increase in $\delta^{34}S_{CAS}$ to ~26‰.

Above Abu Mahara glacial strata, $\delta^{34}S_{pyr}$ (Figure 1d) increases from 4‰ to 17‰ in the mid Masirah Bay. There is a gradual decrease in $\delta^{34}S_{pyr}$ to -10‰ in the upper Khufai. $\delta^{34}S_{pyr}$ increases slightly in the basal Shuram calcareous sandstones and then decreases through the red shales to -22.5‰ in the upper Shuram interbedded carbonates. There is an increase in $\delta^{34}S_{pyr}$ to ~ -10‰ in the uppermost Shuram and lower Buah, followed by a drop to -25‰ in the uppermost Buah.

Examining $\Delta\delta^{34}S$, the fractionation between coeval sulphate and pyrite, provides a more meaningful way to interpret $\delta^{34}S_{pyr}$ by eliminating covariation with sulphate $\delta^{34}S$. Here we find $\Delta\delta^{34}S$ increases from less than 1‰ at the top of the post-glacial cap carbonate to ~ 35‰ at the top Khufai. The basal Shuram is characterized by $\Delta\delta^{34}S = 39$‰, which decreases slightly in the lower Shuram and remains relatively constant (35.2 ± 4.1‰, n = 49) throughout the duration of the Shuram excursion. As the Shuram excursion ends in the upper Buah, $\Delta\delta^{34}S$ increases to an average of 47‰ (n = 14), with 10 samples having fractionations indicative of BSD.

Evaluating diagenesis:
Evidence for primary $\delta^{13}C_{carb}$ during the Shuram excursion

We examined two geochemical proxies ($\delta^{18}O$ and Mn/Sr) to assess the likelihood that the $\delta^{13}C_{carb}$ signal of the Shuram excursion was primary (Figure S2a-b). Although there is a correlation between $\delta^{13}C_{carb}$ and $\delta^{18}O_{carb}$ for samples during the Shuram excursion ($r^2 = 0.6$), the range of $\delta^{18}O$ values for the samples during the excursion falls within the variability of those before and after the excursion (Figure S2a). This is consistent with either a partial resetting of the $\delta^{18}O$ signal (KAUFMAN and KNOLL, 1995; KAUFMAN et al., 1992) (e.g., by meteoric diagenesis) or secular trends (VEIZER et al., 1999) in marine $\delta^{18}O$ over the Neoproterozoic. Examination of whole rock Mn/Sr values (Figure S2b) shows that samples that define the Shuram excursion are within the variability of sample values that bound the excursion. In addition, most excursion samples have Mn/Sr < 1, well below the threshold (KAUFMAN and KNOLL, 1995; KAUFMAN et al., 1992) for alteration of primary $\delta^{13}C_{carb}$. This indicates that meteoric diagenesis was insufficient to significantly reset the Mn/Sr ratio and, therefore, highly unlikely to have altered the primary composition of $\delta^{13}C_{carb}$. From these data and from the remarkable uniformity of the Shuram excursion across Oman (inclusive of both surface and subsurface datasets) and other globally correlative sections, we conclude that the $\delta^{13}C_{carb}$ signal is primary.

Evidence for primary $\delta^{34}S_{SO4}$ preserved in Oman

We have examined $\delta^{34}S_{SO4}$ versus several indicators of diagenesis ($\delta^{18}O_{carb}$, Mn/Sr, $\delta^{13}C_{carb}$, and the concentration of carbonate-associated sulphate [SO4] (Figure S2c-f). With the exception of one point (circled in red), there appears to be no indication of diagenetic alteration in our $\delta^{34}S_{SO4}$ data. This point has been excluded from Figure 1 to avoid re-scaling the x-axis; however, it is included in supplementary table S1. The anomalous point comes from the Marinoan-equivalent cap carbonate and may reflect the unusual depositional environment rather than post-depositional alteration. Several samples have anomalously high [SO4] (> 2000ppm) although well within the range reported from modern carbonates. Of these, only the one sample

indicated as possibly altered has a $\Delta\delta^{34}S$ that is small enough such that post-depositional pyrite oxidation might have contributed to the measured [SO4].
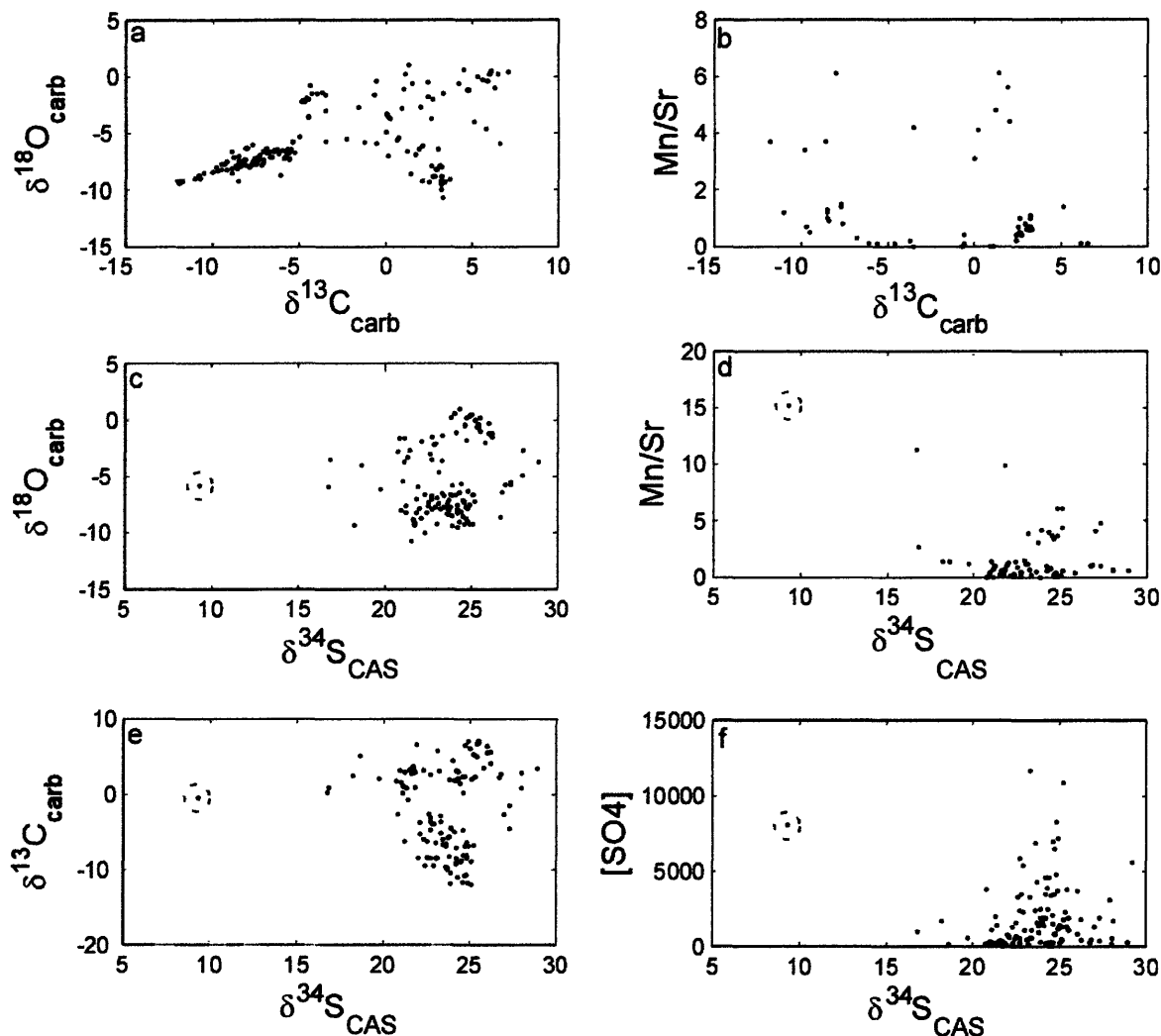
Figure S2: Evaluation of $\delta^{13}C_{carb}$ and $\delta^{34}S_{SO4}$ diagenesis. Samples from the Shuram excursion are in black, while samples bounding it are in blue. a-b) Evaluation of diagenesis of the $\delta^{13}C_{carb}$ signal. a) Cross plot of $\delta^{13}C_{carb}$ vs. $\delta^{18}O_{carb}$. b) Cross plot of $\delta^{13}C_{carb}$ vs. whole-rock Mn/Sr. c-f) Evaluation of diagenetic alteration of $\delta^{34}S_{SO4}$ data. Sample encircled in dashed red line is likely to have been diagenetically altered. c) Cross plot of $\delta^{34}S_{SO4}$ vs. $\delta^{18}O_{carb}$. b) Cross plot of $\delta^{34}S_{SO4}$ vs. whole-rock Mn/Sr. e) Cross plot of $\delta^{34}S_{SO4}$ vs. $\delta^{13}C_{carb}$. f) Cross plot of $\delta^{34}S_{SO4}$ vs. concentration of carbonate-associated sulphate [SO4] (ppm). See above for discussion and Table S1 for data.

Supporting material for oxidation during stage II (Shuram excursion)

Additional evidence for stage II oxidation is found in the ~8‰ decrease in $\delta^{34}S_{SO4}$ across the Shuram excursion, while $\Delta\delta^{34}S$ remains nearly constant. This indicates sulphide oxidation

accompanying the oxidation of DOC during the Shuram excursion. Further support for a more oxidizing environment during deposition of stage II strata comes from pyrite and total organic carbon (TOC) abundances (Figure S3): the Masirah Bay and Khufai formations have relatively abundant pyrite (0.78 ± 0.58 wt%) and TOC (0.70 ± 0.49 wt%), whereas the Shuram and Buah formations have significantly less pyrite (0.064 ± 0.055 wt%) and TOC (0.100 ± 0.030 wt%). It should be noted that pre- (Masirah Bay/Khufai) and post-excursion (Shuram-Buah) data cluster into distinct groupings independent of lithology (siliciclastic vs. carbonate). Both the Masirah Bay-Khufai and Shuram-Buah formations represent upward shallowing sequences of siliciclastic-carbonate packages that are sedimentologically similar; because they plot so distinctly (Figure S3), it suggests that they were formed under different redox conditions, with Shuram-Buah deposition occurring in a significantly more oxidizing environment.
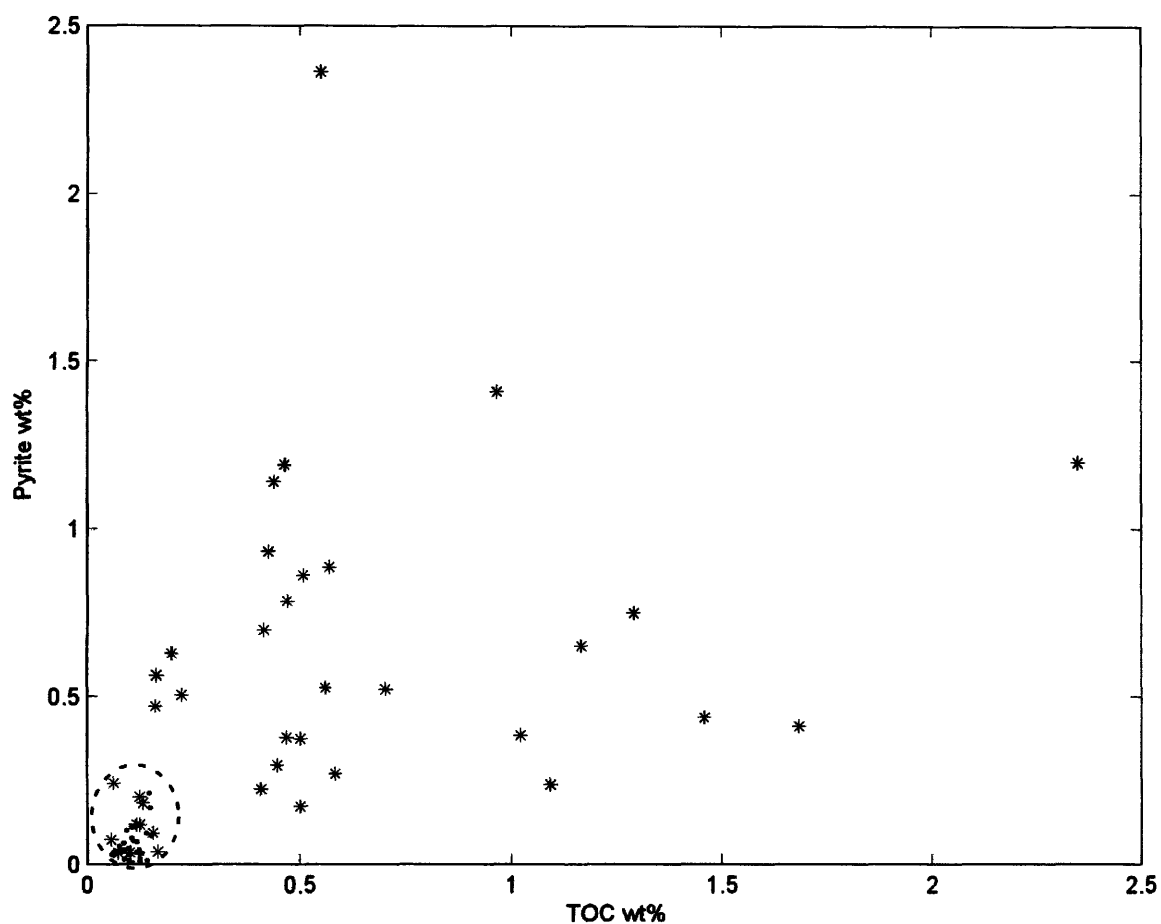
Figure S3: Abundance of pyrite and TOC by formation. Masirah Bay (blue) and Khufai shales and carbonates (black), deposited before the Shuram excursion, define a high pyrite-high TOC realm, whereas all the Shuram (red) and Buah (magenta) shales and carbonates, deposited during and after the Shuram excursion, are confined to a low pyrite-low TOC area (dashed circle). See text for discussion and Table S1 for data.

Construction of $\delta^{13}C_{carb}$ correlation and associated paleobiological indices (Figure 2)

This figure correlates various globally-distributed Ediacaran-age strata that contain the Shuram excursion. Because of variability in sediment accumulation rates and the duration and magnitude of periods of non-deposition and/or erosion, the geometry of the $\delta^{13}C_{carb}$ curve varies between sections (MYROW and GROTZINGER, 2000). Nevertheless, the major components of the curve, particularly the large magnitude of the negative $\delta^{13}C_{carb}$, are present in each section, and help build a composite model. Such composite models provide a useful means to visualize the degree to which globally disparate sections record the same chemostratigraphic signal. The figure was constructed using $\delta^{13}C_{carb}$ from Oman (this study; (AMTHOR et al., 2003)) and U/Pb ages from Oman (AMTHOR et al., 2003) and those from China (CONDON et al., 2005) and Namibia (GROTZINGER et al., 1995) that have been previously correlated to the Oman $\delta^{13}C_{carb}$ chemostratigraphy. The Oman $\delta^{13}C_{carb}$ record was then fit linearly between successive geochronological tie-points to construct a time line for the section, incorporating a reasonable estimate (BOWRING et al., 2007) for the age of the Khufai-Shuram unconformity. Next, the $\delta^{13}C_{carb}$ data from Namibia and China, possessing multiple geochronological constraints were added and aligned to the Omani record by fixing $\delta^{13}C_{carb}$ maxima and minima (e.g., nadir of the Shuram excursion, Buah positive, etc.) with a linear stretch between tie-points and geochronologic data. Data from geochronologically unconstrained sections (Australia, USA) were overlain on this record using a linear stretch between tie-points ($\delta^{13}C_{carb}$ maxima and minima). The absence of high-resolution age constraints for the interval of 630 – 555 Myr is problematic. Therefore, while we believe the shape of the curve will remain accurate, the scaling of this portion of the plot is approximate and the details of timing are likely to change as more dates become available. $\delta^{13}C_{carb}$ data from: Oman (this study; (AMTHOR et al., 2003)); China (CONDON et al., 2005; JIANG et al., 2003); Australia (CALVER, 1995; CALVER, 2000); Namibia (GROTZINGER et al., 1995; SAYLOR et al., 1995; and Death Valley (CORSETTI and KAUFMAN, 2003). U/Pb zircon ages from Oman (AMTHOR et al., 2003), Namibia(GROTZINGER et al., 1995; HOFFMANN et al., 2004), and China (CONDON et al., 2005). The range for acanthomorph acritarchs (GREY, 2005; GREY et al., 2003) is derived from several Australian sections and the upper Duoshantuo Formation, China. Additional work (MOCZYDLOWSKA, 2005; VIDAL and MOCZYDLOWSKA, 1995; XIAO et al., 2004) (indicated by the dashed line) shows other acritarch species evolved during stage I oxidation, but how these are correlated with the ECAP fauna (GREY, 2005) remains unclear. The range (BOWRING et al., 2002; NARBONNE, 2005) for sessile and segmented fronds is for strata in Newfoundland (Mistaken Point) above the Gaskiers glaciation (BOWRING et al., 2002). The range for small metazoa and bilaterian embryos from the Duoshantuo Formation, China summarized in (CONDON et al., 2005). The range (MARTIN et al., 2000) for macroscopic mobile bilaterian is obtained from strata from the White Sea, while the range (CONDON et al., 2005) for macroscopic multicellular algae is taken from the upper Duoshantuo Formation. Finally, the range of weakly calcified metazoa is a composite observation based on both Oman (AMTHOR et al., 2003) and Namibia ((GROTZINGER et al., 1995).

Methods
Sample preparation

All samples examined in this study are drill cuttings sampled every 2m from the Miqrat-1 drill hole in the South Oman Salt Basin (Figure S1). Samples were soaked in distilled de-ionized (DI) water and then rinsed 3x in DI to remove any water soluble drilling contamination. Next, samples were rinsed 3x in methanol, dichloromethane, and hexane to remove any soluble organic

contamination. Samples were powdered using a SPEX 8510 Shatterbox with an alumina ceramic container.

Carbon extraction and isotopic analysis

Carbonate carbon and oxygen isotopes were measured according to the methods described by Ostermann & Curry(2000). Organic carbon isotopes were analyzed as samples of total organic carbon (TOC). For TOC analyses, powdered samples were acidified in 6N HCl for 24 hours to remove carbonate minerals, filtered, rinsed with DI, dried, and the residuum was loaded into tin cups for isotopic analysis. Samples were flash combusted at 1060°C in a Carlo Erba NA1500 Elemental Analyser fitted with an AS200 autosampler. The resulting CO_2 gas was analyzed by continuous flow using a Delta plus XP Isotope Ratio Mass Spectrometer. Carbon isotopes are reported as $\delta^{13}C = (R_{standard}/R_{sample} - 1) * 1000$, where R = the ratio of $^{13}C/^{12}C$, in units of per mil (‰) relative to the V-PDB standard. Calibration of $\delta^{13}C_{org}$ was done by comparison with international standards (IAEA-CH-6, NBS-22) and in-house references ("Acetanilide" and "Penn State Kerogen") interspersed with the sample analyses.

Sulphur extraction and isotopic analysis

Powdered samples were rinsed with DI to remove soluble sulphates (e.g., from sulphide oxidation) and then soaked for 24 hours in DI to remove water-soluble sulphate minerals (e.g., anhydrite). Sulphate $\delta^{34}S$ was examined in the form of carbonate-associated sulphate (BURDETT et al., 1989; GELLATLY and LYONS, 2005; HURTGEN et al., 2002; KAMPSCHULTE et al., 2001; KAMPSCHULTE and STRAUSS, 2004; STAUDT et al., 1994) (CAS), also known as structurally-substituted sulphate, which is sulphate trapped in the carbonate mineral matrix, either through substitution for the carbonate ion or in crystal defects. CAS was obtained by dissolving the powdered sample in 6N HCl for 2 hours at ~60°C under nitrogen gas or in 6N HCl for 24 hours at room temperature. No $\delta^{34}S$ offset was observed between these methods. Following dissolution, samples were filtered to remove insoluble residues and an excess of 1 M $BaCl_2$ solution was added to the solute to precipitate $BaSO_4$. The insoluble residue was kept for pyrite analysis.

Pyrite was extracted as chromium-reducible sulphur (CANFIELD et al., 1986). Pyrite extraction was performed under nitrogen gas by the addition of 6N HCl and 0.4M reduced chromium chloride solution. The reaction was allowed to proceed for 2 hours with the sulphide collected as silver sulphide after bubbling through a sodium citrate buffer (pH 4) and into a silver nitrate (1 M) trap. Rinsed, filtered, and dried $BaSO_4$ and Ag_2S precipitates were then combined with an excess of V_2O_5 and analyzed for S-isotope composition at Indiana University on a Finnigan MAT 252 gas source mass spectrometer fitted with a peripheral elemental analyzer (EA) for on-line sample combustion(STUDLEY et al., 2002). Sulphur isotope compositions are expressed in standard δ-notation as permil (‰) deviations from V-CDT, with analytical error of <0.07‰, calculated from replicate analyses of samples and laboratory standards. Samples were calibrated using the international standards NBS-127 (20.3‰) and S3 (-31.5‰), as well as four internal standards: silver sulphide (ERE-Ag_2S: -4.3‰), chalcopyrite (EMR-CP: 0.9‰), and two barium sulfate standards (BB4-18: 39.5‰; PQB: 38.0‰).

Supplementary References

Amthor, J. E., Grotzinger, J. P., Schroder, S., Bowring, S. A., Ramezani, J., Martin, M. W., and Matter, A., 2003. Extinction of Cloudina and Namacalathus at the Precambrian-Cambrian boundary in Oman. *Geology* **31**, 431-434.

Bowring, S. A., Grotzinger, J. P., Condon, D. J., Ramezani, J., and Newall, M., 2007. Geochronologic constraints on the chronostratigraphic framework of the Neoproterozoic Huqf Supergroup, Sultanate of Oman. *American Journal of Science* **(in press)**.

Bowring, S. A., Myrow, P. M., Landing, E., and Ramezani, J., 2002. Geochronological contraints on terminal Neoproterozoic events and the rise of Metazoans. *Astrobiology* **2**, 457.

Burdett, J. W., Arthur, M. A., and Richardson, M., 1989. A Neogene seawater sulfate isotope age curve from calcareous pelagic microfossils. *Earth and Planetary Science Letters* **94**, 189-198.

Calver, C. R., 1995. Ediacaran isotope stratigraphy of Australia. *PhD Thesis (Macquarie University)*.

Calver, C. R., 2000. Isotope stratigraphy of the Ediacarian (Neoproterozoic III) of the Adelaide Rift Complex, Australia, and the overprint of water column stratification. *Precambrian Research* **100**, 121-150.

Canfield, D. E., Raiswell, R., Westrich, J. T., Reaves, C. M., and Berner, R. A., 1986. The use of chromium reduction in the analysis of reduced inorganic sulfur in sediments and shales. *Chemical Geology* **54**, 149-155.

Condon, D., Zhu, M., Bowring, S., Wang, W., Yang, A., and Jin, Y., 2005. U-Pb Ages from the Neoproterozoic Doushantuo Formation, China. *Science* **308**, 95 - 98.

Corsetti, F. A. and Kaufman, A. J., 2003. Stratigraphic investigations of carbon isotope anomalies and Neoproterozoic ice ages in Death Valley, California. *Geological Society of America Bulletin* **115**, 916-932.

Gellatly, A. M. and Lyons, T. W., 2005. Trace sulfate in mid-Proterozoic carbonates and the sulfur isotope record of biospheric evolution. *Geochimica Et Cosmochimica Acta* **69**, 3813-3829.

Grey, K., 2005. *Ediacaran palynology of Australia*. Association of Australasian Paleontologists.

Grey, K., Walter, M. R., and Calver, C. R., 2003. Neoproterozoic biotic diversification: Snowball Earth or aftermath of the Acraman impact? *Geology* **31**, 459-462.

Grotzinger, J. P., Bowring, S. A., Saylor, B. Z., and Kaufman, A. J., 1995. Biostratigraphic and Geochronological Constraints on Early Animal Evolution. *Science* **270**, 598-604.

Hoffmann, K.-H., Condon, D. J., Bowring, S. A., and Crowley, J. L., 2004. U-Pb zircon date from the Neoproterozoic Ghaub Formation, Namibia: Constraints on Marinoan glaciation. *Geology* **32**, 817-820.

Hurtgen, M. T., Arthur, M. A., Suits, N. S., and Kaufman, A. J., 2002. The sulfur isotopic composition of Neoproterozoic seawater sulfate: implications for a snowball Earth? *Earth and Planetary Science Letters* **203**, 413-429.

Jiang, G., Kennedy, M. J., and Christie-Blick, N., 2003. Stable isotopic evidence for methane seeps in Neoproterozoic postglacial cap carbonates. **426**, 822-826.

Kampschulte, A., Bruckschen, P., and Strauss, H., 2001. The sulphur isotopic composition of trace sulphates in Carboniferous brachiopods: implications for coeval seawater, correlation with other geochemical cycles and isotope stratigraphy. *Chemical Geology* **175**, 149-173.

Kampschulte, A. and Strauss, H., 2004. The sulfur isotopic evolution of Phanerozoic seawater based on the analysis of structurally substituted sulfate in carbonates. *Chemical Geology* **204**, 255-286.

Kaufman, A. J. and Knoll, A. H., 1995. Neoproterozoic Variations in the C-Isotopic Composition of Seawater - Stratigraphic and Biogeochemical Implications. *Precambrian Research* **73**, 27-49.

Kaufman, A. J., Knoll, A. H., and Awramik, S. M., 1992. Biostratigraphic and chemostratigraphic correlation of Neoproterozoic sedimentary successions - Upper Tindir Group, Northwestern Canada, as a test case. *Geology* **20**, 181-185.

Le Guerroue, E., Allen, P. A., and Cozzi, A., 2006a. Chemostratigraphic and sedimentological framework of the largest negative carbon isotopic excursion in Earth history: The Neoproterozoic Shuram Formation (Nafun Group, Oman). *Precambrian Research* **146**, 68 - 92.

Le Guerroue, E., Allen, P. A., Cozzi, A., Etienne, J. L., and Fanning, M., 2006b. 50 million year duration negative carbon isotope excursion in the Ediacaran ocean. *Terra Nova* **18**, 147 - 153.

Martin, M. W., Grazhdankin, D. V., Bowring, S. A., Evans, D. A. n. D., Fedonkin, M. A., and Kirschvink, J. L., 2000. Age of Neoproterozoic Bilatarian Body and Trace Fossils, White Sea, Russia: Implications for Metazoan Evolution. *Science* **288**, 841-845.

McCarron, G., 2000. The sedimentology and chemostratigraphy of the Nafun Group, Huqf Supergroup,Oman. *PhD Thesis (Oxford University)*, 175.

Moczydlowska, M., 2005. Taxonomic review of some Ediacaran acritarchs from the Siberian Platform. *Precambrian Research* **136**, 283-307.

Myrow, P. M. and Grotzinger, J. P., 2000. Chemostratigraphic proxy records; forward modeling the effects of unconformities, variable sediment accumulation rates, and sampling-interval bias. In: Grotzinger, J. P. and James, N. Eds.), *Carbonate sedimentation and diagenesis in the evolving Precambrian world*. SEPM, Tusla, OK.

Narbonne, G. M., 2005. The Ediacara Biota: Neoproterozoic Origin of Animals and Their Ecosystems. *Annu. Rev. Earth Planet. Sci.* **33**, 1 - 22.

Ostermann, D. R. and Curry, W. B., 2000. Calibration of stable isotopic data: An enriched $\delta^{18}O$ standard used for source gas mixing detection and correction. *Paleoceanography* **15**, 353 - 360.

Saylor, B. Z., Grotzinger, J. P., and Germs, G. J. B., 1995. Sequence stratigraphy and sedimentology of the Neoproterozoic Kuibus and Schwarzrand Subgroups (Nama Group), southwestern Namibia. *Precambrian Research* **73**, 153 - 171.

Schröder, S., Schreiber, B. C., Amthor, J. E., and Matter, A., 2003. A depositional model for the terminal Neoproterozoic Early Cambrian Ara Group evaporites in south Oman. *Sedimentology* **50**, 879-898.

Staudt, W. J., Schoonen, M. A. A., Vairavamurthy, M. A. e., Schoonen, M. A. A. e., Eglinton, T. I. e., Luther, G. W., III (editor), and Manowitz, B. e., 1994. Sulfate incorporation into sedimentary carbonates. *Geochemical transformations of sedimentary sulfur. ACS Symposium Series* **612**, 332-345.

Studley, S. A., Ripley, E. M., Elswick, E. R., Dorais, M. J., Fong, J., Finkelstein, D., and Pratt, L. M., 2002. Analysis of sulfides in whole rock matrices by elemental analyzer-continuous flow isotope ratio mass spectrometry. *Chemical Geology* **192**, 141-148.

Veizer, J., Ala, D., Azmy, K., Bruckschen, P., Buhl, D., Bruhn, F., Carden, G. A. F., Diener, A., Ebneth, S., Godderis, Y., Jasper, T., Korte, G., Pawellek, F., Podlaha, O. G., and Strauss, H., 1999. $^{87}Sr/^{86}Sr$, $\delta^{13}C$, and $\delta^{18}O$ evolution of Phanerozoic seawater. *Chemical Geology* **161**, 59-88.

Vidal, G. and Moczydlowska, M., 1995. The Neoproterozoic of Baltica-stratigraphy, palaeobiology and general geological evolution. *Precambrian Research* **73**, 197 - 216.

Xiao, S. H., Bao, H. M., Wang, H. F., Kaufman, A. J., Zhou, C. M., Li, G. X., Yuan, X. L., and Ling, H. F., 2004. The Neoproterozoic Quruqtagh Group in eastern Chinese Tianshan: evidence for a post-Marinoan glaciation. *Precambrian Research* **130**, 1-26.

Table S1: Isotopic and Geochemical data

Unit	Lithology	Depth (m)	$\delta^{13}C_{carb}$	$\delta^{18}O_{carb}$	$\delta^{13}C_{TO}$	$\delta^{34}S_{SO}$	$\delta^{34}S_{py}$	$\Delta\delta^{34}S$	TOC (wt%)	Pyrite (wt%)	[SO4]	Mn/Sr	Mn (ppm)	Sr (ppm)	Fe (wt%)
Buah	silty dolostone	3200	2.4	-1.8	-26.8	24.7	-25.5	50.3			860	0.4	255	601	0.8
Buah	silty dolostone	3202	2.7	-2.0		25.8			0.10	0.03		0.4	209	530	0.5
Buah	silty dolostone	3204	3.3	-1.5	-26.6	26.2	-18.8	45.0			1800				
Buah	silty dolostone	3206	4.8	-1.2	-26.2	26.2	-24.1	50.3			430				
Buah	silty dolostone	3208	4.7	-1.2	-26.7	26.0	-24.1	50.1			830				
Buah	silty dolostone	3210	6.3	-1.0	-25.6	25.5	-23.7	49.2			1100				
Buah	silty dolostone	3212	5.9	-0.4	-25.5	25.4	-23.3	48.7			1300				
Buah	silty dolostone	3216	5.3	0.0	-25.5	25.2	-25.9	51.1			1800				
Buah	silty dolostone	3220	6.0	0.2	-25.8	25.5	-6.7	32.3			1900				
Buah	silty dolostone	3224	5.6	-0.3	-25.9	26.0	-24.0	49.9			3700				
Buah	silty dolostone	3226	6.5	0.2	-25.9	24.7	-24.9	49.6	0.06	0.24	810	0.1	109	1010	0.5
Buah	silty dolostone	3228	4.5	0.6	-24.1	24.0	-24.5	48.5			1700				
Buah	silty dolostone	3240	4.2	-0.6	-25.4	25.4	-14.1	39.5	0.07	0.03	3800				
Buah	silty dolostone	3250	6.1	0.5	-26.3	25.0	-23.7	48.7			1400	0.1	83	869	0.5
Buah	silty dolostone	3260	7.1	0.4	-26.0	24.9	-18.6	43.5			1200				
Buah	silty dolostone	3276	2.4	-0.5	-27.2	24.6	-13.7	38.4	0.12	0.20	270	0.2	183	991	1.2
Buah	silty dolostone	3280	1.5	-0.6		25.3	-13.7	38.9			2300				
Buah	silty dolostone	3300	-0.6	-0.4	-28.2	24.6	-9.2	33.9	0.11	0.12	1500	0.1	160	1250	1.2
Buah	silty dolostone	3320	1.3	1.0		24.3	-11.4	35.7			2500				
Buah	silty dolostone	3326	1.1	0.2	-28.1	23.8	-12.6	36.4	0.12	0.12	940	0.0	86	2090	0.5
Buah	silty dolostone	3340	1.0	-1.1		24.1					1900				
Buah	silty dolostone	3350	0.9	-2.8		20.7	-11.9	32.6	0.06	0.07	160	0.0	118	2920	0.4
Buah	dolostone	3360	0.0	-3.3	-25.3	21.3	-5.6	26.9			2000				
Buah	dolostone	3376	-0.7	-1.6	-27.6	21.1	-12.1	33.2	0.13	0.18	1100	0.0	140	2960	0.8
Buah	dolostone	3380	-1.6	-2.7	-29.3	21.4	-10.6	32.0			1400				
Buah	dolostone	3396	-3.5	-3.0	-30.2	22.6	-3.4	26.0			3300				
Buah	dolostone	3400	-3.5	-1.6	-31.1	20.8	-8.7	29.4	0.17	0.04	3800	0.0	51	2780	0.4
Buah	dolostone	3404	-4.0	-1.5	-32.5	22.7	-13.9	36.7			5900				
Buah	dolostone	3408	-4.4	-0.8											
Buah	dolostone	3412	-4.5	-2.0											
Buah	dolostone	3416	-4.5	-3.5	-29.4	22.7	-7.7	30.4			2400				
Buah	dolostone	3420	-4.5	-3.6	-29.8	23.3	-13.6	36.8			3300				
Buah	dolostone	3426	-4.6	-1.9	-31.2	22.1	-12.3	34.4	0.15	0.09	690	0.1	72	1010	0.3
Buah	dolostone	3428	-4.3	-1.5											
Shuram	silty dolostone	3432	-4.8	-2.1	-31.0	22.9	-12.2	35.1			2300				
Shuram	silty dolostone	3436	-4.7	-2.2											
Shuram	silty dolostone	3440	-4.8	-2.2	-29.9	22.8	-13.7	36.4			3500				
Shuram	silty dolostone	3444	-4.9	-2.2											
Shuram	silty dolostone	3450	-3.7	-1.4	-27.5	23.3	-11.5	34.8	0.14	0.21	11700	0.2	172	1070	0.7
Shuram	silty dolostone	3456	-5.0	-5.3											
Shuram	silty dolostone	3460	-5.4	-5.8	-27.4	23.9	-3.0	26.9			1500				
Shuram	silty dolostone	3464	-5.5	-6.4											
Shuram	silty limestone	3468	-5.3	-6.7	-29.5	23.9	-7.5	31.4			1900				
Shuram	silty limestone	3472	-5.6	-7.3											
Shuram	silty limestone	3476	-5.6	-6.7	-27.8	22.7	-10.1	32.9	0.15	0.17	560	0.1	119	1580	0.4
Shuram	silty limestone	3480	-5.6	-7.2	-31.0	24.6	-9.4	34.0			2100				
Shuram	silty limestone	3486	-5.7	-6.4											
Shuram	silty limestone	3490	-5.8	-6.6	-30.7	24.1	-13.6	37.7			1400				
Shuram	silty limestone	3494	-5.9	-7.2											
Shuram	silty limestone	3500	-6.1	-8.7	-31.6	22.1	-10.7	32.8	0.10	0.11	600	0.1	122	1300	0.4
Shuram	silty limestone	3506	-5.8	-7.0											

Table S1: continued

Unit	Lithology	Depth (m)	δ¹³C_carb	δ¹⁸O_carb	δ¹³C_TOC	δ³⁴S_SO4	δ³⁴S_py	Δδ³⁴S	TOC (wt%)	Pyrite (wt%)	[SO4]	Mn/Sr	Mn (ppm)	Sr (ppm)	Fe (wt%)
Shuram	silty limestone	3510	-6.0	-6.5	-31.3	23.3	-14.9	38.2			580				
Shuram	silty limestone	3512	-6.2	-6.8											
Shuram	silty limestone	3516	-6.3	-6.4											
Shuram	silty limestone	3520	-6.5	-6.6	-30.7	23.8	-14.5	38.4			1400				
Shuram	silty limestone	3526	-6.5	-6.5											
Shuram	silty limestone	3530	-6.8	-6.7	-29.8	23.4	-17.8	41.2			560				
Shuram	silty limestone	3536	-6.9	-6.7											
Shuram	silty limestone	3540	-6.6	-7.1	-29.0	23.7	-16.4	40.1			1600				
Shuram	silty limestone	3546	-6.7	-7.1											
Shuram	silty limestone	3550	-6.8	-6.6	-30.8	22.3	-22.5	44.8			1300	0.3	360	1310	1.0
Shuram	silty limestone	3556	-6.9	-6.3											
Shuram	silty limestone	3560	-7.1	-7.6		21.2	-20.2	41.4	0.09	0.06					
Shuram	silty limestone	3564	-7.1	-6.6											
Shuram	silty limestone	3566	-7.1	-7.3	-28.9	22.5	-14.9	37.4			1600				
Shuram	silty limestone	3570	-7.3	-6.9	-28.6	23.0	-20.2	43.3			1100				
Shuram	silty limestone	3574	-7.4	-7.4		23.6	-14.2	37.8			2400				
Shuram	silty limestone	3576	-7.4	-7.1	-28.7										
Shuram	silty limestone	3580	-7.5	-7.7	-26.8	23.4	-15.7	39.1			1100				
Shuram	silty limestone	3586	-8.1	-7.8											
Shuram	silty limestone	3590	-8.3	-7.7	-24.4	23.8	-16.4	40.2			1500				
Shuram	silty limestone	3596	-8.2	-7.3											
Shuram	silty limestone	3600	-8.5	-9.2		23.0	-10.1	33.2	0.06	0.03		1.2	582	467	1.1
Shuram	silty limestone	3606	-8.4	-7.9											
Shuram	silty limestone	3610	-8.5	-7.8	-29.6	22.0	-15.9	37.9			770	1.3	463	362	1.1
Shuram	silty limestone	3616	-8.4	-7.5											
Shuram	silty limestone	3620	-8.4	-7.6	-28.0	22.5	-8.6	31.0	0.07	0.05	700	0.9	381	428	1.2
Shuram	silty limestone	3624	-9.2	-8.2	-27.1	24.2	-10.3	34.5			1900				
Shuram	silty limestone	3626			-25.7										
Shuram	silty limestone	3630	-9.5	-8.2	-28.5	22.4	-13.6	36.0	0.07	0.04	510	1.4	441	310	1.0
Shuram	silty limestone	3636			-25.8										
Shuram	silty limestone	3644			-27.0										
Shuram	silty limestone	3648	-7.7	-6.0								0.7	445	640	0.8
Shuram	silty limestone	3650	-8.5	-7.0		22.7			0.10	0.03		0.5	411	802	1.3
Shuram	calcareous shale	3652	-8.7	-7.9											
Shuram	calcareous shale	3656			-25.6										
Shuram	calcareous shale	3658	-9.7	-8.3		23.6					6900				
Shuram	calcareous shale	3660	-9.5	-7.7	-27.5	22.9	-15.2	38.1			5400	1.5	433	282	1.7
Shuram	calcareous shale	3662	-9.3	-7.7								0.8	261	316	0.4
Shuram	calcareous shale	3670	-10.0	-8.4		23.7	-9.3	33.0			4300				
Shuram	calcareous shale	3676			-25.8										
Shuram	calcareous shale	3680	-8.8	-7.1		24.5	-12.1	36.5	0.08	0.04		3.7	511	138	3.5
Shuram	calcareous shale	3682	-7.7	-7.7	-25.1	24.7			0.15	0.08	6500				
Shuram	calcareous shale	3686	-7.6	-7.2		25.2	-12.5	37.7	0.14	0.09	10900				
Shuram	calcareous shale	3690	-8.1	-7.3		24.6			0.10	0.08	7000				
Shuram	calcareous shale	3692	-8.5	-7.7	-24.9	24.8			0.12	0.07	8300				
Shuram	calcareous shale	3696	-8.6	-8.1											
Shuram	calcareous shale	3700	-9.2	-7.5		24.2			0.06	0.03		1.0	426	447	1.9
Shuram	calcareous shale	3702	-8.9	-8.1	-24.7	24.4			0.12	0.03	4600				
Shuram	calcareous shale	3706	-7.2	-7.8	-26.1	24.8			0.09	0.10	4800				
Shuram	calcareous shale	3712	-7.7	-7.5	-25.8	24.9			0.11	0.07	7200				
Shuram	calcareous shale	3716	-7.9	-8.0	-25.7	24.2			0.13	0.03	3500				

Table S1: continued

Unit	Lithology	Depth (m)	δ¹³C_carb	δ¹⁸O_carb	δ¹³C_TOC	δ³⁴S_SO4	δ³⁴S_py	Δδ³⁴S	TOC (wt%)	Pyrite (wt%)	[SO4]	Mn/Sr	Mn (ppm)	Sr (ppm)	Fe (wt%)
Shuram	calcareous shale	3720	-8.5	-7.4		23.1			0.07	0.04		1.2	460	371	2.0
Shuram	calcareous shale	3722	-8.5	-7.9	-24.5	24.2			0.12	0.04	4600				
Shuram	calcareous shale	3726	-8.9	-8.5	-26.2	24.5			0.12	0.04	3400				
Shuram	calcareous shale	3730	-10.7	-9.0		24.8	-6.8	31.6	0.06	0.04		3.7	773	211	2.6
Shuram	calcareous shale	3732	-10.8	-8.7	-23.8	24.7			0.12	0.02	3500				
Shuram	calcareous shale	3736	-11.0	-9.0	-25.0	24.3			0.09	0.01	3900				
Shuram	calcareous shale	3740	-11.7	-9.2		24.6			0.07	0.04		3.4	570	169	2.8
Shuram	calcareous shale	3742	-11.9	-9.4	-24.4	23.9			0.12	0.04	290				
Shuram	calcareous shale	3746	-11.8	-9.2	-25.7	24.9			0.10	0.01	3700				
Shuram	calcareous shale	3750	-12.0	-9.2	-25.0	25.1			0.06	0.03	400	6.1	705	115	3.4
Shuram	calcareous shale	3752	-10.7	-8.5	-26.3	25.0			0.14	0.01	240				
Shuram	calcareous shale	3756	-10.5	-8.5	-24.0	24.4			0.11	0.00	280				
Shuram	calcareous shale	3760	-10.5	-8.5		23.9			0.08	0.03		4.2	784	185	3.0
Shuram	calcareous shale	3762	-9.1	-7.4	-26.2	23.9			0.12	0.01	2500				
Shuram	calcareous shale	3770	-9.8	-8.0		23.7	-7.8	31.6	0.07	0.04		3.1	346	112	1.7
Shuram	silty limestone	3780	-7.8	-7.8		23.6			0.08	0.04		0.5	456	917	1.9
Shuram	limestone/sdstone	3790	-8.9	-6.6	-25.3	25.1			0.06	0.03	1300	4.4	587	133	3.6
Shuram	limestone/sdstone	3796	-8.0	-6.3					0.08	0.04		5.6	681	122	2.9
Shuram	limestone/sdstone	3800	-8.1	-6.3		24.8			0.07	0.03		6.1	705	115	3.2
Shuram	limestone/sdstone	3802	-6.4	-5.5											
Shuram	limestone/sdstone	3804	-5.8	-5.5											
Shuram	limestone/sdstone	3806	-5.4	-5.7	-26.8	27.3	-3.7	31.0	0.07	0.04	1900	4.8	594	123	2.8
Shuram	limestone/sdstone	3808			-26.8										
Shuram	limestone/sdstone	3810	-3.5	-5.7	-28.3	27.0	-5.3	32.3	0.10	0.05	1300	4.1	540	131	1.6
Shuram	limestone/sdstone	3812	-3.1	-5.0	-27.2	28.1	-7.4	35.5			1700				
Shuram	limestone/sdstone	3816	-4.3	-5.9	-25.4	27.9	-9.5	37.4			3100				
Shuram	limestone/sdstone	3818			-26.5										
Shuram	limestone/sdstone	3820	-2.3	-5.5	-27.0	27.3	-8.9	36.2			370	1.0	272	280	1.0
Shuram	limestone/sdstone	3822			-26.0										
Shuram	limestone/sdstone	3826	-0.6	-4.5	-26.6	29.2	-9.1	38.3			5600				
Shuram	limestone/sdstone	3830	0.0	-4.9	-27.4	28.0	-10.7	38.7	0.12	0.11	180	0.6	135	229	0.6
Shuram	limestone/sdstone	3832			-25.6										
Shuram	limestone/sdstone	3836	1.8	-3.6											
Khufai	silty dolostone	3840	2.6	-3.7	-30.4	28.9	-6.2	35.1	0.12	0.12	260	0.6	134	228	0.6
Khufai	silty dolostone	3844	2.3	-3.2											
Khufai	silty dolostone	3848	1.5	-3.0											
Khufai	silty dolostone	3850	2.0	-2.7	-30.0	28.0	-4.0	32.0	0.16	0.47	540	0.7	189	261	0.7
Khufai	silty dolostone	3852	1.8	-3.7											
Khufai	silty dolostone	3856	2.2	-6.0											
Khufai	silty dolostone	3860	1.9	-6.4	-29.7	26.8	-1.8	28.6	0.22	0.50	450	1.1	270	253	0.8
Khufai	silty dolostone	3864	2.1	-6.4											
Khufai	silty dolostone	3868	1.9	-6.7											
Khufai	dolostone	3870	1.4	-8.6	-31.7	26.7	-3.5	30.3	0.20	0.63	250	1.0	401	400	1.2
Khufai	dolostone	3872	1.7	-5.9											
Khufai	dolostone	3876	1.9	-5.9											
Khufai	dolostone	3880	1.2	-6.6	-32.7	25.1	-1.5	26.6	0.51	0.86	490	0.6	297	473	1.3
Khufai	dolostone	3882			-31.9										
Khufai	dolostone	3886			-32.5										
Khufai	dolostone	3890	0.6	-5.6	-33.0	24.4	-1.5	26.0	0.57	0.89	80	0.8	301	389	1.7
Khufai	dolostone	3896			-32.6										
Khufai	dolostone	3900	0.2	-3.7	-32.1	21.1	-5.8	26.9	0.42	0.70	240	0.7	219	336	1.3

Table S1: continued

Unit	Lithology	Depth (m)	$\delta^{13}C_{carb}$	$\delta^{18}O_{carb}$	$\delta^{13}C_{TOC}$	$\delta^{34}S_{SO_4}$	$\delta^{34}S_{py}$	$\Delta\delta^{34}S$	TOC (wt%)	Pyrite (wt%)	[SO4]	Mn/Sr	Mn (ppm)	Sr (ppm)	Fe (wt%)
Khufai	dolostone	3904			-31.8										
Khufai	limestone	3908			-31.9										
Khufai	limestone	3910	0.7	-5.4	-31.7	21.0	-4.5	25.5	0.47	0.78	310	1.4	256	185	1.1
Khufai	limestone	3912			-32.0										
Khufai	limestone	3916			-31.8										
Khufai	limestone	3920	2.1	-9.2	-32.2		-6.0		0.56	0.53		0.6	193	318	0.8
Khufai	limestone	3922			-31.9										
Khufai	limestone	3926			-31.9										
Khufai	limestone	3930	2.7	-8.8	-33.1		-2.7		0.70	0.52		0.4	176	490	0.8
Khufai	limestone	3932			-31.8										
Khufai	limestone	3936			-32.0										
Khufai	limestone	3940	2.6	-7.9	-30.3	22.7	-2.4	25.1	0.50	0.37	250	0.4	161	431	0.7
Khufai	limestone	3950	2.8	-8.8	-32.0	21.6	-1.2	22.7	1.02	0.39	400	0.6	227	352	0.6
Khufai	limestone	3960	3.2	-8.8	-32.3		-0.7		1.68	0.41		0.5	165	359	0.6
Khufai	limestone	3970	3.2	-8.0	-32.4	20.9	0.1	20.9	1.46	0.44	180	0.4	154	418	0.6
Khufai	limestone	3980	2.9	-8.2	-31.4	21.8	-0.2	22.0			150	0.7	204	299	0.8
Khufai	limestone	3990	3.1	-7.9	-31.4	23.2	1.6	21.7	0.47	0.38	130	0.7	184	265	0.6
Khufai	limestone	4000	3.2	-9.5	-31.7	24.2	4.0	20.2	0.41	0.22	210	0.6	190	306	0.5
Khufai	limestone	4010	3.2	-9.2	-31.8	21.7	2.1	19.6	0.59	0.27	300	0.3	170	650	0.5
Khufai	limestone	4020	3.2	-10.0	-31.5	22.3	2.2	20.0	1.09	0.24	200	0.2	148	834	0.5
Khufai	limestone	4022	3.0	-8.1											
Khufai	limestone	4030	3.3	-10.7	-31.9	21.5	2.3	19.3	0.50	0.17	320	0.2	133	851	0.4
Khufai	limestone	4040	3.7	-9.1		21.7	1.8	19.8	0.45	0.29	210	0.2	127	664	0.5
Khufai	limestone	4044	3.9	-7.8											
Khufai	limestone	4050	3.4	-9.3		21.7	-3.1	24.8	1.17	0.65	25	0.5	201	370	1.0
Khufai	silty limestone	4060	2.9	-8.2	-30.7	21.2	-0.4	21.6			200	1.0	424	418	3.0
Khufai	silty limestone	4068	2.5	-7.3											
M. Bay	silty limestone	4070	2.1	-6.1	-30.5	19.7	2.2	17.5			560	1.2	433	357	1.4
M. Bay	silty limestone	4072	2.5	-9.3	-31.0	18.2	1.1	17.0	1.29	0.75	1700	1.4	477	334	1.2
M. Bay	silty limestone	4074	2.1	-6.7											
M. Bay	silty limestone	4076	1.8	-6.3											
M. Bay	silty limestone	4080	1.7	-6.9	-31.1		0.7		0.97	1.41		3.9	1240	318	1.4
M. Bay	silty limestone	4090	0.1	-3.5	-29.7	16.8	4.4	12.4	0.55	2.36	1000	2.7	889	334	2.1
M. Bay	silty limestone	4096	2.9	-3.7											
M. Bay	silty limestone	4100	5.1	-4.0		18.6	5.8	12.8	0.44	1.14	150	1.4	469	344	1.6
M. Bay	limestone	4110	6.6	-5.9	-28.5	21.9	10.7	11.2	0.46	1.19	150	1.1	454	420	1.4
M. Bay	silty limestone	4120	5.8	-4.6	-28.6	23.1	12.1	11.1	0.43	0.93	460	3.9	1280	328	1.7
M. Bay	dolomaceous shale	4140	3.0	-6.4		24.3	17.0	7.3	0.16	0.56		4.0	584	145	3.5
M. Bay	dolomaceous shale	4160	0.9	-5.6											
M. Bay	dolomaceous shale	4180	1.4	-4.2											
M. Bay	dolomaceous shale	4200	0.1	-7.0	-30.7	21.8	10.6	11.2	2.35	1.20		9.9	672	68	3.8
M. Bay	dolomaceous shale	4220	1.4	-5.3											
M. Bay	dolomaceous shale	4238	0.3	-5.5											
Hadash	silty dolostone	4240	-1.3	-5.8		9.3	8.5	0.8	0.59	2.59	8100	15.2	1795	118	4.1
Hadash	silty dolostone	4242	-0.1	-5.9											
Hadash	silty dolostone	4244	-0.6	-5.9		16.7	4.2	12.5	0.56	1.42		11.3	1570	139	3.5

39

Appendix C
Ediacaran oxidation and biotic evolution
(comment on Fike et al. 2006. Oxidation of the Ediacaran Ocean,
Nature, 444: 744-747)

K. Grey[1] & C.R. Calver[2]

[1]Geological Survey of Western Australia, Department of Industry and Resources, 100 Plain Street, East Perth, Western Australia 6004. (kath.grey@doir.wa.gov.au)

[2]Mineral Resources Tasmania, PO Box 56, Rosny Park, Tasmania 7018 (ccalver@mrt.tas.gov.au)

The link between the radiation of various lineages of eukaryotes in the latest Proterozoic, and massive environmental changes – oxygenation, global ice ages, and bolide impact – is the focus of much current research interest. Fike *et al.* (2006) used carbon and sulphur isotope-chemostratigraphic data from Oman to propose three stages of oxidation in the Ediacaran oceans, and linked the second and third stages to eukaryote diversification. The second stage, signaled by strongly ^{13}C-depleted sedimentary carbonates (the 'Shuram excursion'), is believed to result from oxidation of a large, deep-ocean reservoir of organic carbon (Fike et al., 2006). Fike *et al.* used our published data (Grey 2005, Calver 2000) to assert that a correlative carbon isotope excursion in Australia coincided with the initial diversification of acanthomorphic acritarchs. Peak diversity is asserted to have coincided with subsequent deposition of ^{13}C-enriched carbonate and the third oxidation stage. However, they appear to have misinterpreted our data, which instead indicates that diversification significantly preceded the Shuram excursion, greatly weakening their argument for a link between the inferred oxidation events and eukaryote

evolution.

In the type area of the Ediacaran System, the Adelaide Rift Complex, no acritarchs have been recovered from the strongly ^{13}C-depleted section (<-5‰, middleWonoka Formation, Fig.1) correlated with the Shuram excursion. This is likely due to high levels of thermal maturity and deep weathering. Nearby drillholes contain sparse acanthomorphs indicating diversification in the underlying Bunyeroo and lowermost Wonoka Formations (Fig. 1), but the remainder of the Wonoka Formation is missing in these drillholes. The acritarch record is much better preserved and more complete in the Officer Basin. Here, acanthomorph diversification begins in the Dey Dey Mudstone (a correlative of the Bunyeroo Formation), within 50 m of the Acraman impact ejecta layer (Willman et al., 2006), and diverse assemblages continue through a thick overlying succession of mudstone and siltstone with interbedded ^{13}C-enriched carbonate (Karlaya Limestone and Tanana Formation) to reach peak diversity in the ^{13}C-enriched Wilari Dolomite Member (Grey 2005; Calver & Lindsay 1998). The increase in acanthomorph species numbers does not coincide with a negative excursion in [13]C (Fig. 1). Not until some 700 m above the first acanthomorph record, and above at least three of our four acanthomorph zones[2], does strongly ^{13}C-depleted carbonate, presumably the onset of the Shuram excursion, appear in the Officer Basin (Grey 2005; Calver & Lindsay 1998). Consistent with this, the Karlaya Limestone and Tanana Formation are older than the ^{13}C-depleted middle Wonoka Formation from Sr isotope stratigraphic and sequence stratigraphic evidences. Acanthomorph abundances and species numbers apparently decline above this level, in stark contrast to the model of Fike *et al.*, although the fossil record is poor in this part of

the Australian succession. Because of unconformities in the Officer Basin and non-preservation of acritarchs in the Adelaide Rift Complex, we are uncertain of the relationship of the peak diversity seen in the Wilari Dolomite Member with the Shuram excursion.

Finally, in contrast to the assertion of Fike *et al.*, our data do not show peak acanthomorph diversity in the Julie Formation (Amadeus Basin). Not a single acritarch was recovered from the Julie Formation. In the Amadeus Basin, acanthomorph diversification begins in the underlying Pertatataka Formation (a correlative of the Bunyeroo Formation), with maximum recorded diversity about 50 m below the base of the Julie Formation. The Australian evidence for peak acanthomorph diversity coinciding with the third oxidation stage of Fike *et al.* is extremely weak.

References
Fike, D.A., Grotzinger, J.P., Pratt, L.M. & Summons, R.E. Oxidation of the Ediacaran Ocean. *Nature* 444, 744-747 (2006).
Grey, K. Ediacaran Palynology of Australia. Memoirs of the Association of Australasian Palaeontologists, 31, 439 p (2005).
Calver, C.R. Isotope stratigraphy of the Ediacarian (Neoproterozoic III) of the Adelaide Rift Complex, South Australia, and the overprint of water column stratification. Precambrian Research 100, 121–150 (2000).
Willman, S., Moczydłowska, M. & Grey, K. Neoproterozoic (Ediacaran) diversification of acritarchs—A new record from the Murnaroo 1 drillcore, eastern Officer Basin, Australia. Review of Palaeobotany and Palynology, 139, 17-39 (2006).
Calver, C.R. & Lindsay, J. F. Ediacarian sequence and isotope stratigraphy of the Officer Basin, South Australia. Australian Journal of Earth Sciences 45, 513–532 (1998)
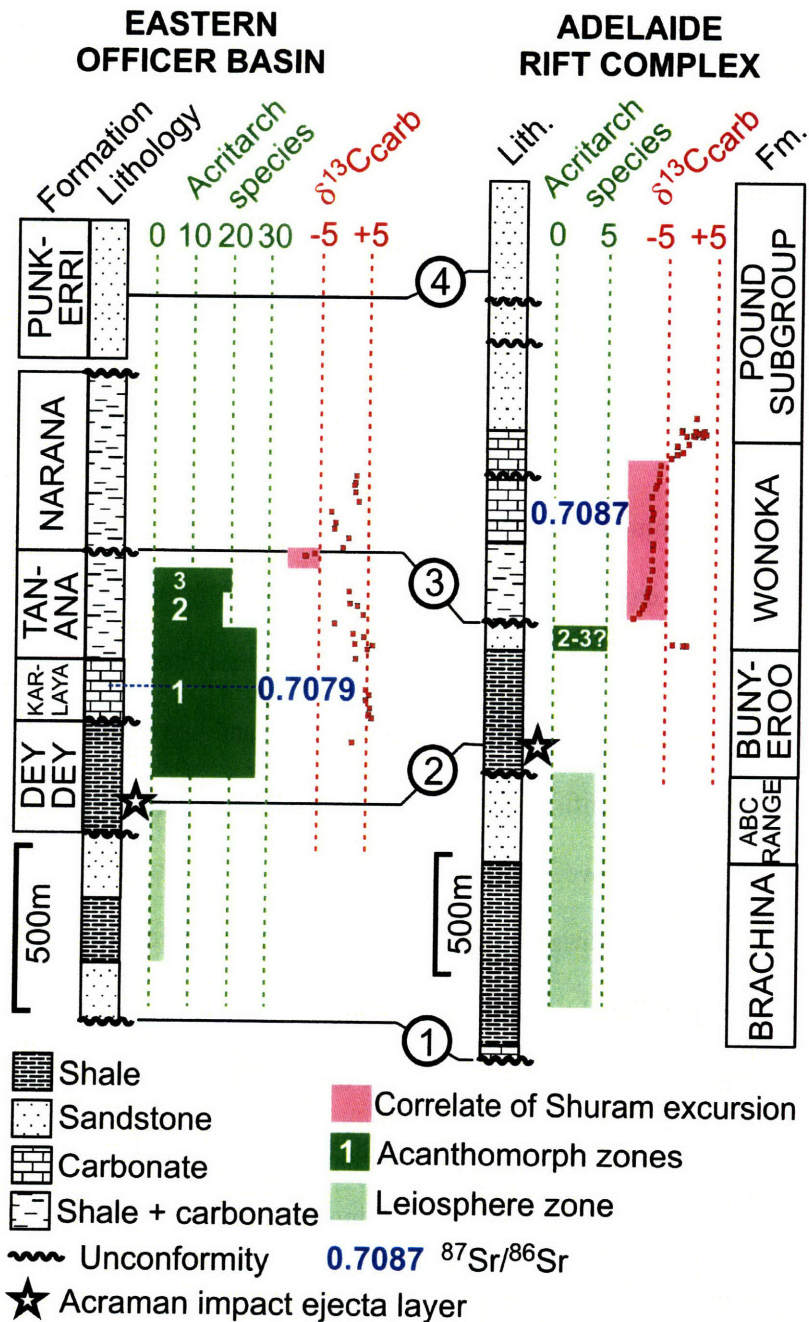
Fig. 1: Ediacaran successions in the eastern Officer Basin (data from Munta-1 drillhole[2,5]) and Adelaide Rift Complex (acritarch data from SCYW1A drillhole[2]; isotope data from Bunyeroo Gorge[3]). Selected correlation tie-lines (circled numbers) are (1) the basal Ediacaran sequence boundary; (2) the Acraman impact ejecta horizon[2,5]; (3) the 'canyon unconformity'[5]; (4) occurrences of Ediacaran animal fossils. Marine [87]Sr/[86]Sr increased monotonically through the Ediacaran; indicated least-altered values are thus consistent with the correlations shown[5].

Appendix D
reply to Grey & Calver 'Ediacaran oxidation and biotic evolution'

D. A. Fike[1], J. P. Grotzinger[2], L.M. Pratt[3], R.E. Summons[1]

[1]Department of Earth, Atmospheric, & Planetary Sciences, Massachusetts Institute of Technology, Cambridge, MA 02139, USA

[2]Division of Geological and Planetary Sciences, California Institute of Technology, Pasadena, CA 91125, USA

[3]Department of Geological Sciences, Indiana University, Bloomington, IN 47405, USA

Calver & Grey point out the difficulties of relating the Australian acritarch record to the global record of environmental change. This results from the lack of documented stratigraphic sections that have overlapping chronologies of both acritarch evolution and global chemostratigraphic proxies, such as $\delta^{13}C_{carb}$, and we agree that such coupled records are required to confirm our hypothesis (FIKE et al., 2006). Until such records exist, any correlations between Australian acritarch-bearing strata and strata containing records of global secular variations in $\delta^{13}C_{carb}$ are necessarily tenuous. This uncertainty, however, does not affect the principal conclusion of our paper, which emphasizes the evidence for sequential chemical oxidation of the Ediacaran ocean. Indeed, our inferred correlation between chemical oxidation and biological evolution has been strongly supported by recent results on strata containing strong geochronologic tie-points and a robust biostratigraphic and chemostratigraphic record (CANFIELD et al., 2007; YIN et al., 2007).

Specifically, Calver & Grey contest our interpretation of an increase in acritarch diversity associated with the onset of the negative excursion in $\delta^{13}C_{carb}$ in the Wonoka Formation of the Adelaide Rift Complex, equivalent to our Stage II oxidation. Despite

this claim, existing data show that the onset of the Wonoka $\delta^{13}C_{carb}$ excursion is found in the most basal Wonoka, just above the Bunyeroo/Wonoka contact (Figure 7, CALVER, 2000). An examination of the Adelaide Rift Complex (Figure 18, GREY, 2005) acritarch record reveals an increase in acritarch diversity (appearance of the *Ab/Am/Gp* assemblage) in the basal Wonoka. We reject the correlation between the Adelaide Rift Complex and Eastern Officer Basin that Calver & Grey present (their Figure 1), particularly the attempt to correlate the Shuram-Wonoka $\delta^{13}C_{carb}$ excursion, which reaches -12‰ in chemostratigraphically well-resolved sections spanning several hundred meters of stratigraphy, with two data points of only moderate depletion (~-6‰) across a contact that is known to be unconformable. Therefore, finding no actual data that preclude our interpretations, we stand by our correlation between acritarch diversification in the basal Wonoka and the onset of the Stage II oxidation.

Calver & Grey correctly point out our error in associating the Julie Formation with the peak in acritarch diversity in the Amadeus basin[1]. The peak diversity is in the uppermost Pertatataka Formation, immediately underlying the Julie Formation. However, in the absence of geochronologic constraints we accept the interpretation that these formations are not broadly separated in time (Figure 32, WALTER et al., 2000). Therefore, this does not discount the central hypothesis of our paper, which argues for increasing biological diversity associated with progressive oxidation throughout Ediacaran time.

_____

[1] The text in Chapter 1 has been modified accordingly to reflect this.

References:

Calver, C. R., 2000. Isotope stratigraphy of the Ediacarian (Neoproterozoic III) of the Adelaide Rift
Complex, Australia, and the overprint of water column stratification. *Precambrian Research* **100**,
121-150.

Canfield, D. E., Poulton, S. W., and Narbonne, G. M., 2007. Late Neoproterozoic Deep Ocean
Oxygenation and the Rise of Animal Life *Science* **315**, 92 - 95.

Fike, D. A., Grotzinger, J. P., Pratt, L. M., and Summons, R. E., 2006. Oxidation of the Ediacaran Ocean.
Nature **444**, 744 - 747.

Grey, K., 2005. *Ediacaran palynology of Australia*. Association of Australasian Paleontologists.

Walter, M. R., Veevers, J. J., Calver, C. R., Gorjan, P., and Hill, A. C., 2000. Dating the 840–544 Ma
Neoproterozoic interval by isotopes of strontium, carbon, and sulfur in seawater, and some
interpretative models. *Precambrian Research* **100**, 371 - 433.

Yin, L., Zhu, M., Knoll, A. H., Yuan, X., Zhang, J., and Hu, J., 2007. Doushantuo embryos preserved
inside diapause egg cysts. *Nature* **446**, 661 - 663.

CHAPTER 2
A paired sulfate-pyrite δ^{34}S approach to understanding the evolution of the Ediacaran-Cambrian sulfur cycle

D. A. Fike[1*] and J. P. Grotzinger[2]

[1]Department of Earth, Atmospheric, & Planetary Sciences, Massachusetts Institute of Technology, Cambridge, MA 02139, USA

[2]Division of Geological and Planetary Sciences, California Institute of Technology, Pasadena, CA 91125, USA

Abstract

An anomalous enrichment in marine sulfate δ^{34}S$_{SO4}$ is preserved in globally-distributed latest Ediacaran – early Cambrian strata. The proximity of this anomaly to the Ediacaran-Cambrian boundary and the associated evolutionary radiation has invited speculation that the two are causally related. Here we present a high resolution record of paired sulfate (δ^{34}S$_{SO4}$) and pyrite (δ^{34}S$_{pyr}$) from sediments spanning ca. 550 – 540 million years ago (Ma) from the Ara Group of the Huqf Supergroup, Sultanate of Oman. We observe an increase in δ^{34}S$_{SO4}$ from ~20‰ to ~42‰, beginning at ca. 550 Ma and continuing at least through ca. 540 Ma. There is a concomitant increase in δ^{34}S$_{pyr}$ over this interval from ~ -15‰ to 10‰. This globally correlative enrichment, here termed the Ara anomaly, constitutes a major perturbation to the sulfur cycle. The Ara anomaly is placed in the context of Ediacaran sulfur cycle and evaluated using a new approach based on paired δ^{34}S$_{SO4}$-δ^{34}S$_{pyr}$ data. These paired data are used to calculate both δ^{34}S$_{in}$, the isotopic composition of the sulfur flux entering the ocean, and f_{pyr}, the fraction of sulfur buried as pyrite. It appears that by the base of the Ediacaran, δ^{34}S$_{in}$ was enriched (~10‰) significantly relative to bulk Earth values (~0‰) and became progressively more enriched through at least the earliest Cambrian (~23‰). The rise in δ^{34}S$_{in}$ is correlated with the known record of increasing Ediacaran ^{87}Sr/^{86}Sr and is believed to result from increased weathering associated with the assembly of Gondwanaland, particularly the rapid recycling of δ^{34}S-enriched Ediacaran strata, and the preferential weathering of sulfates relative to sulfides at low (sub-modern) levels of atmospheric oxygen. Most (20‰) of the ~30% decline in δ^{34}S$_{SO4}$ observed in the Paleozoic is interpreted as representing in part the return of δ^{34}S$_{in}$ toward bulk Earth values. Against the background of increasing Ediacaran δ^{34}S$_{in}$, the Ara anomaly is caused by an increase in f_{pyr}, most likely driven by enhanced primary production, consistent with earlier reports of elevated organic carbon burial and widespread phosphorite deposition. Increased production may have led in turn to eutrophication-driven anoxia and the E-C boundary extinction. The remainder (10‰) of the Paleozoic decrease in δ^{34}S is attributed to decreasing f_{pyr} in association with the rise of pO$_2$ to near modern levels. The data presented here constrain the changes in biogeochemical cycling that caused the Ara anomaly and serve as a contextual framework for understanding the E-C boundary, as well as biological and environmental change into the Paleozoic.

1. INTRODUCTION

The sudden onset of the Cambrian radiation of metazoa at the close of the Ediacaran Period remains an enduring enigma in Earth history. In recent years, it has been shown that this dramatic evolutionary radiation of diverse calcified invertebrates (KNOLL and CARROLL, 1999) occurred shortly after an extinction of the Ediacaran fauna at the Ediacaran-Cambrian (E-C) boundary at ca. 541 million years ago (Ma) (AMTHOR et al., 2003; BOWRING et al., 2007). There is no solid understanding of how evolutionary and environmental changes are coupled, if at all, during the Cambrian radiation (MARSHALL, 2006). If coupled, there is no consensus as to whether environmental change helped to induce the Cambrian explosion (BRASIER and LINDSAY, 2000) or whether the sudden metazoan radiation brought about environmental change (SPERLING and PETERSON, 2007). It is clear, however, that the E-C boundary itself marks significant global biogeochemical change, including evidence for ocean anoxia (KIMURA and WATANABE, 2001; SCHRÖDER and GROTZINGER, 2007), the extinction of Ediacaran *Namacalathus* and *Cloudina* fossil assemblages, and a 7‰ negative excursion in the carbon isotopic composition of carbonate minerals ($\delta^{13}C_{carb}$) of ~1 Myr duration (AMTHOR et al., 2003). This negative excursion in $\delta^{13}C_{carb}$ is increasingly used to correlate different boundary sections in the absence of direct palaeontological or geochronological constraints (BARTLEY et al., 1998; SHIELDS, 1999).

While carbon isotope studies have provided some clues to biogeochemical cycling in the latest Ediacaran, additional paleoenvironmental proxies are needed to further constrain the environmental and evolutionary changes leading up to and across the E-C boundary. Sulfur cycling plays a key role in regulating Earth's surface redox balance

and, because it is mediated by a variety of microbial processes with distinctive metabolic fractionations, serves as a record of ecological variation. Previous studies (e.g., CLAYPOOL et al., 1980; HOLSER, 1977; THODE and MONSTER, 1965) have indicated extreme enrichment in marine sulfate $\delta^{34}S_{SO4}$, the 'Yudomski event' of Holser(1977), in terminal Ediacaran-earliest Cambrian strata (Figure 1). The goal of this paper to interrogate sulfur cycling over latest Ediacaran-earliest Cambrian (ca. 550 – 540 Ma) time, as recorded in the strata of the Ara Group, Sultanate of Oman and to place the resulting $\delta^{34}S$ record into the broader context of the evolution of Ediacaran-Cambrian biogeochemical cycling.
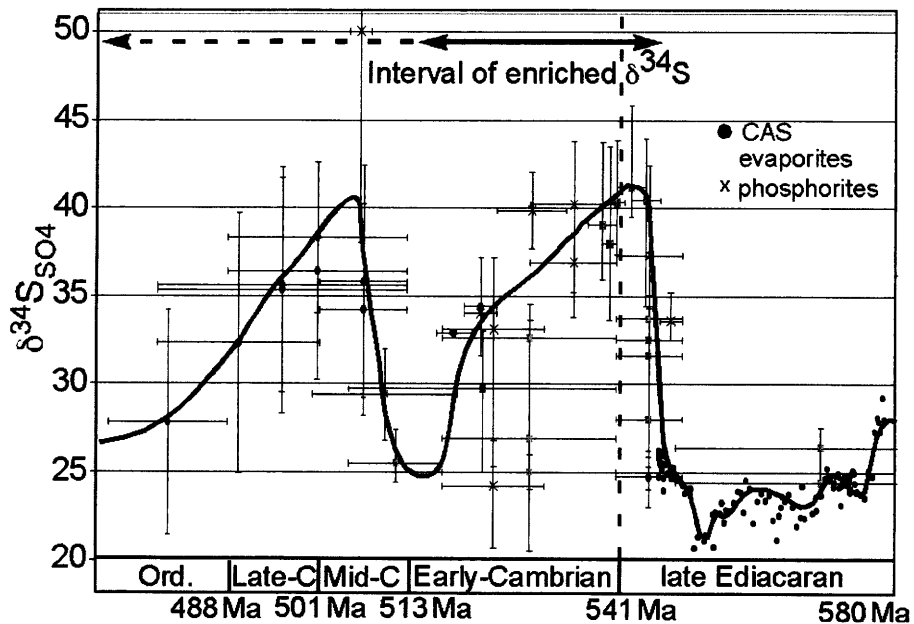
Figure 1: Summary of enriched $\delta^{34}S_{SO4}$ over Ediacaran-Cambrian time. $\delta^{34}S$ is plotted as the mean value reported and the vertical lines represent the total range (or standard deviation, as reported). References are as follows: CAS (FIKE et al., 2006; GOLDBERG et al., 2005; HURTGEN, 2006; KAMPSCHULTE and STRAUSS, 2004); evaporites (BANERJEE et al., 1998; CLAYPOOL et al., 1980; HOUGHTON, 1980; PISARCHIK and GOLUBCHINA, 1975; SCHRÖDER et al., 2004; STRAUSS, 1993; STRAUSS et al., 2001; WALTER et al., 2000); phosphorites: (GOLDBERG et al., 2005; HOUGH et al., 2006; SHEN et al., 2000; SHEN et al., 1998; SHIELDS et al., 1999). Age ranges have been updated to the most recent geochronological constraints where possible.

1.1 Existing record of Ediacaran-Cambrian sulfur cycle

An understanding of the Ediacaran sulfur cycle is essential for interpreting the end-Ediacaran enrichment in $\delta^{34}S_{SO4}$. Above Marinoan glacial deposits (ca. 635 Ma), $\delta^{34}S_{SO4}$ is highly variable in cap carbonates, interpreted to be the result of spatial (lateral and vertical) $\delta^{34}S_{SO4}$ gradients in seawater (HURTGEN, 2006), arising from low concentrations (< 200μM) of oceanic sulfate (FIKE et al., 2006; HURTGEN, 2006). Enriched $\delta^{34}S_{SO4}$ values of ~40‰ occur in the upper portion of these cap carbonates (HURTGEN, 2006), decreasing to ~25‰ shortly above the cap (FIKE et al., 2006). Subsequently, $\delta^{34}S_{SO4}$ is constrained to gradual fluctuations between ~15-30‰ until ca. 550 Ma (FIKE et al., 2006; HURTGEN et al., 2005; KAUFMAN et al., 2007). Sulfate concentrations are deduced to rise to ~5 – 10 mM over the interval from ca. 635 – 580 Ma, coincident with a rise in atmospheric oxygen (FIKE et al., 2006) and possibly to levels as high as ~15 – 25 mM around the time of the E-C boundary (HORITA et al., 2002).

Worldwide the interval straddling the E-C boundary records an anomalous enrichment in $\delta^{34}S_{SO4}$ of marine sulfate preserved in evaporites, phosphorites, and carbonate-associated sulfate (Figure 1). This enrichment is here termed the Ara anomaly because the onset and peak are extremely well represented in the coeval Ara Group, Sultanate of Oman. Enriched $\delta^{34}S_{SO4}$ values during the Ara anomaly are on the order of 40‰ (SCHRÖDER et al., 2004, data presented here), whereas typical values of $\delta^{34}S_{SO4}$ are in the range of ~20-25‰ prior to its onset (FIKE et al., 2006).

The Ara anomaly ushers in a period of enriched $\delta^{34}S$ that lasts throughout the Cambrian (Figure 1). Improved geochronologic constraints are needed to uniquely

reconstruct seawater $\delta^{34}S$ over this interval; however, it appears that there are two distinct periods of enriched $\delta^{34}S$ at E-C boundary (discussed directly in the present paper) and another during the Middle Cambrian (~510 Ma). As of this writing, it is unclear whether the mechanism(s) that caused the Ara anomaly are relevant for understanding enriched $\delta^{34}S$ throughout the Early Cambrian (lasting until ca. 515 Ma) or throughout the entire early Paleozoic interval of enriched $\delta^{34}S$. Even with the conservative view that the Ara anomaly terminates in the Early Cambrian, its magnitude (~20‰) and duration ($\geqslant$ 30 Myr) constrain the Ara anomaly to be one of the largest known perturbations to the sulfur biogeochemical cycle in Earth history. Further, the coincidence of the Ara anomaly and the E-C boundary invites speculation about a causal relationship between these two events. Our goal is to distinguish between possible causes (e.g., biologic vs. tectonic) for the Ara anomaly and to place the $\delta^{34}S$ record in the context of changes in ecology and carbon cycling that occur across the E-C boundary and throughout the ensuing Cambrian radiation.

1.2 Geologic Context

The Huqf Supergroup provides one of the best preserved, most continuous sections of Ediacaran through earliest Cambrian strata (ca. 635 – 540 Myr) (AMTHOR et al., 2003; SCHRÖDER et al., 2004). Huqf strata are preserved both in surface outcrops of the Oman Mountains and the Huqf area, and within subsurface sedimentary basins (Figure 2). The Huqf Supergroup comprises the Abu Mahara, Nafun, and Ara groups.
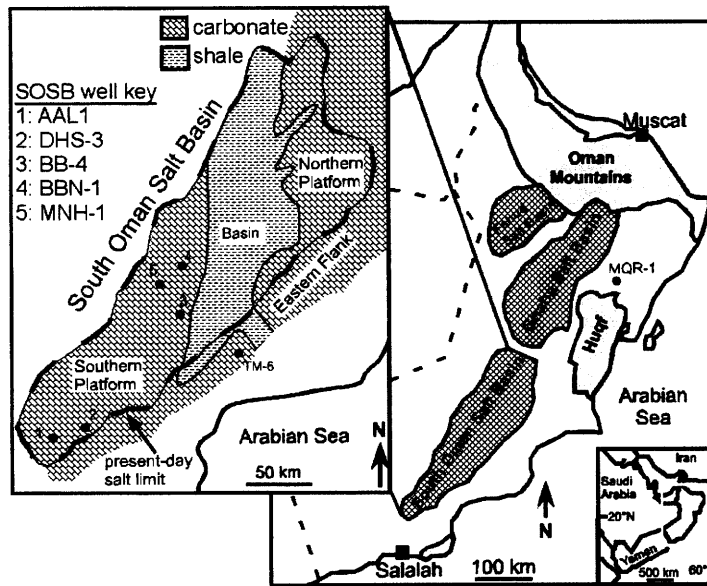
Figure 2: Map of Oman showing locations of Neoproterozoic outcrops (dark grey). Three subsurface salt basins (Fahud, Ghaba, and South Oman Salt Basins are indicated in the interior. The locations of the wells that provided subsurface samples are shown. Nafun Group strata were sampled from well MQR-1 located north of the Huqf region. Ara Group strata (inset) were sampled from wells that penetrate the SOSB (AAL-1, DHS-3, BB-4, BBN-1, MNH-1) or the Eastern Flank (TM-6).

Stratigraphic, lithologic, and geochronologic constraints for the Huqf Supergroup are shown in Figure 3. The Abu Mahara Group contains Marinoan-equivalent glacial deposits (Fiq Formation, ca. 635 Ma) that overlie ca. 800 Ma crystalline basement (BOWRING et al., 2007). Nafun Group sediments were deposited in a regionally extensive sag basin under open, shallow marine conditions, and each formation can be traced laterally for several hundred km across Oman (GROTZINGER et al., 2002; LE GUERROUE et al., 2006a; MATTES and CONWAY-MORRIS, 1990; MCCARRON, 2000). Nafun Group strata comprise two clastic-to-carbonate shallowing-upward successions (Masirah Bay Formation and Khufai Formation; Shuram Formation and Buah Formation) with an unconformity across the Khufai-Shuram boundary (MCCARRON, 2000) that likely includes the interval of Gaskiers glaciation at ca. 580 Ma (BOWRING et al., 2007);

however, Le Guerroue et al. (2006a; 2006b) argue for continuous deposition across this contact. The Shuram excursion, a >15‰ negative excursion in $\delta^{13}C_{carb}$, spans ~ 500m of section from the basal Shuram Formation through the mid-Buah Formation (BURNS and MATTER, 1993; FIKE et al., 2006; LE GUERROUE et al., 2006a). Global correlation of $\delta^{13}C_{carb}$ anomalies provides two age constraints for the Buah Formation (Figure 3): ca. 550 Ma for the mid-Buah (correlation with Doushantuo Formation, China (BOWRING et al., 2007; CONDON et al., 2005)); and ca. 548 Ma for the upper Buah (correlation with Nama Group, Namibia (BOWRING et al., 2007; GROTZINGER et al., 1995)). These ages are consistent with those obtained from the overlying Ara Group.

Ara Group strata were deposited between ca. 547 – 540 Ma (BOWRING et al., 2007). The Ara Group and E-C boundary strata are known definitively only from the subsurface (AMTHOR et al., 2003; MATTES and CONWAY-MORRIS, 1990). In strata beneath the modern day South Oman Salt Basin (SOSB), the Ara Group exists as a series of six carbonate-evaporite shallowing upward cycles, deposited in strongly subsiding block-faulted basin (AMTHOR et al., 2003; SCHRÖDER et al., 2003b). On the margin (termed the Eastern Flank) of the SOSB, Ara Group strata are recorded as a series of evaporite-free carbonates. There is a robust correlation (AMTHOR et al., 2003) between the Ara carbonates interbedded with evaporites on the interior of the SOSB and those deposited on the Eastern Flank, based on the presence of an ash-bed dated to 541 Ma (BOWRING et al., 2007), $\delta^{13}C_{carb}$ chemostratigraphy, drill core logs, and trace element geochemistry. In both the SOSB and the Eastern Flank, the contact between the Buah and overlying Ara Group is marked by a disconformable, karstic surface.

The presence of multiple ash horizons within Ara Group strata (Figure 3) has significantly improved our understanding of the timing and duration of Ara deposition and our ability to correlate the Oman stratigraphy with other sections globally (AMTHOR et al., 2003; BOWRING et al., 2007; GROTZINGER et al., 1995). An age of 546.72 ± 0.22 Ma from the middle of the basal Ara carbonate (A0) constrains the unconformity at the Buah-Ara contact to ~1 Myr (BOWRING et al., 2007). Ash beds at the base (AMTHOR et al., 2003; BOWRING et al., 2007) and top (BOWRING et al., 2007) of the third carbonate unit (A3) yield zircon U/Pb ages of 542.91 ± 0.13 and 542.31 ± 0.14 Ma, respectively. All zircon U/Pb ages cited here were obtained from the same laboratory and calibrated under the same conditions, allowing for a very precise determination of the relative ages of samples (BOWRING et al., 2007). These A3 ages indicate that the deposition of a typical Ara carbonate unit took ~ 1 Ma (BOWRING et al., 2007), consistent with the age difference between the A0 and A4 (see below) carbonates. The base of the A4 carbonate unit contains an ash that yielded a U/Pb age (AMTHOR et al., 2003; BOWRING et al., 2007) of 541.00 ± 0.12 Ma. This age, in combination with a 7‰ negative excursion in carbonate $\delta^{13}C$ and the disappearance of Ediacaran *Namacalathus* and *Cloudina* fossil assemblages, is the basis for the identification of the E-C boundary at the base of the A4 carbonate in Oman (AMTHOR et al., 2003).

Figure 3: Stratigraphic column for the upper Huqf Supergroup, Sultanate of Oman. The dashed line indicates the Ediacaran-Cambrian boundary. Geochronologic constraints are from single zircon U/Pb ages on ashbeds (BOWRING et al., 2007). Ages in black are from Oman, those in gray are correlated to Oman based on $\delta^{13}C_{carb}$ chemostratigraphy (FIKE et al., 2006). Stratigraphy consists of Nafun Group strata from MQR-1 and a compilation of all Ara SOSB data. Data from different SOSB wells are normalized to a uniform thickness for plotting purposes. a) $\delta^{13}C_{carb}$ for reference. b) $\delta^{34}S_{SO4}$ from carbonate-associated sulfate (black circles). The open circles are the mean $\delta^{34}S$ for floor and roof bedded anhydrites (horizontal line through the circle is the standard deviation). c) Pyrite $\delta^{34}S$. d) $\Delta\delta^{34}S = \delta^{34}S_{CAS} - \delta^{34}S_{pyr}$.

Ara strata from the Eastern Flank are preserved as a strictly carbonate succession approximately 200-300m in thickness (Figure 4). There is no record of evaporite

deposition along the Eastern flank. We cannot exclude the possibility that shallow-water sabkha evaporites (WARREN, 1989) were deposited on the Eastern Flank and underwent post-depositional dissolution. However, in the absence of any preserved evaporitic strata or clear geochemical evidence (e.g., $\delta^{13}C_{carb}/\delta^{18}O_{carb}$ enrichment from basin restriction), the most probable interpretation is that the Eastern flank carbonate strata represent deposition during relative sea-level highstands (i.e., syndepositional with SOSB carbonate deposition). Evaporite deposition within the basin is likely associated with periods of non-deposition (subaerial exposure) on the Eastern Flank. Correlation of the A4 unit (containing the E-C boundary) between the margin and interior of the basin is secure, based on the presence of both the 541 Ma ashbed at the base of the A4 carbonate and the overlying E-C boundary $\delta^{13}C_{carb}$ excursion (AMTHOR et al., 2003).
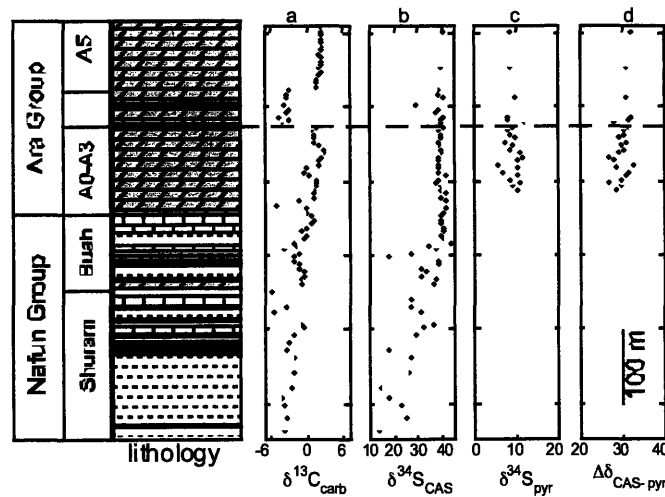
Figure 4: Stratigraphic column for the Upper Nafun Group and the Ara Group strata of the Eastern Flank well TM-6. The dashed line indicates the Ediacaran-Cambrian boundary. The negative $\delta^{13}C_{carb}$ excursion corresponds to the A4 carbonate unit and the Ediacaran-Cambrian boundary (as in Figure 3). Lithologies follow the legend from figure 3. a) $\delta^{13}C_{carb}$ for reference. b) $\delta^{34}S_{SO4}$ from carbonate-associated sulfate. c) Pyrite $\delta^{34}S$. d) $\Delta\delta^{34}S = \delta^{34}S_{CAS} - \delta^{34}S_{pyr}$.

However, the difficulties of correlating hiatal gaps in Eastern Flank strata to the periods

of evaporite deposition within the SOSB hinders correlation above and below the A4

unit. Therefore, the lower Ara strata on the Eastern flank are correlated to the A0-A3

carbonate units and upper Ara strata on the Eastern flank are correlated with the A5/A6

carbonates from within the SOSB (Figure 5). No attempt to further divide Eastern Flank

strata is made.

Samples from this study were taken as cores and cuttings from the following SOSB

wells: AAL-1, BBN-1, DHS-3, BB-4, and MNH-1; as well as the Eastern Flank well TM-

6 (see Appendix A (Table S1) for a complete list of samples). Well locations are shown

in Figure 2 and the stratigraphic distribution of samples is shown in Figure 5. Results for

Nafun Group strata from the well MQR-1 were reported previously (FIKE et al., 2006)

and are here supplemented by basal Ara strata from MQR-1 to provide context over the

Nafun-Ara transition.
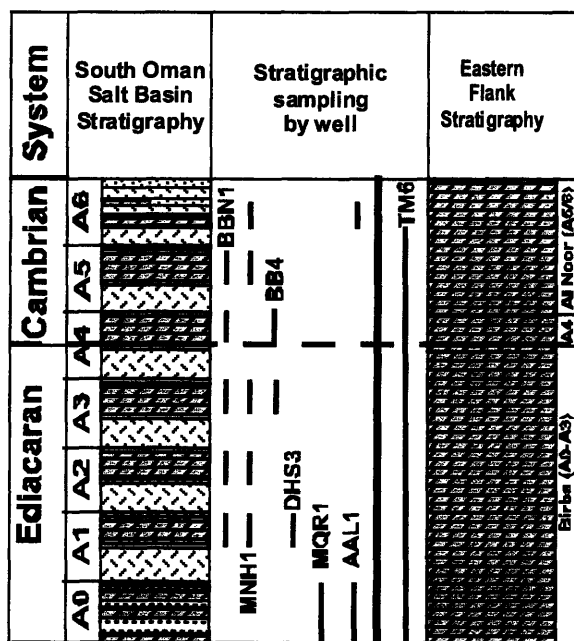
Figure 5: Stratigraphic distribution of Ara Group samples by well from within the SOSB
and the Eastern flank. The lithologic legend is the same as in Figure 3.

2. METHODS

Samples were processed and analyzed as reported previously(FIKE et al., 2006). For anhydrite-bearing SOSB strata, samples were soaked repeatedly in DI to remove water-soluble sulfate minerals. The removal of water-soluble sulfates was also done in a 10% NaCl solution (KAMPSCHULTE and STRAUSS, 2004), which greatly reduced the number of rinses needed to remove water-soluble sulfates, but did not have any noticeable effect on the resulting $\delta^{34}S_{SO4}$ value. Carbonate carbon and oxygen isotopes were measured using standard methods (OSTERMANN and CURRY, 2000). Carbon isotopes are reported as $\delta^{13}C_{carb} = (R_{standard}/R_{sample} - 1) * 1000$, where R = the ratio of $^{13}C/^{12}C$, in units of permil (‰) relative to the V-PDB standard. Oxygen isotopes are analogously reported as $\delta^{18}O_{carb}$, relative to the V-PDB standard. Sulfur isotope compositions are expressed as $\delta^{34}S = (R_{standard}/R_{sample} - 1) * 1000$, where R_i is the ratio of $^{34}S/^{32}S$, reported as permil (‰) deviations from V-CDT, with analytical error of ~0.1‰, calculated from replicate analyses of samples and laboratory standards.

3. RESULTS

Here we present the first high-resolution record of paired sulfate and sulfide $\delta^{34}S$ from Ara Group strata spanning ca. 550 – 540 Ma from the SOSB (Figure 3) and Eastern Flank (Figure 4). We place these data in the context of the Nafun Group (ca. 635 – 550 Ma) sulfur chemostratigraphy (FIKE et al., 2006) to discuss changes in sulfur biogeochemical cycling, and inferentially environmental change, over Ediacaran-early Cambrian time.

3.1 The Ara Anomaly: $\delta^{34}S_{SO4}$

An increase in $\delta^{34}S_{SO4}$ in the mid-Buah Formation marks the onset of the Ara anomaly at ca. 550 Ma. Enriched $\delta^{34}S_{SO4}$ values persist through the remainder of the Buah Formation and through the entirety of the Ara Group. This increase is observed in both the SOSB (Figure 3b) and the Eastern Flank (Figure 4b). We first present the data from SOSB strata and then the Eastern Flank strata. The Eastern Flank strata record the full rise in $\delta^{34}S_{SO4}$ (up to 42‰), whereas the MQR-1 strata are truncated by the sub-Haima unconformity after rising from 20‰ to 26‰. The sub-Haima unconformity is traceable across Oman and separates the Ara Group carbonates from the regionally extensive mid-late Cambrian Haima clastics. Within the SOSB, the rise in $\delta^{34}S_{SO4}$ continues throughout the basal Ara (A0) Group, reaching values as high as 39‰ by the end of A0 deposition (ca. 546 Ma). The A0 carbonates underlie the first known evaporitic sediments and are therefore regarded as having been deposited before the basin underwent its first episode of periodic restriction. $\delta^{34}S_{SO4}$ continues to increase throughout the lower Ara units (A1- A3), reaching a maximum of 42‰ near the top of the A3 carbonate unit, just before the E-C boundary. The A4 carbonate unit (ca. 541 Ma) was deposited during the E-C boundary negative $\delta^{13}C_{carb}$ excursion, and has slightly less enriched $\delta^{34}S_{SO4}$ (~40‰). The uppermost Ara carbonates (A5, A6) are characterized by $\delta^{34}S_{SO4}$ averaging 41‰, indicating that elevated $\delta^{34}S$ continued into the earliest Cambrian (ca. 540 Ma), consistent with Early Cambrian values of ~30–38‰ (KAMPSCHULTE and STRAUSS, 2004). The magnitude of the Ara anomaly in $\delta^{34}S_{SO4}$ is consistent across the SOSB itself and between the SOSB and strata of the non-evaporitic Eastern Flank, and

these enriched values are consistent with reports from globally correlative sections (Figure 1).

3.2 The Ara Anomaly: $\delta^{34}S_{pyr}$

Overall, there is a significant increase in $\delta^{34}S_{pyr}$, relative to typical values from the underlying Nafun Group (~ -15‰), associated with the enriched $\delta^{34}S_{SO4}$ that comprises the Ara anomaly (Figure 3c, 4c). By the basal Ara (A0), $\delta^{34}S_{pyr}$ has risen sharply to ~ 20‰ within strata of the SOSB. Values of $\delta^{34}S_{pyr}$ remain enriched throughout the remainder of Ara deposition (the average SOSB Ara $\delta^{34}S_{pyr}$ is 10‰). In Eastern Flank strata (Figure 4c), pre-A4 samples from TM-6 have an average $\delta^{34}S_{pyr} = 9.3$‰; whereas $\delta^{34}S_{pyr}$ reaches 9.4‰ in A4 strata and 8.6‰ for post-A4 strata. Although not as well-resolved as the $\delta^{34}S_{SO4}$ excursion, the Ara anomaly in $\delta^{34}S_{pyr}$ is consistent across the SOSB itself and between the SOSB and the non-evaporitic Eastern Flank strata. In addition, these $\delta^{34}S_{pyr}$ values are in agreement with reports of enriched $\delta^{34}S_{pyr}$ from contemporaneous strata (CANFIELD et al., 2007; GOLDBERG et al., 2005).

The interpretation of $\delta^{34}S_{pyr}$ is complicated by its dependence on the isotopic composition of sulfate undergoing reduction and on the isotopic fractionation associated with sulfate reduction itself. It is this latter fractionation that is of interest when trying to characterize the sulfur cycle. Therefore, we focus on $\Delta\delta^{34}S = \delta^{34}S_{SO4} - \delta^{34}S_{pyr}$ as a way to interpret variability within the sulfur cycle decoupled from $\delta^{34}S_{SO4}$ (Figures 3d, 4d). In the upper Nafun Group, $\Delta\delta^{34}S$ is ~32‰ in the lower Buah, and increases briefly to ~44‰ in the upper Buah coincident with the onset of enrichment in $\delta^{34}S_{SO4}$ (Figure 3d). These strata are interpreted to represent an interval marked by significant bacterial sulfur

disproportionation, a microbial metabolism that increases $\Delta\delta^{34}S$ (FIKE et al., 2006). Within the SOSB (Figure 3d), the value of $\Delta\delta^{34}S$ decreases in the basal Ara (A0), although the remainder of the Ara Group samples have an average (~27‰) that is within the range of Upper Nafun Group strata. In Eastern Flank strata, pre-A4 and A4 samples from TM-6 have an average $\Delta\delta^{34}S = 31$‰, increasing slightly to 32‰ in post-A4 strata (Figure 4d). The greater variability in $\Delta\delta^{34}S$ in SOSB strata relative to Eastern Flank strata is attributed to the fact that the SOSB strata are primarily samples taken from drill core, whereas the Eastern Flank strata are exclusively samples of cuttings. Cuttings are fragments of rock that are cut from the borehole during drilling. They are 1-3 mm in size and represent a range of stratigraphic levels integrated over approximately 2 meters of stratigraphy. The increased stratigraphic coverage (~2m rather than ~2cm for core samples) for each sample of cuttings has the effect of smoothing high-frequency spatial variability in $\delta^{34}S_{pyr}$ and therefore $\Delta\delta^{34}S$. Despite these differences, $\Delta\delta^{34}S$ is remarkably consistent both within the SOSB and the Eastern Flank throughout the Ara anomaly.

4. ANALYSIS AND INTERPRETATION

4.1 The Ara as a Record of Open Marine Conditions

4.1.1 The $\delta^{34}S_{SO4}$ record

We now assess the evidence that the Ara anomaly is a record of open marine conditions (i.e., globally extensive) and not the result of local basin restriction. This is important since the basin is not only developed on continental crust, but also because the younger strata (A2-A6) were deposited within a rift structure bounded by transtensional faults. Vertical fault motions within this pull-apart structure likely had an important

influence on the episodic restriction required to form basin-wide evaporite sequences. However, as restricted as the basin may have become during evaporite deposition, available data indicate that the evaporating fluids were of marine origin (HORITA et al., 2002; SCHRÖDER et al., 2003a).

First, we note that within the SOSB the majority (18‰) of the increase in $\delta^{34}S_{SO4}$ that constitutes the Ara anomaly occurred in the non-evaporitic facies of the Buah Formation and the A0. The Buah Formation is composed of open marine platform carbonates (COZZI et al., 2004a; COZZI et al., 2004b) that can be traced laterally(McCARRON, 2000) for 100s of km. As such, the Buah formation is interpreted to record global marine composition. Support for this claim is found in the strong similarity between $\delta^{13}C_{carb}$ chemostratigraphy from the Buah Formation (COZZI et al., 2004a) with that from the open marine platform carbonates of the Nama Group, Namibia (GROTZINGER et al., 1995).

By the basal Ara (A0) Group in the SOSB, $\delta^{34}S_{SO4}$ has increased to $\sim$ 39‰. This occurs stratigraphically beneath the first evidence for periodic basin restriction in the Ara Group. The predominant facies observed in cores of the A0 are laminated microbialitic carbonates and carbonate mudstones, interspersed with lenses of gray-green shale and volcanic ash facies. There is no evidence for reworking of these sediments, indicating their deposition in a fairly deep water (below storm wave base) environment. While there is no indication of basin restriction (e.g., evaporites and/or evaporitic enrichment in e.g., $\delta^{13}C_{carb}/\delta^{18}O_{carb}$) in the existing cores or well-logs of the A0, it is inherently difficult to preclude the possibility of (spatially-variable) basin restriction during the Buah-Ara hiatus or contemporaneous with A0 deposition.

For the wells within the SOSB, the remainder (~3‰) of the 21‰ increase in $\delta^{34}S_{SO4}$

that delineates the Ara Anomaly is derived from the Ara Group (A1 – A6) carbonates

interbedded with evaporitic strata. Each of these carbonate units are typically ~ 50 -

100m in thickness and show a characteristic facies progression from outer ramp

mudstones to shallow water grainstones, fossil-rich (A1-A3) thrombolitic reefs, and

peritidal carbonates. There is no correlation observed between facies (mudstones,

grainstones, thrombolitic reefs, or peritidal carbonates) and $\delta^{34}S_{SO4}$ (Figure 6). The

facies-independence of $\delta^{34}S_{SO4}$ argues against local basin restriction as the cause of the

Ara anomaly because evaporite basins are typically characterized by steep facies

gradients as a function of restriction (WARREN, 1989). Ara carbonate units (A1–A6)

have previously been interpreted as open marine sediments (AMTHOR et al., 2003)

because the index fossils *Cloudina* and *Namacalathus,* present in the Ediacaran carbonate

units (A1 – A3), are elsewhere (e.g., Namibia, Canada) associated with open water

environments (GROTZINGER et al., 2000; HOFMANN and MOUNTJOY, 2001). The record

of $\delta^{13}C_{carb}$ derived from the carbonates of the SOSB Ara wells shows no offset with

respect to the $\delta^{13}C_{carb}$ record obtained from the evaporite-free Eastern Flank (AMTHOR et

al., 2003). Similarly, the record of $\delta^{13}C_{carb}$ in the A1-A3 (AMTHOR et al., 2003) matches

the $\delta^{13}C_{carb}$ chemostratigraphy of the terminal Ediacaran Nama Group of Namibia

(GROTZINGER et al., 1995; SAYLOR et al., 1998), which are unequivocally open marine

platform carbonates with excellent geochronologic and palaeontological constraints (see

summary in GROTZINGER and MILLER, 2007) that allow for clear correlation to Oman.

Additionally, the base of the A4 carbonate unit, dated to 541.00 ± 0.12 Myr (AMTHOR et

al., 2003; BOWRING et al., 2007) records the 7‰ $\delta^{13}C_{carb}$ excursion that is used to

globally correlate disparate E-C boundary sections (BARTLEY et al., 1998; GROTZINGER et al., 1995; SHIELDS, 1999). Further, the lack of scatter in $\delta^{13}C_{carb}$ across all of the Ara carbonate units (Figure 3a) suggests that the Ara basin did not evolve extensively while isolated from a global marine reservoir. Similarly, the small scatter in $\delta^{34}S_{SO4}$ between the different Ara units (Figure 3b) argues against variable restriction during deposition.
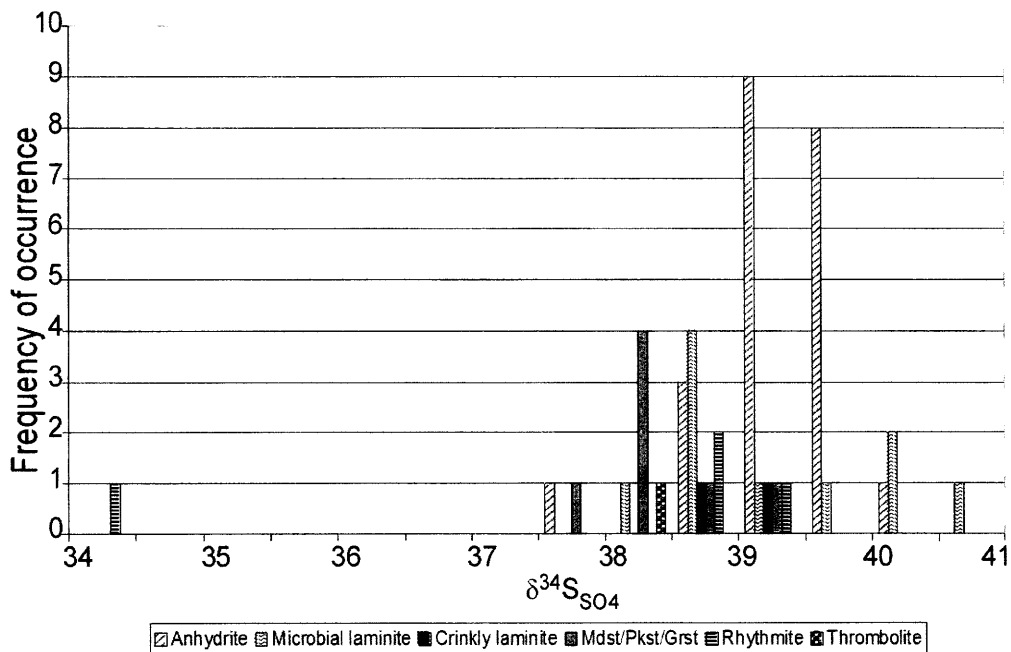
Figure 6: Facies independence of $\delta^{34}S$ in SOSB Ara Group strata. Data are from the A3 and A4 stratigraphic units of well BB-4.

It is clear from the evaporite deposition that the basin did go through periods of restriction from the open ocean. Analysis of elemental composition confirms the evaporites originated from seawater rather than from continental waters (BRENNAN et al., 2004; HORITA et al., 2002; SCHRÖDER et al., 2003a). Despite the evaporitic conditions associated with primary evaporite deposition, stratiform anhydrite is believed to accurately record the isotopic composition of seawater sulfate because of nearly

quantitative removal of seawater sulfate and the small (~1‰) isotopic fractionation associated with gypsum/anhydrite deposition(RAAB and SPIRO, 1991). It is important to note that the anhydrite layers discussed here were probably deposited as gypsum and have undergone recrystallization as anhydrite following dewatering during burial. There has been no definitive study of sulfur isotope fractionation associated with this recrystallization. However, given the lack of a significant fractionation between seawater sulfate and either mineral, it is unlikely that recrystallization altered the original $\delta^{34}S_{SO4}$ composition of the Ara stratiform gypsum deposits. A comparison of $\delta^{34}S_{SO4}$ between carbonate-associated sulfate from the Ara carbonate units and the stratiform anhydrite deposits bounding these units (filled and open circles, respectively, in Figure 3b) reveals that $\delta^{34}S_{anhyd}$ is enriched by ~ 2–4‰ with respect to the less variable $\delta^{34}S_{CAS}$. This small offset between $\delta^{34}S_{CAS}$ and $\delta^{34}S_{anhyd}$ supports an open marine interpretation for the $\delta^{34}S_{CAS}$ signal and indicates a possible minor evaporitic enrichment in $\delta^{34}S_{anhyd}$. Thus, despite evidence for restriction associated with evaporite deposition, the interbedded carbonates (A1-A6) appear to have been deposited in direct connection to the global ocean.

While the above arguments do not prove that the Ara carbonates were in direct connection to the global ocean, they place clear constraints on what type of restriction could have occurred during Ara deposition. First, any restriction must have been small enough to prevent distillation-induced differences between the Ara $\delta^{13}C_{carb}$ record and global chemostratigraphy. It follows that the degree of restriction during deposition of the different carbonate units must have been essentially constant to prevent variability in $\delta^{13}C_{carb}/\delta^{34}S_{CAS}$ between individual Ara units (i.e., between intervals of evaporite

deposition, the basin would have to return the same level of restriction for the duration of deposition of each Ara carbonate unit). The similarity of the $\delta^{34}S_{SO4}$ record between the SOSB (preserved in both $\delta^{34}S_{CAS}$ and $\delta^{34}S_{anhyd}$) and Eastern Flank strata, where there is no record of any evaporite deposition, argues strongly that the Ara anomaly is not an artifact of basin restriction. The agreement between these records requires that any evaporitic effect would have had to have been small enough to prevent distillation-induced differences between the SOSB Ara Group and the non-evaporitic Eastern Flank Ara strata . This would be surprising, as evaporite basins tend to have some of the strongest known gradients in both sedimentology and mineralogy (WARREN, 1989). The reproducibility of the $\delta^{34}S_{SO4}$ Ara anomaly demonstrates a homogeneous sulfur isotope composition across this $\sim 10^5 \, km^2$ basin.

In terms of assessing possible restriction during deposition of Ara Group carbonates it is most useful to compare $\delta^{34}S_{SO4}$ observed in the Ara with that observed in globally correlative strata. A survey of the literature finds similarly enriched sulfate ($\delta^{34}S_{SO4} \sim$ 40‰) widely distributed throughout the globe in latest Ediacaran-earliest Cambrian strata (see Figure 1). The global pattern of enriched $\delta^{34}S$, preserved in CAS, phosphorites, and evaporites, at the time of Ara deposition strongly argues that these enriched values reflect primary seawater $\delta^{34}S_{SO4}$, rather than being the result of multiple independently restricted basins. This provides confidence that the Ara anomaly reflects a perturbation to the global marine sulfur cycle.

4.1.2 The $\delta^{34}S_{pyr}$ record

$\delta^{34}S_{pyr}$ is known to depend on conditions of the local depositional environment (e.g., sedimentation rate, sulfate reduction rate, and sulfate concentration)(CANFIELD, 2001). As such, in comparison to $\delta^{34}S_{SO4}$, it is significantly more difficult to assess the likelihood that a particular range of $\delta^{34}S_{pyr}$ is representative of global marine conditions. Nonetheless, it is important to evaluate whether the observed enrichment in $\delta^{34}S_{pyr}$ seen in the Ara anomaly is representative of global sediments. The similarity of $\delta^{34}S_{pyr}$ between the SOSB and Eastern Flank suggest that it is representative of pyrite deposition over the $\sim10^5$ km^2 basin, despite gradients in sedimentary facies from basin margin to center. These values of $\delta^{34}S_{pyr}$ are in broad agreement with correlative sections in China (GOLDBERG et al., 2005) and Newfoundland (CANFIELD et al., 2007). An estimate of globally averaged $\delta^{34}S_{pyr}$ (~15‰) over this interval (compiled from the data of CANFIELD, 2004; CANFIELD et al., 2007) agrees with the average values of Ara $\delta^{34}S_{pyr}$ (~12‰) observed in this study. Therefore, following the logic outlined above for consideration of $\delta^{34}S_{SO4}$, it is likely that the observed increase in $\delta^{34}S_{pyr}$ is representative of the open ocean.

4.2 Mechanisms to generate the Ara anomaly

We now attempt to constrain possible causative mechanisms for the Ara anomaly. In doing this, we rely on an understanding of the sulfur cycle that is based on the interpretation of high-resolution pairs of $\delta^{34}S_{SO4}$-$\delta^{34}S_{pyr.}$. The steady-state equation relating the isotopic composition of sulfate in the oceans, $\delta^{34}S_{SO4}$, and the isotopic composition of pyrite $\delta^{34}S_{pyr}$ is:

$$\delta^{34}S_{in} = (1 - f_{pyr}) * \delta^{34}S_{SO4} + f_{pyr} * \delta^{34}S_{pyr}. \tag{1}$$

where f_{pyr} is the fraction of sulfur buried as pyrite, and $\delta^{34}S_{in}$ is the isotopic composition of sulfur entering the ocean. This can be rewritten substituting $\Delta\delta^{34}S = \delta^{34}S_{SO4} - \delta^{34}S_{pyr}$:

$$\delta^{34}S_{SO4} = f_{pyr} * \Delta\delta^{34}S + \delta^{34}S_{in}. \tag{2}$$

It follows that there are three ways (Figure 7) to generate the enrichment in $\delta^{34}S_{SO4}$, such as that observed in the Ara anomaly, by varying one of these parameters ($\Delta\delta^{34}S$, f_{pyr}, $\delta^{34}S_{in}$) while holding the others constant. The first mechanism is to increase $\Delta\delta^{34}S$, the biological fractionation between coexisting sulfate and pyrite. This has the effect of enriching $\delta^{34}S_{SO4}$ and depleting $\delta^{34}S_{pyr}$. The second mechanism is to increase f_{pyr}, while the third mechanism is to increase $\delta^{34}S_{in}$. Both of these latter mechanisms result in a parallel enrichment of $\delta^{34}S_{SO4}$ and $\delta^{34}S_{pyr}$. The first two mechanisms have been commonly invoked to explain changes in $\delta^{34}S_{SO4}$ (CANFIELD and TESKE, 1996; CLAYPOOL et al., 1980). On the other hand, $\delta^{34}S_{in}$ is generally assumed to have been relatively invariant throughout geologic history(CANFIELD, 2001; GARRELS and LERMAN, 1981). As such, change in $\delta^{34}S_{in}$ is not typically considered as a possible cause for observed $\delta^{34}S_{SO4}/\delta^{34}S_{pyr}$ variability, although this has been proposed recently to explain unusually enriched $\delta^{34}S$ throughout the Neoproterozoic (CANFIELD, 2004). Previous attempts to identify the cause of $\delta^{34}S_{SO4}$ excursions in the geologic record have been hindered by the lack of coexisting $\delta^{34}S_{SO4}$ and $\delta^{34}S_{pyr}$. Without such data, it is not possible to rigorously identify or preclude any of these mechanisms as the cause of the

observed enrichment in $\delta^{34}S_{SO4}$ during the Ara anomaly. Using the data presented here, we now examine each of these three mechanisms in turn.
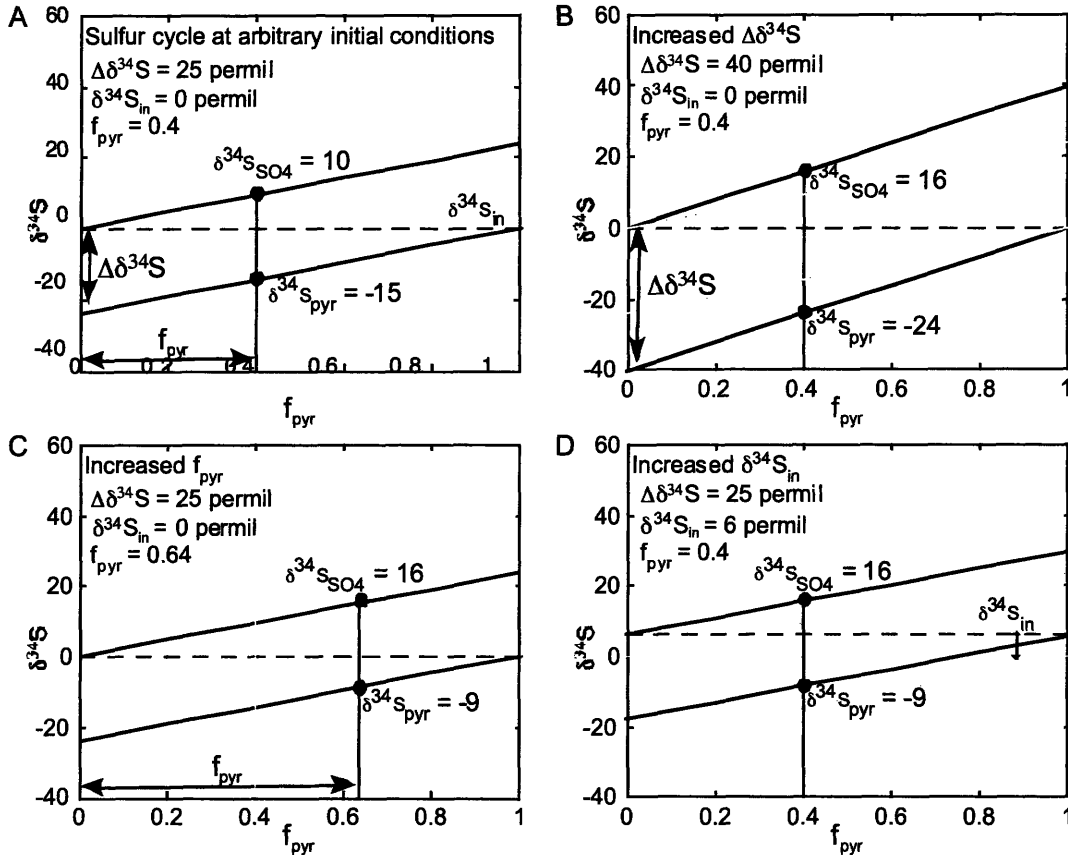
Figure 7: Three steady-state mechanisms to increase $\delta^{34}S_{SO4}$. a) Characterization of the steady-state sulfur cycle, set to arbitrary initial values (inset). $\delta^{34}S_{SO4}$ (upper line) and $\delta^{34}S_{pyr}$ (lower line) are shown to be a function of f_{pyr}, $\Delta\delta^{34}S$, and $\delta^{34}S_{in}$. b) A 15‰ increase in $\Delta\delta^{34}S$ yields a 6‰ increase in $\delta^{34}S_{SO4}$ and a 9‰ decrease in $\delta^{34}S_{pyr}$. c) An increase in f_{pyr} of 0.14 yields a 6‰ increase in both $\delta^{34}S_{SO4}$ and $\delta^{34}S_{pyr}$. d) A 6‰ increase in $\delta^{34}S_{in}$ yields a 6‰ increase in $\delta^{34}S_{SO4}$ and $\delta^{34}S_{pyr}$. Changes in b-d are specified in upper left of each graph. Initial conditions are shown in gray. Note that both (c) and (d) lead to the same change in $\delta^{34}S_{SO4}$ and $\delta^{34}S_{pyr}$.

4.2.1 Increasing $\Delta\delta^{34}S$

Throughout most of the Precambrian, $\Delta\delta^{34}S$ appears to have been dominated by bacterial sulfate reduction (BSR). BSR has typical fractionations (under non-limiting

sulfate conditions) of ~ 25‰ and an apparent maximum value of 46‰ (CANFIELD and

TESKE, 1996). In the modern, and presumably throughout much of the Phanerozoic,

however, there is an additional metabolism that plays a significant role in determining the

overall metabolic fractionation: bacterial sulfur disproportionation (BSD). BSD is a

metabolism that increases $\Delta\delta^{34}S$ through the reworking of intermediate valence (e.g., S^0,

S_2O_3, SO_3^{2-}) sulfur species. As such, fractionation in the modern can reach values as high

as 70‰, with average fractionations typically around 50‰ (CANFIELD and TESKE, 1996).

The expression of BSD is first observed in the Mesoproterozoic (JOHNSTON et al., 2005).

It appears to have become more prevalent in the later Ediacaran, just after the end of the

Shuram $\delta^{13}C_{carb}$ excursion (FIKE et al., 2006), and is widespread throughout the

Phanerozoic (CANFIELD and TESKE, 1996). As such, based on existing data, an increase

in BSD prevalence during Ara time was the most likely explanation for the increase in

$\delta^{34}S_{SO4}$ during the Ara anomaly. Since BSD is associated with more oxidizing

environments, this would be consistent with the pattern of increasing oxygenation

throughout the Ediacaran (CANFIELD et al., 2007; CANFIELD and TESKE, 1996; DES

MARAIS et al., 1992; FIKE et al., 2006). However, examination of the $\delta^{34}S_{pyr}$ record

(Figures 3c,4c) shows it tracks $\delta^{34}S_{SO4}$, increasing to ~12‰ just before the E-C boundary.

That is, with the exception of the upper Buah strata characterized by disproportionation,

$\Delta\delta^{34}S$ is essentially invariant across the Ara anomaly. Based on the data presented here,

an increase in $\Delta\delta^{34}S$ cannot be the cause of the Ara anomaly. Nor does it seem likely,

given $\delta^{34}S_{pyr}$ in contemporaneous sections (e.g., CANFIELD, 2004; CANFIELD et al., 2007;

GOLDBERG et al., 2005), that global $\Delta\delta^{34}S$ was significantly greater than that observed in

the carbonates of the Ara Group. As such, we find increased $\Delta\delta^{34}S$ to be an improbable

explanation for the Ara anomaly.   This precludes the one obviously biological explanation for the anomaly (i.e. a change in the metabolic fractionation associated with sulfur cycling).   We are left to consider the remaining two hypotheses for the Ara anomaly (increased f_{pyr} and $\delta^{34}S_{in}$), both of which likely result from changes in geological and/or geochemical parameters (e.g., weathering rates, riverine input) rather than direct metabolic effects.

4.2.2 Discriminating between f_{pyr} and $\delta^{34}S_{in}$

The synchronous enrichment (Figure 3) of $\delta^{34}S_{SO4}$ and $\delta^{34}S_{pyr}$ suggests that either f_{pyr} or $\delta^{34}S_{in}$ increased. These two scenarios could correspond to distinctly different marine redox environments because increased f_{pyr} is often an indication of a shift to more reducing conditions, while increased $\delta^{34}S_{in}$ would require no change in ocean redox (assuming constant f_{pyr}). As the Ara anomaly occurs over an interval of paleobiological significance, it is crucial to be able to differentiate between these two situations in order to correctly reconstruct the paleoenvironmental conditions during the terminal Ediacaran-earliest Cambrian.

Two thought experiments demonstrate that $\delta^{34}S_{in}$ must vary more than has been appreciated. First, consider a compilation (Figure 8) of calculated f_{pyr} as determined for each pair of $\delta^{34}S_{SO4}$-$\delta^{34}S_{pyr}$ values. Here f_{pyr} is obtained by inverting Eq[2] and assuming a constant value of $\delta^{34}S_{in}$ = 3‰ (CANFIELD, 2004). The data are divided into three stratigraphic zones: the Ara SOSB, the Lower Nafun (Masirah Bay and Khufai formations), and the Upper Nafun (Shuram and Buah formations). While the overall trend may hold some meaning (e.g., average f_{pyr} of Upper Nafun strata is lower than Lower

Nafun strata, consistent with the interpretation of more oxidizing conditions during deposition of the Upper Nafun Group (FIKE et al., 2006)), it is clear that the individual values obtained by this method (particularly for the Lower Nafun and Ara strata) are nonsensical. It is not possible for f_{pyr} to exceed unity, as that would correspond to more than 100% of the sulfur leaving the ocean be in the form of pyrite. Nor is this artificially elevated f_{pyr} the result of a few aberrant points because averaging across each of these three stratigraphic divisions does not yield significantly more reasonable values for f_{pyr} (Lower Nafun: 0.96; Upper Nafun: 0.56; Ara: 1.23). Therefore, provided that Eq[2] (i.e., quasi-static evolution) is a valid description of the sulfur cycle (discussed below), the assumption of constant $\delta^{34}S_{in}$ (~3‰) must be wrong; in particular, $\delta^{34}S_{in} \gg 3‰$ is necessary to prevent f_{pyr} from exceeding unity.
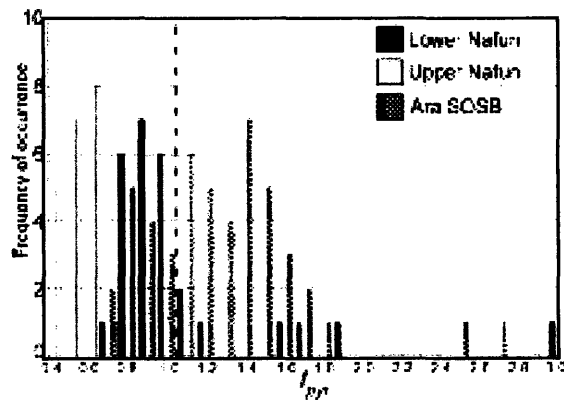
Figure 8: Histogram of f_{pyr} calculated from paired $\delta^{34}S_{SO4}$-$\delta^{34}S_{pyr}$ data assuming steady-state conditions with $\delta^{34}S_{in}$ = 3‰. Data are binned into three stratigraphic intervals: Lower Nafun; Upper Nafun; and Ara SOSB strata. One sample from the Lower Nafun (f_{pyr} = 7.8) is not shown. Vertical dashed line (f_{pyr}=1) denotes maximum possible value. Apparent higher values signify that $\delta^{34}S_{in}$ must be enriched in excess of 3‰.

Secondly, we consider the implications of isotopic mass balance on the sulfur cycle. In a steady-state system, $\delta^{34}S_{in}$ must lie between average $\delta^{34}S_{SO4}$ and average $\delta^{34}S_{pyr}$

(Figure 7, Eq[1]). From this, it is clear that for $\delta^{34}S_{in}$ = 3‰, no value of f_{pyr} is sufficient to explain the Ara anomaly. Specifically, given the average values of paired $\delta^{34}S_{SO4}$ (40‰) and $\delta^{34}S_{pyr}$ (12‰) in the Ara Group carbonates, $\delta^{34}S_{in}$ must exceed 12‰ during Ara time. Therefore, $\delta^{34}S_{in}$ > 12‰ is a necessary condition for an explanation of the Ara anomaly. This line of reasoning is useful for framing the problem, but does not allow us to constrain $\delta^{34}S_{in}$ beyond its minimum value nor to identify to what extent f_{pyr} varied. Nonetheless, this clearly demonstrates that the standard assumption of constant $\delta^{34}S_{in}$ ~3‰ (HOLSER et al., 1988) is not valid for Ediacaran-Cambrian sulfur cycling (at the minimum).

A means to explicitly calculate both f_{pyr} and $\delta^{34}S_{in}$ is therefore required to identify the mechanism responsible for the Ara anomaly. This has not been possible previously because of the lack of paired $\delta^{34}S_{SO4}$ and $\delta^{34}S_{pyr}$ datasets. However, plotting data according to Eq [2], we are able to calculate both f_{pyr} (the slope) and $\delta^{34}S_{in}$ (the y-intercept) from a dataset that contains co-occurring $\delta^{34}S_{SO4}$ and $\delta^{34}S_{pyr}$ (Figure 9; Table 1). We emphasize that paired $\delta^{34}S_{SO4}$-$\delta^{34}S_{pyr}$ data provide the first means of reconstructing $\delta^{34}S_{in}$ (or f_{pyr}) over the geologic record. The linear fit of the data in Figure 9 strongly argue that this approach has merit, at least on basin-scale. Additional paired datasets from globally distributed sections will be necessary to demonstrate that this method accurately describes the global sulfur cycle. However, based on the arguments that the paired $\delta^{34}S_{SO4}$-$\delta^{34}S_{pyr}$ data presented here are globally representative, we deem that they can be meaningfully applied to the global sulfur cycle.
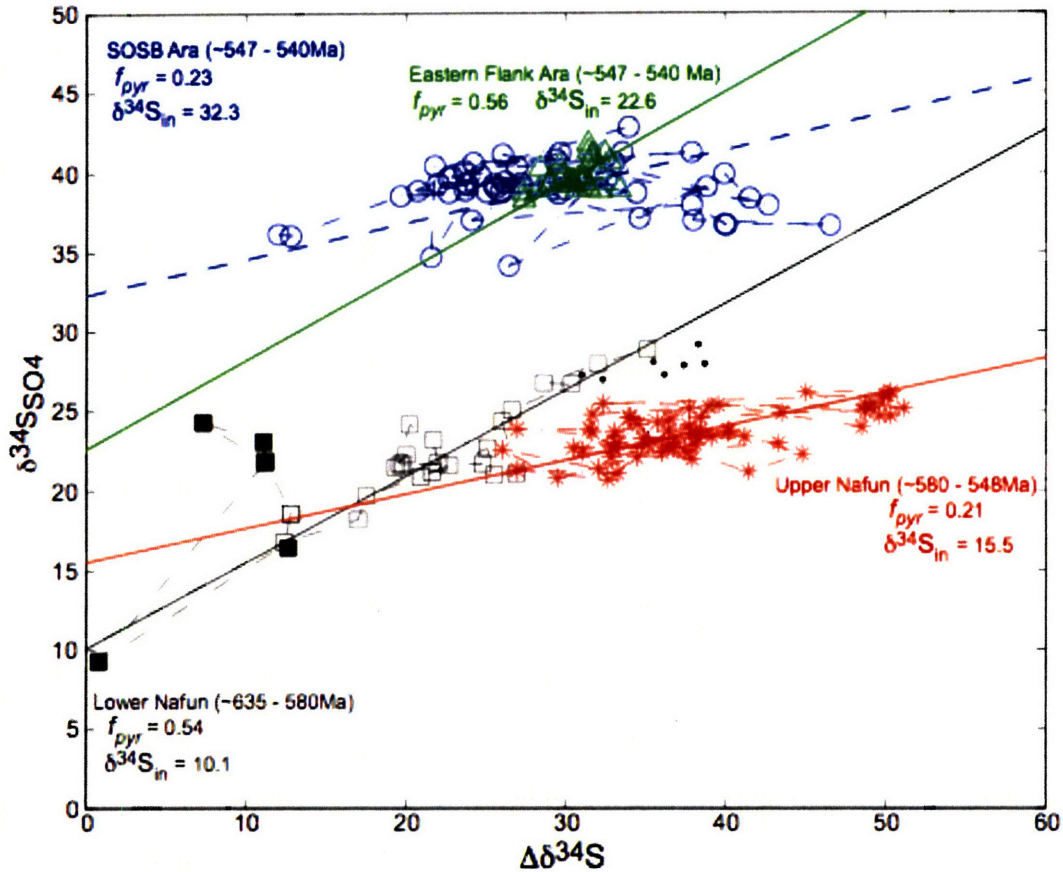
Figure 9: Composite plot of $\delta^{34}S_{SO4}$ vs. $\Delta\delta^{34}S$ for the Eastern Flank of the Ara Group (well TM6: green diamonds) as well as the underlying lower Nafun (Masirah Bay and Khufai formations) and upper Nafun (Shuram and Buah formations) Group samples in black squares and red asterisks, respectively(FIKE et al., 2006). Samples are plotted in stratigraphic order connected by lines to emphasize the stratigraphic variation (secular evolution). The slope of the solid line for each of these three data sets corresponds to f_{pyr} and the y-intercept to $\delta^{34}S_{in}$. Numbers in brackets are the 95% confidence intervals obtained from bootstrapping (n=1000). Black dots are strata at the base of the Shuram Formation (Upper Nafun Group) that are likely composed of reworked Khufai carbonates (Lower Nafun Group) and not included in the best fit line of either unit. Black squares are strata associated with the cap carbonate and immediately overlying Masirah Bay Formation that have not been included in the calculated best fit line for the lower Nafun Group strata (see discussion in text). Data from Ara SOSB strata (blue circles) are fit by a dashed line. This line does not accurately representative sulfur cycling because the slope is artificially shallow due to a sampling artefact (core vs. cuttings samples), as explained in the text and illustrated in Figure 11.

74

Table 1: Parameters for Ediacaran-Cambrian sulfur cycle, determined from Figure 9.

Unit	$\delta^{34}S_{IN}$	f_{pyr}	Note
Lower Nafun Group	10.1 [8.6, 11.3]	0.54 [0.49, 0.60]	cap carbonate strata removed
Lower Nafun Group	12.1 [10.3, 14.9]	0.49 [0.37, 0.55]	all data
Upper Nafun Group	15.5 [14.1, 16.7]	0.21 [0.18, 0.25]	all data
Ara Group (TM-6)	22.6 [17.4, 28.1]	0.56 [0.37, 0.73]	all data
Ara Group (SOSB)	32.3 [30.7, 46.4]	0.23 [-0.25, 0.28]	artificially shallow (non-steady-state) slope

Numbers in brackets are the bootstrap 95% confidence intervals (n=1000). See text for explanation of notes.

In using this formulation there are several caveats that need to be stated. First, as the meaning of the slope (f_{pyr}) and y-intercept ($\delta^{34}S_{in}$) are grounded in the formulism of Eq[1], they are only meaningful provided that the system is evolving in a quasi-static sense. A rigorous treatment of non-steady-state evolution of the sulfur cycle, along with modified expressions for f_{pyr} and $\delta^{34}S_{in}$ for various non-steady-state conditions are developed elsewhere. In order for quasi-static equilibrium to hold, the timescale for the rate of change in any sulfur cycle parameter (e.g., $\delta^{34}S_{in}$, $\Delta\delta^{34}S$, or f_{pyr}) must be much greater than the response time of the sulfur cycle (equivalent to the residence time of sulfate in the ocean). Since $\Delta\delta^{34}S$ is controlled by local controls, particularly redox and microbial ecology, it is the parameter that is expected to have the greatest rate of change. Therefore the condition for quasi-static evolution is $\tau_\Delta \gg \tau_{SO4}$, where τ_Δ is equal to $\Delta\delta^{34}S$ divided by the rate of change of $\Delta\delta^{34}S$ ($d/dt(\Delta\delta^{34}S)$) and τ_{SO4}, the residence time of sulfate in the ocean, is equal to the size of the marine sulfate reservoir (g) divided by the flux of sulfate into the ocean, J_{in} (g/yr). Modern sulfate concentrations ([SO_4^{2-}] = 28 mM) equate to a reservoir of 1.3 x 10^{21} g. Modern J_{in} is ~10^{14} g/yr, corresponding to τ_{SO4}

of ~13 Myr (BERNER, 2001). Typical Ediacaran [SO_4^{2-}] is estimated to be on the order of 5-10 mM, based on values of $\Delta\delta^{34}S$ and isotopic variability in $\delta^{34}S_{SO4}$ (FIKE et al., 2006), whereas [SO_4^{2-}] is estimated at 16-25 mM for terminal Ediacaran-earliest Cambrian strata based on analysis of fluid inclusions (BRENNAN et al., 2004). For the purposes of the following analysis, we assume [SO_4^{2-}] ~ 10 mM and that Ediacaran-Cambrian J_{in} was not significantly different from its modern value. This corresponds to τ_{SO4} ~ 4 Myr for sulfur cycling in the Ediacaran-Cambrian. With the exception of the anomalously large $\Delta\delta^{34}S$ in the upper Buah Formation, typical values of $\Delta\delta^{34}S$ are ~ 30‰ both before and during the Ara anomaly. The condition for quasi-static evolution of the sulfur cycle (i.e., Eq[2] to be valid) is then that $\Delta\delta^{34}S$ changes much slower than ~7‰/Myr. Whether this condition applies to the different intervals under consideration here will be discussed in more detail below.

4.3 Discussion of calculated values for f_{pyr} and $\delta^{34}S_{in}$

The paired $\delta^{34}S_{SO4}$-$\delta^{34}S_{pyr}$ data from the late Ediacaran-earliest Cambrian Ara Group are plotted according to Eq[2] and shown in Figure 9 (green triangles and blue circles). To evaluate the utility of this method and to provide context for the development of the Ediacaran sulfur cycle, paired $\delta^{34}S_{SO4}$-$\delta^{34}S_{pyr}$ data from the underlying Nafun Group (data from FIKE et al., 2006) are also shown in Figure 9 (black squares for the ~ 635 – 590 Ma Lower Nafun Group (Masirah Bay and Khufai formations); red asterisks for the ~ 580 – 550 Ma Upper Nafun Group (Shuram and Buah formations)). The data corresponding to the black dots are from strata at the base of the Shuram Formation that likely comprise reworked material from the lower Nafun strata. As such, they have been excluded from

the following analysis. For each section, $\delta^{34}S_{in}$ and f_{pyr} are determined by fitting a line through the reduced major axis(RAYNER, 1985) of the data and are shown in Table 1 along with the 95% confidence intervals from bootstrap runs (n=1000). The data for each stratigraphic interval in Figure 9 are connected by dashed lines in stratigraphic order. We will first address the interpretation of the Nafun Group data and then enter into a discussion of the Ara Group data.

4.3.1 The Lower Nafun Group

The plots in Figure 9 make use of secular (quasi-static) evolution of the sulfur cycle over time to determine the parameters (f_{pyr} and $\delta^{34}S_{in}$) that characterize the cycle. Therefore, it is ideal for the strata to span a time interval significantly greater than τ_{SO4} to maximize the likelihood of greater secular change and, as a result, a better fit to the data. This is the case for the lower Nafun (Masirah Bay/Khufai formations) data considered here (black squares), which were deposited over ~45 Myr, much greater than the response time of the marine sulfur cycle (τ_{SO4} ~ 7 Myr). These samples fit along a linear trend from the basal Masirah Bay Formation in the lower left to the upper Khufai Formation in the upper right, indicating the trajectory of the evolution of sulfur cycling over this interval.

We turn to examine the six filled squares to the lower left. These are the six stratigraphically lowermost points, corresponding to the Marinoan cap carbonate and immediately overlying strata. Based on the geochemical changes likely to be associated with the end of the Marinoan glaciation, including spatial variability in $\delta^{34}S_{SO4}$ (HURTGEN, 2006) and a very small sulfate reservoir, it is likely that these points do not

meet the condition for quasi-static equilibrium, although in the absence of strict geochronologic constraints it is difficult to assert that with certainty. The fit of the line through the lower Nafun Group data increases significantly when excluding these six points, suggesting they either represent non-quasi-static evolution of the sulfur cycle or an evolutionary trajectory that is significantly different from the remainder of the lower Nafun Group. Using all points, including the filled black squares, the values of f_{pyr} (0.49) and $\delta^{34}S_{in}$ (12.1‰) were obtained. These values are shifted slightly (the slope of the fitted line is steepened) by discarding the six points above the Marinoan cap: f_{pyr} = 0.54; $\delta^{34}S_{in}$ = 10.1. Because of the uncertainties associated with the immediately post-glacial strata, these latter values are used for the remainder of the discussion. The lower Nafun Group data lie along a linear trend from the lower left to upper right of Figure 9, spanning a difference in $\Delta\delta^{34}S$ of ~ 22‰ in ~30 Myr. This meets the condition for quasi-static equilibrium (Eq[4]) and we now proceed to consider the interpretation of the lower Nafun values of f_{pyr} and $\delta^{34}S_{in}$.

The lower Nafun value of f_{pyr} (~0.54) is higher than the average for Phanerozoic strata (CANFIELD, 2004). These strata are characterized by high TOC and pyrite contents(FIKE et al., 2006) as well as enrichments in redox-sensitive trace elements (e.g., uranium, rhenium, and molybdenum; Figure 10). The high value of f_{pyr} is therefore interpreted to reflect an overall reducing (e.g., anoxic to euxinic) environment. The lower Nafun value of $\delta^{34}S_{in}$ (~10‰) is significantly above both the bulk Earth value (0‰) and the modern estimate of $\delta^{34}S_{in}$ (3‰) (CANFIELD, 2004; HOLSER et al., 1988). Mechanisms to explain this will be explored below.
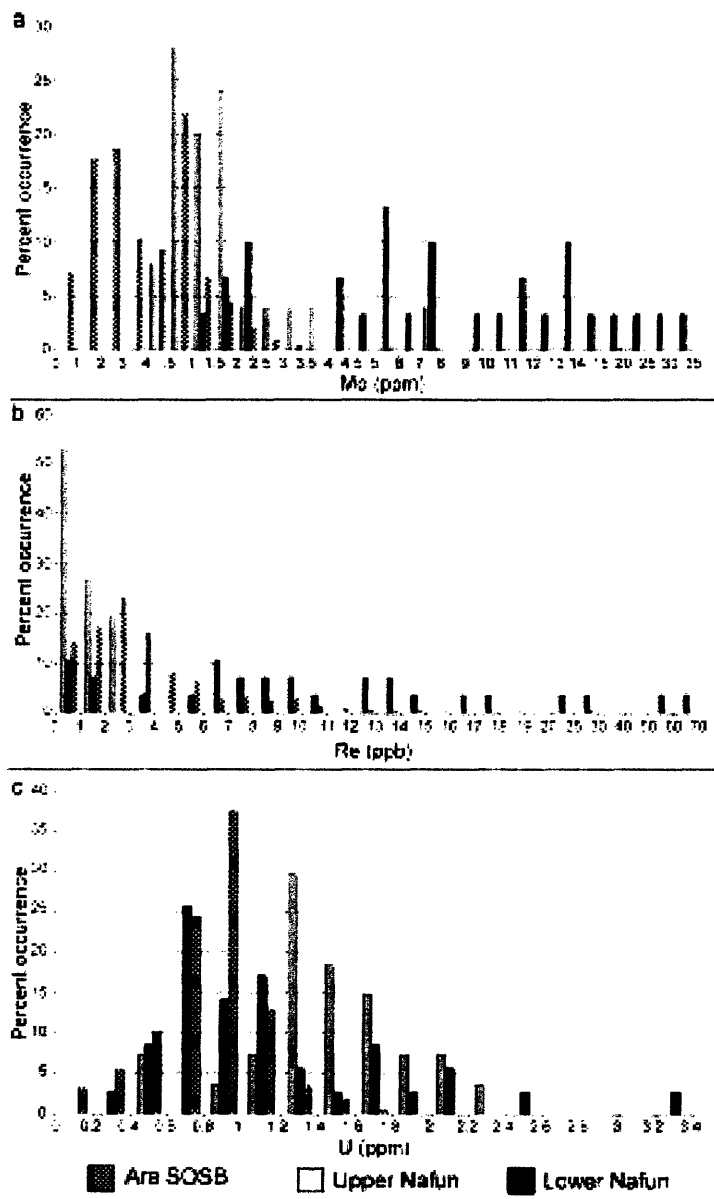
Figure 10. Redox-sensitive trace element abundance of lower and upper Nafun Group and Ara SOSB strata. a) uranium; b) rhenium; c) molybdenum. Ara Group strata cluster with the more oxidized Upper Nafun Group rather than the more reducing Lower Nafun Group.

4.3.2 The Upper Nafun Group

The data (red asterisks) from the upper Nafun Group (Shuram/Buah formations) also fit along a linear trend from the basal Shuram Formation in the lower left to the upper Buah Formation in the upper right. These strata span ~30 Myr, with variation of ~ 24‰ in $\Delta\delta^{34}S$. While there is more variability than in the lower Nafun, with the exception of a single uppermost Buah sample ($\Delta\delta^{34}S = 31‰$, $\delta^{34}S_{SO4} = 25‰$), it is not likely that any of the upper Nafun data violate the condition of quasi-static evolution of the sulfur cycle. The calculated sulfur cycling parameters obtained for the upper Nafun are: $f_{pyr} = 0.21$; $\delta^{34}S_{in} = 15.5‰$. To check whether the slope was dominated by the uppermost Buah Formation strata with high $\Delta\delta^{34}S$ (indicating microbial sulfur disproportionation (FIKE et al., 2006)), we fit the upper Nafun strata without these samples. The results of this segregated fit are not significantly different ($f_{pyr} = 0.29$; $\delta^{34}S_{in} = 12.9‰$), so the grouped values will be used throughout the remainder of the discussion. It is not possible given the limited stratigraphic thickness of the Upper Buah Formation (and therefore limited opportunity for quasi-static evolution to express itself) to make a robust fit of the data just from the Upper Buah. A comparison of upper Nafun strata with and without the upper Buah data does suggest, however, that the upper Buah Formation may have a lower f_{pyr} than the rest of the upper Nafun Group, consistent with the presence of BSD and a higher $\delta^{34}S_{in}$, suggesting a trend toward increasing $\delta^{34}S_{in}$ in younger strata.

The upper Nafun value of f_{pyr} (0.21) is significantly lower than that found in the lower Nafun strata. We interpret this decrease in f_{pyr} to correspond to more oxidizing conditions, consistent with a drop in TOC and pyrite contents (FIKE et al., 2006) as well as in trace element enrichments (Figure 10), relative lower Nafun Group strata.

Additionally, the Upper Nafun strata comprise the interval of the Shuram $\delta^{13}C_{carb}$ excursion, which has been interpreted to record oxidation of the deep ocean (FIKE et al., 2006). A similar transition to more oxidizing conditions is found in the strata of Newfoundland around ~580 Ma (CANFIELD et al., 2007). In the upper Nafun, $\delta^{34}S_{in}$ (~15.5‰) is significantly enriched relative to both the bulk Earth value (0‰) and the value (~10‰) found in the lower Nafun.

4.3.3 The Ara Group (Eastern Flank)

The data from the non-evaporitic Eastern Flank Ara Group strata are plotted in Figure 9 as green triangles. These samples span a limited phase-space in Figure 9, making the fit through them less robust than either the upper or lower Nafun Group strata. Unlike the Nafun Group strata which were deposited over tens of millions of years, the Eastern Flank Ara Group strata were likely deposited over ~7 Myr. This (relatively) short time precludes more extensive secular evolution of seawater $\delta^{34}S_{SO4}$ (a greater range in Figure 9) that could be observed on longer time scales. These samples span a variation of ~6‰ in $\Delta\delta^{34}S$ over the ~7 Myr and exhibit a trend toward increasing $\Delta\delta^{34}S$ in younger strata. As such, it is not likely that any of the Eastern Flank Ara samples violate the condition of quasi-static evolution of the sulfur cycle. However, because of the limited $\delta^{34}S_{SO4}$ variation present in the Eastern Flank strata, the fit of the data is not as well-constrained as the Nafun Group strata (Table 1). The calculated sulfur cycling parameters obtained for the Eastern Flank of the Ara Group are: $f_{pyr} = 0.56$; $\delta^{34}S_{in} = 22.6‰$. This Ara Group value for f_{pyr} (0.56) is significantly higher than that found in the upper Nafun strata and comparable to the value for the lower Nafun Group. A return

to more reducing conditions is supported by increased pyrite and TOC contents in these Ara Group strata. However, increased primary production(ARTHUR and SAGEMAN, 1994) also results in increased pyrite/TOC. There is no evidence for an increase in the abundance of redox-sensitive trace elements (Figure 10). Therefore, there is insufficient evidence to argue for a return to more reducing conditions and we seek another explanation (see discussion below). The trend toward increasing $\delta^{34}S_{in}$ continues in the Ara strata, where $\delta^{34}S_{in}$ (22.6‰) is enriched beyond the values in the Nafun Group (10-15‰).

4.3.4 The Ara Group (SOSB)

The data (blue circles) from the Ara Group strata within the SOSB plot on top of the position from the Ara Group strata from the Eastern Flank (Figure 9). This emphasizes the reproducibility of both $\delta^{34}S_{SO4}$ and $\delta^{34}S_{pyr}$ across the basin. However, there is significantly more variability in $\Delta\delta^{34}S$ in the Ara SOSB strata relative to the Ara Eastern Flank strata. The resulting fit for the SOSB Ara data (dashed line) is significantly shallower than the Ara Eastern Flank strata (Figure 9). Examining the SOSB Ara data, it appears that f_{pyr} changes very little in the transition from the upper Nafun (0.21) to the Ara Group (0.23). However, the transition to Ara deposition in the SOSB is marked by a drastic increase in $\delta^{34}S_{in}$ to 33.3‰. This stands in marked contrast to the values obtained from the Eastern Flank strata. Taking this at face value suggests that, despite similarities in $\delta^{34}S$, there are extreme spatial gradients in the delivery of sulfur to and burial of sulfur within the basin. However, before interpreting these values (and the significant differences between Ara SOSB and Eastern Flank strata), we need to examine whether

the Ara SOSB samples meet the criterion for quasi-static evolution of the sulfur cycle. We first examine the A4 carbonate from BB4, a ~50 m thick carbonate unit believed to have been deposited in ~ 1 Myr (BOWRING et al., 2007). Here we observe repeated variation in $\Delta\delta^{34}$S of ~6‰ in less than 5 meters. Assuming a constant sedimentation rate in the A4, this variability in $\Delta\delta^{34}$S corresponds to a rate of change in $\Delta\delta^{34}$S > 60‰/Myr. Even if we have underestimated the deposition rate of the A4 by an order of magnitude, these fluctuations would still violate the condition of quasi-static equilibrium. Therefore, it is clear that our sampling of the SOSB Ara strata does not record a quasi-statically evolving sulfur cycle. This calls into question what is different about the Ara SOSB samples relative to the other samples examined in this study. The samples for the Nafun Group and the Ara Eastern Flank strata were drill cuttings. The samples of cuttings, collected every 2-5 meters, include chips from all strata encountered within the drilled 2-5 meter-thick intervals. Because multiple chips are required to generate enough mass for analysis, high-frequency variability is averaged out. As such, the cuttings samples therefore provide stratigraphically averaged values for geochemical (and lithologic) records, such as δ^{34}S$_{SO4}$ and δ^{34}S$_{pyr}$. On the other hand, most of the SOSB Ara samples are from drill cores and correspond to ~2 cm of stratigraphy. Clearly, the core samples are characterizing a much smaller stratigraphic window than the cuttings samples and there is no spatial averaging to remove high-frequency variability.

δ^{34}S$_{pyr}$ is known to be spatially variable; in fact this variation is considered one of the hallmarks of biogenic pyrite formation(CANFIELD, 2001). Such variation is likely dependent on local spatial and temporal variability in conditions relative to pyrite formation (e.g., sulfate, iron, or organic substrate availability). Typical facies in the Ara

include rhythmites, microbial laminites, and crinkly laminites (Figure 9). These facies are likely to have been subject to cyclical (e.g., seasonal, annual, or decadal) environmental variability. As such, it is not surprising that the $\delta^{34}S_{pyr}$ record from these samples seems to record oscillatory variability. Such high-frequency oscillations are averaged over the stratigraphic window sampled by the cuttings, allowing (lower-amplitude) secular variation to be distinguished.

Indeed, averaging the data from the Ara SOSB core samples over a several meter window decreases the variability in $\Delta\delta^{34}S$ to values comparable to that obtained from other sections. However, in doing so, the limited number of samples remaining precludes a meaningful fit of the data. Based on the comparison of core vs. cuttings, there are short-term high-amplitude oscillations in $\delta^{34}S_{pyr}$ that dominate the $\Delta\delta^{34}S$ signal for core samples; whereas these oscillations are averaged in the cuttings samples to reveal a longer-term smaller-amplitude secular change in $\Delta\delta^{34}S$. In terms of paleoenvironmental reconstruction, it is this latter signal, averaged over m-scale intervals of stratigraphy, that is the most meaningful in terms of characterizing secular changes in biogeochemical cycling. This suggests that samples of cuttings may be ideal for future investigations that aim to reconstruct (low-amplitude) secular changes in biogeochemical cycling.

The difference in sample (core vs. cuttings) provides a clear explanation of why the SOSB Ara data are characterized by highly variably $\Delta\delta^{34}S$ (relative to the other samples). Now, we proceed to understand how the fit of the SOSB Ara data in Figure 9 is altered by these rapid variations in $\Delta\delta^{34}S$. This is illustrated simply in Figure 11 and described in the following text.

Consider an initial equilibrium position characterized by $\delta^{34}S_{SO4}(t_0)$ and $\Delta\delta^{34}S_{SO4}(t_0)$.

We consider the $\delta^{34}S_{SO4}$ response to an instantaneous increase in $\Delta\delta^{34}S$ (e.g., as the result of shifting microbial communities). Consider a change in $\Delta\delta^{34}S$ by a set amount X (‰), while f_{pyr} and $\delta^{34}S_{in}$ are held constant. The $\Delta\delta^{34}S$ value will immediately jump to its new expected value: $\Delta\delta^{34}S(t_1) = \Delta\delta^{34}S(t_0) + X$. However, $\delta^{34}S_{SO4}$ only asymptotically approaches its new equilibrium values: $\delta^{34}S_{SO4}(t\rightarrow\infty) = \delta^{34}S_{SO4}(t_0) + X*f_{pyr}$. The rate at which $\delta^{34}S_{SO4}$ changes is given by $X*f_{pyr}*(e^{-t/\tau SO4})/\tau_{SO4}$ in ‰/Myr, such that after a given time t, $\delta^{34}S_{SO4}$ will have moved a fraction $X*f_{pyr}*(e^{-t/\tau SO4})$ of its way toward the new equilibrium position. However, if $\Delta\delta^{34}S$ varies at a sufficiently fast rate (as it does in the Ara SOSB strata), then $\Delta\delta^{34}S$ will have changed to a new value before $\delta^{34}S_{SO4}$ reached its equilibrium position. In this manner, for variations in $\Delta\delta^{34}S$ that exceed the condition of quasi-static equilibrium, $\delta^{34}S_{SO4}$ approaches its new equilibrium position more slowly than that equilibrium position varies (as set by the rate of change of $\Delta\delta^{34}S$).
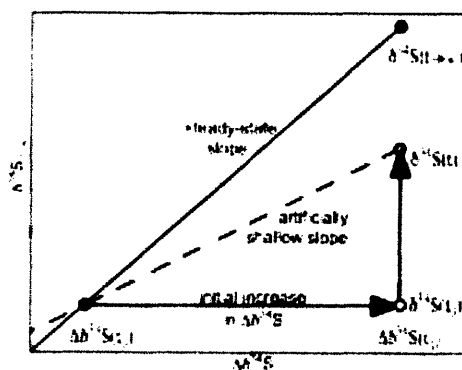
Figure 11. Artificial shallowing in $\delta^{34}S$ vs. $\Delta\delta^{34}S$ due to variation in $\Delta\delta^{34}S$ that occurs faster than the response time of $\delta^{34}S$.

It is important to note that in such a case, there will still be a correlation between $\delta^{34}S_{SO4}$ and $\Delta\delta^{34}S$ (as observed in the Ara SOSB strata). However the slope of that correlation will be artificially shallow (Figure 11), providing both an over-estimate of $\delta^{34}S_{in}$ and an underestimate of f_{pyr}. Thus, the variability in $\Delta\delta^{34}S$ from core samples resulted in an artificially flat fit of the SOSB data relative to the Eastern Flank strata. The artificially shallow slope of the Ara SOSB data can be corrected by requiring the fitted line to pass through the y-intercept ($\delta^{34}S_{in}$ ~22.6‰) obtained for the Ara Eastern Flank data. A completely independent correction (not requiring a "known" $\delta^{34}S_{in}$) can be determined rigorously, provided that the frequency of oscillation in $\Delta\delta^{34}S$ is known. However, the uncertainty in the observed frequency of $\Delta\delta^{34}S$ variation in the Ara SOSB does not make this a useful exercise for this particular data set. The corrected fit has a slope of $f_{pyr} = 0.54$, in agreement with the Ara Eastern Flank value of $f_{pyr} = 0.56$.

5. DISCUSSION

We have presented a novel method based upon paired $\delta^{34}S_{SO4}$-$\delta^{34}S_{pyr}$ data that allows one to calculate f_{pyr} and $\delta^{34}S_{in}$ (Figure 9) for systems behaving quasi-statically, as in the case of the upper and lower Nafun Group and Eastern Flank Ara strata. It appears that by early Ediacaran time $\delta^{34}S_{in}$ (~10‰) was enriched significantly above modern values and became progressively more enriched (~23‰) by the E-C boundary. We observed a decrease in f_{pyr} in the mid-Ediacaran, consistent with increasing oxidation ca. 580 Ma. This is followed by an increase in f_{pyr} associated with the onset of the Ara anomaly. Detailed discussions of these trends in $\delta^{34}S_{in}$ and f_{pyr} follow.

5.1 Enriched $\delta^{34}S_{in}$

The calculated values of $\delta^{34}S_{in}$ for all strata examined here are significantly above both the bulk Earth value (0‰) and the estimate of $\delta^{34}S_{in}$ (~3‰) in the modern (CANFIELD, 2004; HOLSER et al., 1988). The finding of elevated Ediacaran-early Cambrian $\delta^{34}S_{in}$ is in agreement with Canfield (2004), who argued for elevated $\delta^{34}S_{in}$ (>3‰) across the Neoproterozoic based on widespread pyrite enrichment ($\delta^{34}S_{pyr} \gg 0$) over this interval.

We now examine three plausible ways to generate $\delta^{34}S_{in}$ enriched relative to bulk Earth values. The first mechanism for increased $\delta^{34}S_{in}$ relies on a prolonged period of ocean euxinia (CANFIELD, 2004), which is thought to have been prevalent for much of the Proterozoic (ANBAR and KNOLL, 2002; CANFIELD, 1998; POULTON et al., 2004). Under euxinic conditions, water column pyrite formation is frequent (WILKIN et al., 1997; WILKIN et al., 1996) and predominantly distributed over the abyssal ocean, rather than the continental shelf, where most pyrite forms in an oxic ocean. Subduction of this abyssal pyrite, depleted in ^{34}S relative to mantle values (~0‰), will result in an increase in the average isotope composition of the crustal sulfur reservoir (marine and sedimentary sulfates and sulfides, as well as igneous sulfur). Model results of prolonged pyrite subduction over the Proterozoic (CANFIELD, 2004) have yielded $\delta^{34}S_{crust}$ values up to ~70‰ prior to the oxidation of the deep ocean. While $\delta^{34}S_{in}$ is a combination of weathering inputs (related to $\delta^{34}S_{crust}$) and mantle inputs (hydrothermal + volcanic), the weathering flux is the dominant component, comprising up to ~ 90% of total sulfur delivered to the (modern) ocean (CANFIELD, 2004; WALKER, 1986). Therefore, an

increase in $\delta^{34}S_{crust}$ should correspond to increased $\delta^{34}S_{in}$. The rate of change in $\delta^{34}S_{in}$ observed in the Huqf strata presented here (~13‰ over 95 Myr) falls within the rates of change in $\delta^{34}S_{in}$ predicted by models of crustal evolution resulting from pyrite subduction (CANFIELD, 2004).

However, this model requires continued widespread subduction of abundant seafloor pyrite, and therefore euxinic conditions, to generate increasing $\delta^{34}S_{in}$. Once the deep ocean has been oxygenated, $\delta^{34}S_{in}$ will gradually return to bulk Earth values (0‰) (CANFIELD, 2004). Prolonged widespread euxinia is not easily reconciled with the relatively oxidized (CANFIELD et al., 2007; FIKE et al., 2006; SCOTT et al., 2006) conditions of the late Ediacaran (~580 – 550 Ma). Without a euxinic deep ocean, pyrite precipitation is restricted to occur only during sediment diagenesis or in restricted basins (e.g., the modern Black Sea). Given their occurrence today (at modern pO_2), it is likely there were some restricted euxinic basins during ~580 – 550 Ma, although the evidence for increasing oxidation over this interval suggests that their importance was likely minimal. Therefore, while this mechanism may explain the elevated $\delta^{34}S_{in}$ (~10‰) prior to deep ocean oxygenation at ca. 580 Myr, it does not seem to explain the continued rise in $\delta^{34}S_{in}$ across the later Ediacaran. As such, we seek another means to generate enriched $\delta^{34}S_{in}$.

A second mechanism to generate elevated $\delta^{34}S_{in}$ can be found by considering the effects of pO_2 on the weathering of sulfur minerals. Under steady-state sulfur cycling, the weighted isotope composition of sulfur minerals (sulfates + sulfides) in newly formed marine sediments will equal $\delta^{34}S_{in}$. However, while the weathering of sulfates is independent of pO_2, the weathering rate of sulfides (predominantly pyrite) is believed to

depend on pO_2. Laboratory studies of pyrite oxidation (JERZ and RIMSTIDT, 2004) suggest the rate of pyrite oxidation is proportional to the square root of pO_2. Other factors (e.g., exhumation rate, humity, acidity, etc.) also strongly effect the rate of pyrite oxidation (JERZ and RIMSTIDT, 2004; MORTH and SMITH, 1966), although it is beyond the scope of the current study to attempt to constrain how these would affect Ediacaran pyrite oxidation. Recent modeling indicates that pO_2-dependent sulfide weathering is necessary to generate the observed $\delta^{13}C$-$\delta^{34}S$ isotope trends over the Phanerozoic (BERGMAN et al., 2004). In a pO_2-dependent sulfide weathering regime, the riverine flux draining a given set of sedimentary rocks will have an isotope composition inversely proportional to pO_2. That is, the lower pO_2, the slower ^{34}S-depleted sulfides will weather relative to ^{34}S-enriched sulfates, and the higher $\delta^{34}S_{in}$ will be. Therefore, relative to the modern, a preferential weathering of sulfates relative to sulfides, and therefore continued enrichment in $\delta^{34}S_{in}$, would continue as long as pO_2 was significantly below present atmospheric levels (PAL). Given that Ediacaran pO_2 was most likely ~15-20% PAL (BERKNER and MARSHALL, 1965; CANFIELD et al., 2007; CANFIELD and TESKE, 1996), preferential weathering of sulfates relative to sulfides is a plausible explanation for the observed increase in $\delta^{34}S_{in}$, particularly for the Upper Nafun strata believed to have been deposited during a period of deep ocean oxygenation (and hence limited oceanic pyrite subduction).

A final possibility to generate enriched $\delta^{34}S_{in}$ involves the preferential weathering of $\delta^{34}S$-enriched (both $\delta^{34}S_{SO4}$ and $\delta^{34}S_{pyr}$) Ediacaran strata. This 'rapid recycling' hypothesis (BERNER, 2006) reflects the observation that young sedimentary rocks are subject to very rapid weathering relative to older strata. Estimates of weathering sources

at the time of the E-C boundary suggest that both the sulfate and pyrite weathering pools are dominated by young, δ^{34}S-enriched strata (BERNER, 2006). In addition, the late Ediacaran was an interval of low global sea level leading up to the Early Cambrian Sauk transgression (MATTHEWS and COWIE, 1979). This may have resulted in an additional enrichment in δ^{34}S$_{in}$ because of preferential exposure and weathering of Ediacaran sediments known to contain both relatively ^{34}S-enriched sulfates and pyrites (CANFIELD, 2004; CANFIELD et al., 2007; FIKE et al., 2006; GOLDBERG et al., 2005; HURTGEN, 2006; HURTGEN et al., 2005; SHIELDS et al., 1999; STRAUSS, 1993). Furthermore, because the δ^{34}S-enriched Ediacaran strata tend to also be enriched in ^{87}Sr/^{86}Sr (Figure 12), the rapid recycling of Ediacaran strata may well explain part of the covariation between predicted δ^{34}S$_{in}$ and the ^{87}Sr/^{86}Sr record (BURNS et al., 1994; HALVERSON et al., 2007; VEIZER et al., 1999).

Our data indicate that δ^{34}S$_{in}$ is already 10‰ at the base of the Ediacaran. However, there are no datasets of paired δ^{34}S$_{SO4}$-δ^{34}S$_{pyr}$ prior to the Ediacaran that can accurately constrain when δ^{34}S$_{in}$ began to increase from bulk Earth values. However, some predictions can be made. The methods for enriching δ^{34}S$_{in}$ discussed above require an isotopic offset between sulfate and sulfide sedimentary minerals (with sulfates enriched in ^{34}S relative to pyrites). As such, the efficacy of these mechanisms depends on the fractionation during sulfate reduction ($\Delta\delta^{34}$S). Thus, without an isotopic offset between sulfates and sulfides, there would be no effect on δ^{34}S$_{in}$.
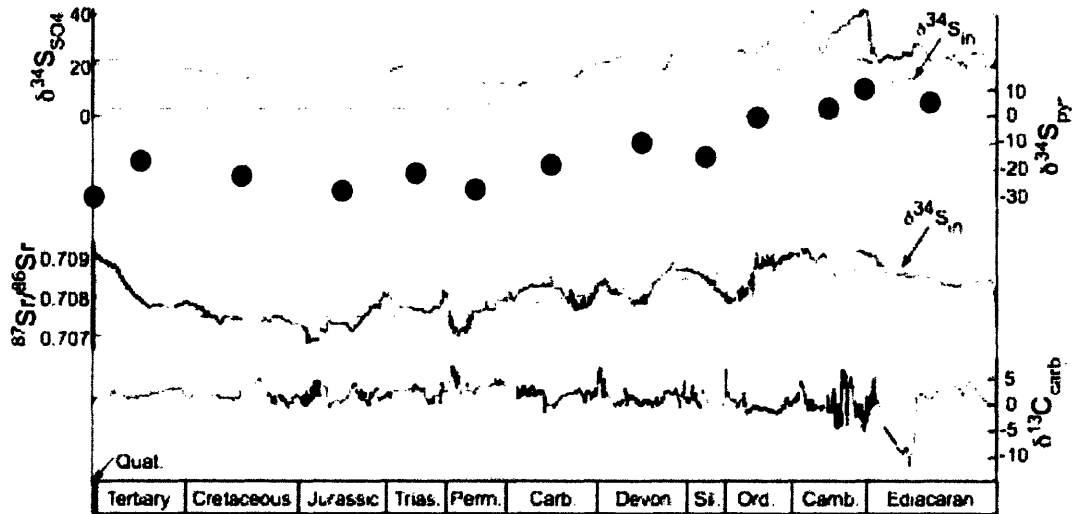
Figure 12. Composite chart of Ediacaran-Phanerozoic chemostratigraphy. a) Smoothed average of $\delta^{34}S_{SO4}$ plotting alongside proposed $\delta^{34}S_{in}$ presented here. $\delta^{34}S_{SO4}$ data are from the literature (see Figure 1) and the present study and are shown as a 5-point running average. $\delta^{34}S_{pyr}$ are from the literature (CANFIELD, 2004; CANFIELD et al., 2007) and the present study. The dashed line shows our inferred decay of $\delta^{34}S_{in}$ over the Paleozoic. b) $^{87}Sr/^{86}Sr$ data are from the literature (BURNS et al., 1994; VEIZER et al., 1999), shown with a 3-point and 10-point running average for the Ediacaran and Phanerozoic, respectively. Projected $\delta^{34}S_{in}$ (as in (a)) is overlain to highlight the similarity between it and $^{87}Sr/^{86}Sr$ over the Ediacaran-Paleozoic. c) $\delta^{13}C_{carb}$ is shown to highlight that the Ediacaran-Paleozoic enrichment in $\delta^{34}S$ is uncoupled to the carbon cycle. Data are from the literature (AMTHOR et al., 2003; FIKE et al., 2006; MALOOF et al., 2005; SALTZMAN, 2005; VEIZER et al., 1999) and the current study, averaged over a 10-point window. Age ranges have been updated to the most recent geochronological constraints where possible.

Sulfate concentrations were low throughout early Earth history and therefore unlikely to generate significant $\Delta\delta^{34}S$ (CANFIELD, 2001; HABICHT et al., 2002). It was not until the Mesoproterozoic (KAH et al., 2004; SHEN et al., 2002) that sulfate concentrations rose to high enough levels (> ~200μM) to generate $\Delta\delta^{34}S>>0$. Thus, an increase $\delta^{34}S_{in}$ would only become possible during and after the Mesoproterozoic. Indeed, time-averaged compilations (CANFIELD, 2004) record a parallel rise in $\delta^{34}S_{SO4}$ and $\delta^{34}S_{pyr}$ from approximately 1.5 – 0.54 Gyr. Given the general trend toward more oxidizing conditions in the Mesoproterozoic (JOHNSTON et al., 2005), this is most

consistent with increased $\delta^{34}S_{in}$ over this interval, although increased pyrite burial cannot be ruled out (*cf.* Figure 7). However, in the absence of paired $\delta^{34}S_{SO4}$-$\delta^{34}S_{pyr}$, this argument cannot be tested directly.

We turn to other geochemical proxies, in particular $^{87}Sr/^{86}Sr$, to attempt to constrain the rise in $\delta^{34}S_{in}$. We note that calculated rise in $\delta^{34}S_{in}$ (and not the $\delta^{34}S_{SO4}$ record) presented here parallels the increase in $^{87}Sr/^{86}Sr$ observed in the Ediacaran (BURNS et al., 1994; HALVERSON et al., 2007), supporting a weathering control on $\delta^{34}S_{in}$. Based on this, we propose that the increase in $\delta^{34}S_{in}$ from bulk earth values (~0‰) to the values we see in the basal Ediacaran (~10‰) occurred in association with a parallel rise in $^{87}Sr/^{86}Sr$ seen in the earlier Neoproterozoic (HALVERSON et al., 2007). Paired $\delta^{34}S_{SO4}$-$\delta^{34}S_{pyr}$ datasets in intervals spanning Mesoproterozoic – Cryogenean strata will be able to constrain the timing of the rise in $\delta^{34}S_{in}$. These datasets will also be able to discern if $\delta^{34}S_{in}$ increases primarily during periods of ocean anoxia (CANFIELD, 2004) or whether variations in $\delta^{34}S_{in}$ are related to changes in the weathering flux via its correlation to $^{87}Sr/^{86}Sr$.

In summary, our preferred explanation for the enriched $\delta^{34}S_{in}$ observed in the Huqf strata of Oman, particularly during the more oxidizing Upper Nafun Group strata, is not the subduction of pyriferous sediments deposited during widespread ocean euxinia (CANFIELD, 2004), but the preferential weathering (rapid recycling) of $\delta^{34}S$-enriched Ediacaran strata, in particular of ^{34}S-enriched sulfates relative to less enriched sulfides under sub-modern pO_2, possibly enhanced by late-Ediacaran global sea level lowstand. This scenario is deemed more likely based on the continued increase in $\delta^{34}S_{in}$ observed during oxidizing conditions represented by the upper Nafun Group, rather than an

observed increase associated solely with strata (e.g., the Lower Nafun) deposited during more reducing times. However, pyrite subduction remains a viable mechanism to enrich $\delta^{34}S_{in}$ to ~10‰ prior to ocean oxidation at ~ 580 Ma.

We now consider the implications of elevated $\delta^{34}S_{in}$ for the Phanerozoic. $\delta^{34}S_{in}$ is predicted to increase following the Ediacaran until pO_2 rose to near PAL. Thenceforth, the balanced weathering of sulfates and sulfides would cause $\delta^{34}S_{in}$ to drift down toward bulk Earth values (~0‰). Although the Cambrian Period currently suffers from a low-resolution $\delta^{34}S_{SO4}$ record, available data indicates that $\delta^{34}S_{SO4}$ remains enriched throughout the Cambrian (HOUGH et al., 2006; KAMPSCHULTE and STRAUSS, 2004). This is consistent with a further increase in $\delta^{34}S_{in}$ over Cambrian time while pO_2 was still at sub-modern levels(HOUGH et al., 2006). From the Ordovician through the Permian, there is a nearly linear decrease in $\delta^{34}S_{SO4}$ from ~40‰ to ~10‰ (KAMPSCHULTE and STRAUSS, 2004; STRAUSS, 1997). This trend dominates the Paleozoic $\delta^{34}S_{SO4}$ curve (Figure 12). A parallel decrease in average $\delta^{34}S_{pyr}$ from ~0‰ to -30‰ occurs over the same interval(CANFIELD, 2004). The traditional interpretation of this dramatic decline has been a redox exchange between the biological carbon and sulfur cycles that maintains pO_2 at constant levels (BERNER, 2006; GARRELS and LERMAN, 1981; VEIZER et al., 1980). In this interpretation, (assuming a constant $\delta^{34}S_{in}$ at modern values (~3‰)), the decrease in $\delta^{34}S_{SO4}$ is driven by a decrease in f_{pyr} from 0.93 to 0.17. There is indeed evidence for a general decrease in f_{pyr} (see below) over the Paleozoic (ARTHUR and SAGEMAN, 1994; BERRY and WILDE, 1978; ULMISHEK and KLEMME, 1990; WILDE, 1987); however, we deem both an early Paleozoic f_{pyr} of near unity and such a drastic decrease in f_{pyr} (by 81%) over the Paleozoic to be implausible and unsupported by the rock record.

Based on the evidence presented here for elevated $\delta^{34}S_{in}$ (~23‰) at the E-C boundary, we propose that $\delta^{34}S_{in}$ decays back to near modern values (~3‰) over the Paleozoic decline in $\delta^{34}S_{SO4}/\delta^{34}S_{pyr}$. Reinterpreting the existing compilations of Cambrian data (CANFIELD, 2004; KAMPSCHULTE and STRAUSS, 2004) under the assumption of $\delta^{34}S_{in}$ ~ 22‰ results in an early Paleozoic f_{pyr} ~0.50. This agrees well with the calculated value (f_{pyr}=0.56) obtained from the Eastern Flank strata of the Ara Group (Figure 9). Allowing $\delta^{34}S_{in}$ to decay from ~22% to ~3‰ over the Paleozoic corresponds to a decrease in f_{pyr} over this interval from 0.50 to 0.17. This is still a considerable drop in f_{pyr}, however, it is in better agreement with estimates of decreased marine black shale deposition (ULMISHEK and KLEMME, 1990) over this period (from ~42% to ~21% of sediment deposition). Allowing $\delta^{34}S_{in}$ to decrease from ~23‰ to ~3‰, apportions the driving mechanism for the decrease in Paleozoic $\delta^{34}S$ primarily to decreased $\delta^{34}S_{in}$ (20‰), with decreased f_{pyr} also having a significant contribution (10‰). That a decrease in $\delta^{34}S_{in}$ and f_{pyr} should occur together is not surprising. Atmospheric oxygen levels are believed to be inversely proportional to f_{pyr} (BERGMAN et al., 2004). pO_2-dependent sulfide weathering also predicts $\delta^{34}S_{in}$ to decrease with rising pO_2. Evidence for a weathering-induced decrease in $\delta^{34}S_{in}$ over the Paleozoic is supported by the observed correlation between Paleozoic $\delta^{34}S_{SO4}$ and $^{87}Sr/^{86}Sr$ (SHIELDS and VEIZER, 2002; VEIZER et al., 1999). It is clear that high-resolution studies of Paleozoic paired $\delta^{34}S_{SO4}$-$\delta^{34}S_{pyr}$ will be needed to resolve Paleozoic $\delta^{34}S_{in}$ and the role it played in the observed decrease in $\delta^{34}S_{SO4}/\delta^{34}S_{pyr}$. Continued correlation of reconstructed $\delta^{34}S_{in}$ with $^{87}Sr/^{86}Sr$ as in the Ediacaran (discussed above) will implicate a weathering control, either in the form of

rapid recycling of Ediacaran strata enriched in $\delta^{34}S_{SO4}/\delta^{34}S_{pyr}$, or pO_2-dependent sulfide weathering as the cause of $\delta^{34}S_{in}$ variability.

5.2 Enhanced f_{pyr} leading up to the E-C boundary

We seek to place the observed increase in f_{pyr} (~0.56) that occurs over the interval of the Ediacaran-Cambrian boundary in the context of the Ediacaran oxidation leading up the period of Ara Group deposition, as well as in the context of environmental change throughout the Paleozoic. The observed decrease in f_{pyr} between the lower and upper Nafun Group strata is consistent with other evidence for mid-Ediacaran oxidation, and likely spurred the evolution of Ediacaran fauna (CANFIELD et al., 2007; FIKE et al., 2006; KAUFMAN et al., 2007; SCOTT et al., 2006). The Shuram $\delta^{13}C_{carb}$ excursion(BURNS and MATTER, 1993; LE GUERROUE et al., 2006a) in the Upper Nafun strata is interpreted to record the oxidation of a large pool of dissolved organic carbon from the deep ocean (FIKE et al., 2006). Alternatively, development of the Ediacaran fauna(SPERLING and PETERSON, 2007) may have led to overall more oxidizing conditions as organisms filtered this proposed abundant marine DOC out of the water column.

Given the evidence for ~ 580 Myr Ediacaran oxidation, how do we reconcile the apparent increase in f_{pyr} in the latest Ediacaran-earliest Cambrian? The value of f_{pyr} is controlled by many factors, including: pO_2, sedimentation rate, ocean circulation, nutrient availability, global temperature, and the availability of sulfate, iron, and organic carbon substrates (ARTHUR and SAGEMAN, 1994; BERNER, 1984; BERNER and RAISWELL, 1983; RAISWELL and BERNER, 1986). These factors group broadly into two factors, those associated with production and those associated with preservation (ARTHUR and

SAGEMAN, 1994). Preservation is affected by the sedimentation rate and redox state of the sediment-water interface, itself dependent on, among others, pO_2, ocean circulation, and global temperature. Production is affected primarily by nutrient and substrate availability.

We examine first the possibility of enhanced preservation to explain the increased f_{pyr} observed in the Ara Group strata. There are two primary factors that result in enhanced preservation of pyrite: increased sedimentation rate and water-column anoxia. The control that sedimentation rate has on preservation appears to arise because increased sedimentation rate partitions sediments from the overlying pool of oxidants, minimizing remineralizaton and/or re-oxidation (ARTHUR and SAGEMAN, 1994). There is evidence for increased sedimentation rates over the Ediacaran – early Paleozoic interval associated with the assembly of Gondwanaland, particularly based on the volume of quartzite sediments accumulating at this time (SQUIRE et al., 2006). However, a direct measure of sedimentation rate is elusive. The record of $^{87}Sr/^{86}Sr$ is generally believed to reflect weathering processes and therefore can serve as a proxy for sedimentation rate. The pronounced peak in $^{87}Sr/^{86}Sr$ across the E-C boundary (BURNS et al., 1994; HALVERSON et al., 2007; VEIZER et al., 1999) supports increased sedimentation rates over this interval. As such, increased sedimentation rate may play a role in enhanced f_{pyr} during Ara time. but its contribution is hard to quantify in the absence of a direct measure of sedimentation rate through time.

The other factor that enhances preservation is anoxia at the site of deposition. Anoxia in the overlying waters limits the exposure of reduced materials to oxidants and, thus, increases the efficiency of organic matter and pyrite burial. The Ara Group strata

contain slightly elevated TOC (~0.3 - 1%) and pyrite (~0.2 - 0.5%) relative to the upper

Nafun Group. These signals are equivocal for resolving whether the Ara Group was

affected by anoxia or increased production as the result of both is to increase TOC and

pyrite abundances(ARTHUR and SAGEMAN, 1994). We turn to redox-sensitive trace

element enrichments to help distinguish between these two options. Overall, Ara Group

strata show no significant enrichment in uranium or rhenium (indicators of anoxia), or

molybdenum (indicator of euxinia), relative to the Upper Nafun Group strata (Figure 10).

This suggests the increase in pyrite burial is driven by increased primary production

rather than more reducing conditions. However, the A4 carbonate containing the E-C

boundary negative $\delta^{13}C_{carb}$ excursion is an exception, and is characterized by elevated

uranium and rhenium concentrations. This is attributed to widespread anoxia, believed to

have been prevalent at the E-C boundary (KIMURA and WATANABE, 2001; SCHRÖDER

and GROTZINGER, 2007), and is associated with the extinction of the Ediacaran organisms

(AMTHOR et al., 2003). Overall, the lack of enrichment in trace elements relative to the

Upper Nafun Group suggests that redox conditions in the global ocean did not change

appreciably during deposition of the Ara Group (excluding the E-C boundary itself).

Support for increased primary production comes from the evidence for abundant

phosphorite deposits during the period of Ara deposition (BRASIER et al., 1997; COOK and

SHERGOLD, 1984). Major phosphorite deposits of late Ediacaran-early Cambrian age are

globally widespread and the peak occurrence of these deposits is in association with the

enriched $\delta^{34}S_{SO4}$ of the Ara anomaly (COOK and SHERGOLD, 1984). Phosphorus is widely

considered the limiting nutrient for productivity (TYRRELL, 1999). The widespread

phosphorite deposits imply that abundant phosphorus would have been available to

enhance biological productivity. Elevated production is also supported by evidence for enhanced organic carbon burial during the latest Ediacaran – earliest Cambrian (SAYLOR et al., 1998). Therefore, we conclude that a change in primary production, rather than a return to more reducing conditions, was responsible for increased f_{pyr} during Ara deposition from ~550 – 540 Ma. Enhanced primary production reconciles increased f_{pyr} with the continued existence of the Ediacaran fauna up until the E-C boundary. The presence of these organisms, including *Namacalathus* and *Cloudina* in the lower Ara Group carbonates, has been interpreted as indicative of oxic conditions (AMTHOR et al., 2003).

Given our interpretation of the $\delta^{34}S_{SO4}$-$\delta^{34}S_{pyr}$ record assuming decreasing $\delta^{34}S_{in}$, the gradual decrease in f_{pyr} across the Paleozoic (from ~0.5 – ~0.2) is in good agreement with the apparent trend toward gradually more oxidizing conditions as recorded by decreased black shale deposition. This trend toward gradually more oxidizing conditions over the Paleozoic(BERRY and WILDE, 1978; ULMISHEK and KLEMME, 1990; WILDE, 1987) suggests a more long-term control on ocean redox state and is likely associated with atmospheric oxygen levels rising to near modern values.

Increasing oxygenation, and subsequent shrinking of oceanic oxygen minimum zones (OMZs), is recorded by changes in the abundance and depositional environment of organic- and pyrite-rich black shales(ARTHUR and SAGEMAN, 1994). There is a decrease in the fraction of sediments that are black shales from the Silurian (~42%) to the Upper Devonian-early Carboniferous (~21%) (ULMISHEK and KLEMME, 1990). This is not to say that black shales monotonically decrease in their abundance. Indeed, black shale deposition in both the Pennsylvanian-Permian and Upper Jurassic becomes more areally

extensive (~27%); however, both intervals are heavily influenced by abundant terrestrial organic carbon (ULMISHEK and KLEMME, 1990).

The environment of major black shale deposition has altered with time as well. Black shale deposition in the late Proterozoic typically occurred in open, shallow shelf environments(ULMISHEK and KLEMME, 1990). In Cambrian through Devonian time, organic-rich facies formed primarily in open shelves at water depths deeper than common in the Ediacaran(ULMISHEK and KLEMME, 1990). Black shale facies deposited during younger periods were customarily limited to basins either partially-restricted (Carboniferous-Cretaceous) or completely-restricted (Tertiary-Quaternary) from the open ocean(ULMISHEK and KLEMME, 1990). Further, when atmospheric and oceanic circulation studies have been able to resolve locations of upwelling, there is strong correlation between zones of upwelling and organic-rich black shales (PARRISH, 1982; PARRISH, 1987; PARRISH and CURTIS, 1982). For example, in the Upper Devonian, a period of widespread black shale deposition (CAPLAN and BUSTIN, 1999; JOACHIMSKI et al., 2001; ULMISHEK and KLEMME, 1990), there is a 92% correlation between the occurrence of organic-rich facies and predicted zones of upwelling (PARRISH, 1982). These data relate the periods of black shale deposition to localized bursts of primary production as opposed to intervals of global anoxia punctuating an otherwise increasingly oxidized ocean.

In summary, we propose that the increased f_{pyr} in the terminal Ediacaran-earliest Cambrian is related to increased primary production, possibly aided by increased sedimentation rate associated with the assembly of Gondwana (SQUIRE et al., 2006). Primary production is generally limited by the flux of nutrients, primarily phosphorus

delivered by riverine input (TYRRELL, 1999). The peak in $^{87}Sr/^{86}Sr$ (a proxy for riverine flux, among others) and in the abundance of phosporate deposits during the time of Ara deposition support increased nutrient input capable of sustaining elevated primary production during the Ara anomaly. We see no compelling evidence that the increase in f_{pyr} is driven by a return to generally more reducing conditions such as characterized the early (pre-Gaskiers) Ediacaran. It is clear, however, that enhanced primary production and anoxia are not completely uncoupled. There is evidence (INGALL et al., 1993) that under anoxic conditions the recycling of phosphate is enhanced, spurring primary production. Similarly, the remineralization of organic matter consumes oxygen and can lead to anoxia during periods of elevated primary production, such as in the wake of algal blooms (PAERL et al., 1998). In light of this, we suggest that the inferred anoxia at the E-C boundary (KIMURA and WATANABE, 2001; SCHRÖDER and GROTZINGER, 2007) is the result of water-column eutrophication resulting from enhanced primary production during the latest Ediacaran (~546 – 541 Ma), rather than resulting from either a return to more reducing conditions globally or the overturn of anoxic oceanic deep water. Following the E-C boundary, f_{pyr} is projected to decrease over the Paleozoic as atmospheric oxygen rises to near modern levels. Further studies will serve to identify the end of the Ara anomaly in the Cambrian and determine the relationship (if any) between the transition to decreased f_{pyr} and the biological and redox evolution of the Paleozoic ocean.

6. Conclusions

A unique high-resolution paired $\delta^{34}S_{SO4}$ – $\delta^{34}S_{pyr}$ dataset from Ediacaran – early Cambrian strata of the Huqf Supergroup, Sultanate of Oman was used to develop a new method for constraining changes to the global sulfur cycle, allowing for the determination of both $\delta^{34}S_{in}$ and f_{pyr}. We observe $\delta^{34}S_{in}$ to be significantly enriched relative to bulk Earth (0%), increasing from ~10‰ in the basal Ediacaran to ~22‰ around the Ediacaran-Cambrian boundary. The rise in $\delta^{34}S_{in}$ is likely due to the rapid recycling of $\delta^{34}S$-enriched Ediacaran strata and the preferential weathering of sulfates relative to sulfides under sub-modern levels of pO_2. $\delta^{34}S_{in}$ is projected to decrease to modern values over the Paleozoic influencing the observed decrease in Paleozoic $\delta^{34}S_{SO4}$ and $\delta^{34}S_{pyr}$. A decrease in f_{pyr} is observed in the late Ediacaran (~580 – 550 Ma), consistent with previous reports for ocean oxygenation at this time. Against the background of increasing $\delta^{34}S_{in}$, anomalously enriched $\delta^{34}S_{SO4}$ and $\delta^{34}S_{pyr}$ during latest Ediacaran-earliest Cambrian time (~550 – 540 Ma) is interpreted to result from increased f_{pyr}, ultimately driven by enhanced primary production in nutrient-rich waters. Future studies of paired $\delta^{34}S_{SO4}$-$\delta^{34}S_{pyr}$ can illuminate both the temporal evolution of $\delta^{34}S_{in}$ and f_{pyr} over geologic history, as well as decipher the relationship between changes in these parameters and biological evolution.

REFERENCES

Amthor, J. E., Grotzinger, J. P., Schroder, S., Bowring, S. A., Ramezani, J., Martin, M. W., and Matter, A., 2003. Extinction of Cloudina and Namacalathus at the Precambrian-Cambrian boundary in Oman. *Geology* **31**, 431-434.

Anbar, A. D. and Knoll, A. H., 2002. Proterozoic ocean chemistry and evolution: a bioinorganic bridge? *Science* **297**, 1137 - 1142.

Arthur, M. A. and Sageman, B. B., 1994. Marine Black Shales - Depositional Mechanisms and Environments of Ancient-Deposits. *Annual Review of Earth and Planetary Sciences* **22**, 499-551.

Banerjee, D. M., Strauss, H., Bhattacharya, S. K., Kumar, V., and Mazumdar, A., 1998. Isotopic composition of carbonates and sulphates, potash mineralisation and basin architecture of the Nagaur–Gangnagar evaporite basin (northwestern India) and their implications on the Neoproterozoic exogenic cycle. *Mineralogical Magazine* **62A**, 106 - 107.

Bartley, J. K., Pope, M., Knoll, A. H., Semikhatov, M. A., and Petrov, P. Y. U., 1998. A Vendian-Cambrian boundary succession from the northwestern margin of the Siberian Platform: stratigraphy, palaeontology, chemostratigraphy and correlation. *Geological Magazine* **135**, 473-494.

Bergman, N. M., Lenton, T. M., and Watson, A. J., 2004. COPSE: A new model of biogeochemical cycling over Phanerozoic time. *American Journal of Science* **304**, 397-437.

Berkner, L. V. and Marshall, L. C., 1965. On the Origin and Rise of Oxygen Concentration in the Earth's Atmosphere. *Journal of the Atmospheric Sciences* **22**, 225-261.

Berner, R. A., 1984. Sedimentary pyrite formation: an update. *Geochimica et Cosmochimica Acta* **48**, 605 - 615.

Berner, R. A., 2001. Modeling atmospheric O_2 over Phanerozoic time. *Geochimica et Cosmochimica Acta* **65**, 685- 694.

Berner, R. A., 2006. GEOCARBSULF: A combined model for Phanerozoic atmospheric O2 and CO2. *Geochimica et Cosmochimica Acta* **70**, 5653 - 5664.

Berner, R. A. and Raiswell, R., 1983. Burial of organic carbon and pyrite sulfur in sediments over Phanerozoic time: a new theory. *Geochimica et Cosmochimica Acta* **47**, 855 - 862.

Berry, W. B. N. and Wilde, P., 1978. Progressive ventilation of the oceans -- an explanation for the distribution of the lower Paleozoic black shales. *American Journal of Science* **278**, 257 - 275w.

Bowring, S. A., Grotzinger, J. P., Condon, D. J., Ramezani, J., and Newall, M., 2007. Geochronologic constraints on the chronostratigraphic framework of the Neoproterozoic Huqf Supergroup, Sultanate of Oman. *American Journal of Science* (**in press**).

Brasier, M., Green, O., and Shields, G., 1997. Ediacarian sponge spicule clusters from southwestern Mongolia and the origins of the Cambrian fauna. *Geology* **25**, 303-306.

Brasier, M. D. and Lindsay, J. F., 2000. Did supercontinent amalgamation trigger the 'Cambrian explosion'? In: Riding, R. and Zhuravlev, A. Y. Eds.), *Ecology of the Cambrian Radiation*. Columbia University Press, New York.

Brennan, S. T., Lowenstein, T. K., and Horita, J., 2004. Seawater chemistry and the advent of biocalcification. *Geology* **32**, 473-476.

Burns, S. J., Haudenschild, U., and Matter, A., 1994. The Strontium Isotopic Composition of Carbonates from the Late Precambrian (Approximate-to-560-540 Ma) Huqf Group of Oman. *Chemical Geology* **111**, 269-282.

Burns, S. J. and Matter, A., 1993. Carbon isotopic record of the latest Proterozoic from Oman. *Eclogae Geologicae Helvetiae* **86**, 595-607.

Canfield, D. E., 1998. A new model for Proterozoic ocean chemistry. *Nature* **396**, 450 - 453.

Canfield, D. E., 2001. Biogeochemistry of sulfur isotopes. *Reviews in Mineralogy & Geochemistry: Stable Isotope Geochemistry* **43**, 607-636.

Canfield, D. E., 2004. The evolution of the Earth surface sulfur reservoir. *American Journal of Science* **304**, 839-861.

Canfield, D. E., Poulton, S. W., and Narbonne, G. M., 2007. Late Neoproterozoic Deep Ocean Oxygenation and the Rise of Animal Life *Science* **315**, 92 - 95.

Canfield, D. E. and Teske, A., 1996. Late Proterozoic rise in atmospheric oxygen concentration inferred from phylogenetic and sulphur-isotope studies. *Nature* **382**, 127-132.

Caplan, M. L. and Bustin, R. M., 1999. Devonian-Carboniferous Hangenberg mass extinction event, widespread organic-rich mudrock and anoxia: causes and consequences. *Palaeogeography Palaeoclimatology Palaeoecology* **148**, 187 - 207.

Claypool, G. E., Holser, W. T., Kaplan, I. R., Sakai, H., and Zak, I., 1980. The age curves of sulfur and oxygen isotopes in marine sulfate and their mutual interpretation. *Chemical Geology* **28**, 199-260.

Condon, D., Zhu, M., Bowring, S., Wang, W., Yang, A., and Jin, Y., 2005. U-Pb Ages from the Neoproterozoic Doushantuo Formation, China. *Science* **308**, 95 - 98.

Cook, P. J. and Shergold, J. H., 1984. Phosphorus, phosphorites, and skeletal evolution at the Precambrian-Cambrian boundary. *Nature* **308**, 231 - 236.

Cozzi, A., Allen, P. A., and Grotzinger, J. P., 2004a. Understanding carbonate ramp dynamics using delta C-13 profiles: examples from the Neoproterozoic Buah Formation of Oman. *Terra Nova* **16**, 62-67.

Cozzi, A., Grotzinger, J. P., and Allen, P. A., 2004b. Evolution of a terminal Neoproterozoic carbonate ramp system (Buah Formation, Sultanate of Oman): Effects of basement paleotopography. *Geological Society of America Bulletin* **116**, 1367 - 1384.

Des Marais, D. J., Strauss, H., Summons, R. E., and Hayes, J. M., 1992. Carbon Isotope Evidence for the Stepwise Oxidation of the Proterozoic Environment. *Nature* **359**, 605-609.

Fike, D. A., 2007. Evolution of the Ediacaran-Cambrian environment: insights from carbon and sulfur cycling. PhD, MIT.

Fike, D. A., Grotzinger, J. P., Pratt, L. M., and Summons, R. E., 2006. Oxidation of the Ediacaran Ocean. *Nature* **444**, 744 - 747.

Garrels, R. M. and Lerman, A., 1981. Phanerozoic cycles of sedimentary carbon and sulfur. *Proceedings of the National Academy of Sciences USA* **78**.

Goldberg, T., Poulton, S. W., and Strauss, H., 2005. Sulphur and oxygen isotope signatures of late Neoproterozoic to early Cambrian sulphate, Yangtze Platform, China: Diagenetic constraints and seawater evolution. *Precambrian Research* **137**, 223-241.

Grotzinger, J. P., Al-Siyabi, A. H., Al-Hashimi, R. A., and Cozzi, A., 2002. New model for tectonic evolution of Neoproterozoic-Cambrian Huqf Supergroup basins, Oman. *GeoArabia* **7**, 241.

Grotzinger, J. P., Bowring, S. A., Saylor, B. Z., and Kaufman, A. J., 1995. Biostratigraphic and Geochronological Constraints on Early Animal Evolution. *Science* **270**, 598-604.

Grotzinger, J. P. and Miller, R., 2007. The Nama Group. In: Miller, R. (Ed.), *The Geology of Namibia*.

Grotzinger, J. P., Watters, W. A., and Knoll, A. H., 2000. Calcified metazoans in thrombolite-stromatolite reefs of the terminal Proterozoic Nama Group, Namibia. *Paleobiology* **26**, 334-359.

Habicht, K. S., Gade, M., Thamdrup, B., Berg, P., and Canfield, D. E., 2002. Calibration of Sulfate Levels in the Archean Ocean. *Science* **298**, 2372-2374.

Halverson, G. P., Dudas, F. O., Maloof, A. C., and Bowring, S. A., 2007. Evolution of the $^{87}Sr/^{86}Sr$ Composition of Neoproterozoic Seawater. *Palaeogeography Palaeoclimatology Palaeoecology* **in press**.

Hofmann, H. J. and Mountjoy, E. W., 2001. *Namacalathus-Cloudina* assemblage in Neoproterozoic Miette Group (Byng Formation), British Columbia: Canada's oldest shelly fossils. *Geology* **29**, 1091-1094.

Holser, W. T., 1977. Catastrophic Chemical Events in History of Ocean. *Nature* **267**, 403-408.

Holser, W. T., Schidlowski, M., Mackenzie, F. T., and Maynard, J. B., 1988. Geochemical cycles of carbon and sulfur. In: Gregor, C. B., Garrels, R. M., MacKenzie, F. T., and Maynard, J. B. Eds.), *Chemical cycles in the evolution of the Earth*. John Wiley & Sons, New York.

Horita, J., Zimmermann, H., and Holland, H. D., 2002. Chemical evolution of seawater during the Phanerozoic: Implications from the record of marine evaporites. *Geochimica Et Cosmochimica Acta* **66**, 3733-3756.

Hough, M. L., Shields, G. A., Evins, L. Z., Strauss, H., Henderson, R. A., and Mackenzie, S., 2006. A major sulphur isotope event at c.510 Ma: a possible anoxia-extinction-volcanism connection during the Early-Middle Cambrian transition? *Terra Nova* **18**, 257-263.

103

Houghton, M. L., 1980. Geochemistry of the Proterozoic Hormuz evaporites, Southern Iran. MSc Thesis, University of Oregon.

Hurtgen, M. T., 2006. Sulfur cycling in the aftermath of a Neoproterozoic (Marinoan) snowball glaciation: Evidence for a syn-glacial sulfidic deep ocean. *Earth and Planetary Science Letters* **245**, 551 - 570.

Hurtgen, M. T., Arthur, M. A., and Halverson, G. P., 2005. Neoproterozoic sulfur isotopes, the evolution of microbial sulfur species, and the burial efficiency of sulfide as sedimentary pyrite. *Geology* **33**, 41-44.

Ingall, E. D., Bustin, R. M., and Vancappellen, P., 1993. Influence of Water Column Anoxia on the Burial and Preservation of Carbon and Phosphorus in Marine Shales. *Geochimica Et Cosmochimica Acta* **57**, 303-316.

Jerz, J. K. and Rimstidt, J. D., 2004. Pyrite oxidation in moist air. *Geochimica et Cosmochimica Acta* **68**, 701 - 714.

Joachimski, M. M., Ostertag-Henning, C., Pancost, R. D., Strauss, H., Freeman, K. H., Littke, R., Damste, J. S. S., and Racki, G., 2001. Water column anoxia, enhanced productivity and concomitant changes in delta C-13 and delta S-34 across the Frasnian-Famennian boundary (Kowala Holy Cross Mountains/Poland). *Chemical Geology* **175**, 109-131.

Johnston, D. T., Wing, B. A., Farquhar, J., Kaufman, A. J., Strauss, H., Lyons, T. W., Kah, L. C., and Canfield, D. E., 2005. Active microbial sulfur disproportionation in the Mesoproterozoic. *Science* **310**, 1477-1479.

Kah, L. C., Lyons, T. W., and Frank, T. D., 2004. Low marine sulphate and protracted oxygenation of the proterozoic biosphere. *Nature* **431**, 834-838.

Kampschulte, A. and Strauss, H., 2004. The sulfur isotopic evolution of Phanerozoic seawater based on the analysis of structurally substituted sulfate in carbonates. *Chemical Geology* **204**, 255-286.

Kaufman, A. J., Corsetti, F. A., and Varni, M. A., 2007. The effect of rising atmospheric oxygen on carbon and sulfur isotope anomalies in the Neoproterozoic Johnnie Formation, Death Valley, USA. *Chemical Geology* **in press**.

Kimura, H. and Watanabe, Y., 2001. Oceanic anoxia at the Precambrian-Cambrian Boundary. *Geology* **29**, 995 - 998.

Knoll, A. H. and Carroll, S. B., 1999. Early animal evolution; emerging views from comparative biology and geology. *Science* **284**, 2129 - 2137.

Le Guerroue, E., Allen, P. A., and Cozzi, A., 2006a. Chemostratigraphic and sedimentological framework of the largest negative carbon isotopic excursion in Earth history: The Neoproterozoic Shuram Formation (Nafun Group, Oman). *Precambrian Research* **146**, 68 - 92.

Le Guerroue, E., Allen, P. A., Cozzi, A., Etienne, J. L., and Fanning, M., 2006b. 50 million year duration negative carbon isotope excursion in the Ediacaran ocean. *Terra Nova* **18**, 147 - 153.

Maloof, A. C., Schrag, D. P., Crowley, J. L., and Bowring, S. A., 2005. An expanded record of Early Cambrian carbon cycling from the Anti-Atlas Margin, Morocco. *Canadian Journal of Earth Sciences* **42**, 2195-2216.

Marshall, C. R., 2006. Explaining the Cambrian "explosion" of animals. *Annual Review of Earth and Planetary Sciences* **34**.

Mattes, B. W. and Conway-Morris, S., 1990. Carbonate/evaporite deposition in the Late Precambrian–Early Cambrian Ara Formation of southern Oman. In: Robertson, A. H. F., Ed2, Ed3, Ed4, Ed5, and Ed6 Eds.), *The geology and tectonics of the Oman region*. Geological Society, London.

Matthews, S. C. and Cowie, J. W., 1979. Early Cambrian transgression. *Journal of the Geological Society* **136**, 133 - 135.

McCarron, G., 2000. The sedimentology and chemostratigraphy of the Nafun Group, Huqf Supergroup,Oman. *PhD Thesis (Oxford University)*, 175.

Morth, A. H. and Smith, E. E., 1966. Kinetics of the sulfide-to-sulfate reaction. *Am. Chem. Soc. Div. Fuel Chem. Preprints* **10**, 83 - 92.

Ostermann, D. R. and Curry, W. B., 2000. Calibration of stable isotopic data: An enriched $\delta^{18}O$ standard used for source gas mixing detection and correction. *Paleoceanography* **15**, 353 - 360.

Paerl, H. W., Pinckney, J. L., Fear, J. M., and Peierls, B. L., 1998. Ecosystem responses to internal and watershed organic matter loading: consequences for hypoxia in the eutrophying Neuse river estuary, North Carolina, USA. *Marine Ecology-Progress Series* **166**, 17-25.

Parrish, J. T., 1982. Upwelling and petroleum source beds, with reference to Paleozoic. *American Association of Petroleum Geologists Bulletin* **66**, 750 - 774.

Parrish, J. T., 1987. Palaeo-upwelling and the distribution of organic-rich rocks. In: Brooks, J. and Fleet, A. J. Eds.), *Marine petroleum source rocks*. Geological Society Special Publication, London.

Parrish, J. T. and Curtis, R. L., 1982. Atmospheric circulation, upwelling, and organic-rich rocks in the Mesozoic and Cenozoic eras. *Palaeogeography Palaeoclimatology Palaeoecology* **40**, 31 - 66.

Pisarchik, Y. K. and Golubchina, M. N., 1975. Sulfur isotope composition for Cambrian calcium sulfates from the Siberian platform. *Geochem. Int.* **8**, 227 - 230.

Poulton, S. W., Fralick, P. W., and Canfield, D. E., 2004. The transition to a sulphidic ocean ~1.84 billion years ago. *Nature* **431**, 173 - 177.

Raab, M. and Spiro, B., 1991. Sulfur isotopic variations during seawater evaporation with fractional crystallization. *Chemical Geology* **86**, 323 - 333.

Raiswell, R. and Berner, R. A., 1986. Pyrite and organic matter in Phanerozoic normal marine shales. *Geochimica et Cosmochimica Acta* **50**, 1967 - 1976.

Rayner, J. M. V., 1985. Linear relations in biomechanics: the statistics of scaling functions. *Journal of Zoology, London* **A206**, 415 - 439.

Saltzman, M. R., 2005. Phosphorus, nitrogen, and the redox evolution of the Paleozoic oceans. *Geology* **33**, 573-576.

Saylor, B. Z., Kaufman, A. J., Grotzinger, J. P., and Urban, F., 1998. A composite reference section for terminal Proterozoic strata of southern Namibia. *Journal of Sedimentary Research* **68**, 1223-1235.

Schröder, S. and Grotzinger, J. P., 2007. Evidence for anoxia at the Ediacaran-Cambrian boundary: the record of redox-sensitive trace elements and rare earth elements in Oman. *Journal of the Geological Society* **164**, 175-187.

Schröder, S., Schreiber, B. C., Amthor, J. E., and Matter, A., 2003a. A depositional model for the terminal Neoproterozoic - Early Cambrian Ara Group evaporites in south Oman. *Sedimentology* **50**, 879-898.

Schröder, S., Schreiber, B. C., Amthor, J. E., and Matter, A., 2003b. A depositional model for the terminal Neoproterozoic Early Cambrian Ara Group evaporites in south Oman. *Sedimentology* **50**, 879-898.

Schröder, S., Schreiber, B. C., Amthor, J. E., and Matter, A., 2004. Stratigraphy and environmental conditions of the terminal Neoproterozoic-Cambrian period in Oman: evidence from sulphur isotopes. *Journal of the Geological Society* **161**, 489-499.

Scott, C., Lyons, T. W., Bekker, A., Anbar, A. D., and Williams, G., 2006. Geochemical evidence for the restriction of oxic depositional environments in the Proterozoic ocean *Geological Society of America Annual Meeting.* GSA, Philadelphia.

Shen, Y., Canfield, D. E., and Knoll, A. H., 2002. Middle Proterozoic ocean chemistry: evidence from the McArthur Basin, Northern Australia. *American Journal of Science* **302**, 81 - 109.

Shen, Y., Schidlowski, M., and Chu, X., 2000. Biogeochemical approach to understanding phosphogenic events of the terminal Proterozoic to Cambrian. *Palaeogeography Palaeoclimatology Palaeoecology* **158**, 99 - 108.

Shen, Y. N., Zhao, R., Chu, X. L., and Lei, J. J., 1998. The carbon and sulfur isotope signatures in the Precambrian-Cambrian transition series of the Yangtze Platform. *Precambrian Research* **89**, 77-86.

Shields, G., 1999. Working towards a new stratigraphic calibration scheme for the Neoproterozoic-Cambrian. *Eclogae Geologicae Helvetiae* **92**, 221-233.

Shields, G. and Veizer, J., 2002. Precambrian marine carbonate isotope database: Version 1.1. *Geochemistry Geophysics Geosystems* **3**.

Shields, G. A., Strauss, H., Howe, S. S., and Siegmund, H., 1999. Sulphur isotope compositions of sedimentary phosphorites from the basal Cambrian of China: implications for Neoproterozoic-Cambrian biogeochemical cycling. *Journal of the Geological Society* **156**, 943-955.

Sperling, E. A. and Peterson, K. J., 2007. Poriferan Paraphyly and its Implications for Precambrian Paleobiology. *Journal of the Geological Society, London* **in press**.

Squire, R. J., Campbell, I. H., Allen, C. M., and Wilson, C. J. L., 2006. Did the Transgondwanan Supermountain trigger the explosive radiation of animals on Earth? *Earth and Planetary Science Letters* **250**, 116-133.

Strauss, H., 1993. The Sulfur Isotopic Record of Precambrian Sulfates - New Data and a Critical-Evaluation of the Existing Record. *Precambrian Research* **63**, 225-246.

Strauss, H., 1997. The isotopic composition of sedimentary sulfur through time. *Palaeogeography Palaeoclimatology Palaeoecology* **132**, 97-118.

Strauss, H., Banerjee, D. M., and Kumar, V., 2001. The sulfur isotopic composition of Neoproterozoic to early Cambrian seawater - evidence from the cyclic Hanseran evaporites, NW India. *Chemical Geology* **175**, 17-28.

Thode, H. G. and Monster, J., 1965. Sulfur-isotope geochemistry of petroleum, evaporites, and ancient seas. In: Young, A. and Galley, J. E. Eds.), *Fluids in subsurface environments*. AAPG, Tulsa.

Tyrrell, T., 1999. The relative influences of nitrogen and phosphorus on oceanic primary production. *Nature* **400**, 525 - 531.

Ulmishek, G. F. and Klemme, H. D., 1990. *Depositional controls, distribution, and effectiveness of world's petroleum source rocks*. US Geological Survey, Washington, D.C.

Veizer, J., Ala, D., Azmy, K., Bruckschen, P., Buhl, D., Bruhn, F., Carden, G. A. F., Diener, A., Ebneth, S., Godderis, Y., Jasper, T., Korte, G., Pawellek, F., Podlaha, O. G., and Strauss, H., 1999. ^{87}Sr/^{86}Sr, δ^{13}C, and δ^{18}O evolution of Phanerozoic seawater. *Chemical Geology* **161**, 59-88.

Veizer, J., Holser, W. T., and Wilgus, C. K., 1980. Correlation of ^{13}C/^{12}C and ^{34}S/^{32}S secular variations. *Geochimica et Cosmochimica Acta* **44**, 579 - 587.

Walker, J. C. G., 1986. Global geochemical cycles of carbon, sulfur and oxygen. *Marine Geology* **70**, 159 - 174.

Walter, M. R., Veevers, J. J., Calver, C. R., Gorjan, P., and Hill, A. C., 2000. Dating the 840–544 Ma Neoproterozoic interval by isotopes of strontium, carbon, and sulfur in seawater, and some interpretative models. *Precambrian Research* **100**, 371 - 433.

Warren, J. K., 1989. *Evaporite sedimentology*. Prentice Hall, Englewood Cliffs, NJ.

Wilde, P., 1987. Model of progressive ventilation of the late Precambrian-early Paleozoic ocean. *American Journal of Science* **287**, 442 - 459.

Wilkin, R. T., Arthur, M. A., and Dean, W. E., 1997. History of water-column anoxia in the Black Sea indicated by pyrite framboid size distributions. *Earth and Planetary Science Letters* **148**, 517 - 525.

Wilkin, R. T., Barnes, H. L., and Brantley, S. L., 1996. The size distribution of framboidal pyrite in modern sediments: An indicator of redox conditions. *Geochimica et Cosmochimica Acta* **60**, 3897 - 3912.

Appendix A:

Table S1: Isotopic data for subsurface core and cuttings samples

Table S1: Isotopic data for subsurface core and cuttings samples

Well	Unit	Depth	Type	$\delta^{13}C$	$\delta^{18}O$	$\delta^{34}S_{CAS}$	$\delta^{34}S_{pyr}$	$\Delta\delta$
AAL1	A6C	2256.0	ctgs			38.4	-3.1	41.5
AAL1	A0C	3820.0	ctgs			39.0		
AAL1	A0C	3823.1	core				17.8	
AAL1	A0C	3829.0	core			39.7	17.1	22.6
AAL1	A0C	3838.6	core			36.1	23.3	12.8
AAL1	A0C	3845.8	core			36.2	24.2	12.0
AAL1	A0C	3852.0	ctgs			36.7		
AAL1	A0C	3952.0	ctgs			35.0		
AAL1	A0C	4000.0	ctgs			32.9		
AAL1	A0C	4052.0	ctgs			33.1		
AAL1	A0C	4096.0	ctgs			35.9		
BB4	A4C	2905.8	core	-2.7	-2.4	39.3	13.8	25.5
BB4	A4C	2907.7	core	-2.4	-2.2	38.8	12.9	25.9
BB4	A4C	2908.7	core	-2.6	-2.0		16.6	
BB4	A4C	2909.3	core	-2.6	-2.0	38.8	13.7	25.0
BB4	A4C	2910.8	core	-2.6	-2.5	38.5	18.9	19.6
BB4	A4C	2911.4	core	-2.7	-2.2	38.7	16.1	22.6
BB4	A4C	2911.5	core	-2.7	-2.5	38.9	18.2	20.7
BB4	A4C	2919.3	core	-2.6	-2.2	39.3	15.5	23.8
BB4	A4C	2925.6	core	-2.4	-3.2	38.9	15.2	23.7
BB4	A4C	2928.8	core	-2.5	-1.0	38.7	9.2	29.5
BB4	A4C	2929.4	core	-2.2	-3.1	39.3	10.4	28.9
BB4	A4C	2931.4	core	-2.8	-3.9	39.3	17.4	22.0
BB4	A4C	2932.1	core	-2.8	-3.8			
BB4	A4C	2932.9	core	-2.8	-3.3	39.7	7.7	32.0
BB4	A4C	2937.1	core	-3.1	-4.5	39.0	13.4	25.6
BB4	A4C	2937.8	core	-3.1	-4.5			
BB4	A4C	2939.8	core	-3.1	-4.2	39.6	7.1	32.5
BB4	A4C	2940.1	core	-3.1	-4.4	39.7	16.9	22.8
BB4	A4C	2940.9	core	-3.2	-4.3			
BB4	A4C	2944.7	core	-4.4	-4.2	39.2	6.1	33.0
BB4	A4C	2945.2	core	-3.9	-3.6	38.9	9.1	29.9
BB4	A4C	2945.9	core	-3.9	-4.6			
BB4	A4C	2948.6	core	-4.6	-2.9	39.4	13.3	26.1
BB4	A4C	2949.9	core	-5.0	-3.4	39.3	12.2	27.2
BB4	A4C	2950.0	core	-4.5	-3.0	39.8	15.2	24.6
BB4	A4C	2950.2	core	-4.3	-2.5	34.7	13.2	21.5
BB4	A4C	2950.6	core	-2.9	-1.8			
BB4	A3C	3029.7	core	3.3	-3.5	40.4	13.4	26.9
BB4	A3C	3032.3	core	3.2	-4.6	41.2	11.6	29.6
BB4	A3C	3033.6	core	3.2	-4.8	40.9		
BB4	A3C	3034.0	core	3.4	-4.3	40.5		
BB4	A3C	3035.0	core	3.7	-3.1	41.1	15.1	26.0
BBN1	A5C	3534.0	ctgs	-0.7	-4.9	40.5		
BBN1	A5C	3540.0	ctgs	0.8	-0.9			
BBN1	A5C	3546.0	ctgs	1.8	1.6	40.3		
BBN1	A5C	3563.0	ctgs	2.8	0.3			
BBN1	A5C	3568.0	ctgs	2.8	0.7			
BBN1	A4C	3682.0	ctgs	-6.7	-3.7	38.7		
BBN1	A4C	3685.0	ctgs	-2.6	-3.0	36.9		
BBN1	A4C	3716.0	ctgs	-2.6	-3.1	38.1		

Table S1: continued

Well	Unit	Depth	Type	$\delta^{13}C$	$\delta^{18}O$	$\delta^{34}S_{CAS}$	$\delta^{34}S_{DVr}$	$\Delta\delta$
BBN1	A4C	3734.0	ctgs	-0.6	-3.5	39.6		
BBN1	A4C	3736.0	ctgs	-2.6	-3.8			
BBN1	A4C	3740.0	ctgs	-1.9	-3.5			
BBN1	A3C	3781.0	ctgs	3.3	1.8	37.9	-4.8	42.7
BBN1	A3C	3831.0	ctgs	3.2	-1.2	38.7	4.3	34.4
BBN1	A3C	3868.0	ctgs	2.6	-0.6	40.8		
BBN1	A2C	4194.0	ctgs	2.1	-0.7			
BBN1	A2C	4237.0	ctgs	0.0	-1.0			
BBN1	A2C	4259.0	ctgs	0.6	0.9			
BBN1	A2C	4264.0	ctgs	-0.5	-0.7			
BBN1	A1C	4358.0	ctgs	2.7	0.2			
DHS3	A1C	2956.6	core	2.3	1.1	34.2	7.7	26.4
DHS3	A1C	2963.5	core			34.2		
DHS3	A1C	2990.1	core	2.2	-2.9	40.6	7.6	33.0
DHS3	A1C	3000.9	core			42.8	8.9	33.9
MNH1	A6C	3394.0	ctgs	2.1	0.0	37.8		
MNH1	A6C	3410.0	ctgs	2.4	0.0	39.9	0.0	39.9
MNH1	A6C	3450.0	ctgs			37.0		
MNH1	A6C	3460.0	ctgs	2.8	0.1		10.9	
MNH1	A5C	3640.0	ctgs	2.8	0.0	40.6		
MNH1	A5C	3690.0	ctgs	2.3	0.0			
MNH1	A5C	3700.0	ctgs	2.0	0.0	37.1	2.5	34.6
MNH1	A5C	3710.0	ctgs	2.7	0.0	41.2		
MNH1	A5C	3800.0	ctgs	2.7	0.0	41.4		
MNH1	A5C	3810.0	ctgs	2.1	-3.4	39.5		
MNH1	A5C	3820.0	ctgs	2.2	-1.3	42.5		
MNH1	A3C	3960.0	ctgs			39.7		
MNH1	A3C	3976.0	core			40.4		
MNH1	A3C	3979.0	core	2.9	1.7	40.4	18.7	21.8
MNH1	A3C	3979.4	core	0.3	-4.2	41.2		
MNH1	A3C	3983.5	core	1.5	0.3	41.2	3.4	37.9
MNH1	A3C	3988.7	core			39.9		
MNH1	A2C	4171.0	core	3.4	0.6	40.1	16.5	23.6
MNH1	A2C	4176.0	core	3.4	1.4	40.5		
MNH1	A2C	4187.3	core			40.8	11.5	29.3
MNH1	A2C	4190.4	core	3.2	2.6	41.3		
MNH1	A2C	4246.0	ctgs	2.9	1.4	40.6	16.4	24.2
MNH1	A2C	4260.0	ctgs			41.3	7.7	33.5
MNH1	A1C	4496.0	ctgs	2.6	0.7	39.1	0.3	38.8
MNH1	A1C	4500.0	ctgs	2.2	0.6	37.0	-1.0	38.0
MNH1	A1C	4504.0	ctgs	2.5	0.5	36.7	-9.9	46.5
MNH1	A1C	4512.0	ctgs	3.5	0.1	36.7	-3.2	39.9
MNH1	A1C	4516.0	ctgs	1.7	0.4	36.7	-3.4	40.0
MNH1	A1C	4520.0	ctgs	1.5	0.6	38.0	0.1	37.9
MNH1	A1C	4528.0	ctgs	1.8	0.3	37.0	12.9	24.1
MQ1	A0	2906.0	ctgs	1.2	-5.2			
MQ1	A0	2926.0	ctgs	1.5	-5.1	27.3		
MQ1	A0	2958.0	ctgs	2.2	-2.5	31.8		
MQ1	A0	3018.0	ctgs	2.0	-2.1	26.7		
MQ1	A0	3026.0	ctgs	1.4	-4.3	30.2		
MQ1	A0	3070.0	ctgs	1.7	-1.7			

108

Table S1: continued

Well	Unit	Depth	Type	$\delta^{13}C$	$\delta^{18}O$	$\delta^{34}S_{CAS}$	$\delta^{34}S_{pyr}$	$\Delta\delta$
MQ1	A0	3110.0	ctgs	2.0	-0.7	23.0		
MQ1	A0	3134.0	ctgs	2.4	-1.2	24.1		
MQ1	A0	3142.0	ctgs	1.0	-2.4	24.5		
MQ1	A0	3150.0	ctgs	1.0	-2.7	25.3		
MQ1	A0	3158.0	ctgs	0.1	-2.3	25.7		
MQ1	A0	3180.0	ctgs	2.0	-1.4	23.8		
MQ1	A0	3192.0	ctgs	2.1	-1.9	25.2		
MQ1	A0	3198.0	ctgs	2.2	-1.0	23.7		
TM6	Post-A4	1990.0	ctgs	2.1	-3.3			
TM6	Post-A4	1995.0	ctgs	2.4	-4.0			
TM6	Post-A4	2000.0	ctgs	2.5	-3.3	41.2	8.7	32.5
TM6	Post-A4	2005.0	ctgs	2.5	-3.4			
TM6	Post-A4	2010.0	ctgs	2.6	-3.5			
TM6	Post-A4	2015.0	ctgs	2.6	-2.7			
TM6	Post-A4	2020.0	ctgs	2.8	-2.8			
TM6	Post-A4	2025.0	ctgs	2.6	-2.1			
TM6	Post-A4	2030.0	ctgs	2.3	-3.7			
TM6	Post-A4	2035.0	ctgs	2.5	-3.7			
TM6	Post-A4	2040.0	ctgs	2.7	-3.9			
TM6	Post-A4	2045.0	ctgs	2.6	-3.6			
TM6	Post-A4	2050.0	ctgs	2.3	-3.4	39.6	8.5	31.1
TM6	Post-A4	2055.0	ctgs	2.5	-3.3			
TM6	Post-A4	2060.0	ctgs	2.3	-3.2			
TM6	Post-A4	2065.0	ctgs	1.7	-1.1			
TM6	Post-A4	2070.0	ctgs	1.7	-2.9			
TM6	Post-A4	2075.0	ctgs	1.9	-1.0			
TM6	A4	2080.0	ctgs	-2.7	-2.6	39.3		
TM6	A4	2085.0	ctgs	-3.1	-1.8	39.2		
TM6	A4	2090.0	ctgs	-3.1	-1.8	41.3	9.9	31.4
TM6	A4	2100.0	ctgs	-3.7	-1.4	29.7		
TM6	A4	2105.0	ctgs	-2.8	-3.3	38.9		
TM6	A4	2110.0	ctgs	-3.1	-3.0	38.2		
TM6	A4	2115.0	ctgs	-4.4	-4.2	40.7	7.9	32.8
TM6	A4	2120.0	ctgs	-2.9	-3.6	40.0	7.9	32.1
TM6	A4	2125.0	ctgs	-3.8	-3.1	40.3	11.9	28.4
TM6	Pre-A4	2130.0	ctgs	1.8	-4.1	41.1	9.4	31.7
TM6	Pre-A4	2135.0	ctgs	1.2	-2.9	38.9	8.2	30.7
TM6	Pre-A4	2140.0	ctgs	1.4	-2.8	39.6	8.8	30.8
TM6	Pre-A4	2145.0	ctgs	1.5	-2.4	39.7	9.9	29.8
TM6	Pre-A4	2150.0	ctgs	1.4	-2.7	39.0	7.6	31.4
TM6	Pre-A4	2155.0	ctgs	2.2	-2.7	39.3	9.3	30.0
TM6	Pre-A4	2160.0	ctgs	3.0	-2.2	39.7	8.7	31.0
TM6	Pre-A4	2165.0	ctgs	3.2	-3.2	40.4	10.8	29.6
TM6	Pre-A4	2170.0	ctgs	2.7	-3.0	38.7	11.4	27.3
TM6	Pre-A4	2175.0	ctgs	2.4	-3.4	38.9	10.6	28.3
TM6	Pre-A4	2180.0	ctgs	2.3	-3.4	38.9	5.5	33.4
TM6	Pre-A4	2185.0	ctgs	0.2	-5.6	39.2	10.2	29.0
TM6	Pre-A4	2190.0	ctgs	-0.2	-6.5	38.9	6.7	32.2
TM6	Pre-A4	2195.0	ctgs	0.7	-4.2	41.8	10.4	31.4
TM6	Pre-A4	2200.0	ctgs	1.8	-3.3	39.2	8.8	30.5
TM6	Pre-A4	2205.0	ctgs	1.7	-1.6	38.3	10.9	27.4

Table S1: continued

Well	Unit	Depth	Type	$\delta^{13}C$	$\delta^{18}O$	$\delta^{34}S_{CAS}$	$\delta^{34}S_{pyr}$	$\Delta\delta$
TM6	Pre-A4	2210.0	ctgs	1.9	-3.1	39.5	9.1	30.4
TM6	Pre-A4	2215.0	ctgs	1.6	-3.3	39.4	10.4	29.1
TM6	Pre-A4	2220.0	ctgs	1.5	-2.2	41.8		
TM6	Pre-A4	2225.0	ctgs	1.4	-3.0	39.8		
TM6	Pre-A4	2230.0	ctgs	-1.0	-1.9	42.4		
TM6	Pre-A4	2235.0	ctgs	-4.7	-3.5			
TM6	Pre-A4	2240.0	ctgs	0.2	-0.2	42.3		
TM6	Pre-A4	2245.0	ctgs	0.3	-0.8	41.3		
TM6	A0	2250.0	ctgs	1.0	-2.4	39.5		
TM6	A0	2255.0	ctgs	1.5	-2.5	40.2		
TM6	A0	2260.0	ctgs	1.0	-2.4	39.6		
TM6	A0	2265.0	ctgs	0.2	-1.9	40.7		
TM6	A0	2270.0	ctgs	-0.5	-1.1	40.8		
TM6	A0	2275.0	ctgs	0.0	-1.6	39.6		
TM6	A0	2280.0	ctgs	-0.1	-2.0	40.5		
TM6	A0	2285.0	ctgs	-2.0	-1.8	44.3		
TM6	A0	2290.0	ctgs	-1.7	-2.3	34.9		
TM6	A0	2295.0	ctgs	-3.4	-3.2	37.9		
TM6	A0	2300.0	ctgs	-1.1	-2.8	27.1		
TM6	A0	2305.0	ctgs	-2.0	-2.3	18.3		
TM6	A0	2310.0	ctgs	-1.8	-2.7	39.1		
TM6	A0	2315.0	ctgs	-1.1	-2.7	38.4		
TM6	A0	2320.0	ctgs	-1.2	-2.7	31.8		
TM6	A0	2325.0	ctgs	-0.2	-2.9	33.7		
TM6	A0	2330.0	ctgs	-0.2	-2.8	31.9		
TM6	A0	2335.0	ctgs	-0.9	-2.9	38.1		
TM6	A0	2340.0	ctgs	-0.8	-2.7	37.1		
TM6	Buah Fm.	2360.0	ctgs			27.8		
TM6	Buah Fm.	2370.0	ctgs	-3.2	-3.1	27.2		
TM6	Buah Fm.	2380.0	ctgs	-5.3	-3.9	31.7		
TM6	Buah Fm.	2395.0	ctgs	-0.5	-3.7	36.5		
TM6	Buah Fm.	2400.0	ctgs	-0.2	-3.3	33.0		
TM6	Buah Fm.	2410.0	ctgs	-2.0	-0.4	29.9		
TM6	Buah Fm.	2420.0	ctgs	-2.7	-3.0	8.0		
TM6	Shuram Fm.	2430.0	ctgs	-3.2	-3.5	18.1		
TM6	Shuram Fm.	2440.0	ctgs	-1.7	-4.1	27.1		
TM6	Shuram Fm.	2460.0	ctgs	-1.8	-3.5	27.0		
TM6	Shuram Fm.	2480.0	ctgs	-2.2	-3.9	14.8		
TM6	Shuram Fm.	2495.0	ctgs	-3.7	-3.7	18.6		
TM6	Shuram Fm.	2505.0	ctgs	-3.4	-4.3	23.3		
TM6	Shuram Fm.	2520.0	ctgs	-3.0	-3.4	25.7		
TM6	Shuram Fm.	2540.0	ctgs	-3.4	-3.3	13.9		

CHAPTER 3
Detection of variable basin restriction using sulfate δ^{34}S in carbonate-evaporite strata:
An example from the Ediacaran-Cambrian Ara Group, Sultanate of Oman

D. A. Fike[1] & J.P. Grotzinger[2]

[1]Department of Earth, Atmospheric, & Planetary Sciences, Massachusetts Institute of Technology, Cambridge, MA 02139, USA

[2]Division of Geological and Planetary Sciences, California Institute of Technology, Pasadena, CA 91125, USA

Abstract

Recent analyses of carbonate-associated sulfate (CAS) demonstrate the potential to generate a high-resolution record of sulfur cycling over most of Earth history. However, significant enrichments or depletions (up to 4‰) are often observed between evaporite and δ^{34}S$_{CAS}$. Here we present high-resolution δ^{34}S measurements from the Ara Group, a series of six carbonate-evaporite sequences spanning ~ 546 – 540 Ma in the Sultanate of Oman. Floor and roof anhydrites bound each of the carbonate units of the Ara Group and were analyzed for δ^{34}S$_{anhyd}$. These anhydrites are compared to previously collected δ^{34}S$_{CAS}$, which shows very little deviation from reconstructed seawater sulfate – with the exception of a transient (~4‰) negative anomaly at the anhydrite-carbonate contact. On the other hand, we observe repeated progressive enrichments in δ^{34}S$_{anhyd}$ (up to 4‰) transitioning from the carbonate-anhydrite to the anhydrite-halite contact. This trends opposes what would be expected solely from sulfate deposition during fractionation crystallization. Rather, we attribute the observed enrichment in δ^{34}S$_{anhyd}$ to continued sulfate reduction in a progressively smaller pool of sulfate. These distillation effects, and those arising solely from fractional crystallization, impart significant variability to evaporite δ^{34}S. We conclude that δ^{34}S$_{CAS}$ recorded in open marine (non-restricted) carbonates may provide the most faithful record of seawater sulfate δ^{34}S for reconstructing sulfur biogeochemical cycling.

Introduction

Biogeochemical cycles define the principal pathways through which the Earth's surface has

evolved over geologic time. In particular, the evolution of the carbon and sulfur cycles has

played a major role in recording the rise of oxygen over Earth history (Berner, 2006; Garrels

and Lerman, 1981; Hayes and Waldbauer, 2006). Abundant carbonate and organic-rich sediments throughout the geologic record have been able to provide a good understanding of the evolution of the carbon cycle (Hayes et al., 1999). In contrast, sulfur cycling is less well understood because the record of sulfate $\delta^{34}S_{SO4}$ has traditionally relied on sparsely distributed marine sulfate evaporite sediments composed of gypsum or anhydrite (Claypool et al., 1980; Holser, 1977; Thode and Monster, 1965). Despite deposition in restricted basins, these minerals are believed to generally record seawater $\delta^{34}S$ within ±2‰ (Raab and Spiro, 1991). As such, evaporite $\delta^{34}S$ has usually been regarded as a sufficiently accurate record of the isotopic composition of seawater sulfate $\delta^{34}S$ (Claypool et al., 1980; Raab and Spiro, 1991).

In attempting to provide a more complete marine $\delta^{34}S_{SO4}$ record, recent studies have turned to non-evaporite sulfate-containing minerals (Burdett et al., 1989; Paytan et al., 1998; Shields et al., 1999). Studies of marine barites yield high-resolution $\delta^{34}S_{SO4}$ records that are resistant to diagenetic alteration (Paytan et al., 1998, 2004). These are, however, limited by the distribution of marine sediments and existing studies have yet to generate the high-resolution records in strata older than the Cretaceous. The technique with the most promise to reconstruct the sulfur cycle through deep time is the analysis of carbonate-associated-sulfate (CAS) – sulfate ions incorporated into carbonate minerals either as lattice substituents for the carbonate ion, in crystal defects, or as small inclusions of calcium sulfate (Burdett et al., 1989; Staudt and Schoonen, 1995). Analyses of $\delta^{34}S_{CAS}$ in modern (unaltered) carbonates indicate that CAS accurately records seawater $\delta^{34}S_{SO4}$ (Lyons et al., 2004; Staudt and Schoonen, 1995). Compilations of $\delta^{34}S_{CAS}$ have the potential to generate a high-resolution record of sulfur cycling over most of Earth history (Kampschulte and Strauss, 2004), particularly in strata

older than the existing marine barite record. The first-order trends in $\delta^{34}S_{SO4}$ from CAS and evaporites are similar; however, significant offsets (>10‰) are observed between $\delta^{34}S$ compilations of evaporites and CAS over the Phanerozoic (Kampschulte and Strauss, 2004). While some of these isotopic differences could be attributed to secular $\delta^{34}S_{SO4}$ variability differentially recorded in non-contemporaneous carbonates and evaporites, it is unlikely that secular changes can account for all of the offsets. In particular, in sections that contain interbedded carbonate and evaporites (thereby eliminating errors due to correlation and secular variability), $\delta^{34}S_{CAS}$ can be enriched or depleted by up to 4‰ with respect to evaporite $\delta^{34}S$ (Kah et al., 2004). As the sulfate $\delta^{34}S$ record becomes better resolved, it is important to understand the cause of these isotopic offsets and determine how best to reconstruct seawater sulfate $\delta^{34}S$ and, thereby, the record of sulfur biogeochemical cycling. It is the aim of this paper to investigate possible isotopic offsets between $\delta^{34}S_{anhydrite}$ and $\delta^{34}S_{CAS}$ as preserved in the Ara Group strata of the Sultanate of Oman.

Geological setting

The Ara Group comprises a series of six carbonate-evaporite cycles (A1, oldest; A6, youngest) (Amthor et al., 2003; Schröder et al., 2003) deposited between ~ 546 and 540 Ma (Bowring et al., 2007) in the subsurface South Oman Salt Basin (SOSB), Sultanate of Oman (Figure 1). Each of these cycles can be divided into a three phases (Amthor et al., 2000): 1) a transition from halite to anhydrite to carbonate deposition, recording successive freshening of the basin; 2) an open marine phase marked carbonate platform development where thrombolite reefs with *Cloudina* and *Namacalathus* existed; and 3) increasing basin restriction indicated by a transition from carbonate to anhydrite to halite deposition.
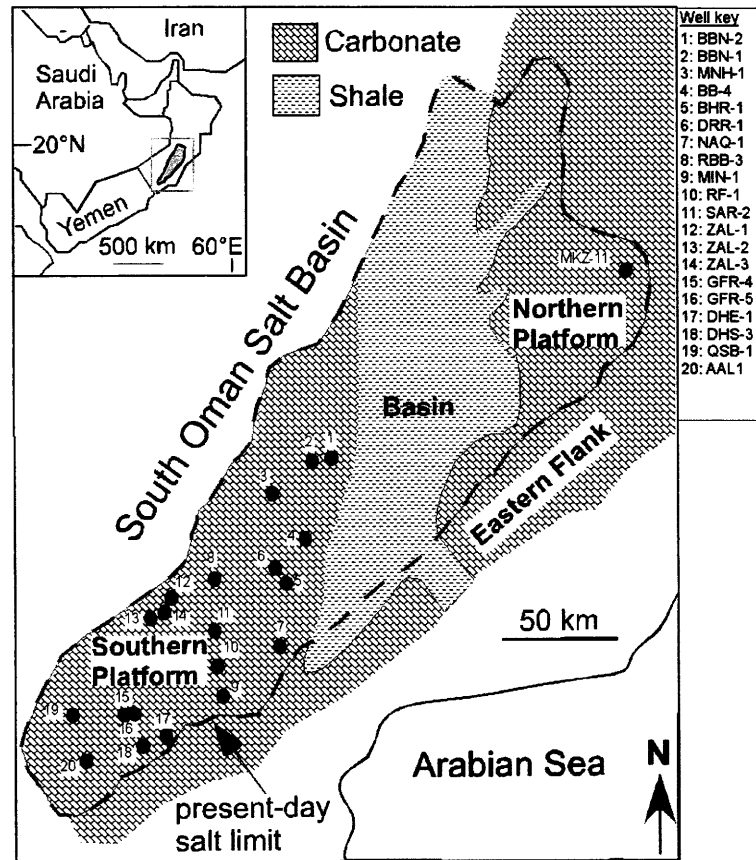
Figure 1: Map of Oman showing Neoproterozoic outcrops and locations of wells that provided subsurface samples.

The maximum flooding surface (MFS) is commonly located close to the anhydrite-carbonate transition and occasionally is characterized by a thin layer of shale (Schröder et al., 2003). The anhydrite immediately below the MFS likely represents a dissolution surface as open marine waters, undersaturated with respect to sulfate evaporites, entered the restricted basin and dissolved the surface layer of anhydrite. Thus, many of the preserved contacts between floor anhydrite (FA) and overlying carbonate are abrupt (Figure 2a,d,g), while others preserve a more gradual transition (Figure 2b,f). The contacts between carbonate and overlying roof anhydrite (RA) are typically gradual (Figure 2e) with the uppermost several meters of

carbonate frequently representing stromatolitic carbonates deposited at or above wave base (Schröder et al., 2003). Subaerial exposure surfaces are not developed at the contacts. The anhydrite with the RAs and FAs ranges from essentially pure anhydrite (Figure 2i,c), to those that contain significant carbonate (Figure 2a), or siliciclastic (Figure 2h,j) contributions.
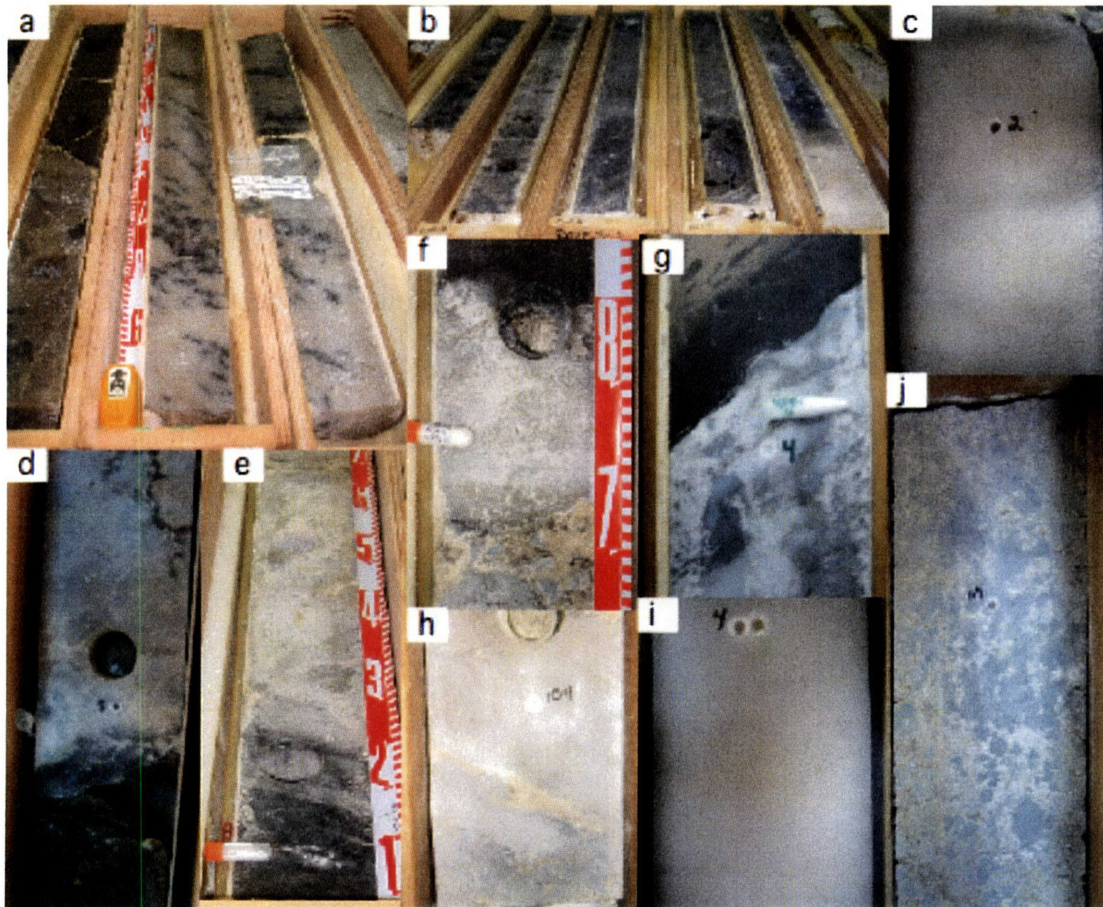
Figure 2: Images of floor and roof anhydrites and carbonate-anhydrite contacts. a) A2 floor anhydrite with a sharp dissolution contact to the basal A2 carbonate unit (shallowing from lower right to upper left, well MNH1). b) A3C floor anhydrite with a gradual contact to the A3 carbonates (shallowing from lower right to upper left, well BHR1). c) Pure A1 anhydrite from well DHE1. d) Transitions from A1 carbonate to A1 roof anhydrite in well DHS3. e) Carbonate to anhydrite transition in the A2 (well QSB1). f) Anhydrite to carbonate transition in the A2 (well QSB1). g) Sharp contact between the A2 floor anhydrite and A2 carbonate in well RBB3. h) Floor anhydrite from the A4 (well BB4). i) Pure A1 anhydrite from well DHE1. j) Floor anhydrite from the A4 (well BB4).

In addition, pyrite is found dispersed throughout the anhydrite and is frequently concentrated

along the MFS, suggesting ongoing bacterial sulfate reduction during the periods of restriction

(Figure 3). It should be noted that the anhydrites bounding the base and top of the Ara

carbonates were most likely deposited as gypsum and underwent recrystallization to anhydrite

during burial. However, the transformation of gypsum to anhydrite is believed to accurately

preserve the original $\delta^{34}S$ composition (Worden et al., 1997). Thus, the anhydrites of the Ara

likely preserve primary $\delta^{34}S_{SO4}$. Analysis of fluid inclusions with the halite of the Ara Group

reveal depleted Ca^{2+} and excess SO_4^{2-}, indicating the continued presence of abundant sulfate

ions throughout deposition of the anhydrite units. Further analyses (Horita et al., 2002;

Schröder et al., 2003) confirm that the evaporitic fluid is derived from seawater; we therefore

preclude possible alteration of evaporitic fluids by non-marine (continental) brines.
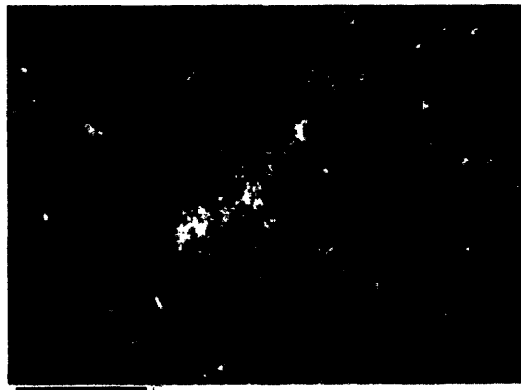
Figure 3: Microprobe image of strata near the anhydrite – carbonate (dolomite) contact in the basal A4 (well BB4). Mineralogy determined using EDS.

Deposition of the Ara Group was accompanied by a shift to an arid climate, and uplift of

basement blocks to form a set of smaller basins that accumulated evaporites and carbonates.

The Ediacaran-Cambrian boundary occurs at the base of the A4 carbonate (Amthor et al.,

2003), based on the 7‰ negative excursion in carbonate $\delta^{13}C$, the disappearance of Ediacaran

Namacalathus and *Cloudina* fossil assemblages, and an intercalated ash bed that yields an age

of 541.0 ± 0.1 Ma (Bowring et al., 2007). The Ara Group stratigraphically straddles the

'Infracambrian' $\delta^{34}S_{SO4}$ maximum (Claypool et al., 1980) and is known to have anhydrite

(Schröder et al., 2004) and CAS (Fike and Grotzinger, 2007) enriched in $\delta^{34}S$. Ara Group

strata are known definitively only from the subsurface. Anhydrite samples analyzed in the

present study were collected from drill core and cuttings from multiple wells across the Ara

basin (Figure 1). These data are compared with previously reported values of carbonate-

associated sulfate $\delta^{34}S$ from the Ara Group carbonates (Fike and Grotzinger, 2007).

Results

High-resolution measurements of anhydrite $\delta^{34}S_{SO4}$ were obtained throughout the floor

(FA) and roof (RA) anhydrites that bound Ara platform carbonates as well as from

intermittent anhydrite cements (AC) within the carbonate units (Figure 4). We observe a

secular trend in $\delta^{34}S$ over the period of Ara deposition, visible in both $\delta^{34}S_{CAS}$ (Fike and

Grotzinger, 2007) and the anhydrite $\delta^{34}S$ presented here. The secular $\delta^{34}S$ trend defines an

increase in $\delta^{34}S$ from ~33‰ at the base of the A1 to a maximum of 41‰ at the A3 carbonate

and then relatively constant $\delta^{34}S$ for the remainder of Ara deposition, with a ~1‰ decrease

during the A4 associated with the Ediacaran-Cambrian boundary $\delta^{13}C_{carb}$ excursion (Amthor

et al., 2003). Superimposed on this trend, CAS $\delta^{34}S$ shows very little (< ~1‰) scatter within

each carbonate unit, except for a transient decrease (up to 4‰) immediately adjacent to the

anhydrite-carbonate contact. Anhydrite $\delta^{34}S$, on the other hand, is variably enriched, where

enrichments are smallest at the carbonate-anhydrite contact and largest (up to 4‰) at the

halite-anhydrite contacts
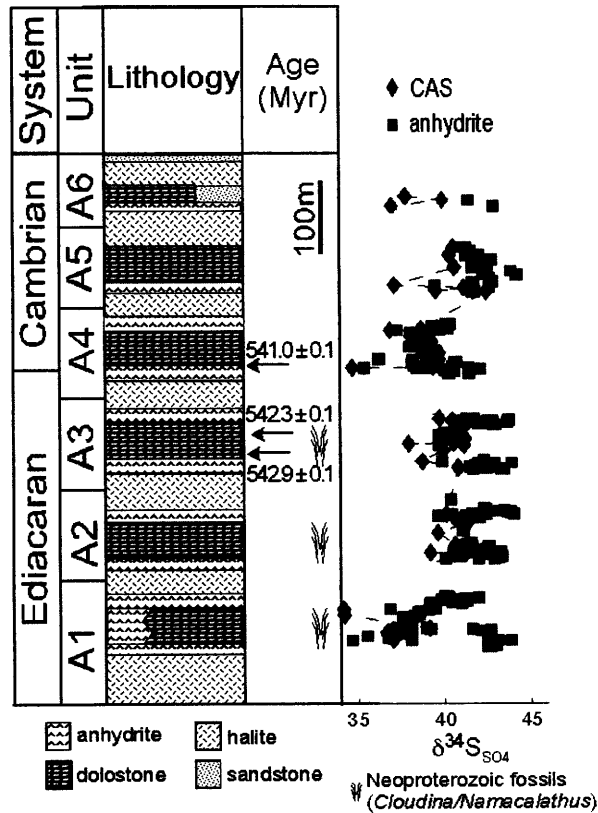
Figure 4: Ara Group $\delta^{34}S$ chemostratigraphy. Anhydrite $\delta^{34}S$ (blue) is typically enriched with respect to CAS (black) by up to several permil.

These patterns can be seen most clearly by examining one Ara cycle in detail. Figure 5

presents the $\delta^{34}S$ variability over the A4 cycle from the well BB4, which has the highest

sampling density. In the basal anhydrite, $\delta^{34}S_{anhyd}$ at the halite-anhydrite contact is enriched

by 3‰ relative to the seawater sulfate, as estimated by the $\delta^{34}S_{CAS}$ trend, and becomes

progressively depleted until it approximates seawater sulfate just below the anhydrite-

carbonate contact. The anhydrite-carbonate contact is characterized by $\delta^{34}S_{CAS}$ (and $\delta^{34}S_{anhyd}$)

depleted by 4‰ relative to seawater sulfate. Throughout the remainder of carbonate

deposition, $\delta^{34}S_{CAS}$ is remarkably consistent and does not deviate from the secular trend by

more than ~ 1‰. This well lacks a sharp carbonate-anhydrite contact and the upper

carbonates show evidence of increasing restriction (e.g., anhydrite cementation). Here the

enrichment in $\delta^{34}S$ begins within the uppermost carbonates (indicated by * in Figure 4) rather

than precisely at the carbonate-anhydrite boundary. The base of the roof anhydrite proper (i.e.,

when there is no longer significant carbonate) then begins with $\delta^{34}S_{anhyd}$ enriched slightly with

respect to inferred seawater and becoming progressively more enriched toward the anhydrite-

halite contact. The symmetric enrichment (most enriched at the anhydrite-halite contact, least

enriched at the anhydrite-carbonate contact) suggests a relationship to changing basin

restriction and the connection to the global ocean.
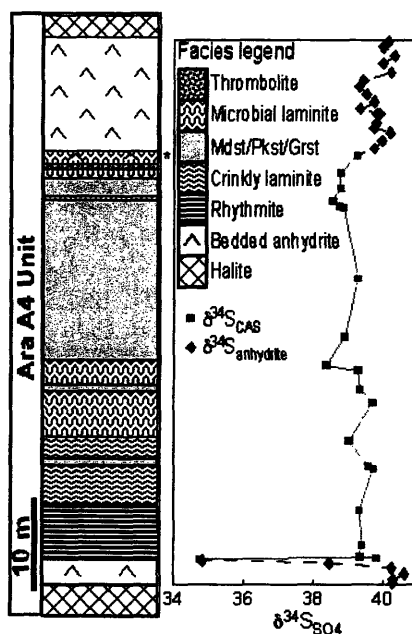
Figure 5: Variability in $\delta^{34}S$ over an entire carbonate-evaporite cycle. Here the A4 cycle (halite-anhydrite-carbonate-anhydrite-halite) from well BB-4 is shown. Carbonate facies are predominantly dolomite and have been mapped in detail (Schröder et al., 2003)

This pattern of $\delta^{34}S_{anhyd}$ variability is observed in each of the Ara units (A1-A5) that has a well-defined FA-carbonate or carbonate-RA transition (Figure 5). In particular, we observe a sharp decrease in $\delta^{34}S_{CAS}$ and $\delta^{34}S_{anhyd}$ across the FA-carbonate contact at the base of each Ara unit. Similarly, we see well-defined enrichment in $\delta^{34}S_{anhyd}$ to 4‰ above coeval seawater sulfate throughout each of the boundary anhydrite units. As such, we believe that this pattern of variable $\delta^{34}S$ is likely to be commonly associated with the deposition of carbonate-evaporite sequences and can be used to understand offsets between CAS and evaporite $\delta^{34}S$ throughout the geologic record.

Enrichment of $\delta^{34}S_{anhyd}$

In open marine conditions, $\delta^{34}S_{CAS}$ records seawater $\delta^{34}S_{SO4}$ including secular variability. Throughout the Ara Group, $\delta^{34}S_{CAS}$ demonstrates very little (inferentially) non-secular variability, which is consistent with previous interpretations of carbonate deposition during open marine conditions (Amthor et al., 2003). The deposition of each Ara unit (anhydrite-carbonate-anhydrite) is believed to have taken ~ 1 Myr (Bowring et al., 2007); deposition of the individual (floor and roof) anhydrite units are likely to have taken significantly less time. Given reasonable estimates (Brennan et al., 2004; Fike and Grotzinger, 2007) for seawater sulfate concentrations (5–16 mM), secular variability during the deposition of each Ara anhydrite unit could not have exceeded ~1‰ (Kah et al., 2004). [Secular (global) $\delta^{34}S$ variability is also highly unlike to oscillate with the same frequency as local (basin) lithologic changes (anhydrite-carbonate).] Thus, the observed enrichment in $\delta^{34}S_{anhyd}$ bounding each of the Ara carbonate units must be a local (i.e., basinal) effect that does not reflect secular change in the global sulfate reservoir.

We now consider the variability observed in both the floor and roof anhydrites. Although the stratigraphic trends in the floor anhydrites $\delta^{34}S$ (decreasing upsection) are opposite those in the roof anhydrites (increasing upsection), both anhydrite units demonstrate increased $\delta^{34}S$ at the halite-anhydrite contact and decreased $\delta^{34}S$ at the anhydrite-carbonate interface. There are undoubtedly second- and third-order changes in restriction during deposition of each anhydrite unit, the first order trend is from maximally restricted at the halite-anhydrite contact to least restricted at the anhydrite-carbonate contact. Thus, there is a correlation between enrichment in $\delta^{34}S_{anhyd}$ and increasing basin restriction, observed in both the floor and roof anydrites for each of the Ara cycles.

We note that this pattern of progressive enrichment in $\delta^{34}S$ with continued basin restriction is opposite that observed in evaporites deposited as a result of progressive evaporation during a single evaporative episode (Raab and Spiro, 1991 and references therein): in these cases, anhydrite/gypsum precipitated during the initial stages of basin restriction is enriched relative to anhydrite/gypsum precipitated during more restricted conditions (e.g., interbedded within halite). Thus, the source of the $\delta^{34}S$ enrichment must be related to evolution of the basinal sulfate reservoir beyond the abiotic equilibrium fractionation associated with the precipitation of sulfate evaporite minerals. These processes result in a ^{34}S-depleted brine and progressively greater depletion in $\delta^{34}S_{evap}$ as gypsum precipitation continues. Specifically, to explain the observed $\delta^{34}S_{anhyd}$ enrichment a process must have been operating during deposition of the Ara anhydrites that resulted in a progressive enrichment in sulfate $\delta^{34}S$ as the basin became more isolated from the ocean. Such mechanisms are abundant and arise chiefly from the biological (microbial) processing of sulfate. Of these, the most common process is bacterial

sulfate reduction (BSR). BSR results in the production of ^{34}S-depleted sulfide and leaves the remaining sulfate brine enriched in δ^{34}S.

The enrichment in $\delta^{34}S_{SO4}$ depends on fractionation factor during BSR and the fraction of sulfate that is reduced to sulfide. Typical fractionations during BSR are ~ 25-35‰ with an experimental range of 4-46‰ (Canfield and Teske, 1996) has been reported and theoretical calculations suggest the upper limit for fractionation may be as high as 70‰ (Brunner and Bernasconi, 2005). The effect of hypersalinity on the rate and isotopic fractionation during BSR remains poorly constrained. Experiments have shown no significant offset between fractionation by freshwater and marine bacteria (Habicht et al., 2002), with the trend toward increasing fractionation with higher sulfate concentrations. A similar fractionation (~30‰) is observed for disseminated pyrites ($\delta^{34}S_{pyr}$ ~ 10‰) within anhydrites of the Ara (Fike, 2007). Nor does elevated salinity necessarily affect the rate of BSR, as significant sulfate reduction is found in sites of active gypsum precipitation (Canfield et al., 2004). Thus, while more work on the salinity dependence of sulfate reduction needs to be done, all existing evidence suggests that hypersaline conditions support active sulfate reduction characterized by sizeable isotopic fractionations. Significant fractionations are expected to continue as long as the sulfate reservoir is not consumed during precipitation of gypsum, as low concentrations of sulfate are known to lead to little or no isotopic fractionation during BSR (Habicht et al., 2002). In the Ara evaporites, however, fluid inclusion work shows that sulfate ions remain abundant throughout halite deposition (Brennan et al., 2004; Horita et al., 2002), suggesting that gypsum deposition was terminated as a result of depleted calcium ions while sulfate concentrations were sufficient for non-limited BSR fractionation.

The observed enrichment in $\delta^{34}S_{anhyd}$ across the Ara strata can be explained as the natural result of continued bacterial sulfate reduction during basin restriction. Here the primary isotopic consequence of basin restriction is that it limits the reservoir of sulfate available both for gypsum/anhydrite deposition and for bacterial sulfate reduction (BSR). Specifically, for a given rate of sulfate reduction, the ^{34}S-enrichment of a sulfate pool would scale inversely with size of the remaining sulfate reservoir. Thus, all other things being equal, a greater enrichment in $\delta^{34}S_{SO4}$ would be expected under more restricted conditions, where less sulfate is available.

Initial gypsum deposition would be enriched relative to seawater by ~1.6‰ (Raab and Spiro, 1991). At this stage, BSR (assuming sulfide is depleted of ~30‰) must reduce sulfate at 5% the rate of evaporite deposition to prevent a depletion in $\delta^{34}S$ during further gypsum deposition. However, to generate further enrichments (up to a total of 4‰ relative to seawater, or 2.4‰ relative to initial gypsum deposition), the relative rate of BSR must increase to 10-15‰ the rate of evaporite deposition. Such elevated rates could be maintained because gypsum deposition became limited by the consumption of available Ca^{2+} ions (Brennan et al., 2004). There are undoubtedly complicating factors to this simple model: the gradient in basin restriction across the anhydrite from halite deposition to carbonate deposition is unlikely to be linear; and microbial sensitivity to salinity changes may result in variable fractionation during BSR. However, the observed consistency of the trends in $\delta^{34}S_{anhyd}$ in each of the Ara units, during both the freshening (halite-anhydrite-carbonate) and restriction (carbonate-anhydrite-halite) phases suggests that BSR-induced enrichment in $\delta^{34}S$ during basin restriction may be a common feature of carbonate-gypsum/anhydrite sequences.

The anhydrite-carbonate transition and $\delta^{34}S$ minimum

A sharp negative excursion (up to 4‰) in $\delta^{34}S$ is observed in each Ara cycle at the anhydrite-carbonate contact. This closely coincides with the maximum flooding surface of each cycle (MFS; Figure 4) and represents the incursion of marine waters into the restricted basin. Relative to the evaporitic brine, the incoming water would have likely been cold and well-oxygenated, resulting in the dissolution of surficial gypsum until the fluid reached sulfate-saturation. However, as outlined above, the $\delta^{34}S$ of gypsum undergoing dissolution would have been equivalent to or slightly enriched relative to the incoming seawater – and therefore not a possible source of the negative $\delta^{34}S$ anomaly at the MFS. Rather, we invoke the oxidation of ^{34}S-depleted sulfides as the cause of the depleted $\delta^{34}S$ at the MFS. The oxidized sulfides were likely the products of BSR, either hydrogen sulfide or sedimentary iron-sulfides (pyrite or metastable iron monosulfides). Disseminated pyrites, depleted in $\delta^{34}S$ (~10‰), are preserved throughout the anhydrite unit and are often concentrated at anhydrite-carbonate contacts (Figure 3). This concentration could be due to gypsum dissolution during the incursion of marine waters or, more likely, the result of stimulated BSR (and pyrite production) due to nutrient influx associated with basin flooding. Oxidative dissolution of such sulfides accompanying the return to open marine conditions could generate the transitory negative excursion in $\delta^{34}S$ observed at the MFS. The stratigraphic extent of depleted $\delta^{34}S$ is minimal (~ 10 cm) and consists of the uppermost few cm of anhydrite (likely influenced by dissolution/re-precipitation) and very basal carbonate sediments. To generate the maximum negative excursion observed (~5‰), oxidized sulfide would have to contribute approximately 15% to the local sulfate pool at the time of maximum flooding. Alternatively, rather than being oxic, the marine waters entering the basin may have been euxinic, carrying ^{34}S-depleted

hydrogen sulfide that oxidized within the basin. The mechanism (sulfide oxidation) for explaining the negative anomaly is the same in these two scenarios, but the source of the sulfide (dissolution of pre-existing evaposedimentary sulfides vs. euxinic marine water) is very different, with significantly different implications for marine redox conditions. There is no evidence for a sulfidic water column during evaporite deposition (e.g., from enrichment of redox-sensitive trace elements or biomarkers indicative of photic-zone euxinia (Fike, 2007)). Given this and the evidence for late Ediacaran ocean oxidation(Canfield et al., 2007; Fike et al., 2006; Kaufman et al., 2007; Scott et al., 2006), a sulfidic ocean reservoir seems unlikely and thus, oxidation of sedimentary sulfides seems the most likely explanation for the transient $\delta^{34}S$ anomaly at the MFS. Despite the relatively short stratigraphic thickness of this anomaly, its presence in each of the Ara cycles indicates that such deviations are likely to be commonly associated with evaporite-carbonate transitions in the rock record.

Conclusions

The Ara Group consists of stacked interbedded carbonate-evaporite cycles. This stratigraphy presents an ideal setting to examine the fidelity of the $\delta^{34}S$ record across multiple carbonate-evaporite transitions, in particular to address systematic offsets between these two seawater sulfate proxies reported in the literature. High-resolution measurements of anhydrite $\delta^{34}S$ were made through the floor and roof anhydrites bounding each carbonate unit in the Ara Group. These data were compared with the existing $\delta^{34}S_{CAS}$ record, which is believed to accurately reflect open marine values (Fike and Grotzinger, 2007). In the Ara Group, $\delta^{34}S_{CAS}$ shows negligible non-secular variation, except for a transitory depletion (up to 4‰ over ~10cm), also observed in $\delta^{34}S_{anhyd}$, across the anhydrite-carbonate contact that is attributed to

sulfide oxidation at the time of basin freshening. In contrast, anhydrite $\delta^{34}S$, representing restricted marine values, is characterized by coherent repeated enrichments (up to 4‰) of anhydrite near the anhydrite-halite contact relative to the anhydrite-carbonate contact. The enrichment in anhydrite is attributed to ongoing bacterial sulfate reduction during progressive basin restriction. In showing how basin restriction can alter $\delta^{34}S_{anhyd}$, we provide a framework for filtering the evaporite $\delta^{34}S$ record to excise artifacts associated with basin restriction. Similarly, our analysis indicates that caution must be used to interpret $\delta^{34}S_{CAS}$ immediately above evaporite-carbonate contacts, particularly when depleted relative to carbonate further from the contact. Based on the parallel study of anhydrite and CAS, we conclude that $\delta^{34}S_{CAS}$, which reflects deposition under open marine (non-restricted) conditions, may be a more faithful record of seawater $\delta^{34}S_{SO4}$ than evaporite $\delta^{34}S$, which can be shifted (enriched or depleted) by as much as 4‰ by as a consequence of basin restriction and freshening.

References

Amthor, J.E., Grotzinger, J.P., Schroder, S., Bowring, S.A., Ramezani, J., Martin, M.W., and Matter, A., 2003, Extinction of Cloudina and Namacalathus at the Precambrian-Cambrian boundary in Oman: Geology, v. 31, p. 431-434.

Amthor, J.E., Reinhardt, J., Grotzinger, J.P., and Cross, N., 2000, Platform to basin transition in terminal Neoproterozoic to Early Cambrian intrasalt carbonates, Ara Group, South Oman Salt Basin, Carbonate Reservoir Characterization and Modeling for Enhanced Hydrocarbon Discovery and Recovery: El Paso, AAPG.

Berner, R.A., 2006, GEOCARBSULF: A combined model for Phanerozoic atmospheric O2 and CO2: Geochimica et Cosmochimica Acta, v. 70, p. 5653 - 5664.

Bowring, S.A., Grotzinger, J.P., Condon, D.J., Ramezani, J., and Newall, M., 2007, Geochronologic constraints on the chronostratigraphic framework of the Neoproterozoic Huqf Supergroup, Sultanate of Oman: American Journal of Science, v. (in press).

Brennan, S.T., Lowenstein, T.K., and Horita, J., 2004, Seawater chemistry and the advent of biocalcification: Geology, v. 32, p. 473-476.

Brunner, B., and Bernasconi, S.M., 2005, A revised isotope fractionation model for dissimilatory sulfate reduction in sulfate reducing bacteria: Geochimica et Cosmochimica Acta, v. 69, p. 4759 - 4771.

Burdett, J.W., Arthur, M.A., and Richardson, M., 1989, A Neogene seawater sulfate isotope age curve from calcareous pelagic microfossils: Earth and Planetary Science Letters, v. 94, p. 189-198.

Canfield, D.E., Poulton, S.W., and Narbonne, G.M., 2007, Late Neoproterozoic Deep Ocean Oxygenation and the Rise of Animal Life Science, v. 315, p. 92 - 95.

Canfield, D.E., Sorensen, K.B., and Oren, A., 2004, Biogeochemistry of a gypsum-encrusted microbial ecosystem: Geobiology, v. 2, p. 133-150.

Canfield, D.E., and Teske, A., 1996, Late Proterozoic rise in atmospheric oxygen concentration inferred from phylogenetic and sulphur-isotope studies: Nature, v. 382, p. 127-132.

Claypool, G.E., Holser, W.T., Kaplan, I.R., Sakai, H., and Zak, I., 1980, The age curves of sulfur and oxygen isotopes in marine sulfate and their mutual interpretation: Chemical Geology, v. 28, p. 199-260.

Fike, D.A., 2007, Carbon and Sulfur Isotopic Constraints on Ediacaran Biogeochemical Processes, Huqf Supergroup, Sultanate of Oman [PhD thesis]: Cambridge, MA, Massachusetts Institute of Technology.

Fike, D.A., and Grotzinger, J.P., 2007, A paired sulfate-pyrite δ 34S approach to understanding the evolution of the Ediacaran-Cambrian sulfur cycle: Geochimica et Cosmochimica Acta, v. submitted.

Fike, D.A., Grotzinger, J.P., Pratt, L.M., and Summons, R.E., 2006, Oxidation of the Ediacaran Ocean: Nature, v. 444, p. 744 - 747.

Garrels, R.M., and Lerman, A., 1981, Phanerozoic cycles of sedimentary carbon and sulfur: Proceedings of the National Academy of Sciences USA, v. 78.

Habicht, K.S., Gade, M., Thamdrup, B., Berg, P., and Canfield, D.E., 2002, Calibration of Sulfate Levels in the Archean Ocean: Science, v. 298, p. 2372-2374.

Hayes, J.M., Strauss, H., and Kaufman, A.J., 1999, The abundance of C-13 in marine organic matter and isotopic fractionation in the global biogeochemical cycle of carbon during the past 800 Ma: Chemical Geology, v. 161, p. 103-125.

Hayes, J.M., and Waldbauer, J.R., 2006, The carbon cycle and associated redox processes through time: Philos Trans R Soc Lond B Biol Sci, v. 361, p. 931-50.

Holser, W.T., 1977, Catastrophic Chemical Events in History of Ocean: Nature, v. 267, p. 403-408.

Horita, J., Zimmermann, H., and Holland, H.D., 2002, Chemical evolution of seawater during the Phanerozoic: Implications from the record of marine evaporites: Geochimica Et Cosmochimica Acta, v. 66, p. 3733-3756.

Kah, L.C., Lyons, T.W., and Frank, T.D., 2004, Low marine sulphate and protracted oxygenation of the proterozoic biosphere: Nature, v. 431, p. 834-838.

Kampschulte, A., and Strauss, H., 2004, The sulfur isotopic evolution of Phanerozoic seawater based on the analysis of structurally substituted sulfate in carbonates: Chemical Geology, v. 204, p. 255-286.

Kaufman, A.J., Corsetti, F.A., and Varni, M.A., 2007, The effect of rising atmospheric oxygen on carbon and sulfur isotope anomalies in the Neoproterozoic Johnnie Formation, Death Valley, USA: Chemical Geology, v. in press.

Lyons, T.W., Walter, L.M., Gellatly, A.M., Martini, A.M., Blake, R.E., Amend, J.P.e., Edwards, K.J.e., and Lyons, T.W.e., 2004, Sites of anomalous organic remineralization in the carbonate sediments of South Florida, USA; the sulfur cycle and carbonate-associated sulfate.: Sulfur biogeochemistry; past and present., v. 379, p. 161-176.

Paytan, A., Kastner, M., Campbell, D., and Thiemens, M.H., 1998, Sulfur isotopic composition of Cenozoic seawater sulfate: Science, v. 282, p. 1459-1462.

—, 2004, Seawater sulfur isotope fluctuations in the cretaceous: Science, v. 304, p. 1663-1665.

Raab, M., and Spiro, B., 1991, Sulfur isotopic variations during seawater evaporation with fractional crystallization: Chemical Geology, v. 86, p. 323 - 333.

Schröder, S., Schreiber, B.C., Amthor, J.E., and Matter, A., 2003, A depositional model for the terminal Neoproterozoic - Early Cambrian Ara Group evaporites in south Oman: Sedimentology, v. 50, p. 879-898.

—, 2004, Stratigraphy and environmental conditions of the terminal Neoproterozoic-Cambrian period in Oman: evidence from sulphur isotopes: Journal of the Geological Society, v. 161, p. 489-499.

Scott, C., Lyons, T.W., Bekker, A., Anbar, A.D., and Williams, G., 2006, Geochemical evidence for the restriction of oxic depositional environments in the Proterozoic ocean, Geological Society of America Annual Meeting: Philadelphia, GSA.

Shields, G.A., Strauss, H., Howe, S.S., and Siegmund, H., 1999, Sulphur isotope compositions of sedimentary phosphorites from the basal Cambrian of China: implications for Neoproterozoic-Cambrian biogeochemical cycling: Journal of the Geological Society, v. 156, p. 943-955.

Staudt, W.J., and Schoonen, M.A.A., 1995, Sulfate incorporation into sedimentary carbonates., *in* Vairavamurthy, M.A., Schoonen, M.A.A., Eglinton, T.I., Luther, G.W., III, and Manowitz, B., eds., Geochemical transformations of sedimentary sulfur. ACS Symposium Series, Volume 612: Washington, DC, United States, p. 332-345.

Thode, H.D., and Monster, J., 1965, Sulfur-isotope geochemistry of petroleum, evaporites, and ancient seas, Fluids in Subsurfaces Environments, Memoir 4, Volume Memoir 4: Tulsa, OK, American Association of Petroleum Geologists, p. 367 - 77.

Worden, R.H., Smalley, P.C., and Fallick, A.E., 1997, Sulfur cycle in buried evaporites: Geology, v. 25, p. 643 - 646.

Appendix A

Table S1: Isotopic data

Table S1: Isotopic data

Well	Sample	Unit	Depth	$\delta^{34}S_{Anhyd}$	$\delta^{34}S_{CAS}$
BBN1	BN-1	A5	3534.0	41.24	40.55
BBN1	BN-2	A5	3540.0	41.51	
BBN1	BN-3	A5	3546.0	41.99	40.30
BBN1	BN-4	A5	3552.0	41.64	
BBN1	BN-5	A5	3560.0	41.85	
BBN1	BN-6	A5	3562.0	42.22	
BBN1	BN-7	A5	3563.0	42.51	
BBN1	BN-8	A5	3565.0	42.31	
BBN1	BN-9	A5	3566.0	42.66	
BBN1	BN-10	A5	3568.0	42.81	
BBN1	BN-11	A4	3682.0	39.32	38.66
BBN1	BN-12	A4	3685.0	37.21	36.87
BBN1	BN-13	A4	3716.0	38.45	38.08
BBN1	BN-14	A4	3734.0	40.59	39.56
BBN1	BN-15	A4	3736.0	41.39	
BBN1	BN-16	A4	3737.0	42.09	
BBN1	BN-17	A4	3740.0	41.42	
BBN1	BN-18	A3	3781.0	39.73	37.93
BBN1	BN-19	A3	3831.0	39.87	38.71
BBN1	BN-20	A3	3868.0	42.42	40.80
BBN1	BN-21	A2	4183.0	42.29	
BBN1	BN-22	A2	4185.0	42.36	
BBN1	BN-23	A2	4194.0	42.11	
BBN1	BN-25	A2	4237.0	41.11	
BBN1	BN-26	A2	4259.0	40.88	
BBN1	BN-27	A2	4264.0	40.02	
BBN1	BN-28	A1	4342.0	39.15	
BBN1	BN-29	A1	4346.0	39.40	
BBN1	BN-30	A1	4358.0	38.93	
BBN1	BN-31	A1	4368.0	38.05	
BBN2	BBN2-102	A4	3843.8	39.60	
BBN2	BBN2-98	A4	3846.7	39.70	
BBN2	BBN2-18	A4	3911.3	40.70	
BBN2	BBN2-17	A4	3912.2	40.48	
BBN2	BBN2-6	A4	3919.1	40.47	
BBN2	BBN2-1	A2	3923.5	40.35	
BHR1	BHR1-52	A3	2484.0	41.97	
BHR1	BHR1-26	A3	2511.0	40.76	

Table S1: continued

Well	Sample	Unit	Depth	$\delta^{34}S_{Anhyd}$	$\delta^{34}S_{CAS}$
BHR1	BHR1-21	A3	2516.2	39.96	
BHR1	BHR1-19	A3	2518.3	40.29	
BHR1	BHR1-12	A3	2525.6	40.95	
BHR1	BHR1-2	A3	2536.0	40.54	
BB4	BB4-90	A4	2893.2	40.13	
BB4	BB4-89	A4	2893.8	40.32	
BB4	BB4-88	A4	2894.7	40.31	
BB4	BB4-87	A4	2895.6	40.16	
BB4	BB4-86	A4	2896.5	40.22	
BB4	BB4-85	A4	2897.4	39.43	
BB4	BB4-84	A4	2898.1	39.30	
BB4	BB4-83	A4	2899.1	39.52	
BB4	BB4-82	A4	2899.8	39.74	
BB4	BB4-81	A4	2900.5	39.34	
BB4	BB4-80	A4	2901.1	39.86	
BB4	BB4-78	A4	2902.2	39.81	
BB4	BB4-77	A4	2902.7	39.73	
BB4	BB4-76	A4	2903.2	40.20	
BB4	BB4-75	A4	2904.1	39.95	
BB4	4-74	A4	2905.0	39.74	
BB4	4-73	A4	2905.8	39.40	39.26
BB4	4-70	A4	2907.7	38.75	38.78
BB4	4-68	A4	2908.7	38.04	
BB4	4-67	A4	2909.3	38.92	38.77
BB4	4-65	A4	2910.8	38.79	38.54
BB4	4-64	A4	2911.4	38.98	38.74
BB4	4-63	A4	2911.5	38.76	38.87
BB4	4-54	A4	2919.3	38.72	39.27
BB4	4-45	A4	2925.6	37.97	38.90
BB4	4-41	A4	2928.8	39.24	38.67
BB4	4-40	A4	2929.4		39.27
BB4	4-37	A4	2931.4	39.50	39.33
BB4	4-36	A4	2932.1	38.75	
BB4	4-35	A4	2932.9	39.54	39.71
BB4	4-29	A4	2937.1	39.33	39.02
BB4	4-28	A4	2937.8	39.54	
BB4	4-25	A4	2939.8	36.22	39.58
BB4	4-24	A4	2940.1	39.47	39.73

Table S1: continued

Well	Sample	Unit	Depth	$\delta^{34}S_{Anhyd}$	$\delta^{34}S_{CAS}$
BB4	4-23*	A4	2940.9	38.15	
BB4	4-18	A4	2944.7	38.10	39.19
BB4	4-17	A4	2945.2	39.14	38.94
BB4	4-13	A4	2948.6	38.25	39.40
BB4	4-9	A4	2949.9	39.54	39.34
BB4	4-8	A4	2950.0	38.89	39.82
BB4	4-7	A4	2950.2	35.37	34.70
BB4	4-5	A4	2950.6	38.46	
BB4	BB4-4	A4	2951.2	40.24	
BB4	BB4-3	A4	2951.8	40.61	
BB4	BB4-2	A4	2952.4	40.28	
BB4	4-1	A4	2952.8	40.26	
BB4	3-9	A3	3029.7	39.65	40.36
BB4	3-6	A3	3032.3	40.92	41.22
BB4	BB4 3-4	A3	3033.6	40.71	40.93
BB4	BB4 3-3	A3	3034.0		40.50
BB4	3-1	A3	3035.0	39.66	41.15
DHE1	DHE-23	A1	2677.5	40.14	
DHE1	DHE-22	A1	2678.8	40.01	
DHE1	DHE-21	A1	2679.5	41.97	
DHE1	DHE-18	A1	2682.1	40.22	
DHE1	DHE-13	A1	2687.3	41.31	
DHE1	DHE-12	A1	2688.1	41.19	
DHE1	DHE-11	A1	2689.2	40.54	
DHE1	DHE-10	A1	2690.3	40.39	
DHE1	DHE-9	A1	2690.9	39.80	
DHE1	DHE-7	A1	2693.4	41.15	
DHE1	DHE-5	A1	2695.1	41.27	
DHE1	DHE-4	A1	2696.2	40.96	
DHE1	DHE-3	A1	2697.0	40.73	
DHE1	DHE-2	A1	2698.3	40.45	
DHE1	DHE-1	A1	2699.3	40.96	
DHS3	DH-2	A1	2956.6	36.79	34.16
DHS3	DH-7h	A1	2963.5		34.19
DHS3	DH-1	A2	2990.1	40.88	40.63
DHS3	DHS3-5	A1	2998.9	43.09	
DHS3	DHS3-4	A1	2999.5	42.55	
DHS3	DHS3-2	A1	3000.8	42.68	

Table S1: continued

Well	Sample	Unit	Depth	$\delta^{34}S_{Anhyd}$	$\delta^{34}S_{CAS}$
DHS3	DHS3-1a	A1	3002.0	42.60	
DRR1	DR-1	A3	2953.5	42.60	
DRR1	DR-2	A3	2953.8	42.15	
DRR1	DR-3	A3	2955.0	42.79	
DRR1	DR-4	A3	2955.6	42.52	
DRR1	DR-5	A3	2956.3	42.81	
DRR1	DR-7	A3	2956.9	42.92	41.24
DRR1	DRR1-3	A3	3009.2	43.88	
DRR1	DRR1-2	A3	3009.4	42.92	
DRR1	DRR1-1	A2	3010.2	43.47	
GFR4	GFR4-8	A3	4636.8	42.25	
GFR4	GFR4-7	A3	4639.7	42.11	
GFR4	GFR4-6	A3	4641.8	42.73	
GFR4	GFR4-5	A3	4642.9	41.79	
GFR4	GFR4-4	A3	4643.9	42.53	
GFR4	GFR4-3	A3	4644.9	41.54	
GFR4	GFR4-2	A3	4645.8	42.30	
GFR4	GFR4-1	A2	4646.7	43.29	
GFR5	GFR5-4	A3	4305.8	41.97	
GFR5	GFR5-3	A3	4311.2	42.72	
GFR5	GFR5-2	A3	4311.4	42.84	
GFR5	GFR5-1	A2	4312.7	41.66	
MIN1	MIN1-4	A1	3448.8	43.82	
MIN1	MIN1-3	A1	3449.8	42.48	
MIN1	MIN1-2	A1	3454.7	42.96	
MIN1	MIN1-1	A1	3455.4	42.44	
MKZ11	MKZ11-1	A3	2184.5	43.73	
MKZ11	MKZ11-2185	A3	2185.0	42.74	
MKZ11	MKZ11-2185.3	A3	2185.3	42.55	
MKZ11	MKZ11-2	A3	2185.5	43.64	
MKZ11	MKZ11-3	A3	2186.5	43.64	
MKZ11	MKZ11-4	A3	2187.9	41.98	
MNH1	MNH1-79	A6	3394.0		37.78
MNH1	MNH1-76	A6	3410.0	41.43	39.92
MNH1	MNH1-75	A6	3450.0	42.88	37.01
MNH1	MNH1-73	A5	3610.0	41.13	
MNH1	MNH1-72	A5	3620.0	41.28	
MNH1	MNH1-71	A5	3630.0	42.74	

Table S1: continued

Well	Sample	Unit	Depth	$\delta^{34}S_{Anhyd}$	$\delta^{34}S_{CAS}$
MNH1	MNH1-70	A5	3640.0	41.69	40.62
MNH1	MNH1-69	A5	3650.0	43.88	
MNH1	MNH1-68	A5	3660.0	44.22	
MNH1	MNH1-65	A5	3690.0	41.69	
MNH1	MNH1-64	A5	3700.0	39.50	37.13
MNH1	MNH1-63	A5	3710.0	42.63	41.16
MNH1	MNH1-59	A5	3800.0	41.35	41.44
MNH1	MNH1-58	A5	3810.0	41.64	39.50
MNH1	MNH1-57	A5	3820.0	41.78	42.45
MNH1	MNH1-53	A3	3960.0	41.27	39.70
MNH1	MNH1-52	A3	3970.0	41.69	
MNH1	MNH1-51	A3	3972.0	41.43	
MNH1	MNH1-50	A3	3976.0	41.69	40.44
MNH1	MNH1-49	A3	3979.0	40.75	40.43
MNH1	MNH1-2h	A3	3979.4		41.18
MNH1	MNH1-5h	A3	3983.5		41.24
MNH1	MNH1-7h	A3	3988.7		39.94
MNH1	MNH1-46	A2	4170.0	41.59	
MNH1	MNH1-45	A2	4171.0	40.41	40.11
MNH1	MNH1-44	A2	4176.0	41.21	40.47
MNH1	MNH1-43	A2	4178.0	42.00	
MNH1	MNH1-42	A2	4179.0	41.67	
MNH1	MNH1-12	A2	4187.3		40.81
MNH1	MNH1-13	A2	4190.4		41.32
MNH1	MNH1-40	A2	4210.0	41.06	
MNH1	MNH1-37	A2	4238.0	41.54	
MNH1	MNH1-36	A2	4242.0	41.44	
MNH1	MNH1-35	A2	4246.0	41.55	40.62
MNH1	MNH1-32	A2	4260.0	41.98	41.26
MNH1	MNH1-28	A1	4424.0	39.44	
MNH1	MNH1-27	A1	4428.0	39.11	
MNH1	MNH1-26	A1	4432.0	39.16	
MNH1	MNH1-25	A1	4436.0	39.24	
MNH1	MNH1-23	A1	4444.0	39.06	
MNH1	MNH1-22	A1	4448.0	38.56	
MNH1	MNH1-21	A1	4452.0	38.45	
MNH1	MNH1-20	A1	4456.0	38.45	
MNH1	MNH1-19	A1	4460.0	38.22	

Table S1: continued

Well	Sample	Unit	Depth	$\delta^{34}S_{Anhyd}$	$\delta^{34}S_{CAS}$
MNH1	MNH1-18	A1	4464.0	37.59	
MNH1	MNH1-17	A1	4468.0	38.06	
MNH1	MNH1-16	A1	4472.0	37.92	
MNH1	MNH1-15	A1	4476.0	37.66	
MNH1	MNH1-14	A1	4480.0	37.60	
MNH1	MNH1-13	A1	4484.0	37.56	
MNH1	MNH1-10	A1	4496.0	39.13	39.11
MNH1	MNH1-9	A1	4500.0	38.02	36.99
MNH1	MNH1-8	A1	4504.0	37.27	36.66
MNH1	MNH1-6	A1	4512.0	37.02	36.74
MNH1	MNH1-5	A1	4516.0	35.49	36.69
MNH1	MNH1-4	A1	4520.0	36.68	37.96
MNH1	MNH1-2	A1	4528.0	34.64	37.01
NAQ1	NAQ1-62	A2	3295.8	42.40	
NAQ1	NAQ1-61	A2	3296.8	41.88	
NAQ1	NAQ1-60	A2	3297.8	39.60	
NAQ1	NAQ1-28	A2	3329.9	41.42	
QSB1	QSB1-6	A2	5564.5	42.66	
QSB1	QSB1-5	A2	5565.5	42.79	
QSB1	QSB1-4	A2	5566.1	41.73	
QSB1	QB-7bh	A2	5567.0		40.51
QSB1	QSB1-3	A2	5567.0	42.79	
QSB1	QSB1-2	A2	5571.1	43.13	
QSB1	QSB1-1	A2	5571.7	42.88	
RBB3	RB-5h	A2	4728.9		39.61
RBB3	RBB3-4	A2	4729.4	43.24	
RBB3	RBB3-3	A2	4729.7	42.37	
RBB3	RBB3-2	A2	4730.1	43.29	
RBB3	RBB3-1	A2	4730.8	41.96	
RF1	RF1-3	A1	3790.8	41.60	
RF1	RF1-2	A1	3791.7	42.67	
RF1	RF1-1	A1	3792.1	42.11	
SAR2	SAR2-4	A3	4144.3	42.87	
SAR2	SAR2-3	A3	4145.3	42.43	
SAR2	SAR2-2	A3	4146.0	42.62	
SAR2	SAR2-1	A3	4147.3	41.48	
ZAL1	Z1-2	A2	5038.0	40.49	39.17
ZAL1	Z1-1	A2	5042.0	40.76	

Table S1: continued

Well	Sample	Unit	Depth	$\delta^{34}S_{Anhyd}$	$\delta^{34}S_{CAS}$
ZAL2	ZAL2-7	A2	4914.6	43.46	
ZAL2	ZAL2-6	A2	4915.5	43.16	
ZAL2	ZAL2-5	A2	4916.5	43.79	
ZAL2	ZAL2-4	A2	4917.5	43.68	
ZAL2	ZAL2-3	A2	4918.5	43.86	
ZAL2	ZAL2-2	A2	4919.5	43.99	
ZAL3	ZAL3-6	A2	5017.9	41.26	
ZAL3	ZAL3-5	A2	5018.5	42.55	
ZAL3	ZAL3-4	A2	5019.1	42.32	
ZAL3	ZAL3-3	A2	5020.5	42.59	

CHAPTER 4
The Ediacaran-Cambrian boundary:
a two-stage record of ecological and geochemical change

D. A. Fike[1], J. P. Grotzinger[2], G. D. Love[3], and R. E. Summons[1]

[1]Department of Earth, Atmospheric, & Planetary Sciences, Massachusetts Institute of Technology, Cambridge, MA 02139, USA

[2]Division of Geological and Planetary Sciences, California Institute of Technology, Pasadena, CA 91125, USA

[3]Department of Earth Sciences, University of California Riverside, Riverside, CA 92521, USA

ABSTRACT

The Ediacaran-Cambrian (E-C) Boundary (~541 Ma) straddles a record of extinction of Ediacaran organisms and the subsequent radiation of skeletal invertebrates during the Cambrian explosion. Globally, E-C boundary sections are characterized by a negative excursion in $\delta^{13}C_{carb}$ previously interpreted to have resulted from anoxia. Here we document $\delta^{13}C_{org}$, $\delta^{15}N_{org}$, redox-sensitive trace elements, and a suite of lipid biomarkers in strata spanning the E-C boundary excursion from the Ara Group of Oman. This 7‰ $\delta^{13}C_{carb}$ excursion is attributed to the remineralization of organic matter with no evidence for enhanced methane release. An accompanying but smaller (4‰) $\delta^{13}C_{org}$ excursion indicates a change in organic reworking and preservation. A coeval positive excursion in $\delta^{15}N_{org}$ indicates water-column denitrification, supported by elevated V/Cr. Rhenium, uranium, and molybdenum enrichments indicate periodic anoxia throughout the E-C boundary $\delta^{13}C_{carb}$ excursion. In the strata immediately preceding the $\delta^{13}C_{carb}$ excursion, there is evidence for a collapse of photic zone primary production, characterized by decreased abundance of (cyano-)bacterial and microalgal biomarkers, coupled to localized occurrence of anoxia. Immediately after the E-C boundary, however, biomarkers indicate a rapid recovering of the microbial community with a well-oxygenated photic zone that persists throughout the negative excursion. This constrains anoxia/euxinia to be limited to near-sediment environments. Nonetheless, persistent anoxia following the excursion likely had a role in the disappearance of the bottom-dwelling Ediacaran fauna.

INTRODUCTION

The Ediacaran-Cambrian (E-C) Boundary, ca. 541 million years ago (Ma) (Bowring et al., 2007) marks the sudden extinction of the first metazoan (Ediacaran soft-bodied and lightly calcified faunas) and sets the stage for the subsequent radiation of skeletalized invertebrates in the Cambrian (Amthor et al., 2003; Brasier and Lindsay, 2000; Marshall, 2006). The E-C boundary is coincident with a 7‰ negative excursion (Amthor et al., 2003) in the carbon isotopic composition of carbonate minerals ($\delta^{13}C_{carb}$), lasting ~ 1 Myr, which is often used to correlate different boundary sections in the absence of palaeontological or geochronological constraints (Bartley et al., 1998). Despite significant study (Bartley et al., 1998; Kimura and Watanabe, 2001; Schröder and Grotzinger, 2007), the origin of the $\delta^{13}C_{carb}$ excursion and the degree to which it can be causally related (Brasier and Lindsay, 2000; Marshall, 2006) to the extinction and subsequent radiation remain poorly understand. Previous work has ascribed the $\delta^{13}C$ excursion to changes in primary productivity (Bartley et al., 1998), methane release (Kirschvink and Raub, 2003), ecosystem reorganization (Bambach et al., 2002), and anoxia, based on enrichments in redox-sensitive trace elements (Kimura and Watanabe, 2001; Schröder and Grotzinger, 2007). There is, however, no concrete understanding of how widespread anoxia would have been, its cause, or how, if at all, it relates to putative changes in primary production or ecosystem reorganization.

We have attempted to constrain the nature of the $\delta^{13}C_{carb}$ excursion by examining multiple geochemical and isotope proxies from replicate sections that pass through the E-C boundary as preserved in the Ara Group, Sultanate of Oman. To complement this approach, we investigate the changes over this interval in a suite of lipid biomarkers, chemical compounds originating from organisms previously living in the water column or in sediments.

These compounds can be traced to specific phylogenetic taxa (e.g, eukaryotes, cyanobacteria) or to specific metabolic pathways (e.g., oxygenic photosynthesis, methanogenesis) (Brocks and Summons, 2003) and, thus, can characterize ecological change across the E-C boundary.

GEOLOGICAL SETTING

Ara Group strata of the Sultanate of Oman were deposited between ca. 547 – 540 Ma (BOWRING et al., 2007). The Ara Group and E-C boundary strata are known definitively only from the subsurface (AMTHOR et al., 2003; MATTES and CONWAY-MORRIS, 1990). The basal contact between the Ara Group and the underlying Buah Formation is marked by a disconformable, karstic surface (Loosveld et al., 1996). The Ara Group is separated from the overlying middle Cambrian to Silurian age clastics of the Haima Supergroup by a regionally extensive angular unconformity (Millson et al., 1996). The Ara Group exists as a series of six carbonate-evaporite shallowing upward cycles, deposited in strongly subsiding block-faulted basin (Amthor et al., 2003; Schröder et al., 2003). Because of very high basin subsidence (Grotzinger et al., 2002), the Ara Group contains an expanded record the E-C boundary and likely includes strata not well represented in other sections (e.g., Namibia, Siberia). In addition, the Ara Group strata have very low thermal maturity, preserving a minimally compromised record of ecological conditions. As such, the Ara strata may provide an unparalleled window into the biogeochemical processes operating across the E-C boundary.

The presence of multiple volcanic ash horizons within Ara Group strata has significantly improved our understanding of the timing and duration of Ara deposition and our ability to correlate the Oman stratigraphy with other sections globally (AMTHOR et al., 2003; BOWRING et al., 2007; GROTZINGER et al., 1995). An age of 546.72 ± 0.22 Ma from the middle of the

basal Ara carbonate (A0) constrains the unconformity at the Buah-Ara contact to ~1 Myr

(BOWRING et al., 2007). Ash beds at the base (AMTHOR et al., 2003; BOWRING et al., 2007)

and top (BOWRING et al., 2007) of the third carbonate unit (A3) yield zircon U/Pb ages of

542.91 ± 0.13 and 542.31 ± 0.14 Ma, respectively. These A3 ages indicate that deposition of

an Ara carbonate unit took ~ 1 Ma. The base of the A4 carbonate unit contains an ash that

yielded a U/Pb age (AMTHOR et al., 2003; BOWRING et al., 2007) of 541.00 ± 0.12 Ma. This

age, in combination with a 7‰ negative excursion in carbonate $\delta^{13}C$ and the disappearance of

Ediacaran *Namacalathus* and *Cloudina* fossil assemblages, is the basis for the identification of

the E-C boundary at the base of the A4 carbonate in Oman (AMTHOR et al., 2003). There is a

robust correlation of the A4 unit (containing the E-C boundary) across the basin, based on the

presence of both the 541 Ma ash at the base of the A4 carbonate and the overlying E-C

boundary $\delta^{13}C_{carb}$ excursion (AMTHOR et al., 2003).Strata spanning the E-C boundary (A3-A5

carbonates) were sampled from different locations, spanning more than 100 km (Figure 1).
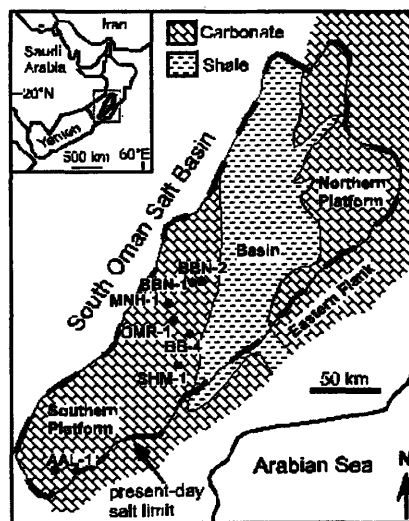
Figure 1: Map of the Sultanate of Oman, highlighting the location of the modern day South Oman Salt Basin. The locations of wells that provided subsurface samples for this study are shown.

In addition, basal Ara (A0) and A2 carbonates were examined to better constrain biomarker variability leading up to the E-C boundary. Wells analyzed in the present study are shown in Figure 1.

GEOCHEMICAL RESULTS

We have examined geochemical and isotopic variation in strata from five wells, placing the E-C boundary excursion within the A4 carbonate in the context of the underlying A3 and overlying A5 carbonates. This provides a baseline against which to compare changes across the E-C boundary. Here we present $\delta^{13}C_{org}$, $\delta^{15}N_{org}$, and redox-sensitive trace elements in their lithostratigraphic context referenced to the E-C boundary by their $\delta^{13}C_{carb}$ chemostratigraphy and the presence of the 541.0 Ma ash bed (Figure 2, Table S1). The Ara Group is characterized by a relatively constant $\delta^{13}C_{carb} \sim 3‰$ through its entirety – with the exception of the E-C boundary excursion (Figure 2a). Here, $\delta^{13}C_{carb}$ decreases to -5‰ in the basal A4 carbonate at the nadir of the E-C boundary excursion, before gradually rising to -2‰ at the top of the A4 carbonate. By the base of the A5 carbonate, $\delta^{13}C_{carb}$ has returned to the pre-excursion baseline of +3‰. We note that there is no parallel shift in $\delta^{18}O$ during the $\delta^{13}C$ excursion (Table S1), making a diagenetic origin for the $\delta^{13}C_{carb}$ excursion unlikely.

A negative excursion of the same duration, but smaller magnitude (4‰) is seen in $\delta^{13}C_{org}$ (Figure 2b). The baseline value for $\delta^{13}C_{org}$ from the A3 carbonate is -31‰. The most depleted samples contain $\delta^{13}C_{org}$ of -35‰, increasing slightly toward the top of the A4 carbonate. In contrast to $\delta^{13}C_{carb}$, there is no return in $\delta^{13}C_{org}$ to less depleted values in the A5. There is more scatter in the $\delta^{13}C_{org}$ signal than in $\delta^{13}C_{carb}$, particularly at the anhydrite-carbonate transitions, which is attributed to changing biological fractionation and/or

community structure associated with the transition from restricted to open marine conditions. The parallel excursions in $\delta^{13}C_{carb}$ and $\delta^{13}C_{org}$ also indicate a diagenetic origin for the $\delta^{13}C_{carb}$ excursion is improbable. The $\delta^{13}C_{org}$ excursion is seen in both total organic carbon (TOC) and in bitumen (solvent extractable organic matter) (Table S1). This agreement between $\delta^{13}C_{org}$ from TOC and bitumen and the observed co-variation between $\delta^{13}C_{carb}$ and $\delta^{13}C_{org}$ are evidence that the bitumen in these rocks is indigenous and has not migrated. This is important for evaluating $\delta^{15}N_{org}$ and the biomarker distributions that are analyzed from bitumen extracts (see below).
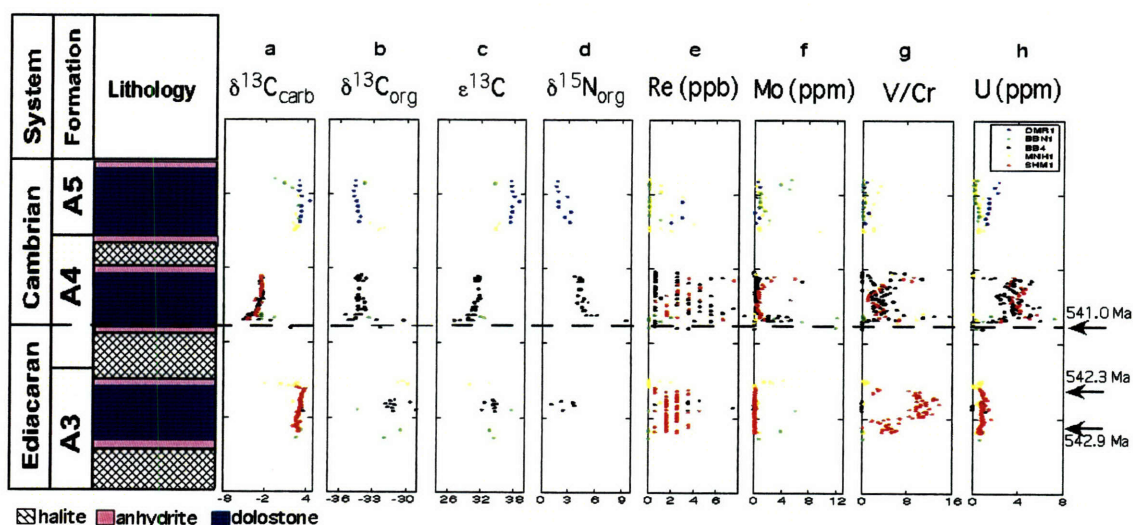
Figure 2: Isotope and trace element chemostratigraphy of the A3-A5 units of the Ara Group. The E-C boundary is indicated by the dashed line. U/Pb ages from Bowring et al. (2007) are shown on the right. a) $\delta^{13}C_{carb}$ showing the EC boundary negative excursion. b) $\delta^{13}C_{org}$. c) ε = $\delta^{13}C_{carb} - \delta^{13}C_{org}$. d) Bitumen $\delta^{15}N_{org}$. e) Rhenium (ppb), f) Molybdenum (ppm). g) Redox-sensitive ratio V/Cr. h) Uranium (ppm). Data are color coded by well (legend upper right).

It is difficult to interpret $\delta^{13}C_{org}$ values in isolation because they depend on both the initial composition of DIC that becomes incorporated into biomass and the isotopic fractionation associated with carbon fixation, in addition to changes in biogenic input and preservation. To

understand changes in carbon cycling independent of variations in $\delta^{13}C$, it is useful to examine $\varepsilon = \delta^{13}C_{carb} - \delta^{13}C_{org}$, the offset between the isotopic composition of carbonate and organic carbon (Figure 2c). Observations of ε allows for ready recognition of changes in $\delta^{13}C_{org}$ relative to $\delta^{13}C_{carb}$, such as may be expected to result from changes in (micro)biological community structure (Hayes, 2001) and/or environmental conditions (Laws et al., 1995; van Dongen et al., 2006; Van Kaam-Peters et al., 1998), and to differentiate these from changes in organic carbon burial (constant ε). Following the recognition of parallel trends in both $\delta^{13}C_{carb}$ and $\delta^{13}C_{org}$ (Knoll et al., 1986), it has become standard practice in studies with paired $\delta^{13}C_{carb}$ - $\delta^{13}C_{org}$ data to assume constant ε, align $\delta^{13}C_{carb}$ and $\delta^{13}C_{org}$ and treat the combined data as a single variable (Calver, 2000; Kaufman et al., 1991; Kimura et al., 1997). This practice of asserting an invariant ε masks the natural variability in ε and the information this variability provides about community structure. Here, we observe a decrease in ε from 34‰ to 31‰ across the E-C boundary excursion (Figure 2c). After the excursion, ε increases beyond its pre-excursion values (up to 37‰) in the A5 carbonate.

There is a positive excursion in $\delta^{15}N_{org}$ (Figure 2d) across the E-C boundary with the same duration as that found in $\delta^{13}C$. Here, $\delta^{15}N$ rises from a baseline of ~2‰ to a maximum of ~9‰ at the nadir of the $\delta^{13}C$ excursion, gradually declining to ~4‰ at the top of the A4. By the base of the A5 carbonate, $\delta^{15}N_{org}$ has returned to its baseline of ~2‰. Bitumen (rather than TOC) samples were used for $\delta^{15}N_{org}$ analysis to avoid any possible alteration to the TOC $\delta^{15}N_{org}$ due to inorganic nitrogen (e.g., nitrogen adsorption onto clay particles). Based on the similarity in bitumen $\delta^{13}C_{org}$ and $\delta^{13}C_{carb}$ profiles, we are confident that the bitumen is indigenous and, thus, the bitumen $\delta^{15}N$ signal is representative of co-occurring bulk $\delta^{15}N_{org}$.

By analyzing only bitumen from unmetamorphosed strata of low thermal maturity, we have minimized post-depositional alteration in the $\delta^{15}N_{org}$ record.

The redox-sensitive trace elements are variously enriched across the A4, relative to the A3 and A5 carbonates (Figure 2e-h). Rhenium is a redox-sensitive trace element that is conservative in seawater, but typically enriched in anoxic sediments following iron and uranium reduction (Crucius et al., 1996). There is a slight Re enrichment in the A4 and the A5 carbonates have less Re than the A3 carbonates (Figure 2e). Overall, however, typical Re concentrations were not significantly above the detection level to observe any clear signal and these data are not discussed further. Molybdenum is typically enriched in reducing (sulfidic) sediments, where it binds to organic matter or iron sulfides (Zheng et al., 2000). Significant Mo enrichment, though, depends on a continued supply of molybdate from oxic waters and is believed to be an indication of euxinic (oxic-sulfidic transition within the water-column) conditions (Crucius et al., 1996; Lyons et al., 2003). There is considerable Mo enrichment (Figure 2f) across the lower portion of the A4 carbonate, during the most negative portion of the $\delta^{13}C$ excursion. Vanadium and chromium are redox-sensitve trace elements that have their redox-transition under conditions associated with nitrate reduction (Jones and Manning, 1994; Piper, 1994). The ratio V/Cr can be used to identify redox conditions more reducing than nitrate reduction (Piper and Isaacs, 1995). The ratio V/Cr (Figure 2g) is enriched across the entire A4, with elevated enrichment in the basal A4 with the most negative $\delta^{13}C$. The A4 enrichment in V/Cr is observed in all wells, suggesting uniform environmental conditions. Interestingly, V/Cr is also enriched in one section in the A3 (well SHM1), possibly suggesting spatially localized anoxia. Uranium is enriched under anoxic conditions typical of sulfate reduction in the marine environment, either by adsorption or direct precipitation (Jones and

Manning, 1994; Piper and Isaacs, 1995). Uranium (Figure 2h) concentrations are uniformly enriched throughout the A4 carbonate relative to values in the A3 and A5 carbonates.

BIOMARKER DATA

We have measured a series of lipid biomarker parameters across the excursion to relate the observed geochemical changes to those in the microbial ecosystem (Table S2). Specifically, biomarkers were quantified from samples in the Ara A0, A2, A3, A4, and A5 carbonate units. Counter to our expectations, the suite of A4 biomarkers is not significantly different from those in the basal Ara (A0) or in the upper Ara (A5), suggesting minimal impact to the planktonic microbial ecosystem associated with the metazoan decline, Ediacaran organisms, $\delta^{13}C_{carb}$ negative excursion, and apparent anoxia at the E-C boundary. However, several biomarker parameters record dramatic shifts in the A2 and A3 carbonates, deposited in the interval immediately preceding the E-C boundary (Figure 3).

Lipid biomarkers are classified into broad groups by their parent hydrocarbon backbone. The majority of biomarkers in the present study fall into two categories: steranes, tetracyclic triterpenoids biosynthesized by eukaryotes, with minor and structurally distinctive components from some bacteria (Brocks and Summons, 2003; Volkman, 2003, 2005); and hopanes, pentacyclic triterpenoids derived from the bacteriohopanepolyols (BHPs) biosynthesized by diverse bacteria, including cyanobacteria and methylotrophs (Brocks and Summons, 2003; Summons and Jahnke, 1992; Summons et al., 1999). In addition, we have quantified the abundance of tricyclic terpenoids, biosynthesized by phylogenetically unresolved bacteria (Peters et al., 2005). The overall abundances of tricyclics, steranes, and hopanes, relative to TOC, are significantly decreased in the A2 (Figure 3a).
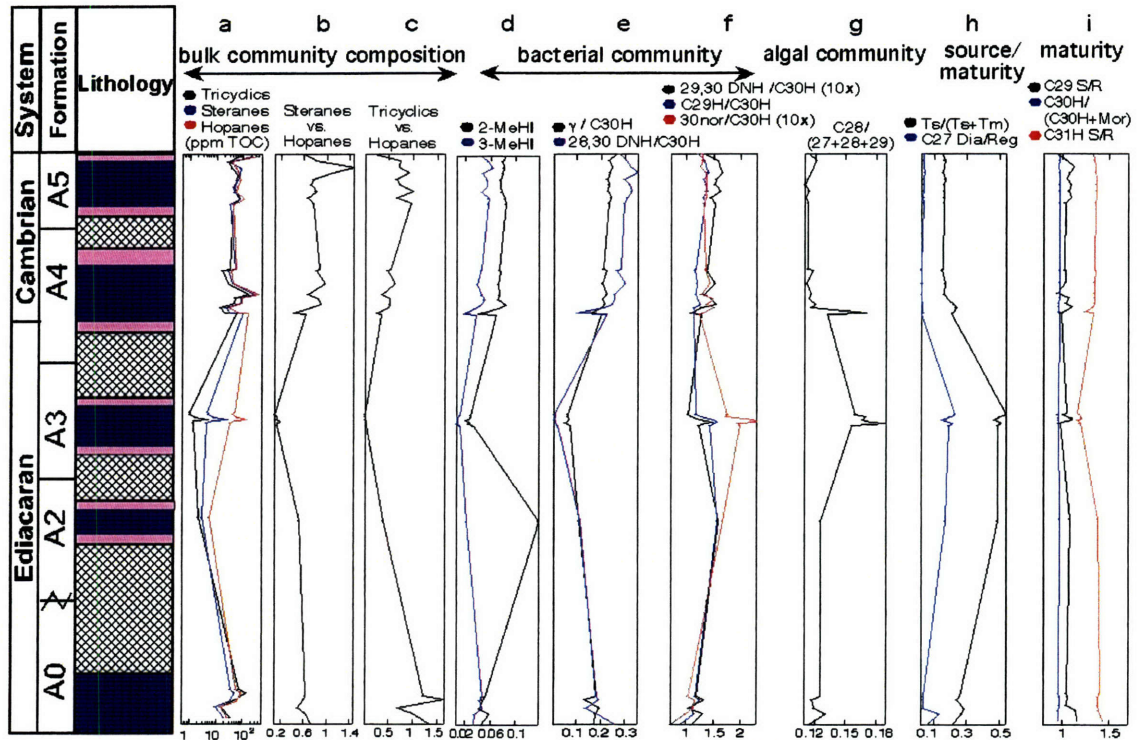
Figure 3: Biomarker stratigraphy of the A0, A2, A3, A4, and A5 units of the Ara Group. The E-C boundary lies at the base of the A4 unit. Lithologies are the same as in Figure 2.

Hopanes return to previous levels in the A3, although it is not until the A4 that tricyclics and steranes are restored to prior abundances. The ratio of steranes to hopanes (S/H), is an approximates of the relative contribution of eukaryotic *versus* bacterial biomass in the ecosystem (Gely et al., 1993; Peters et al., 2005). S/H (Figure 3b) decreases from its baseline value of 0.6 in the A0 to less than 0.2 in the uppermost A3, and gradually rises through the A4 to stabilize at ~0.8 in the upper A4 and A5 units. The ratio of tricyclics to hopanes (T/H) also has a minimum (0.2) in the A3 with a post-excursion abundance (~0.6) less than the pre-excursion value (~1.2) (Figure 3c). Data for hydrocarbon concentrations (ppm TOC) show that the A3 decrease in S/H and T/H is caused primarily by a recovery in hopane abundance (Figure 3a), although the overall contents of both steranes and hopanes are lower in the A2 and A3 than the remainder of the Ara. Since the sterane/hopane ratio is a first-order

characterization of an ecosystem, such significant changes indicate a considerable shift in microbial community structure. These changes are apparent in both the bacterial and microalgal communities. The 2-methylhopane (2-MeHI = 2α-methyl-$\alpha\beta$-hopane/(2α-methyl-$\alpha\beta$-hopane + $\alpha\beta$-hopane) and the 3-methylhopane (3-MeHI = 3β-methyl-$\alpha\beta$-hopane/(3β-methyl-$\alpha\beta$-hopane + $\alpha\beta$-hopane) indices (Figure 3d) are proposed to record the relative contribution of cyanobacterial (2-MeHI) and methylotrophic/methanotrophic (3-MeHI) input to generalized bacterial biomass (Brocks and Summons, 2003). The 2-MeHI rises sharply in the A2, decreases in the A3, and returns to previous and slightly higher values in the A4 and A5 units, respectively. The 3-MeHI decreases in the A2 and A3 units relative to the other Ara carbonates.

Additional proxies for bacterial community composition are found in the relative abundance of gammacerane (γ) and 28,30-dinorhopane (DNH), normalized to $\alpha\beta$-hopane (C_{30}) (Brocks and Summons, 2003; Peters et al., 2005). Decreases in these proxies during the A3 (Figure 3e) argue against elevated salinity or stratification as possible explanations for the observed variations in bulk community composition (Brocks and Summons, 2003). Correlated increases throughout the A2/A3 in several hopane breakdown products (Figure 3f), particularly the relative abundances of 29,30-DNH, C_{29} $\alpha\beta$-hopane, and 30-nor-$\alpha\beta$-hopane normalized to $\alpha\beta$-hopane, indicate a change in organofacies and/or the composition of original organic material, particularly with regard to the distribution pattern of (poly)functionalized side-chains of BHPs (Rohmer et al., 1992). While unable to unambiguously point to specific phylogenetic alterations within the microbial community, these data indicate significant change in bulk bacterial community composition within the A2/A3.

Also within the A3, we see evidence for a reorganization of the microalgal community. In particular, there is an increase in the relative abundance of C_{28} steranes (Figure 3g), which are diagnostic for chlorophyll *c*-containing algae (Peters et al., 2005; Volkman, 2003). This increased abundance of C_{28} steranes persists through the early A4. Throughout all Ara units, however, chlorophytes (green algae) are the dominant algal input as signified by high amounts of C_{29} steranes relative to other sterane carbon numbers.

A change in organofacies is indicated by increases in the A2 and A3 of the biomarker parameters that are sensitive to organic source, specifically the ratio of Ts/(Ts+Tm) C_{27} hopanes and the relative abundance of C_{27} diasteranes to C_{27} regular steranes (Figure 3h). Both of these ratios are also sensitive to thermal maturity (Peters et al., 2005); however, standard maturity indicators (Figure 3i), such as C_{29} sterane 20S/20R, C31 hopane 22S/22R and the ratio of hopane to its less thermodynamically stable moretane ($\alpha\beta$-hopane/($\alpha\beta$-hopane + $\beta\alpha$-hopane)), show that the biomarker suite is essentially uniformly mature. Thus, the variations during the A3 shown in Figure 3h can be confidently attributed to variations within the depositional environment, such as increased abundance of clay minerals, an increase in the clay/TOC ratio, or a change in abundance of the specific compounds that undergo diagenetic rearrangement (Peters et al., 2005; van Kaam-Peters et al., 1998).

INTERPRETATIONS

By their very nature, geochemical proxies and lipid biomarkers can reflect both water column and sedimentary environments as well as conditions during deposition and diagenesis. Despite these complications, parallel application of these proxies can extract significant environmental and ecological information that would be otherwise unavailable. Here, we can

use geochemical speciation and biomarker distributions to understand ecological change leading up to and across the E-C boundary.

Precursor events to the E-C boundary

In all Ara units, biomarker patterns (particularly C_{29}/C_{30} hopane >1, low diasterane content, low $Ts/(Ts+Tm)$, and significant 28,30-dinorhopane and 24-n-propylcholestane contents) are consistent with these being derived from a marine carbonate environment. Trace element abundances indicate overall oxic water-column conditions throughout the lower Ara strata. The presence of oxic conditions in the lower Ara is consistent with the appearance of bacterial sulfur disproportionation and the oxidative sulfur cycle in the uppermost Buah Formation immediately underlying the basal Ara (Fike et al., 2006) and the reports of oxic conditions in other sections globally (Canfield et al., 2007; Kaufman et al., 2007). Despite overlying oxic conditions, pristane/phytane ratios of ~0.4 throughout the Ara indicate reducing conditions persisted in the sediment throughout Ara depositon. During A2/A3 time we see significant decreases in the total biomarkers for eukaryotes and bacteria, with a relative increase in bacterial biomass particularly cyanobacteria. Combined with the other evidence for major ecosystem change, we infer there was a reorganization of the microbial ecosystem at this time, particularly primary production within the photic zone, which dominates total hopane and sterane production (Brocks and Summons, 2003; Peters et al., 2005). This occurs in parallel with evidence for (at least spatially restricted) water-column denitrification (Figure 2g).

The E-C boundary

The E-C boundary, marked in Oman by the onset of the negative $\delta^{13}C_{carb}$ excursion (Amthor et al., 2003), appears to usher in an interval of more widespread anoxia that spans the period of A4 deposition (~ 1 Myr, Bowring et al. 2007). The recovery of biomarker abundances and parameters in the A4, after their anomalous A2 and A3 values, suggest a rapid resurgence of photic zone primary production within the E-C boundary $\delta^{13}C$ excursion. Further, the constancy of these parameters and the absence of aryl isoprenoids, which are indicative of photic zone euxinia, argue for predominantly oxic surface conditions throughout the $\delta^{13}C_{carb}$ excursion in the A4. This requires that any anoxic/euxinic conditions were confined to near the sediment-water interface.

Anoxia has been previously reported in the A4 unit, both in shallow and deep water (Athel basin: Figure 1) facies as the result of redox-sensitive trace element enrichment (Schröder and Grotzinger, 2007). Here we have added several new wells to that record, which support the interpretation of anoxia during the A4. Mo enrichment is found throughout the basal A4, in association with the most depleted $\delta^{13}C_{carb}$ and most enriched $\delta^{15}N_{org}$ values (Figure 2), pointing toward at least intermittently sulfidic conditions. Both V/Cr and U concentrations are enriched throughout the A4. The increase in V/Cr indicates that the nitrate reduction zone is at least partially within the water-column.

Water-column denitrification is supported by $\delta^{15}N_{org}$, which records a 7‰ positive excursion across the E-C boundary. Denitrification is accompanied by an isotope fractionation of ~ 20-30‰ that enriches the residual pool of nitrate (Sigman et al., 2005). Expression of this fractionation is suppressed under nitrate-limiting conditions, such as are typical of marine sediments (Sigman et al., 2001). The observed $\delta^{15}N$ enrichment of 7‰ would correspond to open system reduction of 30% of available nitrate in the water column,

or a comparatively higher fraction under more nitrate-limited conditions. Since water column denitrification only proceeds in the absence of measurable O_2, this supports the interpretation of anoxia during the E-C boundary excursion, especially as the peak of the $\delta^{15}N$ excursion aligns with the nadir of the $\delta^{13}C_{carb}$ excursions.

The coeval depletion in $\delta^{13}C_{carb}$ and $\delta^{13}C_{org}$ (without a parallel excursion in $\delta^{18}O_{carb}$) in the A4 argues that these data record a primary record of carbon cycling (Knoll et al., 1986). There are many possible causes for a decrease in $\delta^{13}C_{carb}$, including decreased carbon burial, decreased fractionation during carbon fixation (ε), the catastrophic release of methane, and the oxidation of organic matter (Kirschvink and Raub, 2003; Kump and Arthur, 1999). The extent of the $\delta^{13}C_{carb}$ minimum (-5‰) and the rapidity of its onset ($<< 1$ Myr) precludes a steady-state explanation in which the negative excursion is caused by decreased carbon burial (essentially no organic carbon burial, inconsistent with geological observations) or decreased fractionation (inconsistent with measured ε). The absence of an increase in 3-MeHI during the A4, argues against catastrophic methane release as a possible cause of the E-C boundary $\delta^{13}C_{carb}$ excursion (Kirschvink and Raub, 2003), as such methane would have likely spurred the growth of 3-MeBHP producing methanotrophs. The most plausible interpretation is that the $\delta^{13}C_{carb}$ excursion results from the remineralization (oxidation) of ^{13}C-depleted organic matter. Depleted $\delta^{13}C$ and anoxia are intimately related: it is the oxidation of ^{13}C-depleted organic matter that drives $\delta^{13}C_{carb}$ negative and consumes available oxidants, oxygen foremost. The oxidized organic matter likely derived from elevated primary production and organic carbon burial that is believed to characterize the terminal Ediacaran (Arthur and Sageman, 1994; Grotzinger et al., 1995; Saylor et al., 1998).

The variation observed in ε can shed light on the changes across the E-C boundary. The value that ε takes in sedimentary rocks depends on many factors, including community composition, the relative abundance of isotopically-distinct carbon fixation pathways, diagenesis and, specifically for phototrophs, the availability of CO_2 and growth rate (Hayes, 2001; Laws et al., 1995; van Dongen et al., 2006; Van Kaam-Peters et al., 1998). Superimposed over the $\delta^{13}C_{carb}$ excursion, we observe a transient decrease in ε to ~ 28‰, followed by ε ~ -31‰ over the remainder of the A4. These values of ε are the lowest recorded in the Huqf Supergroup (data here and (Fike et al., 2006)). We see four possible mechanisms for generating depleted ε during the E-C excursion: increased abundance of organisms using the reverse-TCA cycle, which has a smaller fractionation during carbon fixation (Hayes, 2001); decreased CO_2 availability (Laws et al., 1995); increased heterotrophic processing, which results in the ^{13}C-enriched residual organic (Hayes, 1993); and preferential preservation of carbohydrate-rich material under anoxic conditions (van Dongen et al., 2006; Van Kaam-Peters et al., 1998). We see no evidence for increased abundance of aryl isoprenoids or other biomarkers for organisms using the reverse-TCA cycle during the A4. Nor can we reconcile decreased CO_2 availability with enhanced remineralization of organic matter. Constraining the amount of heterotrophic reworking is non-trivial and in the absence of a reliable proxy for this, we can neither discount nor support this option. We do, however, find supporting evidence for preferential preservation of ^{13}C-enriched material during A4 time. The mechanism for incorporating ^{13}C-enriched compounds, particularly carbohydrates and proteins, invokes early diagenetic sulfidization (van Dongen et al., 2006; Van Kaam-Peters et al., 1998). Coincident with decreased ε, we see enriched molybdenum (Figure 2f) and pyrite abundances throughout the A4, with increased enrichment

in the basal A4 coincident with the minimum in ε (Figure 2c). As noted above, however, there are multiple possible parameters controlling ε. Despite this, there are distinct values in pre-, syn-, and post-excursion strata, suggesting the environmental/species variability in each of these times was much less than the variability between them.

SYNTHESIS

Oxidizing surface ocean conditions prevail throughout middle to late Ediacaran time (Canfield et al., 2007; Fike et al., 2006; Kaufman et al., 2007), at least partly due to the onset of high organic carbon burial that occurs ca. 550 Ma (Grotzinger et al., 1995; Saylor et al., 1998). Synthesizing the data presented here, E-C boundary biogeochemical processes define two stages. In the first, there is a collapse and reorganization of microbial community, likely representing a crash in photic zone primary production, in the A2 and A3 carbonates, immediately below the E-C boundary. Over this interval, we see the first evidence of localized anoxia. The E-C boundary ushers in a period of at least episodic anoxia/euxinia localized to near-sediment environments beneath a surface-mixed, oxic photic zone characterized by a return to increased primary production throughout the A4. This interval was characterized by increased mineralization of organic matter ($\delta^{13}C_{carb}$) leading to anoxia (U,Re), including water-column denitrification ($\delta^{15}N$; V/Cr), and episodic euxinia (Mo) associated with enhanced preservation of ^{13}C-enriched biomass (ε). The deposition of the A5 indicates the return to more oxidizing conditions and the restriction of anoxia to within the sediments.

Based on the prevalence of the $\delta^{13}C_{carb}$ excursion at E-C boundary sections across the globe (Amthor et al., 2003; Bartley et al., 1998; Maloof et al., 2005; Shields, 1999) and on

previous reports of trace element enrichment (Kimura and Watanabe, 2001; Schröder and

Grotzinger, 2007), this anoxia is likely to be a global phenomenon. The Ediacaran calcifying

metazoa *Namacalathus* and *Cloudina* are absent above A3 strata in Oman, and are interpreted

to have become extinct (Amthor et al., 2003). In Oman, this coincides with the E-C boundary

$\delta^{13}C_{carb}$ excursion. Globally, these organisms are not found above this excursion. Similarly,

Ediacaran soft-bodied organisms are also absent above the E-C boundary $\delta^{13}C_{carb}$ excursion,

suggesting global extinction, most plausibly related to this period of anoxia. There is no

evidence for shallow water anoxia prior to this boundary event in the interval ~580 - 542 Myr

(Canfield et al., 2007; Fike et al., 2006). Thus, the (largely bottom-dwelling) Ediacaran

organisms, which first appear ~ 575 Myr, were likely unable to survive the decreased oxygen

availability across the E-C boundary, although sponges and stem-group bilaterians, with their

lower oxygen requirements survived. With the return to oxic conditions after ca. 540 Myr,

the newly vacated environmental niche-space likely spurred the evolution of metazoa during

the Cambrian radiation.

REFERENCES
Amthor, J.E., Grotzinger, J.P., Schroder, S., Bowring, S.A., Ramezani, J., Martin, M.W., and Matter, A., 2003, Extinction of Cloudina and Namacalathus at the Precambrian-Cambrian boundary in Oman: Geology, v. 31, p. 431-434.
Arthur, M.A., and Sageman, B.B., 1994, Marine Black Shales - Depositional Mechanisms and Environments of Ancient-Deposits: Annual Review of Earth and Planetary Sciences, v. 22, p. 499-551.
Bambach, R.K., Knoll, A.H., and Sepkoski, J.J., 2002, Anatomical and ecological constraints on Phanerozoic animal diversity in the marine realm: Proceedings of the National Academy of Sciences of the United States of America, v. 99, p. 6854-6859.
Bartley, J.K., Pope, M., Knoll, A.H., Semikhatov, M.A., and Petrov, P.Y.U., 1998, A Vendian-Cambrian boundary succession from the northwestern margin of the Siberian Platform: stratigraphy, palaeontology, chemostratigraphy and correlation: Geological Magazine, v. 135, p. 473-494.

Bowring, S.A., Grotzinger, J.P., Condon, D.J., Ramezani, J., and Newall, M., 2007, Geochronologic constraints on the chronostratigraphic framework of the Neoproterozoic Huqf Supergroup, Sultanate of Oman: American Journal of Science, v. (in press).

Brasier, M.D., and Lindsay, J.F., 2000, Did supercontinent amalgamation trigger the 'Cambrian explosion'?, *in* Riding, R., and Zhuravlev, A.Y., eds., Ecology of the Cambrian Radiation: New York, Columbia University Press, p. 69 - 89.

Brocks, J.J., and Summons, R.E., 2003, Sedimentary hydrocarbons, biomarkers for early life, *in* Holland, H.D., and Turekian, K.K., eds., Treatise on Geochmistry, Volume 8, Elsevier, p. 63 - 115.

Calver, C.R., 2000, Isotope stratigraphy of the Ediacarian (Neoproterozoic III) of the Adelaide Rift Complex, Australia, and the overprint of water column stratification: Precambrian Research, v. 100, p. 121-150.

Canfield, D.E., Poulton, S.W., and Narbonne, G.M., 2007, Late Neoproterozoic Deep Ocean Oxygenation and the Rise of Animal Life Science, v. 315, p. 92 - 95.

Crucius, J., Calvert, S., Pedersen, T.F., and Sage, D., 1996, Rhenium and molybdenum enrichments in sediments as indicators of oxic, suboxic and sulfidic conditions of deposition: Earth and Planetary Science Letters, v. 145, p. 65 - 78.

Fike, D.A., Grotzinger, J.P., Pratt, L.M., and Summons, R.E., 2006, Oxidation of the Ediacaran Ocean: Nature, v. 444, p. 744 - 747.

Gely, J.-P., Blanc-Valleron, M.-M., Fache-Dany, F., Schuler, M., and Ansart, M., 1993, Characterization of organic-rich material in an evaporitic environment: the Lower Oligocene of the Mulhouse Basin (Alsace, France): Geologische Rundschau, v. 82, p. 718 - 725.

Grotzinger, J.P., Al-Siyabi, A.H., Al-Hashimi, R.A., and Cozzi, A., 2002, New model for tectonic evolution of Neoproterozoic-Cambrian Huqf Supergroup basins, Oman: GeoArabia, v. 7, p. 241.

Grotzinger, J.P., Bowring, S.A., Saylor, B.Z., and Kaufman, A.J., 1995, Biostratigraphic and Geochronological Constraints on Early Animal Evolution: Science, v. 270, p. 598-604.

Hayes, J.M., 1993, Factors controlling the 13C contents of sedimentary organic compounds: Principles and evidence: Marine Geology, v. 113.

—, 2001, Fractionation of carbon and hydrogen isotopes in biosynthetic processes, Stable Isotope Geochemistry, Volume 43: Reviews in Mineralogy & Geochemistry, p. 225-277.

Jones, B., and Manning, D.A.C., 1994, Comparison of geochemical indices used for the interpretation of palaeoredox conditions in ancient mudstones: Chemical Geology, v. 111, p. 111 - 129.

Kaufman, A.J., Corsetti, F.A., and Varni, M.A., 2007, The effect of rising atmospheric oxygen on carbon and sulfur isotope anomalies in the Neoproterozoic Johnnie Formation, Death Valley, USA: Chemical Geology, v. in press.

Kaufman, A.J., Hayes, J.M., Knoll, A.H., and Germs, G.J.B., 1991, Isotopic compositions of carbonates and organic-carbon from upper Proterozoic successions in Namibia - stratigraphic variation and the effects of diagenesis and metamorphism: Precambrian Research, v. 49, p. 301-327.

Kimura, H., Matsumoto, R., Kakuwa, Y., Hamdi, B., and Zibaseresht, H., 1997, The Vendian-Cambrian $\delta^{13}C$ record, North Iran: evidence for overturning of the ocean before the Cambrian Explosion: Earth and Planetary Science Letters, v. 147, p. E1 - E7.

Kimura, H., and Watanabe, Y., 2001, Oceanic anoxia at the Precambrian-Cambrian Boundary: Geology, v. 29, p. 995 - 998.

Kirschvink, J.L., and Raub, T.D., 2003, A methane fuse for the Cambrian explosion: carbon cycles and true polar wander: Comptes Rendus Geosciences, v. 335, p. 65-78.

Knoll, A.H., Hayes, J.M., Kaufman, A.J., Swett, K., and Lambert, I.B., 1986, Secular Variation in Carbon Isotope Ratios from Upper Proterozoic Successions of Svalbard and East Greenland: Nature, v. 321, p. 832-838.

Kump, L.R., and Arthur, M.A., 1999, Interpreting carbon-isotope excursions: carbonates and organic matter: Chemical Geology, v. 161, p. 181-198.

Laws, E.A., Popp, B.N., Bidigare, R.R., Kennicutt, M.C., and Macko, S.A., 1995, Dependence of phytoplankton carbon isotopic composition on growth-rate and [CO2](aq) - theoretical considerations and experimental resutls: Geochimica Et Cosmochimica Acta, v. 59, p. 1131-1138.

Loosveld, R.J.H., Bell, A., and Terken, J.J.M., 1996, The tectonic evolution of interior Oman: GeoArabia (Manama), v. 1, p. 28-51.

Lyons, T.W., Werne, J.P., Hollander, D.J., and Murray, R.W., 2003, Contrasting sulfur geochemistry and Fe/Al and Mo/Al ratios across the last oxic-to-anoxic transition in the Cariaco Basin, Venezuela: Chemical Geology, v. 195, p. 131-157.

Maloof, A., Schrag, D., Crowley, J., and Bowring, S., 2005, An expanded record of early Cambrian carbon cycling from the Anti-Atlas margin, Morocco: Canadian Journal of Earth Science, v. 42, p. 2195 - 2216.

Marshall, C.R., 2006, Explaining the Cambrian "explosion" of animals: Annual Review of Earth and Planetary Sciences, v. 34.

Mattes, B.W., and Conway-Morris, S., 1990, Carbonate/evaporite deposition in the Late Precambrian–Early Cambrian Ara Formation of southern Oman, in Robertson, A.H.F., Ed2, Ed3, Ed4, Ed5, and Ed6, eds., The geology and tectonics of the Oman region, Volume 69: Special Publication: London, Geological Society, p. 617 - 636.

Millson, J.A., Mercadier, C.G.L., Livera, S.E., and Peters, J.M., 1996, The Lower Palaeozoic of Oman and its context in the evolution of a Gondwanan continental margin: Journal of the Geological Society, v. 153, p. 213 - 230.

Peters, K.E., Walters, C.C., and Moldowan, J.M., 2005, The biomarker guide: Cambridge, UK, Cambridge University Press.

Piper, D.Z., 1994, Seawater as the source of minor elements in black shales, phosphorites and other sedimentary rocks: Chemical Geology, v. 114, p. 95 - 114.

Piper, D.Z., and Isaacs, C.M., 1995, Minor elements in Quaternary sediments from the Sea of Japan: a record of surface-water productivity and intermediate water redox conditions: Geological Society of America Bulletin, v. 107, p. 54 - 67.

Rohmer, M., Bisseret, P., and Neunlist, S., 1992, The hopanoids, prokaryotic triterpenoids and precursors of ubiquitous molecular fossils, in Moldowan, J.M., Albrecht, P., and Philip, R.P., eds., Biological markers in sediments and petroleum: Englewood Cliffs, NJ, Prentice Hall, p. 1 - 17.

Saylor, B.Z., Kaufman, A.J., Grotzinger, J.P., and Urban, F., 1998, A composite reference section for terminal Proterozoic strata of southern Namibia: Journal of Sedimentary Research, v. 68, p. 1223-1235.

Schröder, S., and Grotzinger, J.P., 2007, Evidence for anoxia at the Ediacaran-Cambrian boundary: the record of redox-sensitive trace elements and rare earth elements in Oman: Journal of the Geological Society, v. 164, p. 175-187.

Schröder, S., Schreiber, B.C., Amthor, J.E., and Matter, A., 2003, A depositional model for the terminal Neoproterozoic Early Cambrian Ara Group evaporites in south Oman: Sedimentology, v. 50, p. 879-898.

Shields, G., 1999, Working towards a new stratigraphic calibration scheme for the Neoproterozoic-Cambrian: Eclogae Geologicae Helvetiae, v. 92, p. 221-233.

Sigman, D.M., Casciotti, K.L., Andreani, M., Barford, C., Galanter, M., and Bohlke, J.K., 2001, A bacterial method for the nitrogen isotopic analysis of nitrate in seawater and freshwater: Analytical Chemistry, v. 73, p. 4145-4153.

Sigman, D.M., Granger, J., DiFiore, P.J., Lehmann, M.M., Ho, R., Cane, G., and van Geen, A., 2005, Coupled nitrogen and oxygen isotope measurements of nitrate along the eastern North Pacific margin: Global Biogeochemical Cycles, v. 19.

Summons, R.E., and Jahnke, L.L., 1992, Hopenes and hopanes methylated in ring-A: correlation of the hopanoids from extant methylotrophic bacteria with their fossil analogues., in Moldowan, J.M., Albrecht, P., and Philip, R.P., eds., Biological Markers in Sediments and Petroleum: Englewood Cliffs, NJ, Prentice Hall, p. 182 - 200.

Summons, R.E., Jahnke, L.L., Hope, J.M., and Logan, G.A., 1999, 2-Methylhopanoids as biomarkers for cyanobacterial oxygenic photosynthesis: Nature, v. 400, p. 554-557.

van Dongen, B.E., Schouten, S., and Sinnighe Damste, J.S., 2006, Preservation of carbohydrates through sulfurization in a Jurassic euxinic shelf sea: Examination of the Blackstone Band TOC cycle in the Kimmeridge Clay Formation, UK Organic Geochemistry, v. 37, p. 1052 - 1073.

van Kaam-Peters, H.M.E., Koster, J., van der Gaast, S.J., Dekker, M., De Leeuw, J.W., and Damste, J.S.S., 1998, The effect of clay minerals on diasterane/sterane ratios: Geochimica Et Cosmochimica Acta, v. 62, p. 2923-2929.

Van Kaam-Peters, H.M.E., Schouten, S., Koster, J., and Damste, J.S.S., 1998, Controls on the molecular and carbon isotopic composition of organic matter deposited in a Kimmeridgian euxinic shelf sea: Evidence

for preservation of carbohydrates through sulfurisation: Geochimica Et Cosmochimica Acta, v. 62, p. 3259-3283.

Volkman, J.K., 2003, Sterols in microorganisms: Applied Microbiology and Biotechnology, v. 60, p. 495-506.

—, 2005, Sterols and other triterpenoids: source specificity and evolution of biosynthetic pathways: Organic Geochemistry, v. 36, p. 139-159.

Zheng, Y., Anderson, R.F., van Geen, A., and Kuwabara, J., 2000, Authigenic molybdenum formation in marine sediments: a link to pore water sulfide in the Santa Barbara Basin: Geochimica et Cosmochimica Acta, v. 64, p. 4165 - 4178.

APPENDICES

Appendix A (Methods)

Appendix B (Table S1: Geochemical data)

Appendix C (Table S2: Biomarker parameters)

Appendix A

<u>Sample preparation and methodology</u>

Samples analyzed in the present study occur as two forms: drill core and cuttings. Cuttings are rock chips (typically 1–5 mm in size) produced during drilling that are collected every 2-5 meters. The main difference between samples of core and cuttings is that a core sample typically covers ~ 2cm of stratigraphy, whereas the cuttings in a given sample cover 2-5 meters of stratigraphy. Thus, cuttings represent a geochemical and lithological average, which has the tendency to smooth high-frequency variations in measured parameters. All biomarker samples in this study came from core material. Geochemical data were collected for both core and cuttings samples. In comparing the samples analyzed in this study, no systematic offset is observed between core and cuttings samples.

Samples were rinsed with DI to remove any water-soluble drilling contamination. and then rinsed 3x each in methanol, dichloromethane, and hexane to remove any soluble organic contamination. Samples were powdered using a SPEX 8510 Shatterbox with an alumina ceramic container. Carbonate carbon and oxygen isotopes were measured according to standard procedure (Ostermann and Curry, 2000). For TOC analyses, powdered samples were acidified in 6N HCl for 24 hours to remove carbonate minerals, filtered, rinsed with DI, dried, and the insoluble residue was loaded into tin cups for isotopic analysis. Bitumen(1) was obtained by extraction of whole rock powder in a mixture of dichloromethane and methanol (9:1 v/v) using a Dionex Accelerated Solvent Extraction ASE-200. Activated copper was used to remove elemental sulfur from the

bitumen(1) extract, which was then dried under nitrogen to remove the remaining solvents so that the extract yield could be measured. Bitumen(2) was the obtained from select samples where bitumen(1) had been extracted according to the following procedure. After acidification to remove carbonate (as described above), the residual material was re-extracted using the ASE. The yield from this second extraction is bitumen(2). For isotopic analysis, both bitumen(1) and bitumen(2) were re-dissolved in dichloromethane and 0.3mg were pipetted into tin cups, from which the solvent was allowed to evaporate away. For samples that had undergone bitumen removal, the organic residue that remained following acidification and extraction is termed kerogen, although it had not been acidified with HF to remove siliciclastic components. Kerogen was prepared for isotopic analysis by rinsing with DI, drying, and being loaded into tin cups. Organic carbon ($\delta^{13}C_{org}$) isotopes were analyzed as samples of total organic carbon (TOC), bitumen(1), bitumen(2), or kerogen. Nitrogen isotopic data are only presented from bitumen extracts; contamination by siliciclastic-bound nitrogen compounds precluded reproducible $\delta^{15}N$ results from TOC samples.

For isotopic analysis, samples were flash combusted at 1060°C in a Carlo Erba NA1500 Elemental Analyser fitted with an AS200 autosampler. The resulting CO_2 gas was analyzed by continuous flow using a Delta Plus XP Isotope Ratio Mass Spectrometer. Carbon isotopes are reported as $\delta^{13}C = (R_{sample}/R_{standard} - 1) * 1000$, where R = the ratio of $^{13}C/^{12}C$, in units of per mil (‰) relative to the V-PDB standard. Calibration of $\delta^{13}C_{org}$ was done by comparison with international standards (IAEA-CH-6, NBS-22) and in-house references ("Acetanilide" and "Penn State Kerogen") interspersed with the sample analyses. Trace element abundances were determined commercially

(Activation Labs, Ontaria, CA) using their Ultra-Trace-2 analysis package (combined ICP-OES and ICP/MS techniques).

Biomarkers were obtained from the bitumen(1) extract using the following procedure. First, asphaltenes were precipitated from the bitumen using n-pentane. The remaining fraction was separated by liquid chromatography using a silica gel column, eluting first with hexane, then hexane/dichloromethane (8:2 v/v), and finally dichloromethane/methanol (7:3 v/v) to yield the saturated hydrocarbon fraction, the aromatic hydrocarbon fraction, and the resin fraction, respectively. Biomarker analysis was performed on the saturated hydrocarbon fraction after n-alkanes were separated using a silicalite molecular sieve, leaving the branched and cyclic hydrocarbons.

These hydrocarbons (predominantly steranes and hopanes) were then analyzed for biomarker abundance by metastable reaction monitoring gas chromatography-mass spectrometry (MRM GC-MS) using the Autospec Ultima mass spectrometer. Specific biomarkers were identified by their elution time for a given precursor-product transition. Biomarker quantification was done against an internal standard (D4).

<u>References:</u>

Ostermann, D.R., and Curry, W.B., 2000, Calibration of stable isotopic data: An enriched $d^{18}O$ standard used for source gas mixing detection and correction: Paleoceanography, v. 15, p. 353 - 360.

Table S1: Isotopic and Geochemical data

Well	Unit	Depth	δ13C carb	δ18O carb	Mo (ppm)	Re (ppm)	V/Cr	V (ppm)	Cr (ppm)	U (ppm)	Bit1 δ13C	Bit1 δ15N	Bit2 δ13C	Bit2 δ15N	Ker δ13C	TOC δ13C	Bit1 ε	Bit2 ε	Ker ε	TOC ε
OMR1	A5	2846.6	2.9	-3.4	0.46	b.d.	0.89	4.90	5.50	2.30	-34.5	1.7	n.a.	n.a.	n.a.	n.a.	37.5	n.a.	n.a.	n.a.
OMR1	A5	2847.8	3.0	-3.4	0.80	b.d.	0.26	3.54	13.48	1.92	-34.6	1.6	n.a.	n.a.	n.a.	n.a.	37.5	n.a.	n.a.	n.a.
OMR1	A5	2849.2	2.9	-3.4	0.48	b.d.	0.26	2.51	9.50	2.20	-34.8	1.8	n.a.	n.a.	n.a.	n.a.	37.6	n.a.	n.a.	n.a.
OMR1	A5	2850.5	3.3	-3.5	0.47	b.d.	-	b.d.	15.92	1.40	-34.7	2.9	n.a.	n.a.	n.a.	n.a.	38.0	n.a.	n.a.	n.a.
OMR1	A5	2851.7	4.4	-0.8	0.80	0.003	0.09	2.72	31.00	1.41	-34.5	1.8	n.a.	n.a.	n.a.	n.a.	38.9	n.a.	n.a.	n.a.
OMR1	A5	2853.3	3.2	-3.7	0.71	b.d.	0.11	2.64	23.83	1.39	-34.4	1.8	n.a.	n.a.	n.a.	n.a.	37.6	n.a.	n.a.	n.a.
OMR1	A5	2854.8	3.2	-3.4	0.09	b.d.	1.11	2.00	1.81	1.31	-34.4	3.3	n.a.	n.a.	n.a.	n.a.	37.6	n.a.	n.a.	n.a.
OMR1	A5	2856.6	3.1	-3.2	0.74	0.003	-	b.d.	7.29	1.07	-34.1	2.5	n.a.	n.a.	n.a.	n.a.	37.3	n.a.	n.a.	n.a.
OMR1	A5	2858.5	3.0	-3.3	0.27	0.002	0.49	2.01	4.09	1.26	-34.3	3.1	n.a.	n.a.	n.a.	n.a.	37.3	n.a.	n.a.	n.a.
BBN1	A5	3534.0	-0.7	-4.9	5.49	b.d.	0.15	22.70	156.52	0.38	n.a.	n.a.	n.a.	n.a.	n.a.	n.a.	n.a.	n.a.	n.a.	n.a.
BBN1	A5	3540.0	0.8	-0.9	3.87	b.d.	0.08	4.41	58.67	0.12	n.a.	n.a.	n.a.	n.a.	n.a.	-33.8	n.a.	n.a.	n.a.	34.5
BBN1	A5	3546.0	1.8	1.6	5.16	b.d.	0.06	3.71	63.14	0.10	n.a.	n.a.	n.a.	n.a.	n.a.	n.a.	n.a.	n.a.	n.a.	n.a.
BBN1	A5	3552.0	n.a.	n.a.	0.96	0.001	0.49	5.92	12.12	0.13	n.a.	n.a.	n.a.	n.a.	n.a.	n.a.	n.a.	n.a.	n.a.	n.a.
BBN1	A5	3560.0	n.a.	n.a.	0.65	b.d.	0.25	5.86	23.61	0.12	n.a.	n.a.	n.a.	n.a.	n.a.	n.a.	n.a.	n.a.	n.a.	n.a.
BBN1	A5	3562.0	n.a.	n.a.	0.86	b.d.	0.39	6.27	16.29	0.14	n.a.	n.a.	n.a.	n.a.	n.a.	n.a.	n.a.	n.a.	n.a.	n.a.
BBN1	A5	3563.0	2.8	0.3	0.91	b.d.	0.20	3.15	15.35	0.45	n.a.	n.a.	n.a.	n.a.	n.a.	n.a.	n.a.	n.a.	n.a.	n.a.
BBN1	A5	3565.0	n.a.	n.a.	1.66	b.d.	-	b.d.	16.32	0.42	n.a.	n.a.	n.a.	n.a.	n.a.	n.a.	n.a.	n.a.	n.a.	n.a.
BBN1	A5	3566.0	n.a.	n.a.	1.11	b.d.	0.10	1.16	11.37	0.50	n.a.	n.a.	n.a.	n.a.	n.a.	n.a.	n.a.	n.a.	n.a.	n.a.
BBN1	A5	3568.0	2.8	0.7	2.22	0.001	0.21	3.72	18.09	0.38	n.a.	n.a.	n.a.	n.a.	n.a.	n.a.	n.a.	n.a.	n.a.	n.a.
BBN1	A4	3685.0	-2.6	-3.0	2.24	0.001	0.07	7.46	106.38	1.62	n.a.	n.a.	n.a.	n.a.	n.a.	n.a.	n.a.	n.a.	n.a.	n.a.
BBN1	A4	3716.0	-2.6	-3.1	12.14	0.002	0.20	4.50	22.44	7.28	n.a.	n.a.	n.a.	n.a.	n.a.	-34.5	n.a.	n.a.	n.a.	31.9
BBN1	A4	3734.0	-0.6	-3.5	2.98	b.d.	0.35	4.39	12.39	0.25	n.a.	n.a.	n.a.	n.a.	n.a.	-33.3	n.a.	n.a.	n.a.	32.7
BBN1	A4	3736.0	-2.6	-3.8	5.11	b.d.	0.30	5.08	16.80	0.91	n.a.	n.a.	n.a.	n.a.	n.a.	n.a.	n.a.	n.a.	n.a.	n.a.
BBN1	A4	3737.0	n.a.	n.a.	6.99	0.001	0.12	1.76	15.23	b.d.	n.a.	n.a.	n.a.	n.a.	n.a.	n.a.	n.a.	n.a.	n.a.	n.a.
BBN1	A4	3740.0	-1.9	-3.5	11.93	b.d.	0.04	1.72	38.41	0.30	n.a.	n.a.	n.a.	n.a.	n.a.	n.a.	n.a.	n.a.	n.a.	n.a.
BBN1	A3	3781.0	3.3	1.8	6.13	b.d.	0.08	6.96	86.85	0.78	n.a.	n.a.	n.a.	n.a.	n.a.	-34.3	n.a.	n.a.	n.a.	37.6
BBN1	A3	3831.0	3.2	-1.2	3.98	b.d.	0.07	1.52	21.92	0.93	n.a.	n.a.	n.a.	n.a.	n.a.	-30.5	n.a.	n.a.	n.a.	33.7
BBN1	A3	3868.0	2.6	-0.6	0.73	b.d.	0.19	6.31	32.47	0.64	n.a.	n.a.	n.a.	n.a.	n.a.	-31.9	n.a.	n.a.	n.a.	34.5
BB4	A4	2893.2	n.a.	n.a.	n.a.	n.a.	n.a.	n.a.	n.a.	n.a.	n.a.	n.a.	n.a.	n.a.	n.a.	n.a.	n.a.	n.a.	n.a.	n.a.
BB4	A4	2893.8	n.a.	n.a.	n.a.	n.a.	n.a.	n.a.	n.a.	n.a.	n.a.	n.a.	n.a.	n.a.	n.a.	n.a.	n.a.	n.a.	n.a.	n.a.
BB4	A4	2894.7	n.a.	n.a.	n.a.	n.a.	n.a.	n.a.	n.a.	n.a.	n.a.	n.a.	n.a.	n.a.	n.a.	n.a.	n.a.	n.a.	n.a.	n.a.
BB4	A4	2895.6	n.a.	n.a.	n.a.	n.a.	n.a.	n.a.	n.a.	n.a.	n.a.	n.a.	n.a.	n.a.	n.a.	n.a.	n.a.	n.a.	n.a.	n.a.
BB4	A4	2896.5	n.a.	n.a.	n.a.	n.a.	n.a.	n.a.	n.a.	n.a.	n.a.	n.a.	n.a.	n.a.	n.a.	n.a.	n.a.	n.a.	n.a.	n.a.
BB4	A4	2897.4	n.a.	n.a.	0.03	b.d.	-	b.d.	1.05	b.d.	n.a.	n.a.	n.a.	n.a.	n.a.	n.a.	n.a.	n.a.	n.a.	n.a.
BB4	A4	2898.1	n.a.	n.a.	0.03	b.d.	5.08	6.11	1.20	b.d.	n.a.	n.a.	n.a.	n.a.	n.a.	n.a.	n.a.	n.a.	n.a.	n.a.

Table S1: continued

Well	Unit	Depth	δ^{13}C carb	δ^{18}O carb	Mo (ppm)	Re (ppm)	V/Cr	V (ppm)	Cr (ppm)	U (ppm)	Bit1 δ^{13}C	Bit1 δ^{15}N	Bit2 δ^{13}C	Bit2 δ^{15}N	Ker δ^{13}C	TOC δ^{13}C	Bit1 ε	Bit2 ε	Ker ε	TOC ε
BB4	A4	2899.1	n.a.	n.a.	0.06	b.d.	5.89	8.41	1.43	b.d.	n.a.	n.a.	n.a.	n.a.	n.a.	n.a.	n.a.	n.a.	n.a.	n.a.
BB4	A4	2899.8	n.a.	n.a.	0.03	0.002	7.63	13.82	1.81	b.d.	n.a.	n.a.	n.a.	n.a.	n.a.	n.a.	n.a.	n.a.	n.a.	n.a.
BB4	A4	2900.5	n.a.	n.a.	0.00	b.d.	-	b.d.	1.29	b.d.	n.a.	n.a.	n.a.	n.a.	n.a.	n.a.	n.a.	n.a.	n.a.	n.a.
BB4	A4	2901.1	n.a.	n.a.	0.05	b.d.	-	b.d.	1.10	b.d.	n.a.	n.a.	n.a.	n.a.	n.a.	n.a.	n.a.	n.a.	n.a.	n.a.
BB4	A4	2901.1	n.a.	n.a.	0.05	b.d.	-	b.d.	0.00	b.d.	n.a.	n.a.	n.a.	n.a.	n.a.	n.a.	n.a.	n.a.	n.a.	n.a.
BB4	A4	2902.2	n.a.	n.a.	0.09	b.d.	-	b.d.	1.16	b.d.	n.a.	n.a.	n.a.	n.a.	n.a.	n.a.	n.a.	n.a.	n.a.	n.a.
BB4	A4	2902.7	n.a.	n.a.	0.07	b.d.	1.07	2.51	2.36	b.d.	n.a.	n.a.	n.a.	n.a.	n.a.	n.a.	n.a.	n.a.	n.a.	n.a.
BB4	A4	2903.2	n.a.	n.a.	0.07	b.d.	-	b.d.	1.50	b.d.	n.a.	n.a.	n.a.	n.a.	n.a.	n.a.	n.a.	n.a.	n.a.	n.a.
BB4	A4	2904.1	n.a.	n.a.	0.08	b.d.	-	b.d.	1.40	b.d.	n.a.	n.a.	n.a.	n.a.	n.a.	n.a.	n.a.	n.a.	n.a.	n.a.
BB4	A4	2905.0	n.a.	n.a.	0.11	b.d.	-	b.d.	1.59	b.d.	-34.0	n.a.	n.a.	n.a.	n.a.	n.a.	n.a.	n.a.	n.a.	n.a.
BB4	A4	2905.8	-2.7	-2.4	0.36	0.002	1.45	3.97	2.74	0.93	-34.3	3.7	n.a.	n.a.	n.a.	n.a.	31.6	n.a.	n.a.	n.a.
BB4	A4	2906.3	-2.7	-2.4	0.43	b.d.	-	b.d.	1.78	1.96	n.a.	n.a.	n.a.	n.a.	n.a.	n.a.	n.a.	n.a.	n.a.	n.a.
BB4	A4	2907.2	-2.6	-2.1	1.87	0.006	10.59	28.06	2.65	1.60	n.a.	n.a.	n.a.	n.a.	n.a.	n.a.	n.a.	n.a.	n.a.	n.a.
BB4	A4	2907.7	-2.4	-2.2	0.85	0.005	10.72	24.90	2.32	3.77	-34.2	4.3	n.a.	n.a.	-34.3	n.a.	31.8	n.a.	31.9	n.a.
BB4	A4	2908.4	-2.4	-2.4	17.85	0.022	6.85	24.96	3.64	4.11	n.a.	n.a.	n.a.	n.a.	n.a.	n.a.	n.a.	n.a.	n.a.	n.a.
BB4	A4	2908.7	-2.6	-2.0	0.48	b.d.	5.10	10.21	2.00	4.20	-34.4	4.3	-33.6	n.a.	-34.1	n.a.	31.9	31.0	31.5	n.a.
BB4	A4	2909.3	-2.6	-2.0	0.39	b.d.	1.59	2.24	1.41	3.48	-34.3	4.6	n.a.	4.3	n.a.	n.a.	31.7	n.a.	n.a.	n.a.
BB4	A4	2909.8	-2.7	-1.4	0.61	0.002	-	b.d.	1.31	5.23	n.a.	n.a.	n.a.	n.a.	n.a.	n.a.	n.a.	n.a.	n.a.	n.a.
BB4	A4	2910.8	-2.6	-2.5	7.06	b.d.	-	b.d.	2.07	3.35	-34.3	4.5	n.a.	n.a.	n.a.	n.a.	31.7	n.a.	n.a.	n.a.
BB4	A4	2911.4	-2.7	-2.2	0.47	0.002	-	b.d.	b.d.	3.66	n.a.	4.1	n.a.	n.a.	n.a.	n.a.	n.a.	n.a.	n.a.	n.a.
BB4	A4	2911.5	-2.7	-2.5	0.41	b.d.	1.92	3.12	1.62	3.04	-33.8	4.5	n.a.	n.a.	n.a.	n.a.	31.1	n.a.	n.a.	n.a.
BB4	A4	2912.2	-2.7	-2.5	0.45	0.003	2.11	4.59	2.17	5.04	n.a.	n.a.	n.a.	n.a.	n.a.	n.a.	n.a.	n.a.	n.a.	n.a.
BB4	A4	2913.3	-2.7	-2.3	0.45	0.002	2.13	3.89	1.82	3.60	n.a.	n.a.	n.a.	n.a.	n.a.	n.a.	n.a.	n.a.	n.a.	n.a.
BB4	A4	2913.9	-2.6	-2.3	0.44	0.004	3.46	7.40	2.14	3.65	n.a.	n.a.	n.a.	n.a.	n.a.	n.a.	n.a.	n.a.	n.a.	n.a.
BB4	A4	2914.8	-2.7	-1.6	0.35	0.002	3.82	7.37	1.93	2.90	n.a.	n.a.	n.a.	n.a.	n.a.	n.a.	n.a.	n.a.	n.a.	n.a.
BB4	A4	2915.5	-2.4	-2.1	0.35	b.d.	4.95	9.84	1.99	3.11	n.a.	n.a.	n.a.	n.a.	n.a.	n.a.	n.a.	n.a.	n.a.	n.a.
BB4	A4	2916.5	-2.5	-2.4	0.30	b.d.	5.96	11.50	1.93	4.65	n.a.	n.a.	n.a.	n.a.	n.a.	n.a.	n.a.	n.a.	n.a.	n.a.
BB4	A4	2917.2	-2.5	-2.6	0.30	0.004	4.46	8.45	1.89	4.36	n.a.	n.a.	n.a.	n.a.	n.a.	n.a.	n.a.	n.a.	n.a.	n.a.
BB4	A4	2917.7	-2.5	-2.3	0.78	b.d.	3.51	5.91	1.69	3.33	n.a.	n.a.	n.a.	n.a.	n.a.	n.a.	n.a.	n.a.	n.a.	n.a.
BB4	A4	2919.3	-2.6	-2.2	0.27	b.d.	-	b.d.	1.75	3.60	n.a.	4.4	-34.2	4.2	n.a.	n.a.	n.a.	31.6	n.a.	n.a.
BB4	A4	2920.0	-2.5	-2.8	0.27	0.004	2.10	3.93	1.88	4.38	n.a.	n.a.	n.a.	n.a.	n.a.	n.a.	n.a.	n.a.	n.a.	n.a.
BB4	A4	2920.3	-2.6	-2.5	0.25	0.002	3.48	5.50	1.58	3.69	n.a.	n.a.	n.a.	n.a.	n.a.	n.a.	n.a.	n.a.	n.a.	n.a.
BB4	A4	2921.2	-2.7	-1.5	0.19	0.002	1.64	2.31	1.41	3.90	n.a.	n.a.	n.a.	n.a.	n.a.	n.a.	n.a.	n.a.	n.a.	n.a.
BB4	A4	2921.9	-2.4	-2.2	0.27	b.d.	5.04	10.63	2.11	2.80	n.a.	n.a.	n.a.	n.a.	n.a.	n.a.	n.a.	n.a.	n.a.	n.a.
BB4	A4	2922.6	-2.4	-1.9	0.27	b.d.	4.39	9.62	2.19	2.39	n.a.	n.a.	n.a.	n.a.	n.a.	n.a.	n.a.	n.a.	n.a.	n.a.

Table S1: continued

Well	Unit	Depth	$\delta^{13}C$ carb	$\delta^{18}O$ carb	Mo (ppm)	Re (ppm)	V/Cr	V (ppm)	Cr (ppm)	U (ppm)	Bit1 $\delta^{13}C$	Bit1 $\delta^{15}N$	Bit2 $\delta^{13}C$	Bit2 $\delta^{15}N$	Ker $\delta^{13}C$	TOC $\delta^{13}C$	Bit1 ϵ	Bit2 ϵ	Ker ϵ	TOC ϵ
BB4	A4	2923.3	-2.4	-1.3	0.15	0.002	2.46	4.72	1.92	2.80	n.a.	n.a.	n.a.	n.a.	n.a.	n.a.	n.a.	n.a.	n.a.	n.a.
BB4	A4	2924.0	-2.3	-2.7	0.24	0.002	3.99	7.48	1.88	2.16	n.a.	n.a.	n.a.	n.a.	n.a.	n.a.	n.a.	n.a.	n.a.	n.a.
BB4	A4	2924.9	-2.3	-3.1	0.41	0.005	3.49	6.92	1.98	3.16	n.a.	n.a.	n.a.	n.a.	n.a.	n.a.	n.a.	n.a.	n.a.	n.a.
BB4	A4	2925.6	-2.4	-3.2	0.33	b.d.	1.69	3.09	1.83	2.23	-34.3	4.1	n.a.	n.a.	n.a.	n.a.	31.9	n.a.	n.a.	n.a.
BB4	A4	2926.8	-2.4	-3.0	0.24	0.003	2.54	4.55	1.79	3.30	n.a.	n.a.	n.a.	n.a.	n.a.	n.a.	n.a.	n.a.	n.a.	n.a.
BB4	A4	2927.5	-2.6	-2.7	0.29	0.001	2.32	4.07	1.76	2.46	n.a.	n.a.	n.a.	n.a.	n.a.	n.a.	n.a.	n.a.	n.a.	n.a.
BB4	A4	2928.3	-2.5	-2.7	0.26	0.002	1.91	3.69	1.94	4.32	n.a.	n.a.	n.a.	n.a.	n.a.	n.a.	n.a.	n.a.	n.a.	n.a.
BB4	A4	2928.8	-2.5	-1.0	0.26	0.003	2.96	6.11	2.07	3.36	-34.2	4.8	n.a.	n.a.	-34.4	n.a.	31.7	n.a.	32.0	n.a.
BB4	A4	2929.4	-2.2	-3.1	0.35	0.003	3.69	9.78	2.65	4.30	-33.8	n.a.	n.a.	n.a.	n.a.	n.a.	31.6	n.a.	n.a.	n.a.
BB4	A4	2930.0	-2.7	-2.9	0.35	b.d.	3.05	11.71	3.84	3.45	n.a.	n.a.	n.a.	n.a.	n.a.	n.a.	n.a.	n.a.	n.a.	n.a.
BB4	A4	2930.7	-2.9	-3.9	0.44	0.004	5.62	19.35	3.45	4.07	n.a.	n.a.	n.a.	n.a.	n.a.	n.a.	n.a.	n.a.	n.a.	n.a.
BB4	A4	2931.4	-2.8	-3.9	0.35	b.d.	3.65	8.77	2.40	2.73	-34.3	4.6	n.a.	n.a.	n.a.	n.a.	31.5	n.a.	n.a.	n.a.
BB4	A4	2932.1	-2.8	-3.8	0.38	0.002	3.35	6.39	1.91	2.46	n.a.	5.3	n.a.	n.a.	n.a.	n.a.	n.a.	n.a.	n.a.	n.a.
BB4	A4	2932.9	-2.8	n.a.	0.28	0.003	4.23	9.91	2.34	3.60	-33.7	4.0	n.a.	n.a.	n.a.	n.a.	30.9	n.a.	n.a.	n.a.
BB4	A4	2933.7	-2.8	-3.7	0.34	0.002	3.92	9.11	2.32	4.87	n.a.	n.a.	n.a.	n.a.	n.a.	n.a.	n.a.	n.a.	n.a.	n.a.
BB4	A4	2934.4	-2.9	-3.8	0.35	0.002	2.07	4.38	2.11	3.53	n.a.	n.a.	n.a.	n.a.	n.a.	n.a.	n.a.	n.a.	n.a.	n.a.
BB4	A4	2934.9	-2.9	-3.9	0.21	0.005	2.86	5.90	2.07	3.84	n.a.	n.a.	n.a.	n.a.	n.a.	n.a.	n.a.	n.a.	n.a.	n.a.
BB4	A4	2935.7	-2.8	-3.9	0.42	0.004	2.55	5.72	2.24	5.94	n.a.	n.a.	n.a.	n.a.	n.a.	n.a.	n.a.	n.a.	n.a.	n.a.
BB4	A4	2936.3	-2.8	-3.5	0.38	0.004	3.15	6.91	2.20	5.40	n.a.	n.a.	n.a.	n.a.	n.a.	n.a.	n.a.	n.a.	n.a.	n.a.
BB4	A4	2937.1	-3.1	-4.5	0.24	b.d.	2.01	4.08	2.03	3.57	-34.3	4.5	n.a.	n.a.	n.a.	n.a.	31.2	n.a.	n.a.	n.a.
BB4	A4	2937.8	-3.1	-4.5	0.35	0.007	3.68	8.15	2.21	3.85	-33.7	n.a.	n.a.	n.a.	n.a.	n.a.	30.6	n.a.	n.a.	n.a.
BB4	A4	2938.5	-3.0	-3.8	0.30	0.003	6.23	12.95	2.08	3.49	n.a.	n.a.	n.a.	n.a.	n.a.	n.a.	n.a.	n.a.	n.a.	n.a.
BB4	A4	2939.3	-3.1	-3.7	0.31	0.003	4.34	7.50	1.73	4.10	n.a.	n.a.	n.a.	n.a.	n.a.	n.a.	n.a.	n.a.	n.a.	n.a.
BB4	A4	2939.8	-3.1	-4.2	0.33	b.d.	2.24	3.17	1.42	3.60	-34.0	4.7	n.a.	n.a.	n.a.	n.a.	30.9	n.a.	n.a.	n.a.
BB4	A4	2940.1	-3.1	-4.4	0.33	0.005	2.49	4.26	1.71	2.81	-33.6	4.9	-34.3	n.a.	n.a.	n.a.	30.5	31.2	n.a.	n.a.
BB4	A4	2940.9	-3.2	-4.3	0.60	0.004	3.83	8.16	2.13	3.64	n.a.	4.6	n.a.	n.a.	n.a.	n.a.	n.a.	n.a.	n.a.	n.a.
BB4	A4	2941.7	-3.3	-3.7	0.48	0.006	3.84	11.28	2.94	4.17	n.a.	n.a.	n.a.	n.a.	n.a.	n.a.	n.a.	n.a.	n.a.	n.a.
BB4	A4	2942.4	-3.4	-3.9	0.35	0.003	3.43	9.04	2.63	3.66	n.a.	n.a.	n.a.	n.a.	n.a.	n.a.	n.a.	n.a.	n.a.	n.a.
BB4	A4	2943.1	-3.4	-3.6	0.41	0.006	2.38	8.57	3.60	5.16	n.a.	n.a.	n.a.	n.a.	n.a.	n.a.	n.a.	n.a.	n.a.	n.a.
BB4	A4	2943.9	-3.7	-4.3	1.04	0.005	7.53	30.91	4.11	5.19	n.a.	n.a.	n.a.	n.a.	n.a.	n.a.	n.a.	n.a.	n.a.	n.a.
BB4	A4	2944.7	-4.4	-4.2	3.67	0.010	15.66	110.59	7.06	4.99	-34.0	6.2	-34.3	5.6	-35.4	n.a.	29.7	29.9	31.0	n.a.
BB4	A4	2945.2	-3.9	-3.6	2.13	0.008	13.01	62.09	4.77	2.82	-34.5	5.1	n.a.	n.a.	n.a.	n.a.	30.6	n.a.	n.a.	n.a.
BB4	A4	2945.9	-3.9	-4.6	4.86	0.009	10.96	78.09	7.12	4.08	n.a.	n.a.	n.a.	n.a.	n.a.	n.a.	n.a.	n.a.	n.a.	n.a.
BB4	A4	2946.8	-4.2	-3.4	3.50	0.012	10.96	34.47	3.15	2.42	n.a.	n.a.	n.a.	n.a.	n.a.	n.a.	n.a.	n.a.	n.a.	n.a.
BB4	A4	2947.6	-4.4	-3.2	2.11	0.009	4.80	27.23	5.68	2.69	n.a.	n.a.	n.a.	n.a.	n.a.	n.a.	n.a.	n.a.	n.a.	n.a.

Table S1: continued

Well	Unit	Depth	δ¹³C carb	δ¹⁸O carb	Mo (ppm)	Re (ppm)	V/Cr	V (ppm)	Cr (ppm)	U (ppm)	Bit1 δ¹³C	Bit1 δ¹⁵N	Bit2 δ¹³C	Bit2 δ¹⁵N	Ker δ¹³C	TOC δ¹³C	Bit1 ε	Bit2 ε	Ker ε	TOC ε
BB4	A4	2948.6	-4.6	-2.9	1.93	0.013	2.18	5.92	2.71	2.90	-34.5	n.a.	n.a.	n.a.	n.a.	n.a.	29.8	n.a.	n.a.	n.a.
BB4	A4	2948.9	-4.5	-3.3	1.33	0.006	6.02	13.68	2.27	1.81	n.a.	n.a.	n.a.	n.a.	n.a.	n.a.	n.a.	n.a.	n.a.	n.a.
BB4	A4	2949.3	-4.5	-3.3	1.47	0.006	1.24	8.67	6.97	6.02	n.a.	n.a.	n.a.	n.a.	n.a.	n.a.	n.a.	n.a.	n.a.	n.a.
BB4	A4	2949.6	-4.9	-3.2	5.43	0.024	2.69	3.29	1.22	2.93	n.a.	n.a.	n.a.	n.a.	n.a.	n.a.	n.a.	n.a.	n.a.	n.a.
BB4	A4	2949.9	-5.0	-3.4	2.78	0.012	-	b.d.	1.42	2.15	-34.8	9.4	-34.8	n.a.	n.a.	n.a.	29.8	29.8	n.a.	n.a.
BB4	A4	2950.0	-4.5	-3.0	3.98	0.016	-	b.d.	1.55	1.66	-34.9	9.6	-35.1	n.a.	n.a.	n.a.	30.5	30.7	n.a.	n.a.
BB4	A4	2950.2	-4.3	n.a.	2.28	b.d.	-	b.d.	8.97	1.37	-32.6	n.a.	n.a.	n.a.	n.a.	n.a.	28.3	n.a.	n.a.	n.a.
BB4	A4	2950.6	-2.9	n.a.	2.09	0.004	0.87	8.38	9.59	0.40	n.a.	n.a.	n.a.	n.a.	n.a.	n.a.	n.a.	n.a.	n.a.	n.a.
BB4	A4	2950.6	n.a.	n.a.	0.06	0.005	-	b.d.	2.15	b.d.	-30.2	n.a.	n.a.	n.a.	n.a.	n.a.	27.3	n.a.	n.a.	n.a.
BB4	A4	2950.7	-1.2	n.a.	n.a.	n.a.	n.a.	n.a.	n.a.	n.a.	n.a.	n.a.	n.a.	n.a.	n.a.	n.a.	n.a.	n.a.	n.a.	n.a.
BB4	A4	2951.2	n.a.	n.a.	n.a.	n.a.	n.a.	n.a.	n.a.	n.a.	n.a.	n.a.	n.a.	n.a.	n.a.	n.a.	n.a.	n.a.	n.a.	n.a.
BB4	A4	2951.8	n.a.	n.a.	n.a.	n.a.	n.a.	n.a.	n.a.	n.a.	n.a.	n.a.	n.a.	n.a.	n.a.	n.a.	n.a.	n.a.	n.a.	n.a.
BB4	A4	2952.4	n.a.	n.a.	n.a.	n.a.	n.a.	n.a.	n.a.	n.a.	n.a.	n.a.	n.a.	n.a.	n.a.	n.a.	n.a.	n.a.	n.a.	n.a.
BB4	A4	2952.8	n.a.	n.a.	n.a.	n.a.	n.a.	n.a.	n.a.	n.a.	-32.3	n.a.	n.a.	n.a.	n.a.	n.a.	n.a.	n.a.	n.a.	n.a.
BB4	A4	2953.0	1.8	n.a.	n.a.	n.a.	n.a.	n.a.	n.a.	n.a.	n.a.	n.a.	n.a.	n.a.	n.a.	n.a.	n.a.	n.a.	n.a.	n.a.
BB4	A3	3029.7	3.3	-3.5	0.03	0.004	-	b.d.	1.16	0.85	-31.0	n.a.	n.a.	n.a.	n.a.	n.a.	34.3	n.a.	n.a.	n.a.
BB4	A3	3030.8	3.2	-4.0	0.07	0.003	-	b.d.	1.43	0.89	-31.4	2.3	n.a.	n.a.	n.a.	n.a.	34.5	n.a.	n.a.	n.a.
BB4	A3	3031.3	3.3	-4.0	0.07	0.003	-	b.d.	2.23	0.61	-29.6	3.6	n.a.	n.a.	n.a.	n.a.	32.9	n.a.	n.a.	n.a.
BB4	A3	3032.3	3.2	-4.6	0.03	b.d.	-	b.d.	b.d.	b.d.	-31.8	1.2	-31.3	n.a.	n.a.	n.a.	35.0	34.5	n.a.	n.a.
BB4	A3	3032.8	3.4	-3.6	0.06	0.002	-	b.d.	1.17	b.d.	-31.0	3.7	n.a.	n.a.	n.a.	n.a.	34.4	n.a.	n.a.	n.a.
BB4	A3	3033.6	3.2	-4.8	0.07	0.007	-	b.d.	1.10	b.d.	n.a.	n.a.	n.a.	n.a.	-31.6	n.a.	n.a.	n.a.	34.8	n.a.
BB4	A3	3034.0	3.4	-4.3	0.05	0.002	-	b.d.	b.d.	b.d.	n.a.	n.a.	n.a.	n.a.	-31.2	n.a.	n.a.	n.a.	34.6	n.a.
BB4	A3	3034.5	3.3	-4.7	0.07	0.003	-	b.d.	1.53	1.16	-29.1	2.4	n.a.	n.a.	n.a.	n.a.	32.4	n.a.	n.a.	n.a.
BB4	A3	3035.0	3.7	-3.1	n.a.	n.a.	n.a.	n.a.	n.a.	n.a.	-31.1	n.a.	n.a.	n.a.	n.a.	n.a.	34.8	n.a.	n.a.	n.a.
MNH1	A5	3610.0	n.a.	n.a.	0.69	b.d.	1.64	4.87	2.96	b.d.	n.a.	n.a.	n.a.	n.a.	n.a.	n.a.	n.a.	n.a.	n.a.	n.a.
MNH1	A5	3620.0	n.a.	n.a.	0.31	0.001	3.24	4.35	1.34	b.d.	n.a.	n.a.	n.a.	n.a.	n.a.	n.a.	n.a.	n.a.	n.a.	n.a.
MNH1	A5	3630.0	n.a.	n.a.	0.49	0.001	2.71	4.87	1.80	0.10	n.a.	n.a.	n.a.	n.a.	n.a.	n.a.	n.a.	n.a.	n.a.	n.a.
MNH1	A5	3640.0	2.8	0.0	1.63	0.003	0.17	0.75	4.39	0.86	n.a.	n.a.	n.a.	n.a.	n.a.	n.a.	n.a.	n.a.	n.a.	n.a.
MNH1	A5	3650.0	n.a.	n.a.	0.82	0.000	2.07	8.03	3.89	0.51	n.a.	n.a.	n.a.	n.a.	n.a.	n.a.	n.a.	n.a.	n.a.	n.a.
MNH1	A5	3660.0	n.a.	n.a.	1.33	0.000	1.50	8.73	5.83	0.55	n.a.	n.a.	n.a.	n.a.	n.a.	n.a.	n.a.	n.a.	n.a.	n.a.
MNH1	A5	3690.0	2.3	0.0	1.11	0.002	1.47	9.03	6.14	0.92	n.a.	n.a.	n.a.	n.a.	n.a.	n.a.	n.a.	n.a.	n.a.	n.a.
MNH1	A5	3700.0	2.0	0.0	2.07	0.004	3.30	24.97	7.56	1.01	n.a.	n.a.	n.a.	n.a.	n.a.	-33.3	n.a.	n.a.	n.a.	35.3
MNH1	A5	3710.0	2.7	0.0	0.75	0.000	2.02	9.35	4.64	0.45	n.a.	n.a.	n.a.	n.a.	n.a.	n.a.	n.a.	n.a.	n.a.	n.a.
MNH1	A5	3800.0	2.7	0.0	0.45	0.001	0.00	0.00	2.72	0.46	n.a.	n.a.	n.a.	n.a.	n.a.	-32.0	n.a.	n.a.	n.a.	34.7
MNH1	A5	3810.0	2.1	-3.4	0.80	0.000	2.08	10.94	5.25	0.92	n.a.	n.a.	n.a.	n.a.	n.a.	-32.5	n.a.	n.a.	n.a.	34.6

Well	Unit	Depth	$\delta^{13}C$ carb	$\delta^{18}O$ carb	Mo (ppm)	Re (ppm)	V/Cr	V (ppm)	Cr (ppm)	U (ppm)	Bit1 $\delta^{13}C$	Bit1 $\delta^{15}N$	Bit2 $\delta^{13}C$	Bit2 $\delta^{15}N$	Ker $\delta^{13}C$	TOC $\delta^{13}C$	Bit1 ϵ	Bit2 ϵ	Ker ϵ	TOC ϵ
MNH1	A5	3820.0	2.2	-1.3	9.54	0.002	0.33	10.61	32.35	0.44	n.a.	n.a.	n.a.	n.a.	n.a.	n.a.	n.a.	n.a.	n.a.	n.a.
MNH1	A3	3960.0	n.a.	n.a.	4.28	0.000	0.22	4.29	19.49	0.89	n.a.	n.a.	n.a.	n.a.	n.a.	n.a.	n.a.	n.a.	n.a.	n.a.
MNH1	A3	3970.0	n.a.	n.a.	2.33	0.001	1.05	7.79	7.43	0.50	n.a.	n.a.	n.a.	n.a.	n.a.	n.a.	n.a.	n.a.	n.a.	n.a.
MNH1	A3	3972.0	n.a.	n.a.	1.44	0.000	0.64	3.43	5.33	0.50	n.a.	n.a.	n.a.	n.a.	n.a.	n.a.	n.a.	n.a.	n.a.	n.a.
MNH1	A3	3976.0	n.a.	n.a.	1.52	0.002	0.84	6.74	8.02	0.54	n.a.	n.a.	n.a.	n.a.	n.a.	-30.3	n.a.	n.a.	n.a.	n.a.
MNH1	A3	3979.0	2.9	1.7	2.85	0.000	0.51	6.73	13.26	0.74	n.a.	n.a.	n.a.	n.a.	n.a.	-30.8	n.a.	n.a.	n.a.	33.6
MNH1	A3	3979.1	-2.0	-9.6	0.07	0.000	-	4.02	b.d.	b.d.	n.a.	n.a.	n.a.	n.a.	n.a.	-30.8	n.a.	n.a.	n.a.	n.a.
MNH1	A3	3979.4	0.3	-4.2	0.07	0.000	-	1.94	b.d.	b.d.	n.a.	n.a.	n.a.	n.a.	n.a.	-29.8	n.a.	n.a.	n.a.	30.1
MNH1	A3	3981.7	2.4	2.5	0.07	0.000	-	2.55	b.d.	0.13	n.a.	n.a.	n.a.	n.a.	n.a.	n.a.	n.a.	n.a.	n.a.	n.a.
MNH1	A3	3983.5	1.5	0.3	0.17	0.000	-	4.37	b.d.	0.52	n.a.	n.a.	n.a.	n.a.	n.a.	n.a.	n.a.	n.a.	n.a.	n.a.
MNH1	A3	3987.9	2.1	2.2	0.62	0.001	0.35	9.05	26.04	0.40	n.a.	n.a.	n.a.	n.a.	n.a.	n.a.	n.a.	n.a.	n.a.	n.a.
MNH1	A3	3988.7	n.a.	n.a.	n.a.	n.a.	n.a.	n.a.	n.a.	n.a.	n.a.	n.a.	n.a.	n.a.	n.a.	n.a.	n.a.	n.a.	n.a.	n.a.
MNH1	A3	3990.8	2.6	0.2	0.99	0.001	0.43	23.06	54.13	0.23	n.a.	n.a.	n.a.	n.a.	n.a.	n.a.	n.a.	n.a.	n.a.	n.a.
BBN2	A4	3843.8	n.a.	n.a.	0.11	b.d.	5.33	8.63	1.62	b.d.	n.a.	n.a.	n.a.	n.a.	n.a.	n.a.	n.a.	n.a.	n.a.	n.a.
BBN2	A4	3846.7	n.a.	n.a.	0.27	n.a.	n.a.	n.a.	n.a.	n.a.	n.a.	n.a.	n.a.	n.a.	n.a.	n.a.	n.a.	n.a.	n.a.	n.a.
BBN2	A4	3911.3	n.a.	n.a.	0.08	b.d.	10.96	23.10	2.11	b.d.	n.a.	n.a.	n.a.	n.a.	n.a.	n.a.	n.a.	n.a.	n.a.	n.a.
BBN2	A4	3912.2	n.a.	n.a.	0.24	b.d.	9.86	24.26	2.46	0.33	n.a.	n.a.	n.a.	n.a.	n.a.	n.a.	n.a.	n.a.	n.a.	n.a.
BBN2	A4	3919.1	n.a.	n.a.	0.10	b.d.	6.18	12.17	1.97	b.d.	n.a.	n.a.	n.a.	n.a.	n.a.	n.a.	n.a.	n.a.	n.a.	n.a.
BBN2	A4	3923.5	n.a.	n.a.	0.02	n.a.	n.a.	n.a.	n.a.	n.a.	n.a.	n.a.	n.a.	n.a.	n.a.	n.a.	n.a.	n.a.	n.a.	n.a.
SHM1	A4	2538.0	-2.7	-3.0	2.91	0.009	9.24	47.99	5.19	3.63	n.a.	n.a.	n.a.	n.a.	n.a.	n.a.	n.a.	n.a.	n.a.	n.a.
SHM1	A4	2540.0	-2.5	-2.7	5.93	0.003	7.33	47.09	6.43	9.56	n.a.	n.a.	n.a.	n.a.	n.a.	n.a.	n.a.	n.a.	n.a.	n.a.
SHM1	A4	2542.0	-2.6	-2.5	2.48	0.007	8.77	40.26	4.59	3.38	n.a.	n.a.	n.a.	n.a.	n.a.	n.a.	n.a.	n.a.	n.a.	n.a.
SHM1	A4	2546.0	-2.5	-2.6	1.17	0.002	3.53	14.28	4.04	3.26	n.a.	n.a.	n.a.	n.a.	n.a.	n.a.	n.a.	n.a.	n.a.	n.a.
SHM1	A4	2548.0	-2.5	-2.5	1.47	0.004	4.12	17.11	4.15	4.23	n.a.	n.a.	n.a.	n.a.	n.a.	n.a.	n.a.	n.a.	n.a.	n.a.
SHM1	A4	2550.0	-2.4	-2.3	1.15	0.004	3.11	14.84	4.78	4.61	n.a.	n.a.	n.a.	n.a.	n.a.	n.a.	n.a.	n.a.	n.a.	n.a.
SHM1	A4	2552.0	-2.6	-2.3	0.57	0.002	3.21	12.26	3.82	4.37	n.a.	n.a.	n.a.	n.a.	n.a.	n.a.	n.a.	n.a.	n.a.	n.a.
SHM1	A4	2554.0	-2.6	-2.4	0.71	0.002	2.25	18.29	8.13	4.50	n.a.	n.a.	n.a.	n.a.	n.a.	n.a.	n.a.	n.a.	n.a.	n.a.
SHM1	A4	2556.0	-2.6	-2.2	0.65	0.003	1.28	6.11	4.77	4.03	n.a.	n.a.	n.a.	n.a.	n.a.	n.a.	n.a.	n.a.	n.a.	n.a.
SHM1	A4	2558.0	-2.6	-2.4	0.72	0.001	1.02	3.64	3.57	3.48	n.a.	n.a.	n.a.	n.a.	n.a.	n.a.	n.a.	n.a.	n.a.	n.a.
SHM1	A4	2560.0	-2.6	-2.2	0.71	0.003	0.95	4.16	4.36	3.95	n.a.	n.a.	n.a.	n.a.	n.a.	n.a.	n.a.	n.a.	n.a.	n.a.
SHM1	A4	2562.0	-3.3	-5.1	5.36	0.004	0.94	10.45	11.07	3.48	n.a.	n.a.	n.a.	n.a.	n.a.	n.a.	n.a.	n.a.	n.a.	n.a.
SHM1	A4	2564.0	-3.5	-5.2	0.88	b.d.	1.89	10.90	5.75	3.35	n.a.	n.a.	n.a.	n.a.	n.a.	n.a.	n.a.	n.a.	n.a.	n.a.
SHM1	A4	2566.0	-2.5	-2.7	0.25	0.002	2.47	6.09	2.46	4.13	n.a.	n.a.	n.a.	n.a.	n.a.	n.a.	n.a.	n.a.	n.a.	n.a.
SHM1	A4	2568.0	n.a.	n.a.	0.48	0.001	2.85	11.72	4.11	3.92	n.a.	n.a.	n.a.	n.a.	n.a.	n.a.	n.a.	n.a.	n.a.	n.a.
SHM1	A4	2572.0	-3.0	-3.5	0.53	0.003	3.79	17.82	4.71	4.22	n.a.	n.a.	n.a.	n.a.	n.a.	n.a.	n.a.	n.a.	n.a.	n.a.

Well	Unit	Depth	$\delta^{13}C$ carb	$\delta^{18}O$ carb	Mo (ppm)	Re (ppm)	V/Cr	V (ppm)	Cr (ppm)	U (ppm)	Bit1 $\delta^{13}C$	Bit1 $\delta^{15}N$	Bit2 $\delta^{13}C$	Bit2 $\delta^{15}N$	Ker $\delta^{13}C$	TOC $\delta^{13}C$	Bit1 ε	Bit2 ε	Ker ε	TOC ε
SHM1	A4	2574.0	-3.1	-4.0	0.67	0.001	3.29	10.95	3.33	4.07	n.a.	n.a.	n.a.	n.a.	n.a.	n.a.	n.a.	n.a.	n.a.	n.a.
SHM1	A4	2576.0	-3.3	-4.2	1.06	0.001	2.42	8.45	3.49	5.67	n.a.	n.a.	n.a.	n.a.	n.a.	n.a.	n.a.	n.a.	n.a.	n.a.
SHM1	A4	2578.0	-3.4	-4.2	0.83	0.001	4.09	12.37	3.03	4.62	n.a.	n.a.	n.a.	n.a.	n.a.	n.a.	n.a.	n.a.	n.a.	n.a.
SHM1	A4	2580.0	-3.2	-3.7	0.80	0.002	3.00	10.24	3.41	5.01	n.a.	n.a.	n.a.	n.a.	n.a.	n.a.	n.a.	n.a.	n.a.	n.a.
SHM1	A4	2582.0	-4.3	-3.1	1.61	0.006	6.59	20.16	3.06	2.61	n.a.	n.a.	n.a.	n.a.	n.a.	n.a.	n.a.	n.a.	n.a.	n.a.
SHM1	A4	2584.0	-4.6	-3.2	37.48	0.009	-	58.17	b.d.	2.38	n.a.	n.a.	n.a.	n.a.	n.a.	n.a.	n.a.	n.a.	n.a.	n.a.
SHM1	A3	2676.0	2.7	-2.6	0.24	b.d.	2.67	4.65	1.74	0.61	n.a.	n.a.	n.a.	n.a.	n.a.	n.a.	n.a.	n.a.	n.a.	n.a.
SHM1	A3	2678.0	3.0	-3.2	0.29	b.d.	3.19	6.86	2.15	0.62	n.a.	n.a.	n.a.	n.a.	n.a.	n.a.	n.a.	n.a.	n.a.	n.a.
SHM1	A3	2680.0	3.9	-2.4	0.21	b.d.	2.91	6.06	2.08	0.67	n.a.	n.a.	n.a.	n.a.	n.a.	n.a.	n.a.	n.a.	n.a.	n.a.
SHM1	A3	2682.0	3.8	-2.1	0.25	0.003	8.36	32.28	3.86	0.81	n.a.	n.a.	n.a.	n.a.	n.a.	n.a.	n.a.	n.a.	n.a.	n.a.
SHM1	A3	2684.0	3.7	-1.6	0.18	0.002	10.34	33.17	3.21	0.81	n.a.	n.a.	n.a.	n.a.	n.a.	n.a.	n.a.	n.a.	n.a.	n.a.
SHM1	A3	2686.0	3.7	-1.7	0.16	0.001	9.45	24.68	2.61	0.94	n.a.	n.a.	n.a.	n.a.	n.a.	n.a.	n.a.	n.a.	n.a.	n.a.
SHM1	A3	2688.0	3.7	-1.6	0.26	b.d.	1.95	3.44	1.77	0.81	n.a.	n.a.	n.a.	n.a.	n.a.	n.a.	n.a.	n.a.	n.a.	n.a.
SHM1	A3	2690.0	3.6	-1.5	0.14	0.003	9.55	18.81	1.97	0.91	n.a.	n.a.	n.a.	n.a.	n.a.	n.a.	n.a.	n.a.	n.a.	n.a.
SHM1	A3	2692.0	3.5	-1.5	0.17	0.003	9.28	22.68	2.45	0.86	n.a.	n.a.	n.a.	n.a.	n.a.	n.a.	n.a.	n.a.	n.a.	n.a.
SHM1	A3	2694.0	3.4	-1.4	0.18	0.002	10.16	18.22	1.79	0.86	n.a.	n.a.	n.a.	n.a.	n.a.	n.a.	n.a.	n.a.	n.a.	n.a.
SHM1	A3	2698.0	3.4	-1.5	0.15	0.001	10.29	19.36	1.88	0.89	n.a.	n.a.	n.a.	n.a.	n.a.	n.a.	n.a.	n.a.	n.a.	n.a.
SHM1	A3	2700.0	3.4	-1.5	0.16	0.002	9.75	23.29	2.39	0.92	n.a.	n.a.	n.a.	n.a.	n.a.	n.a.	n.a.	n.a.	n.a.	n.a.
SHM1	A3	2702.0	3.3	-1.3	0.16	0.002	12.90	25.27	1.96	1.11	n.a.	n.a.	n.a.	n.a.	n.a.	n.a.	n.a.	n.a.	n.a.	n.a.
SHM1	A3	2704.0	3.3	-3.7	0.12	0.002	13.33	23.90	1.79	1.18	n.a.	n.a.	n.a.	n.a.	n.a.	n.a.	n.a.	n.a.	n.a.	n.a.
SHM1	A3	2706.0	3.3	-3.8	0.13	0.002	12.71	23.34	1.84	1.08	n.a.	n.a.	n.a.	n.a.	n.a.	n.a.	n.a.	n.a.	n.a.	n.a.
SHM1	A3	2708.0	3.2	-2.1	0.25	0.001	10.74	21.64	2.02	1.30	n.a.	n.a.	n.a.	n.a.	n.a.	n.a.	n.a.	n.a.	n.a.	n.a.
SHM1	A3	2710.0	3.1	-2.0	0.18	0.002	9.79	15.95	1.63	0.81	n.a.	n.a.	n.a.	n.a.	n.a.	n.a.	n.a.	n.a.	n.a.	n.a.
SHM1	A3	2712.0	3.2	-1.3	0.21	0.001	11.42	16.50	1.45	0.77	n.a.	n.a.	n.a.	n.a.	n.a.	n.a.	n.a.	n.a.	n.a.	n.a.
SHM1	A3	2714.0	3.2	-0.9	0.16	0.002	11.28	15.25	1.35	0.71	n.a.	n.a.	n.a.	n.a.	n.a.	n.a.	n.a.	n.a.	n.a.	n.a.
SHM1	A3	2716.0	3.3	-1.5	0.11	0.001	11.44	16.89	1.48	0.75	n.a.	n.a.	n.a.	n.a.	n.a.	n.a.	n.a.	n.a.	n.a.	n.a.
SHM1	A3	2718.0	3.2	-0.9	0.19	0.001	13.79	19.49	1.41	1.07	n.a.	n.a.	n.a.	n.a.	n.a.	n.a.	n.a.	n.a.	n.a.	n.a.
SHM1	A3	2720.0	3.3	-1.0	0.11	0.001	10.44	13.29	1.27	0.75	n.a.	n.a.	n.a.	n.a.	n.a.	n.a.	n.a.	n.a.	n.a.	n.a.
SHM1	A3	2722.0	3.3	-2.5	0.12	0.001	11.40	15.56	1.37	0.99	n.a.	n.a.	n.a.	n.a.	n.a.	n.a.	n.a.	n.a.	n.a.	n.a.
SHM1	A3	2724.0	3.3	-1.6	0.26	0.002	10.32	15.78	1.53	0.89	n.a.	n.a.	n.a.	n.a.	n.a.	n.a.	n.a.	n.a.	n.a.	n.a.
SHM1	A3	2726.0	3.2	-0.4	0.22	0.001	9.64	14.67	1.52	0.77	n.a.	n.a.	n.a.	n.a.	n.a.	n.a.	n.a.	n.a.	n.a.	n.a.
SHM1	A3	2730.0	3.3	-0.6	0.21	0.002	12.07	14.67	1.22	0.93	n.a.	n.a.	n.a.	n.a.	n.a.	n.a.	n.a.	n.a.	n.a.	n.a.
SHM1	A3	2732.0	3.2	-2.2	0.42	0.002	9.58	15.68	1.64	1.39	n.a.	n.a.	n.a.	n.a.	n.a.	n.a.	n.a.	n.a.	n.a.	n.a.
SHM1	A3	2734.0	3.2	-1.9	0.21	0.002	8.56	13.91	1.63	0.75	n.a.	n.a.	n.a.	n.a.	n.a.	n.a.	n.a.	n.a.	n.a.	n.a.
SHM1	A3	2736.0	3.2	-1.1	0.17	0.001	9.60	16.07	1.67	0.99	n.a.	n.a.	n.a.	n.a.	n.a.	n.a.	n.a.	n.a.	n.a.	n.a.

Well	Unit	Depth	$\delta^{13}C$ carb	$\delta^{18}O$ carb	Mo (ppm)	Re (ppm)	V/Cr	V (ppm)	Cr (ppm)	U (ppm)	Bit1 $\delta^{13}C$	Bit1 $\delta^{15}N$	Bit2 $\delta^{13}C$	Bit2 $\delta^{15}N$	Ker $\delta^{13}C$	TOC $\delta^{13}C$	Bit1 ε	Bit2 ε	Ker ε	TOC ε
SHM1	A3	2738.0	3.1	-0.9	0.12	0.004	11.50	13.95	1.21	0.81	n.a.	n.a.	n.a.	n.a.	n.a.	n.a.	n.a.	n.a.	n.a.	n.a.
SHM1	A3	2740.0	3.1	-1.3	0.16	b.d.	11.15	13.90	1.25	0.77	n.a.	n.a.	n.a.	n.a.	n.a.	n.a.	n.a.	n.a.	n.a.	n.a.
SHM1	A3	2742.0	3.1	-1.2	0.19	0.003	10.14	12.78	1.26	0.71	n.a.	n.a.	n.a.	n.a.	n.a.	n.a.	n.a.	n.a.	n.a.	n.a.
SHM1	A3	2744.0	3.0	-1.3	0.08	0.001	11.56	10.14	0.88	0.71	n.a.	n.a.	n.a.	n.a.	n.a.	n.a.	n.a.	n.a.	n.a.	n.a.
SHM1	A3	2746.0	2.6	-3.6	0.05	0.002	12.63	10.58	0.84	0.65	n.a.	n.a.	n.a.	n.a.	n.a.	n.a.	n.a.	n.a.	n.a.	n.a.
SHM1	A3	2748.0	2.9	-3.7	0.15	0.001	10.11	10.50	1.04	0.79	n.a.	n.a.	n.a.	n.a.	n.a.	n.a.	n.a.	n.a.	n.a.	n.a.
SHM1	A3	2750.0	3.0	2.8	0.17	0.001	8.48	7.30	0.86	0.78	n.a.	n.a.	n.a.	n.a.	n.a.	n.a.	n.a.	n.a.	n.a.	n.a.
SHM1	A3	2752.0	3.0	2.8	0.13	0.002	10.98	11.35	1.03	0.78	n.a.	n.a.	n.a.	n.a.	n.a.	n.a.	n.a.	n.a.	n.a.	n.a.
SHM1	A3	2754.0	2.9	2.8	0.07	0.001	10.25	8.42	0.82	0.76	n.a.	n.a.	n.a.	n.a.	n.a.	n.a.	n.a.	n.a.	n.a.	n.a.
SHM1	A3	2756.0	2.8	2.8	0.11	0.001	9.13	7.93	0.87	0.89	n.a.	n.a.	n.a.	n.a.	n.a.	n.a.	n.a.	n.a.	n.a.	n.a.
SHM1	A3	2758.0	2.7	-4.2	0.11	0.002	6.73	5.83	0.87	0.78	n.a.	n.a.	n.a.	n.a.	n.a.	n.a.	n.a.	n.a.	n.a.	n.a.
SHM1	A3	2760.0	2.8	-4.0	0.31	0.002	4.71	6.87	1.46	1.62	n.a.	n.a.	n.a.	n.a.	n.a.	n.a.	n.a.	n.a.	n.a.	n.a.
SHM1	A3	2762.0	2.7	-4.4	0.16	0.001	3.87	4.71	1.22	0.91	n.a.	n.a.	n.a.	n.a.	n.a.	n.a.	n.a.	n.a.	n.a.	n.a.
SHM1	A3	2764.0	2.6	-3.6	0.13	0.001	1.82	2.32	1.28	0.75	n.a.	n.a.	n.a.	n.a.	n.a.	n.a.	n.a.	n.a.	n.a.	n.a.
SHM1	A3	2766.0	n.a.	n.a.	0.13	0.002	1.63	2.04	1.26	0.96	n.a.	n.a.	n.a.	n.a.	n.a.	n.a.	n.a.	n.a.	n.a.	n.a.
SHM1	A3	2768.0	2.6	-3.0	0.11	0.002	2.85	3.67	1.29	0.86	n.a.	n.a.	n.a.	n.a.	n.a.	n.a.	n.a.	n.a.	n.a.	n.a.
SHM1	A3	2770.0	2.6	-2.6	0.27	0.001	3.23	6.85	2.12	0.93	n.a.	n.a.	n.a.	n.a.	n.a.	n.a.	n.a.	n.a.	n.a.	n.a.
SHM1	A3	2772.0	3.2	-1.4	0.16	0.001	6.59	7.47	1.13	0.87	n.a.	n.a.	n.a.	n.a.	n.a.	n.a.	n.a.	n.a.	n.a.	n.a.
SHM1	A3	2774.0	3.1	-1.3	0.14	0.001	4.84	3.27	0.68	0.89	n.a.	n.a.	n.a.	n.a.	n.a.	n.a.	n.a.	n.a.	n.a.	n.a.
SHM1	A3	2776.0	2.8	-2.3	0.09	0.001	-	3.70	b.d.	0.69	n.a.	n.a.	n.a.	n.a.	n.a.	n.a.	n.a.	n.a.	n.a.	n.a.
SHM1	A3	2778.0	2.8	-2.3	0.19	0.003	4.30	2.59	0.60	0.71	n.a.	n.a.	n.a.	n.a.	n.a.	n.a.	n.a.	n.a.	n.a.	n.a.
SHM1	A3	2780.0	2.6	-2.5	0.13	0.001	-	2.95	b.d.	0.61	n.a.	n.a.	n.a.	n.a.	n.a.	n.a.	n.a.	n.a.	n.a.	n.a.
SHM1	A3	2782.0	2.6	-2.9	0.14	0.001	-	b.d.	1.04	0.52	n.a.	n.a.	n.a.	n.a.	n.a.	n.a.	n.a.	n.a.	n.a.	n.a.
SHM1	A3	2784.0	2.1	-1.5	0.12	b.d.	4.75	2.80	0.59	0.46	n.a.	n.a.	n.a.	n.a.	n.a.	n.a.	n.a.	n.a.	n.a.	n.a.
SHM1	A3	2786.0	2.3	-2.1	0.28	0.003	5.32	8.39	1.58	0.44	n.a.	n.a.	n.a.	n.a.	n.a.	n.a.	n.a.	n.a.	n.a.	n.a.
SHM1	A3	2788.0	2.9	-2.3	0.12	0.001	4.35	3.96	0.91	0.51	n.a.	n.a.	n.a.	n.a.	n.a.	n.a.	n.a.	n.a.	n.a.	n.a.
SHM1	A3	2790.0	2.9	-2.8	0.18	0.001	3.62	4.10	1.13	0.66	n.a.	n.a.	n.a.	n.a.	n.a.	n.a.	n.a.	n.a.	n.a.	n.a.
SHM1	A3	2792.0	2.9	-2.1	0.14	0.001	6.11	4.72	0.77	0.54	n.a.	n.a.	n.a.	n.a.	n.a.	n.a.	n.a.	n.a.	n.a.	n.a.
SHM1	A3	2794.0	2.9	-3.3	0.08	0.002	5.79	3.69	0.64	0.42	n.a.	n.a.	n.a.	n.a.	n.a.	n.a.	n.a.	n.a.	n.a.	n.a.
SHM1	A3	2796.0	2.9	-2.4	0.10	0.001	5.24	3.36	0.64	0.84	n.a.	n.a.	n.a.	n.a.	n.a.	n.a.	n.a.	n.a.	n.a.	n.a.
SHM1	A3	2798.0	3.0	-1.9	0.37	b.d.	3.47	2.15	0.62	0.63	n.a.	n.a.	n.a.	n.a.	n.a.	n.a.	n.a.	n.a.	n.a.	n.a.
SHM1	A3	2800.0	3.0	-2.3	0.09	0.002	b.d.	b.d.	b.d.	0.62	n.a.	n.a.	n.a.	n.a.	n.a.	n.a.	n.a.	n.a.	n.a.	n.a.

n.a.: not analyzed

b.d.: below detection

Table S2: Biomarker data

#	Well	Unit	Depth (m)	TOC %	Tris ppm TOC	Ster ppm TOC	Hop ppm TOC	Tris ppm sats	Ster ppm sats	Hop ppm sats	Total Tricyclics	Total Steranes	Total Hopanes
1	OMR1	A5C	2846.6	0.9	69.5	216.1	358.1	5.2E+03	1.6E+04	2.7E+04	2.6E+08	8.1E+08	1.3E+09
2	OMR1	A5C	2847.8	1.0	26.0	29.0	35.2	5.0E+03	5.6E+03	6.8E+03	1.0E+08	1.1E+08	1.4E+08
3	OMR1	A5C	2849.2	0.9	38.9	79.4	54.2	6.7E+03	1.4E+04	9.3E+03	1.3E+08	2.7E+08	1.9E+08
4	OMR1	A5C	2850.5	0.8	62.4	75.6	68.9	9.9E+03	1.2E+04	1.1E+04	2.0E+08	2.4E+08	2.2E+08
5	OMR1	A5C	2851.7	0.6	54.2	62.7	83.3	6.5E+03	7.5E+03	9.9E+03	1.3E+08	1.5E+08	2.0E+08
6	OMR1	A5C	2853.3	1.0	44.3	43.3	60.6	8.5E+03	8.3E+03	1.2E+04	1.7E+08	1.7E+08	2.3E+08
7	OMR1	A5C	2854.8	0.8	55.3	44.2	54.8	8.7E+03	6.9E+03	8.6E+03	1.7E+08	1.4E+08	1.7E+08
8	OMR1	A5C	2856.6	0.8	71.8	71.4	106.1	1.1E+04	1.1E+04	1.7E+04	2.3E+08	2.3E+08	3.4E+08
9	OMR1	A5C	2858.5	0.9	40.2	32.3	42.4	6.9E+03	5.6E+03	7.3E+03	1.4E+08	1.1E+08	1.5E+08
10	BB4	A4C	2907.7	0.9	30.6	49.0	55.6	2.7E+03	4.3E+03	4.9E+03	5.4E+07	8.6E+07	9.8E+07
11	BB4	A4C	2908.7	1.2	15.8	27.1	33.1	1.9E+03	3.3E+03	4.0E+03	3.8E+07	6.5E+07	8.0E+07
12	BB4	A4C	2919.3	0.5	25.1	38.9	40.0	1.3E+03	2.1E+03	2.1E+03	2.7E+07	4.2E+07	4.3E+07
13	BB4	A4C	2928.8	0.1	146.8	258.2	388.0	2.0E+03	3.5E+03	5.2E+03	3.9E+07	6.9E+07	1.0E+08
14	BB4	A4C	2932.1	0.2	48.5	77.9	91.7	1.2E+03	1.9E+03	2.2E+03	2.3E+07	3.7E+07	4.4E+07
15	BB4	A4C	2937.1	0.2	45.1	76.5	86.4	1.0E+03	1.7E+03	2.0E+03	2.1E+07	3.5E+07	3.9E+07
16	BB4	A4C	2940.1	0.4	14.2	20.8	28.6	5.1E+02	7.5E+02	1.0E+03	1.0E+07	1.5E+07	2.1E+07
17	BB4	A4C	2944.7	0.5	19.0	31.6	72.6	9.9E+02	1.6E+03	3.8E+03	2.0E+07	3.3E+07	7.6E+07
18	BB4	A4C	2945.2	0.4	55.9	99.5	158.8	2.0E+03	3.5E+03	5.6E+03	3.9E+07	7.0E+07	1.1E+08
19	BB4	A3C	3030.8	0.1	1.0	4.4	49.9	1.3E+02	5.8E+02	6.5E+03	2.7E+05	1.2E+06	1.3E+07
20	BB4	A3C	3031.3	0.1	1.0	4.8	39.8	1.5E+02	6.8E+02	5.6E+03	2.9E+05	1.4E+06	1.1E+07
21	BB4	A3C	3032.8	0.2	1.7	7.6	61.4	2.6E+02	1.2E+03	9.8E+03	5.3E+05	2.4E+06	2.0E+07
22	BB4	A3C	3033.6	0.2	4.8	27.0	141.0	3.6E+02	2.0E+03	1.1E+04	1.4E+06	8.1E+06	4.2E+07
23	BB4	A3C	3034.0	0.2	1.4	7.3	50.0	2.6E+02	1.3E+03	9.1E+03	5.2E+05	2.7E+06	1.8E+07
24	BB4	A3C	3034.5	0.1	1.3	4.2	31.6	1.8E+02	5.9E+02	4.4E+03	3.6E+05	1.2E+06	8.8E+06
25	MNH1	A2C	4187.3	0.6	2.0	2.7	5.2	2.5E+02	3.4E+02	6.4E+02	5.1E+06	6.7E+06	1.3E+07
26	AAL1	A0C	3825.0	0.5	70.3	35.4	57.0	8.1E+03	4.1E+03	6.6E+03	1.3E+08	6.5E+07	1.1E+08
27	AAL1	A0C	3827.0	0.4	141.4	51.9	85.5	1.2E+04	4.6E+03	7.5E+03	2.5E+08	9.1E+07	1.5E+08
28	AAL1	A0C	3832.1	0.5	42.8	30.3	61.1	5.0E+03	3.6E+03	7.2E+03	8.0E+07	5.7E+07	1.1E+08
29	AAL1	A0C	3835.3	0.5	14.5	9.1	14.4	1.3E+04	8.2E+03	1.3E+04	2.6E+07	1.6E+07	2.6E+07
30	AAL1	A0C	3841.3	0.4	35.5	19.0	26.6	3.2E+04	1.7E+04	2.4E+04	6.3E+07	3.4E+07	4.7E+07

Notation: ster = steranes; hop = hopanes; tris = tricyclics;

#	Ster/ Hop	2- MeHI	3- MeHI	Gam/ C30H	28,30/ C30H	Tricyclics/ Hopanes	C28/ (27+28+29)	29,30/ C30H	C29H/ C30H	30nor/ C30H	Ts/ (Ts+Tm)	C27 Dia/Reg	C29 S/R	C30H/ (C30H+Mor)	C31H S/R
1	0.60	0.08	0.04	0.26	0.28	0.19	0.11	0.13	1.22	0.13	0.15	0.04	0.95	0.96	1.33
2	0.82	0.08	0.05	0.23	0.31	0.74	0.12	0.16	1.34	0.13	0.16	0.04	1.05	0.96	1.34
3	1.46	0.08	0.06	0.25	0.32	0.72	0.12	0.16	1.36	0.13	0.16	0.04	1.13	0.96	1.35
4	1.10	0.08	0.05	0.24	0.35	0.91	0.12	0.17	1.41	0.14	0.15	0.04	1.08	0.96	1.35
5	0.75	0.08	0.05	0.23	0.30	0.65	0.11	0.16	1.32	0.14	0.16	0.04	1.05	0.97	1.36
6	0.72	0.08	0.05	0.23	0.32	0.73	0.11	0.15	1.36	0.14	0.16	0.03	1.09	0.97	1.36
7	0.81	0.08	0.05	0.23	0.33	1.01	0.11	0.16	1.38	0.14	0.16	0.04	1.07	0.97	1.37
8	0.67	0.08	0.06	0.24	0.31	0.68	0.11	0.14	1.31	0.14	0.16	0.03	1.09	0.97	1.36
9	0.76	0.08	0.06	0.23	0.29	0.95	0.11	0.15	1.34	0.13	0.16	0.03	1.03	0.97	1.35
10	0.88	0.07	0.04	0.21	0.28	0.55	0.11	0.14	1.17	0.14	0.15	0.02	1.02	0.97	1.34
11	0.82	0.08	0.04	0.22	0.27	0.48	0.12	0.14	1.16	0.13	0.15	0.02	1.03	0.96	1.35
12	0.97	0.07	0.04	0.21	0.30	0.63	0.11	0.15	1.19	0.14	0.17	0.03	1.04	0.97	1.34
13	0.67	0.07	0.04	0.23	0.26	0.38	0.12	0.13	1.18	0.13	0.16	0.02	0.95	0.96	1.34
14	0.85	0.07	0.05	0.21	0.25	0.53	0.11	0.15	1.19	0.15	0.18	0.02	1.07	0.97	1.34
15	0.89	0.08	0.04	0.22	0.25	0.52	0.12	0.16	1.25	0.14	0.22	0.03	1.04	0.96	1.34
16	0.73	0.07	0.03	0.20	0.21	0.50	0.12	0.13	1.13	0.15	0.23	0.03	1.10	0.96	1.33
17	0.44	0.04	0.02	0.16	0.10	0.26	0.17	0.11	1.16	0.13	0.21	0.03	1.01	0.96	1.24
18	0.63	0.07	0.04	0.20	0.23	0.35	0.13	0.13	1.14	0.12	0.21	0.03	1.00	0.96	1.33
19	0.09	0.03	0.01	0.06	0.01	0.02	0.16	0.10	1.18	0.17	0.54	0.22	1.05	0.96	1.16
20	0.12	0.03	0.01	0.06	0.01	0.03	0.17	0.11	1.28	0.17	0.50	0.20	1.01	0.95	1.18
21	0.12	0.02	0.01	0.07	0.01	0.03	0.17	0.13	1.50	0.22	0.47	0.14	1.10	0.96	1.21
22	0.19	0.03	0.01	0.06	0.01	0.03	0.17	0.15	1.57	0.23	0.50	0.19	1.10	0.95	1.16
23	0.15	0.02	0.01	0.05	0.01	0.03	0.19	0.14	1.51	0.19	0.50	0.21	0.99	0.96	1.18
24	0.13	0.03	0.01	0.07	0.02	0.04	0.16	0.12	1.43	0.20	0.48	0.19	0.98	0.95	1.19
25	0.52	0.14	0.02	0.11	0.11	0.39	0.12	0.16	1.56	0.17	0.49	0.17	1.08	0.96	1.38
26	0.62	0.05	0.05	0.18	0.18	1.23	0.13	0.12	1.18	0.10	0.26	0.03	1.05	0.96	1.40
27	0.61	0.05	0.04	0.14	0.19	1.65	0.12	0.13	1.26	0.11	0.24	0.04	1.06	0.96	1.38
28	0.50	0.04	0.05	0.20	0.14	0.70	0.12	0.11	1.09	0.11	0.28	0.04	1.05	0.96	1.38
29	0.63	0.06	0.03	0.18	0.18	1.01	0.13	0.13	1.16	0.10	0.27	0.13	1.15	0.96	1.39
30	0.72	0.05	0.03	0.18	0.26	1.34	0.11	0.11	0.90	0.07	0.21	0.06	1.16	0.96	1.43

Notation: Gam = gammacerane; 28,30 = 28,30 BNH; 29,30 = 29,30 BNH; Mor = Moretane

CHAPTER 5
Intrabasinal sulfur isotope chemostratigraphy of the Ediacaran-Cambrian Huqf Supergroup, Sultanate of Oman: a synthesis of subsurface and outcrop data

D. A. Fike[1*] and J. P. Grotzinger[2]

[1]Department of Earth, Atmospheric, & Planetary Sciences, Massachusetts Institute of Technology, Cambridge, MA 02139, USA

[2]Division of Geological and Planetary Sciences, California Institute of Technology, Pasadena, CA 91125, USA

ABSTRACT
Variations in the isotopic record of marine sulfate ($\delta^{34}S_{SO4}$) are used to infer paleoenvironmental conditions and reconstruct the global sulfur biogeochemical cycle. However, there is still significant uncertainty as to how representative a given isotopic record is of local, regional, or global conditions. To assess this, we have generated a paired $\delta^{13}C_{carb}$-$\delta^{34}S_{SO4}$ chemostratigraphy from multiple sections through the subsurface and outcrops of the Ediacaran – earliest Cambrian Huqf Supergroup, Sultanate of Oman. The large-scale features of the $\delta^{34}S$ curve, such as the transition from Nafun Group strata, characterized by $\delta^{34}S_{SO4} \sim 25‰$ to Ara Group strata ($\sim 40‰$) are reproduced across this $\sim$ 1,000 km basin. The $\delta^{34}S_{SO4}$ stratigraphy was able to verify existing correlations based on $\delta^{13}C_{carb}$ chemostratigraphy and lithostratigraphy. In addition, $\delta^{34}S_{SO4}$ has the potential to resolve uncertain stratigraphic assignments in strata lacking diagnostic $\delta^{13}C_{carb}$ signatures or lithologies.

INTRODUCTION

The results of chemostratigraphic studies provide one of the few reliable ways to reconstruct local to global environmental conditions recorded by sedimentary strata. Examples of previous studies focus on reconstruction of the carbon (HAYES et al., 1999; ROTHMAN et al., 2003) and sulfur (CLAYPOOL et al., 1980; FIKE and GROTZINGER, 2007a; KAMPSCHULTE and STRAUSS, 2004) biogeochemical cycles, ocean/atmosphere redox condition (ARNOLD et al., 2004; FARQUHAR and WING, 2003), and weathering fluxes to

the oceans (VEIZER et al., 1999). However, the strength of any paleoenvironmental reconstruction depends on how representative the proxy under study is of local, regional, or global conditions.

Chemostratigraphic studies commonly use the carbon, and more recently, the sulfur isotopic compositions of sedimentary minerals. The carbon isotopic composition of materials is measured in permil (‰) using the standard δ-notation: $\delta^{13}C = (R_x/R_{std}-1) \cdot 10^3$, where R_x is $^{13}C/^{12}C$ in a sample normalized to the international standard Vienna Pee Dee Belemnite). Both carbonate minerals ($\delta^{13}C_{carb}$) and organic matter ($\delta^{13}C_{org}$) are routinely analyzed for their carbon isotopic composition. Similarly, the sulfur isotopic composition ($\delta^{34}S_x = (R_x/R_{std}-1) \cdot 10^3$, where R_x is the $^{34}S/^{32}S$ of a sample normalized to the international standard Vienna Canyon Diablo Troilite) of sedimentary sulfates ($\delta^{34}S_{SO4}$) and pyrites ($\delta^{34}S_{pyr}$) are frequently measured as part of chemostratigraphic studies. In terms of correlation potential, a set of chemostratigraphic data (e.g., $\delta^{13}C$ or $\delta^{34}S$) can be used to correlate between two or more sections, or to evaluate the merits of a previously proposed correlation based upon an independent set of attributes, such as lithology or fossil content. This study aims to do both: using $\delta^{34}S_{SO4}$ to test existing correlations based upon $\delta^{13}C_{carb}$ chemostratigraphy and lithostratigraphy, and to develop new correlations using $\delta^{34}S_{SO4}$ in strata that do not contain diagnostic lithologies, fossils, and/or carbon isotopic signatures.

Sections can be correlated intrabasinally or globally, depending on the proxy chosen and the sampling resolution. For example, the reservoirs of dissolved inorganic carbon (DIC) and sulfate are well mixed in the modern oceans and therefore reasonably homogeneous with respect to their isotopic composition (Canfield, 2001; Ripperdan,

2001). As such, $\delta^{13}C_{carb}$ or $\delta^{34}S_{SO4}$ from age-equivalent strata deposited globally should record the same isotope signatures ($\pm \sim 1\text{‰}$ associated with local and/or oceanographic effects). Although regional and local conditions can induce variability, similar $\delta^{13}C_{carb}$ profiles are found from globally distributed strata (Ripperdan, 1994), demonstrating the utility of $\delta^{13}C_{carb}$ for correlation and allowing the reconstruction of a global $\delta^{13}C_{carb}$ curve through geologic time (Veizer et al., 1999).

For the modern ocean, $\delta^{34}S_{SO4}$ obtained from sedimentary minerals should accurately reflect the sulfur isotope composition of coeval seawater sulfate, as this is essentially uniformly ($\pm 1\text{‰}$) distributed today. This, however, has yet to be convincingly demonstrated for ancient strata. The one published study that explicitly looked at parallel sections of the Marinoan cap carbonate in Namibia found distinctly different $\delta^{34}S_{SO4}$ trends as a function of paleoenvironment, which was attributed to the upwelling of sulfidic waters in the aftermath of a Snowball Earth glaciation (HURTGEN, 2006). While a consensus curve is slowly developing from multiple globally-distributed datasets (Canfield et al., 1996; Claypool et al., 1980; Kampschulte and Strauss, 2004; Strauss, 1993; Thode and Monster, 1965a), there is still no clearly reproducible record from multiple intrabasinal sections that records similar values and trends for the same chronostratigraphic interval. The utility of $\delta^{34}S_{SO4}$, both for correlation and paleoenvironmental reconstruction, depends to a large degree in the confidence one has about how representative of depositional conditions (local, regional, or global) measured values are.

In the sulfur cycle, previous studies (e.g., Claypool et al., 1980; Holser, 1977; Thode and Monster, 1965b) have indicated extreme enrichment in marine sulfate $\delta^{34}S_{SO4}$ in

terminal Ediacaran-earliest Cambrian strata. However, as little is still known about even the basin-wide reproducibility of $\delta^{34}S_{SO4}$, it is difficult to deconvolve observed $\delta^{34}S_{SO4}$ variability into a truly global (secular) component and any contribution from local effects. It is the goal of the present study to investigate the reproducibility of paired $\delta^{13}C_{carb}$-$\delta^{34}S_{SO4}$ as preserved in the sedimentary strata of the Huqf Supergroup, Sultanate of Oman.

Other proxies, such as the isotopic composition of organic carbon ($\delta^{13}C_{org}$) or sedimentary pyrite ($\delta^{34}S_{pyr}$) are more likely to reflect local conditions rather than a global trend. Although both of these reduced species (organic matter and sulfide) are derived from their oxidized counterparts (DIC and marine sulfate), they are formed predominantly through microbial processes in the marine environment with an isotopic fractionation that depends strongly on local conditions, such as redox, microbial community composition, dominant metabolic pathways, and the rate of sulfate reduction or carbon fixation (Canfield, 2001; Hayes, 1993, 2001; Laws et al., 1995). In theory, under invariant depositional conditions, both $\delta^{13}C_{org}$ and $\delta^{34}S_{pyr}$ would reflect the same trends as $\delta^{13}C_{carb}$ and $\delta^{34}S_{SO4}$ (although shifted to isotopically more depleted values because of microbial fractionation effects). However, depositional/environmental conditions can dominate changes in $\delta^{13}C_{org}$ or $\delta^{34}S_{pyr}$, resulting in uncorrelated or anti-correlated variability relative to $\delta^{13}C_{carb}$ or $\delta^{34}S_{SO4}$, respectively (Fike et al., 2006; Laws et al., 1995; Rothman et al., 2003). Despite this, there is evidence that both $\delta^{34}S_{pyr}$ and $\delta^{13}C_{org}$ can form coherent chemostratigraphic datasets on at least a local or regional (basin-wide), if not global, scale (Canfield, 2004; Popp et al., 1997; Ross et al., 1995).

As such, compilations of $\delta^{13}C_{org}$ and/or $\delta^{34}S_{pyr}$ can be of aid in constructing and evaluating correlations based on $\delta^{13}C_{carb}$ or $\delta^{34}S_{SO4}$.

GEOLOGICAL CONTEXT: HUQF SUPERGROUP

The Huqf Supergroup provides one of the best preserved, most continuous sections of Ediacaran through earliest Cambrian (ca. 635 – 540 Myr) strata (Amthor et al., 2003; Bowring et al., 2007; Burns and Matter, 1993; Cozzi et al., 2004a; Cozzi et al., 2004b; Le Guerroue et al., 2006a; Le Guerroue et al., 2006b; Le Guerroue et al., 2006c; McCarron, 2000; Schröder et al., 2004). Huqf strata are preserved in surface outcrops of the Jabal Akhdar in the Oman Mountains and the Huqf area, as well as within subsurface sedimentary basins (Figure 1). Huqf strata are prolific oil and gas producers. As a result, there are numerous exploration wells throughout the region, providing access to replicate sections from the subsurface.
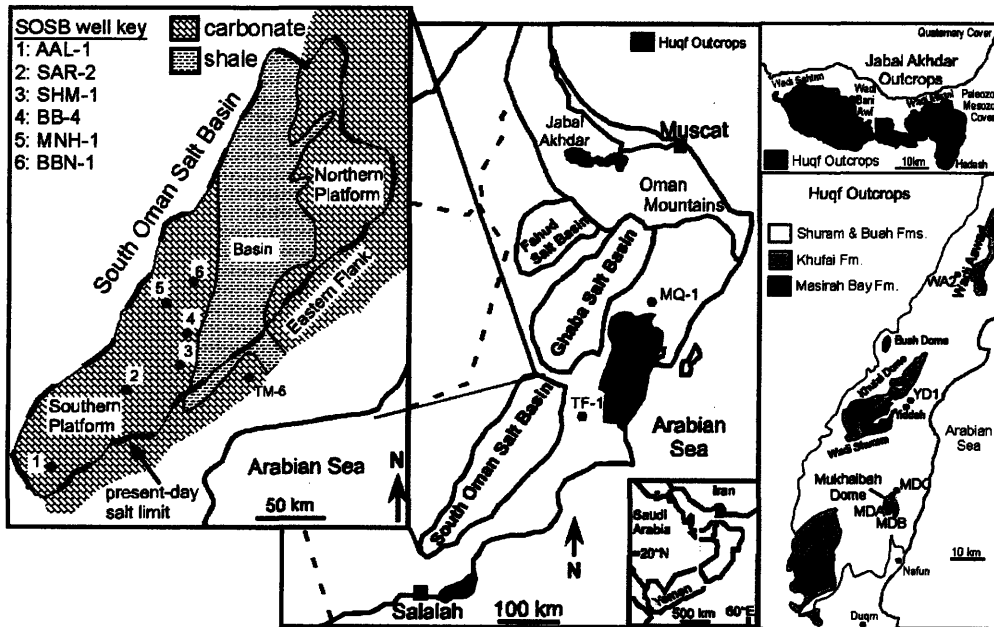
Figure 1: Map of Oman, showing the location of Neoproterozoic outcrops and modern day salt basins. Inset panels highlight the locations of wells within the South Oman Salt Basin (SOSB) and outcrops from the Huqf Ara and Jabal Akhdar.

The Huqf Supergroup comprises the Abu Mahara, Nafun, and Ara groups. Stratigraphic, lithologic, and geochronologic constraints for the Huqf Supergroup are shown in Figure 2, along with the stratigraphic interval sampled by each section studied here.
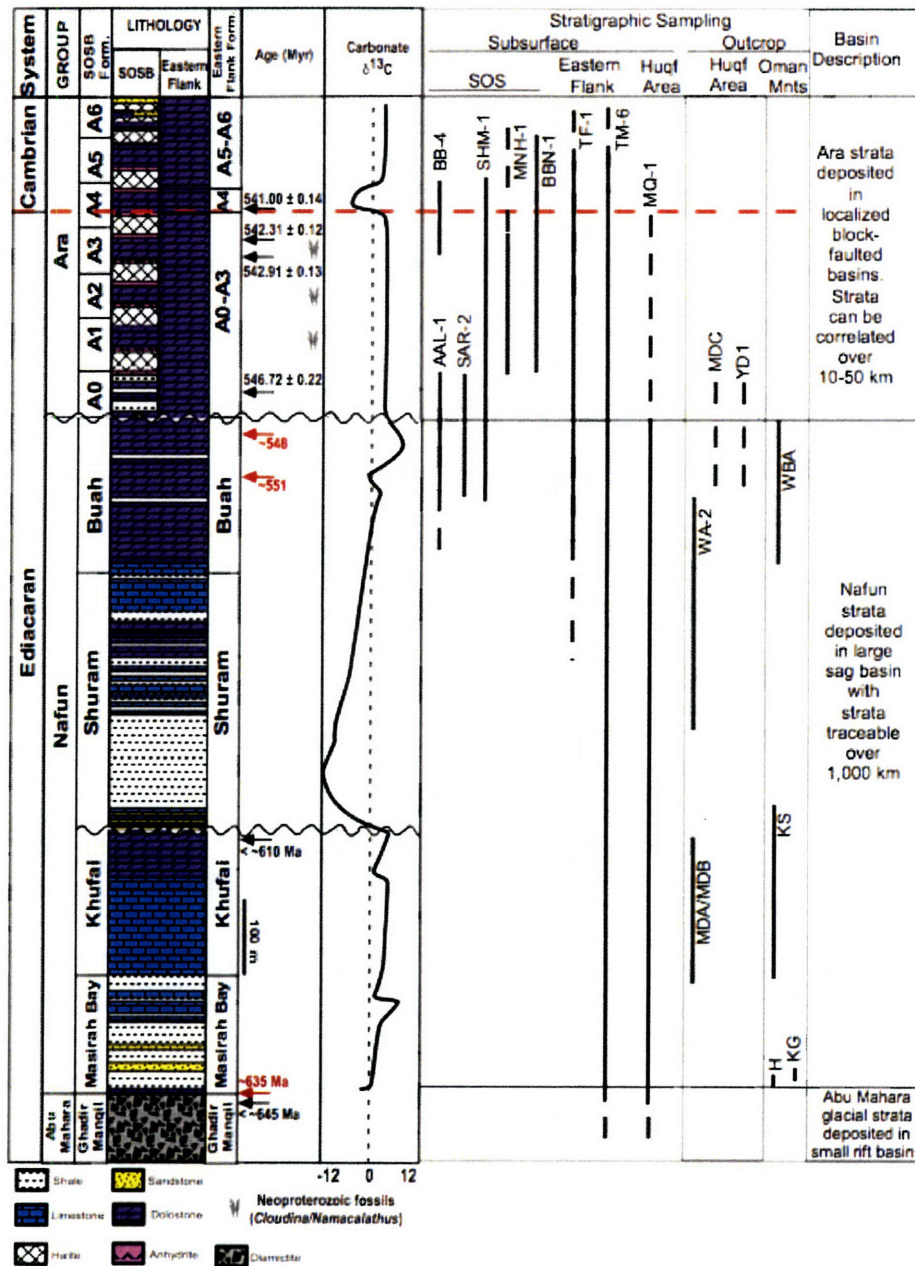
Figure 2: Composite stratigraphy of Oman showing lithology (for both SOSB and Eastern Flank strata), age constraints, fossils, and composite $\delta^{13}C_{carb}$. The stratigraphic range of wells and outcrop sections are shown.

The Abu Mahara Group contains two Neoproterozoic glacial deposits that fill rift basins overlying ca. 800 Ma crystalline basement (BOWRING et al., 2007). The oldest glacial deposits preserved within the Oman Mountains belong to the Ghubrah Formation. A tuffaceous sandstone within Ghubrah strata was originally dated to ca 723 +16/-10 Ma (BRASIER et al., 2000), and recently revised to 713 ± 1 Ma (BOWRING et al., 2007). The Ghubrah is unconformably overlain by the Saqlah volcaniclastics and the younger glaciogenic unit, the Fiq Formation (LEATHER et al., 2002). The existence of an angular unconformity separating the glacial units argues for a depositional hiatus. Detrital zircons indicate that the Fiq formation must have been deposited after 664 Ma (BOWRING et al., 2007). Another population of detrital zircons from a volcanic ash within the glacial diamictite of the LHN-1 core has been dated 645 Ma (BOWRING et al., 2007). These glacial units are correlated and the Fiq glaciation and its overlying Hadash cap carbonate are interpreted to be Marinoan-equivalent (ca 635 Ma).

Nafun Group sediments were deposited in a regionally extensive sag basin under open, shallow marine conditions, and each formation can be traced laterally for several hundred km across Oman (GROTZINGER et al., 2002; LE GUERROUE et al., 2006a; MATTES and CONWAY-MORRIS, 1990; MCCARRON, 2000). Nafun Group strata comprise two clastic-to-carbonate shallowing-upward successions (Masirah Bay Formation and Khufai Formation; Shuram Formation and Buah Formation) with an unconformity across the Khufai-Shuram boundary(MCCARRON, 2000) that likely includes the interval of Gaskiers glaciation at ca. 580 Ma (BOWRING et al., 2007). Le Guerroue et al. (2006a; 2006c), however, argue for continuous deposition across this contact based upon smoothly varying $\delta^{13}C_{carb}$ profiles. The Shuram excursion, a >15‰ negative excursion in

$\delta^{13}C_{carb}$, spans ~ 500m of section from the basal Shuram Formation through the mid-Buah Formation (BURNS and MATTER, 1993; FIKE et al., 2006; LE GUERROUE et al., 2006a; LE GUERROUE et al., 2006c). The excursion has been identified from over 20 separate sections from the subsurface, the Huqf area, and the Jabal Akhdar in the Oman Mountains (Burns and Matter, 1993; Le Guerroue et al., 2006a; Le Guerroue et al., 2006b; McCarron, 2000), and serves as an excellent stratigraphic marker for correlation across Oman. Similarly, detailed depositional and isotopic ($\delta^{13}C_{carb}$) characterization of the Buah Formation (COZZI et al., 2004a; COZZI et al., 2004b) allows for clear correlation of this unit between strata of the Jabal Akhdar in the Oman Mountains, the Huqf area, and the subsurface. Global correlation of $\delta^{13}C_{carb}$ anomalies provides two age constraints for the Buah Formation (Figure 2): ca. 550 Ma for the mid-Buah (correlation with Doushantuo Formation, China (BOWRING et al., 2007; CONDON et al., 2005)); and ca. 548 Ma for the upper Buah (correlation with Nama Group, Namibia (BOWRING et al., 2007; GROTZINGER et al., 1995)). These ages are consistent with those obtained from the overlying Ara Group.

Ara Group strata were deposited between ca. 547 – 540 Ma (BOWRING et al., 2007) and are known definitively only from the subsurface (AMTHOR et al., 2003; MATTES and CONWAY-MORRIS, 1990), although putative Ara-equvalent strata has been identified in the Huqf area (Nicholas, 1999). In strata beneath the modern day South Oman Salt Basin (SOSB), the Ara Group exists as a series of six carbonate-evaporite shallowing upward cycles (A1-A6) overlying non-evaporitic carbonates of the basal Ara (A0) (Amthor et al., 2003; Schröder et al., 2003). Ara strata were deposited in strongly subsiding block-faulted basin (GROTZINGER et al., 2002). On the margin (termed the Eastern Flank) of the

SOSB, Ara Group strata are preserved as a strictly carbonate succession approximately 200-300m in thickness (Figure 2). There is no record of evaporite deposition along the Eastern flank (see discussion in FIKE and GROTZINGER, 2007a). Evaporite deposition within the basin is likely associated with periods of non-deposition (subaerial exposure) on the Eastern Flank. In both the SOSB and the Eastern Flank, the contact between the Buah and overlying Ara Group is marked by a disconformable, karstic surface. There is a robust correlation (AMTHOR et al., 2003) between the A4 carbonate strata within the SOSB and those deposited on the Eastern Flank, based on the presence of an ash-bed dated to 541 Ma (BOWRING et al., 2007), $\delta^{13}C_{carb}$ chemostratigraphy, geophysical well log data, and trace element geochemistry, particularly an enrichment in uranium. However, the difficulties of correlating hiatal gaps in Eastern Flank strata to the periods of evaporite deposition within the SOSB hinders correlation above and below the A4 unit. Therefore, the lower Ara strata on the Eastern flank are correlated to the A0-A3 carbonate units and upper Ara strata on the Eastern flank are correlated with the A5/A6 carbonates from within the SOSB (Figure 2). No attempt to further divide Eastern Flank strata is made.

The presence of multiple ash horizons within Ara Group strata (Figure 2) has significantly improved our understanding of the timing and duration of Ara deposition and our ability to correlate the Oman stratigraphy with other sections globally (AMTHOR et al., 2003; BOWRING et al., 2007; CONDON et al., 2005; GROTZINGER et al., 1995). An age of 546.72 ± 0.22 Ma from the middle of the basal Ara carbonate (A0) constrains the unconformity at the Buah-Ara contact to ~1 Myr (BOWRING et al., 2007). Ash beds at the base (AMTHOR et al., 2003; BOWRING et al., 2007) and top (BOWRING et al., 2007) of the third carbonate unit (A3) yield zircon U/Pb ages of 542.91 ± 0.13 and 542.31 ± 0.14

Ma, respectively. All zircon U/Pb ages cited here were obtained from the same laboratory and calibrated under the same conditions, allowing for a very precise determination of the relative ages of samples (BOWRING et al., 2007). These A3 ages indicate that the deposition of a typical Ara carbonate unit took ~ 1 Ma (BOWRING et al., 2007), consistent with the age difference between the A0 and A4 (see below) carbonates. The base of the A4 carbonate unit contains an ash that yielded a U/Pb age (AMTHOR et al., 2003; BOWRING et al., 2007) of 541.00 ± 0.12 Ma. This age, in combination with a 7‰ negative excursion in carbonate $\delta^{13}C$ and the disappearance of Ediacaran *Namacalathus* and *Cloudina* fossil assemblages, is the basis for the placement in Oman of the E-C boundary at the base of the A4 carbonate (AMTHOR et al., 2003).

SAMPLES

In this paper, we focus on the Nafun and Ara groups of the Huqf Supergroup, deposited between ca. 635 – 540 Ma (BOWRING et al., 2007). These strata were chosen because of the excellent preservation of these strata and the existing understanding of depositional environments and facies variability (Cozzi et al., 2004a; Cozzi et al., 2004b; Le Guerroue et al., 2006a; Le Guerroue et al., 2006b; Le Guerroue et al., 2006c; McCarron, 2000). Samples from this study were taken as cores and cuttings from the following SOSB wells (Figure 1): AAL-1, BB-4, BBN-1, MNH-1, MQ-1, SAR-2, and SHM-1. The Eastern Flank wells TF-1 and TM-6 were also sampled, as was the well MQ-1, located just north of the Huqf outcrop area (Figure 1). Cuttings are rock chips (typically 1–5 mm in size) produced during drilling that are collected by the well-site geologist every 2-5 meters. Our vertical sampling resolution is limited by this constraint.

In contrast, cores are collected intermittently during drilling and allow us to sample the cored interval at much greater resolution. Besides the obvious contextual advantage (e.g., facies identification) in core samples, the main difference between samples of core and cuttings is that a core sample typically covers ~ 2cm of stratigraphy (physical dimension of sample taken from core), whereas the cuttings in a given sample cover 2-5 meters of stratigraphy. Thus, cuttings represent a geochemical and lithological average, which has the tendency to smooth high-frequency variations in measured parameters. Results for Nafun Group strata from the well MQR-1 were reported previously (FIKE et al., 2006). Results for $\delta^{34}S_{CAS}$ and $\delta^{34}S_{anhyd}$ from the subsurface wells of the Ara Group have been described in Chapters 2 and 3.

Outcrop sections were sampled in the Huqf outcrop area and the Jabal Akhdar in the Oman Mountains to complement our subsurface samples (Figure 1). In the Huqf area, Khufai Formation at the Mukhaibah Dome (sections: MDA and MDB) and the Shuram-Buah Formations at Wadi Aswad (section: WA2) were sampled. In addition, we investigated two sections of 'post-Buah' carbonates at the Mukhaibah Dome (section: MDC) and near Yiddah (section: YD1), which are of uncertain stratigraphic affinity, but have been postulated to be outcrop equivalents of the Ara Group (Nicholas, 1999). In the Jabal Akhdar of the Oman Mountains, the following sections were collected (Figure 1): Hadash cap carbonate (section H, adjacent to the Hadash Village:); Hadash to lower Masirah Bay Formations (section KG, locality 2.1 of Allen et al. (2005), located 1km south of Al Jufaf, Wadi Bani Awf); the Khufai to basal Shuram Formations (section KS, locality 2.1 of Allen et al. (2005), located in Wadi Bani Awf approximately 2km south of the road to Wadi Sahtan); and the Buah Fm. (section WBA: in Wadi Bani Awf). All

localities within the Jabal Akhdar are described in detail elsewhere (Allen et al., 2005; Cozzi et al., 2004b).

We have examined 14 outcrop and subsurface sections through Huqf strata to evaluate reproducibility of $\delta^{13}C_{carb}$-$\delta^{34}S_{SO4}$ across the ~1,000 km Huqf basin. In particular, we want to use $\delta^{34}S_{SO4}$ to evaluate existing correlations based on $\delta^{13}C_{carb}$ chemostratigraphy and lithostratigraphy. Further, for those strata lacking distinctive $\delta^{13}C_{carb}$ signatures and lithologies (e.g., the majority of the non-A4 Ara Group), we investigate the utility of $\delta^{34}S_{SO4}$ chemostratigraphy for correlation purposes. The analysis of parallel sections provides us with the opportunity to evaluate a range of depositional and post-depositional factors that may effect the preservation of $\delta^{13}C_{carb}$ and/or $\delta^{34}S_{SO4}$ in these strata. In particular, there is a well established facies gradient during Nafun Group deposition (McCARRON, 2000) from shallow water facies in the Huqf area to deeper water facies in the Oman Mountains. Another facies gradient is found in the Ara Group, between strata of the episodically restricted SOSB and the non-evaporitic Eastern Flank. Subsurface sections have been protected from surface oxidation and provide a comparison to outcrop sections. In addition, subsurface strata have been subjected to a variety of burial depths, which allows us to investigate the effect of burial on the chemical alteration of these sediments. Similarly, while the Huqf outcrops have only undergone shallow burial, the strata in the Oman Mountains were buried to great depth during the overthrusting of the Semail Ophiolite and subjected to low-grade (T ~ 250-280°C) metamorphic conditions (Saddiqi et al., 2006). In comparing the Huqf and Oman Mountain sections with the subsurface data, we hope to be able to detect any original depositional (facies) variability in the isotopic signatures examined or any alteration (or

evidence for the lack thereof) due to the different diagenetic histories of these replicate sections. In seeking to understand variability within $\delta^{13}C_{carb}$ and $\delta^{34}S_{SO4}$, supplemental analyses of $\delta^{13}C_{org}$, $\delta^{34}S_{pyr}$, $\delta^{18}O_{carb}$, and the abundance of major, minor, and trace elements have been performed. These data can further constrain depositional conditions and/or possible post-depositional changes to the samples.

METHODS:

Throughout the course of this study, sample preparation was varied significantly, both as a means to explore possible extraction artefacts and to reflect lessons learned over this time within the sulfur isotope community. Unlike many studies (e.g., Hurtgen et al., 2006), these samples were not subjected to a bleach treatment to remove pyrite and organics prior to CAS analysis. This was done because of the desire to look at both pyrite and organic matter isotopes within the same samples and to minimize treatment steps. All samples underwent repeated water soaking in DI to remove water-soluble sulfates that may have arisen from (post-depositional) pyrite oxidation. This was continued until no further sulfate was liberated (as determined by $BaCl_2$ precipitation). Sulfate liberated during the rinses was typically depleted relative to CAS with the depletion roughly proportional to pyrite yield (Figure 3). Progressive rinses liberated less soluble sulfate and were consistently more enriched (Figure 3) suggesting a smaller contribution from sulfate derived from pyrite oxidation relative to that derived from dissolution of gypsum/anhydrite inclusions.
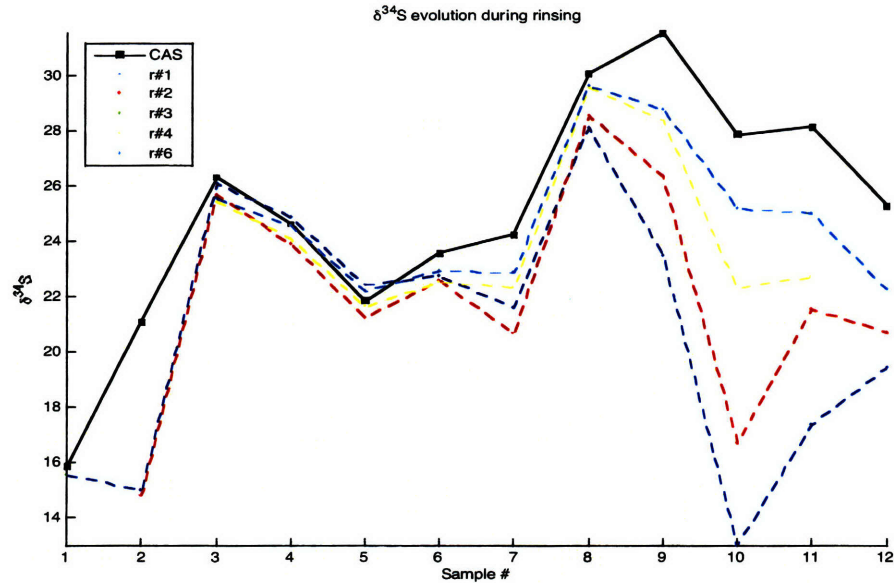
Figure 3: The $\delta^{34}S$ values of sulfate liberated during progressive DI rinses (1-6) are shown and compared to the value obtained for $\delta^{34}S_{CAS}$.

Later extractions involved the addition of NaCl (10 wt %) to the DI (KAMPSCHULTE and STRAUSS, 2004), which has elsewhere been shown to significantly increase the yield of extracted water-soluble sulfate (G. Shields, pers. comm.). Use of this saline rinse can make a significant difference (up to 3‰) in strata with significant pyrite (up to ~ 1‰ wt). Figure 4 compares the observed $\delta^{34}S_{CAS}$ obtained using halite rinses with that obtained using DI rinses. The data from each cleaning procedure track each other remarkably well, although the $\delta^{34}S_{CAS}$ values for the saline-rinsed samples are consistently enriched by ~ 2‰ in samples with significant pyrite (> ~0.1 wt%), suggesting that these were more successful at removing adsorbed sulfates derived from pyrite oxidation. However, no enrichment was observed in samples with low pyrite abundances. Yields of water-soluble sulfate from a single rinse were significantly higher using the saline solution rather than pure DI. Thus, the values of CAS reported in the study on samples from non-saline extractions may include some component of calcium sulfates and/or adsorbed

sulfate and, as such may not reflect purely 'carbonate-associated sulfate'. To the degree that the saline treatment liberates sulfate derived from pyrite oxidation (as in the lower Nafun of MQ-1), its application should minimize $\delta^{34}S$ variability within analyzed sections. However, to the degree that the saline treatment also liberates calcium sulfates or adsorbed sulfate of marine origin and isotopic composition (as in the upper Nafun of MQ-1), then leaching of these water soluble sulfates may not be desirable and, in many cases, may prevent the extraction of sufficient sulfate evolved significantly over the coarse of this study. This is likely to be particularly true in strata that are not pyrite-rich. The community has yet to agree on a common methodology for CAS extractions, although there is widespread recognition for such a protocol to be developed and considerable progress is being made toward this goal.
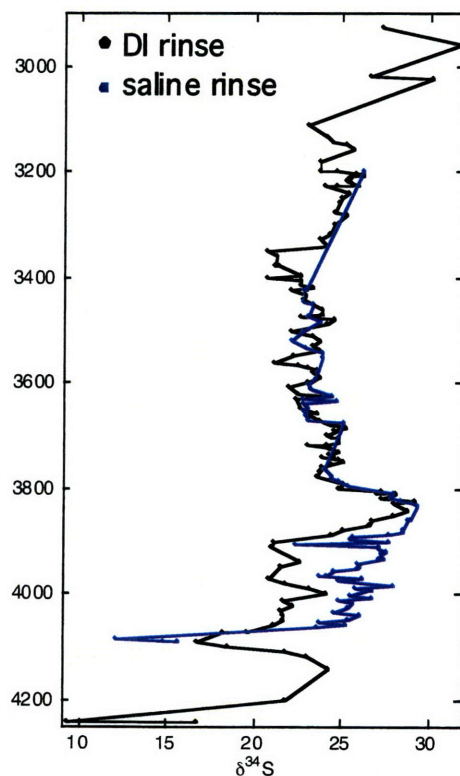
Figure 4: The $\delta^{34}S_{CAS}$ for well MQ-1 obtained as the result of DI rinsing (black) and saline rinsing (blue). There is a trend toward the saline rinsed $\delta^{34}S_{CAS}$ to be ~2‰ heavier. Y-axis is depth in meters.

The carbonate dissolution protocol also evolved over the course of the study. Initial samples were dissolved by addition of 3N HCl under nitrogen for 2 hours at 60°C with constant stirring. Later samples were dissolved overnight in 6N HCl at room temperature. There was no noticeable difference in $\delta^{34}S_{SO4}$ switching between these methods. Sample processing, purification, and analysis of $\delta^{13}C_{carb}/\delta^{18}O_{carb}$, $\delta^{13}C_{org}$, and TEs followed standard protocol, reported previously (FIKE et al., 2006).

RESULTS:

We will present our results for each section, beginning with the subsurface wells and then the outcrops of the Huqf area and the Jabal Akhdar of the Oman Mountains (Figure 1). Each entry will begin with a description of the section and presentation of the geochemical data (typically $\delta^{13}C_{carb}$ and $\delta^{34}S_{SO4}$, but often supplemented by other isotopic and geochemical proxies). This will be followed by a discussion of the degree to which these data are likely to record primary marine signatures, as reflected by the absolute value and stratigraphic variance of the data an comparison with standard indicators of diagenesis, such as $\delta^{18}O_{carb}$ or Mn/Sr (Given and Lohmann, 1986; Kaufman et al., 1991; Veizer, 1983).

Subsurface data:

We have sampled and analyzed nine subsurface sections through Huqf strata. These have a paleogeographic distribution (Figure 1) that ranges between the Huqf area (MQ-1) to the Eastern Flank (TM-6; TF-1) to the SOSB (AAL-1; SAR-2; SHM-1; MNH-1; BBN-

1; and BB-4). Collectively, the wells cover all stratigraphic levels of the Huqf Supergroup. Wells MQ-1 and TM-6 preserve the entire Nafun Group strata, including well-defined examples of the Shuram $\delta^{13}C_{carb}$ excursion, and expressions of the basal Nafun (Hadash cap carbonate) $\delta^{13}C_{carb}$ negative excursion. These wells also preserve portions of the Ara Group. Wells TF-1, AAL-1, SAR-2, and SHM-1, penetrate the upper Nafun and variable amounts of the Ara Group, providing additional context for the poorly understand Nafun – Ara transition. Wells MNH-1, BBN-1, and BB-4 are restricted to Ara Group strata. Wells BB-4, SHM-1, BBN-1, TF-1, and TM-6 all contain the A4 unit, as evidenced by uranium enrichment, depleted $\delta^{13}C_{carb}$, and the presence of a volcanic ash layer dated to 541.0 Ma (Bowring et al., 2007). The discussion of the wells will be presented in ascending stratigraphic order, with data and discussion grouped into Nafun and Ara strata when a well penetrates both units.

Well: MQ-1

The well MQ-1 penetrates the entire Nafun Group and the stratigraphy of the lower Ara. Samples from MQ-1 are exclusively cuttings. One sample was collected for every 2m of stratigraphy. Analyzed samples have a coverage between every 2m (during the onset of the Shuram excursion and the uppermost Buah) to ~20m in the lowermost Masirah Bay and some portions of the Ara strata. Earlier work has identified the well MQ-1 as having one of the most complete sections through the Nafun stratigraphy, based on the $\delta^{13}C_{carb}$ profile (AMTHOR et al., 2003; BURNS and MATTER, 1993). Previously, we have filled in the Nafun $\delta^{13}C_{carb}$ record and added parallel records of $\delta^{13}C_{org}$, $\delta^{34}S_{SO4}$, and $\delta^{34}S_{pyr}$ (FIKE et al., 2006). Here, we address the finer structure of these data, particularly

with regard to the Shuram $\delta^{13}C_{carb}$ excursion, and explore the stratigraphy overlying the Nafun Group, which include 'post-Buah' carbonates of uncertain stratigraphic affinity that have been assigned to the undifferentiated lower Ara Group (Figure 5).

The Nafun Group of MQ-1 contains all of its four constituent formations with lithology as observed in outcrop: the shales and sandstones of the Masirah Bay Fm. grade up into the limestones and dolostones of the Khufai Fm. The Khufai is sharply overlain by the carbonates and sandstones of the lower Shuram Fm., grading up into the calcareous red shales of the middle-upper Shuram Fm. and into the dolostones of the Buah Formation. The Ara strata of MQ-1 are separated from the underlying Buah Fm. by a disconformity, with non-deposition likely lasting no more than 1 Myr (BOWRING et al., 2007) and overlain unconformably by the Cambrian-Ordovician Haima clastics. There is no evidence for the Ara A4 carbonate unit, which is normally expressed by a simultaneous enrichment in uranium and a depletion in $\delta^{13}C_{carb}$. Thus, these strata have been assigned to the (undifferentiated) lower Ara Group (A0-A3).

The general geochemical and isotopic trends in the Nafun Group data of MQ-1 have been discussed previously (Fike et al., 2006). Here we make some additional observations about the stratigraphic variability of these isotope proxies. There is a sharp lithologic boundary in the mid-Khufai Fm, marking the transition from limestone to dolostone that is marked by a minimum in $\delta^{13}C_{carb}$. Progressing upsection, the remainder of the dolomitic Khufai becomes progressively more enriched in $\delta^{13}C_{carb}$ (by 2.5‰), $\delta^{18}O_{carb}$ (by 4‰) and $\delta^{34}S_{CAS}$ (by 8‰). In outcrop, this mineralogic transition marks the onset of progressively more evaporitic conditions in the Khufai and frequent silicification surfaces (see section MDB below and McCarron, 2000). The co-variation in these

isotopes continues beyond the upper Khufai and into the lower Shuram. Here, the onset of the Shuram excursion with the sharp decrease in $\delta^{13}C_{carb}$, also coincides with a decrease in $\delta^{18}O_{carb}$ and $\delta^{34}S_{CAS}$ to values typical of strata before the upper Khufai enrichment. These strata from mid-Khufai to lowermost Shuram are the only portion of MQ-1 stratigraphy marked by clear stratigraphic co-variation. The interpretation of this co-variation is discussed below. Finally, we note that there is a sharp discontinuity in $\delta^{34}S_{CAS}$ (increasing from 20‰ to 24‰) found within the Buah Fm. This offset is significantly larger than the variability observed in adjacent strata.
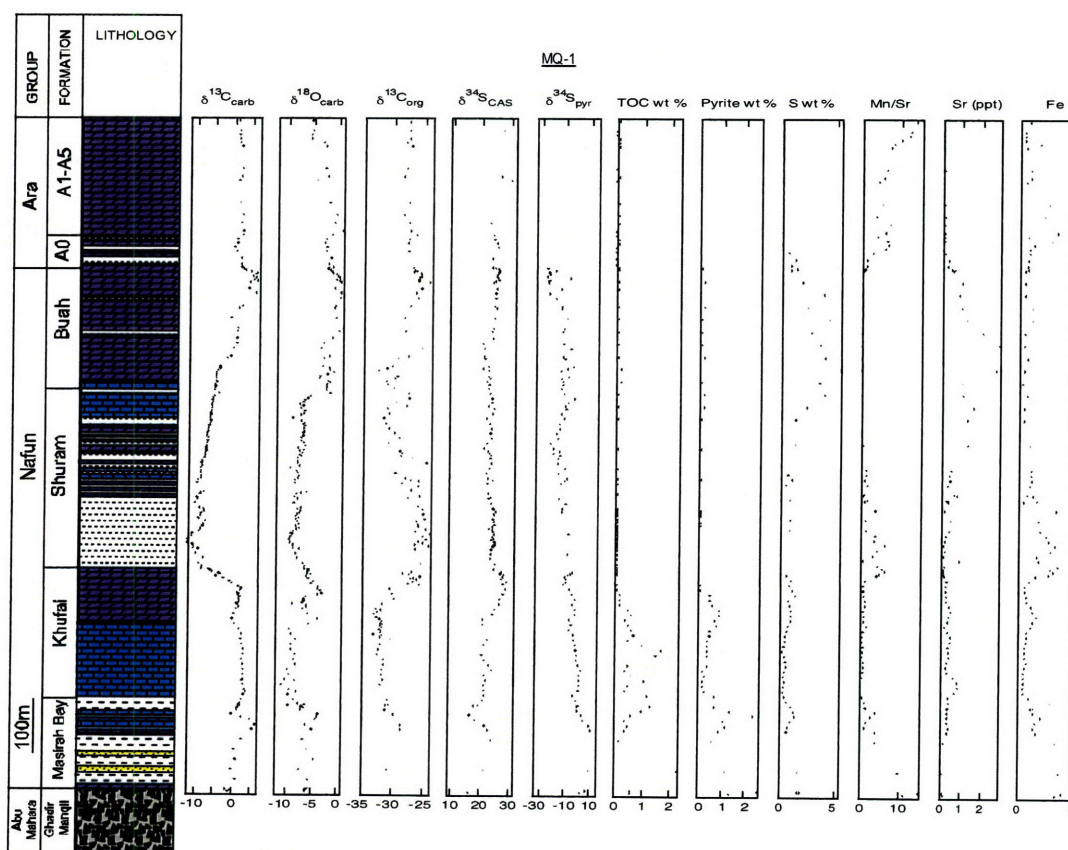
Figure 5: Geochemical and isotopic data from well MQ-1. Nafun Group data reported previously (Fike et al., 2006). Lithology after Figure 2.

- 189 -

We turn now to examine the overlying strata of the (undifferentiated) lower Ara Group (Figure 5). Here, there is no significant change in $\delta^{13}C_{carb}$ (or $\delta^{13}C_{org}$) across the Buah-Ara contact. The Ara strata are marked by exceedingly low TOC (~ 0.05 wt%) and pyrite (~ 0.005 wt%) abundances, which are significantly less than the even the TOC- and pyrite-lean strata of the Upper Nafun in MQ-1. There are further differences observed in many of the geochemical signals across this interval. In particular, we see ~4‰ decrease in $\delta^{18}O_{carb}$, associated with a 100-fold increase in Mn/Sr (driven primarily by decreased [Sr]), and a 50-fold decrease in sulfur abundance. Sulfate concentrations were sufficiently low that only few samples yielded enough CAS for isotopic analyses, and these points generally exhibited more scatter than those in Nafun Group strata. Although the $\delta^{34}S_{CAS}$ trend in MQ-1 continues to increase from the Buah through the Ara, it reaches a maximum of ~ 32‰, well below the values observed in all other Ara sections (except the diagenetically altered TF-1, see below). Accompanying these changes, we see a negligible shift in $\delta^{13}C_{carb}$, with at most a 1‰ decrease with respect to the uppermost Buah strata.

Summarizing these data from MQ-1 we make several observations. First, the observed correlation in $\delta^{13}C-\delta^{18}O-\delta^{34}S$ begins with the enrichment of these values in the upper Khufai at the stratigraphic level where we observe the onset of evaporitic conditions in the outcrop equivalent (section MDB below). These data point to possible restriction from the open ocean with enrichments resulting from closed system consumption of DIC and marine sulfate ($\delta^{13}C/\delta^{34}S$) and/or evaporative enrichment ($\delta^{18}O$). That the co-variation of these isotopes continues through the lowermost Shuram, while $\delta^{18}O$ and $\delta^{34}S_{CAS}$ returning to near their pre-enrichment values suggests a

relationship between the upper Khufai enrichment and the lower Shuram depletion. Given that the lowermost Shuram consists of alternating sandstones and reworked carbonates (section KS below), it is likely that the carbonate record preserved in these strata reflects a mix of syndepositional marine and relict geochemical signals (from the reworked carbonates). Given the inferred unconformity across the Khufai-Shuram boundary, the most likely source for the allochthonous component of the lower Shuram carbonates is the erosion of the evaporitic enriched strata of the uppermost Khufai Formation. As the transgressive systems tract proceeds, any component of reworked Khufai carbonates would become progressively more diluted and the background marine signal would dominant. In the case of MQ-1, this would correspond to an essentially invariant $\delta^{18}O$-$\delta^{34}S$ composition, but with the highly depleted $\delta^{13}C_{carb}$ associated with the Shuram excursion. Finally, we examine the $\delta^{34}S_{CAS}$ record of the lower Buah Formation. Here we observe a jump in $\delta^{34}S$ from 20 to 24‰, coupled with a change in overall trend from decreasing $\delta^{34}S_{CAS}$ below this discontinuity to increasing $\delta^{34}S_{CAS}$ in the overlying strata. Given the lack of variability observed in $\delta^{34}S_{CAS}$ in adjacent strata and this reversal in overall $\delta^{34}S_{CAS}$ trend, we suggest that this jump corresponds to a depositional hiatus. We note that there is no evidence for a change in lithology, $\delta^{13}C_{carb}$, or $\delta^{34}S_{pyr}$ over this interval. There does appear to be a shift in $\delta^{13}C_{org}$ and $\delta^{18}O_{carb}$, these isotopic records are neither sufficiently resolved nor sufficiently understood to differentiate between (gradual) secular change and (sharp) discontinuous deposition. Nonetheless, the discontinuity in $\delta^{34}S_{CAS}$ suggests a break in deposition and highlights the potential for sulfur isotope analyses to identify hiatal gaps in stratigraphy. Continuing upsection into the Ara strata, the geochemical changes observed there (decreased $\delta^{18}O_{carb}$, TOC, pyrite,

S, Sr,) provide clear evidence for diagenetic alteration these strata through the oxidative recrystallization of carbonates (Given and Lohmann, 1986; Veizer, 1983). The contact between the uppermost Buah Formation and the overlying Ara Group is marked by an unconformity that likely involved karstification/cementation of the uppermost (preserved) Buah strata. The Ara strata in MQ-1 are overlain unconformably by the mid-late Cambrian Haima clastic sandstones. This geometry is ideal for fluxing a large volume of water through the Birba Formation, while the cemented Buah-Birba contact likely prevented significant fluid flux into the Nafun Grp strata. Within these strata, the strongest alteration is observed in the least common constituents (e.g., S and Sr) and those that are most common in the altering fluid (e.g., O). The large carbon buffering capacity of carbonates makes the $\delta^{13}C$ composition the most resistant to change. We note that there are no geochemical parallels across the MQ-1 Shuram excursion that would argue for its origin as the result of diagenesis.

Well: TM-6

The strata penetrated by the well TM-6 (Figure 6) include all formations of the Nafun Group and the non-evaporitic equivalent of the Ara Group, as is typical of the Eastern Flank. Samples from TM-6 are exclusively cuttings. One sample was collected for every 5m of stratigraphy. Analyzed samples have a coverage between every 5m (during the onset of the Shuram excursion and in the vicinity of the A4 carbonate) to ~20m in the portions of the Masirah Bay and upper Shuram Formations. The existence of a well-resolved Shuram excursion in the Nafun and the presence of the characteristic A4 carbonate in the Ara Group serve as stratigraphic tie-points for TM-6. The base of

the well is grounded in the shales and sandstones of the Masirah Bay Formation, overlain unconformably by the dolostone of the Khufai Formation. The upper Khufai is marked by a transgressive surface associated with the deposition of the shales and basal carbonates of the Shuram Formation. This transition marks the onset of the Shuram $\delta^{13}C_{carb}$ excursion. Previous data for $\delta^{13}C_{carb}$ are sparse within the middle Shuram, with values returning to near -4‰ by the upper Shuram (BURNS and MATTER, 1993). Over the upper Shuram and lower-mid Buah formations, $\delta^{13}C_{carb}$ rises to +2‰, although throughout this interval it is characterized by more scatter and negative excursions than the $\delta^{13}C_{carb}$ signal in MQ-1 (FIKE et al., 2006) or in equivalent age strata in Namibia (SAYLOR et al., 1998). In addition, the $\delta^{13}C_{carb}$ record in TM-6 does not exhibit the Buah positive anomaly (to $\delta^{13}C_{carb} \sim$ +6‰) as seen in MQ-1, which is correlated to similarly enriched strata in Namibia dated to 548 Ma (BOWRING et al., 2007; GROTZINGER et al., 1995).

New data presented here include increased $\delta^{13}C_{carb}$ resolution, particularly in the Masirah Bay and Shuram formations, paired with $\delta^{18}O_{carb}$ chemostratigraphy, and a new $\delta^{34}S_{CAS}$ record (Figure 6). The $\delta^{13}C_{carb}$ record in the Masirah Bay Formation reveals a negative excursion at the base, suggesting penetration to the Fiq cap carbonate (Marinoan equivalent), observed elsewhere in Oman, both in the subsurface and outcrop, to have a similarly depleted $\delta^{13}C_{carb}$ profile (FIKE et al., 2006; LEATHER et al., 2002). Secondly, we have provided increased resolution in the Shuram Formation that better defines the extent of the Shuram excursion.
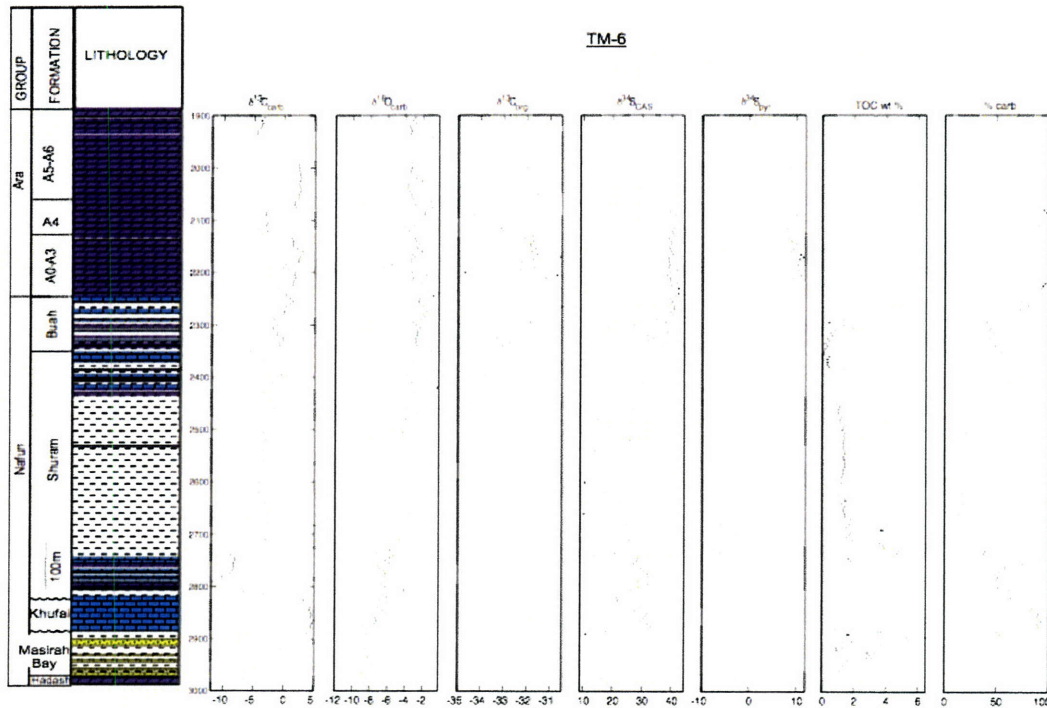
Figure 6: Geochemical and isotopic data from well TM-6. The $\delta^{13}C_{carb}$, $\delta^{34}S_{CAS}$, and $\delta^{34}S_{pyr}$ data have been reported previously (Fike and Grotzinger, 2007a). The TOC data are the results of previous work at PDO. Lithology after Figure 2.

After the initial carbonate beds in the basal Shuram, which record the most depleted values ($\delta^{13}C_{carb}$ = -12‰ – -9‰), the middle Shuram is comprised of calcareous shale, which has an extremely uniform isotopic composition ($\delta^{13}C_{carb}$ = -3 ± 1‰). The sharp gradient in $\delta^{13}C_{carb}$ across the lower-mid Shuram, as compared to MQ-1, and the change in lithology suggest a hiatus in deposition occurred here. The rapid transition from $\delta^{13}C_{carb}$ ~ -3‰ to 0‰ observed in TM-6 at 2400m (assigned to the upper Shuram Formation), is elsewhere observed to occur in the mid-upper Buah Formation (BURNS and MATTER, 1993; COZZI et al., 2004a; COZZI et al., 2004b; FIKE et al., 2006). There is no covariation between $\delta^{13}C_{carb}$-$\delta^{18}O_{carb}$ through the Shuram excursion (Figure 7). The lower portion (Nafun strata) of the TM-6 $\delta^{34}S_{SO4}$ record is more variable than the

equivalent strata in MQ-1, although the general trends are the same (enriched $\delta^{34}S_{CAS}$ in the upper Khufai with a trend toward decreasing values over the course of the Shuram Formation (Fike et al., 2006). The observed rise in $\delta^{34}S_{SO4}$ to ~ 40‰ in TM-6, however, occurs within strata that are currently assigned to the Buah Formation (based on well-log records and pre-existing $\delta^{13}C_{carb}$ data). This cannot be reconciled with the observed values in the Buah in well MQ-1 or in outcrops of the Huqf area (discussed below).
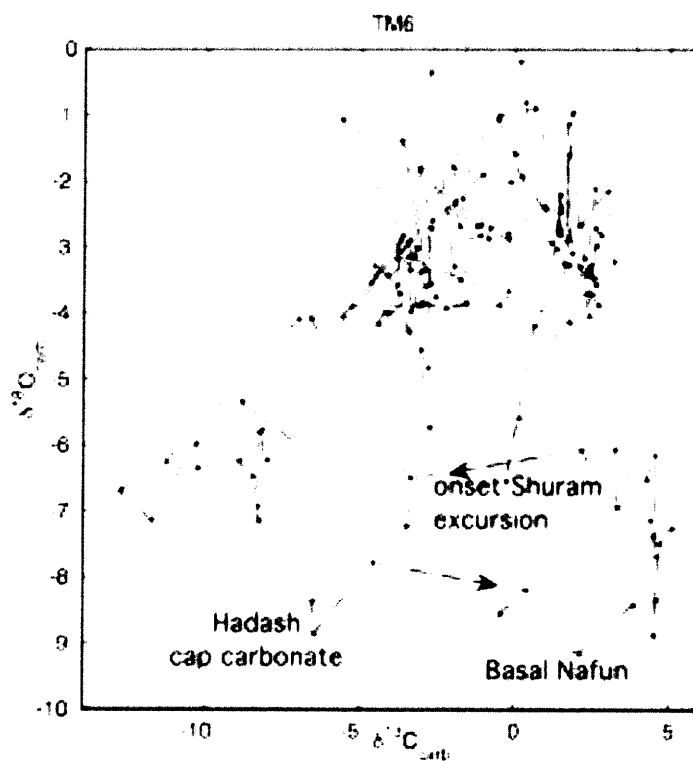
Figure 7: Cross plot of $\delta^{13}C_{carb}$ – $\delta^{18}O_{carb}$ for well TM-6. Data are connected in stratigraphic order. The base of the Nafun Group and the onset of the Shuram $\delta^{13}C_{carb}$ excursion are indicated. There is a general trend toward increasing $\delta^{18}O_{carb}$ upsection and no covariation between $\delta^{13}C$-$\delta^{18}O$ is observed over the Shuram excursion.

Summarizing these data from TM-6, we make several observations. First, there appears to be a general offset between the assigned stratigraphy and geochemical character of TM-6. This is first apparent after the sharp discontinuity in $\delta^{13}C_{carb}$ of the lower Shuram Formation. Here $\delta^{13}C_{carb}$ increases from -8‰ (typical of the lower Shuram) to -3‰, typical of the mid-Buah Formation (Burns and Matter, 1993; Cozzi et al., 2004a; Cozzi et al., 2004b). Secondly, there is the increase in $\delta^{13}C_{carb}$ to ~ 0‰, which is observed in strata assigned to the upper Shuram in TM-6, but occurs elsewhere in the mid-upper Buah Formation (Burns and Matter, 1993; Cozzi et al., 2004a; Cozzi et al., 2004b). The explanation for these offsets in $\delta^{13}C_{carb}$ can be most easily explained if there is an unconformity across $\delta^{13}C_{carb}$ increase in the lower Shuram, placing mid-Buah strata directly on top of lower Shuram strata. The existence of an unconformity is consistent with the sharp lithologic change over this interval.

As the only well containing both the Shuram excursion and the distinctive A4 carbonate unit, TM-6 serves to tie together the chemostratigraphic records from the Nafun and Ara groups. In particular, the $\delta^{34}S_{CAS}$ record from TM-6 preserves the transition from 'Nafun' type $\delta^{34}S_{SO4}$ (20-30‰ to 'Ara'-type $\delta^{34}S_{SO4}$ (~40‰). In TM-6, this transition appears gradual, supporting the notion that this enrichment reflects a global secular trend and is not the result of Ara-specific basin restriction (Fike and Grotzinger, 2007a). However, the current stratigraphic assignments in TM-6 do not fit with the existing understanding of $\delta^{34}S_{CAS}$ within the Huqf Supergroup, namely in TM-6 the 'Nafun-Ara' $\delta^{34}S$ transition occurs within strata of the Shuram and Buah Formations. Thus, either, the 'Buah' strata in TM-6 are not recorded elsewhere and represent the transition between uppermost Buah to basal Ara strata, or the $\delta^{34}S_{CAS}$ from the upper

Buah in MQ-1 (and outcrop sections) has been depleted through diagenesis (pyrite oxidation). The uniformity of the $\delta^{34}S_{CAS}$ signal in MQ-1 argues against diagenetic alteration (Figure 5). As does the existing stratigraphic mismatch (based on $\delta^{13}C_{carb}$) we observe in TM-6. In addition to the inferred unconformity in the lower Shuram of TM-6, the absence of a well-defined Buah positive $\delta^{13}C_{carb}$ anomaly in TM-6 and its presence in MQ-1, existing outcrop sections, and in other globally-dispersed strata (Amthor et al., 2003; Saylor et al., 1998), suggest that there is another hiatus in TM-6 following the Shuram excursion and makes it likely that the overlying 'Buah' strata are younger than the Buah strata preserved in MQ-1.

While the $\delta^{34}S_{CAS}$ record in TM-6 (Figure 6) nicely records the gradual rise in $\delta^{34}S$ to 40‰, the signal is significantly more variable (particularly in the lower strata) then that found in MQ-1 (Figure 5). This is surprising given that the cutting samples from MQ-1 were sampled every 2m, while the cuttings from TM-6 were sampled every 5m. As such, each TM-6 sample integrates over 150% more stratigraphy than each MQ-1 sample. This difference in sampling density would result in a smoothed $\delta^{34}S_{SO4}$ curve in TM-6 relative to MQ-1 – provided that the strata preserved the same record of $\delta^{34}S_{SO4}$ at the time of sampling. The opposite trend observed in TM-6 (noisier data relative to MQ-1) point to alteration of TM-6 $\delta^{34}S_{SO4}$ signal. The Nafun strata of TM-6 are uniformly enriched in TOC and pyrite, relative to their concentrations in MQ-1. This provides increased chance for pyrite oxidation to alter $\delta^{34}S_{SO4}$. This could have occurred during diagenesis, sample storage, or laboratory processing. There is no clear relationship between Mn/Sr or $\delta^{18}O$ and the variability of $\delta^{34}S_{SO4}$ (in contrast to well TF-1, discussed below), providing no evidence for pyrite oxidation and sulfate incorporation as the result of carbonate

diagenesis prior to sampling; however, the unusually noisy $\delta^{13}C_{carb}$ signal in the upper

Shuram and Buah Formations does support some diagenetic alteration occurring within

the subsurface. As does the fact that $\delta^{34}S_{pyr}$ in TM-6 does not seem to track depletions in

$\delta^{34}S_{CAS}$. Had depleted $\delta^{34}S_{CAS}$ in TM-6 been primary, a coincident depletion in $\delta^{34}S_{pyr}$

would be expected. TM-6 was drilled over 30 years ago and stored prior to this study

under poorly controlled temperature and humidity conditions. Pyrite oxidation during

acid dissolution and sulfate extraction is known to be able to cause depletion of $\delta^{34}S_{CAS}$

(MARENCO et al., 2007). However, we feel that, given the maximum pyrite abundances

($\sim$ 1 wt%), this is unlikely to yield more than 1-2‰ depletion in $\delta^{34}S_{SO4}$ at typical $\Delta\delta^{34}S$

($\sim$30‰) observed here. Rather, to the extent that the observed $\delta^{34}S_{CAS}$ record is noisier

than should be expected, we feel that it is most likely attributed to differential pyrite

oxidation, either during diagenesis or during sample storage in the coreshed prior to

analysis. In particular, TM-6 samples were not uniformly treated with the saline solution

(see discussion in methods); as such, complete removal of oxidation products may not

have been achieved.

Well: TF-1

The strata penetrated by the well TF-1 (Figure 8) include all formations of the Nafun

Group and the non-evaporitic equivalent of the Ara Group. However, the Nafun Group

strata of TF-1 are poorly understood, and we have focused on the uppermost Buah

Formation and Ara stratigraphy in the present study. Samples from TF-1 are exclusively

cuttings. One sample was collected for every 2m of stratigraphy. Analyzed samples

have a coverage between every 2m (in the vicinity of the A4 carbonate) to ~8m in the

undifferentiated lower and upper Ara stratigraphy. This well was examined specifically because it was a likely candidate of diagenetic alteration based on its existing $\delta^{13}C_{carb}$ record. In assessing fidelity of the $\delta^{13}C$-$\delta^{34}S_{SO4}$ isotopes, we focused on the Ara Group and in particular on the A4 unit, which is clearly identified by strong uranium enrichment, the presence of the volcanic ash at its base, and the $\delta^{13}C_{carb}$ negative anomaly (Figure 8). $\delta^{34}S$ is strongly depleted and characterized by significant scatter in the strata leading up to and through the A4 carbonate. There is elevated Mn/Sr throughout TF-1 strata with a noticeable increase across the A4 coincident with depleted $\delta^{34}S_{CAS}$.
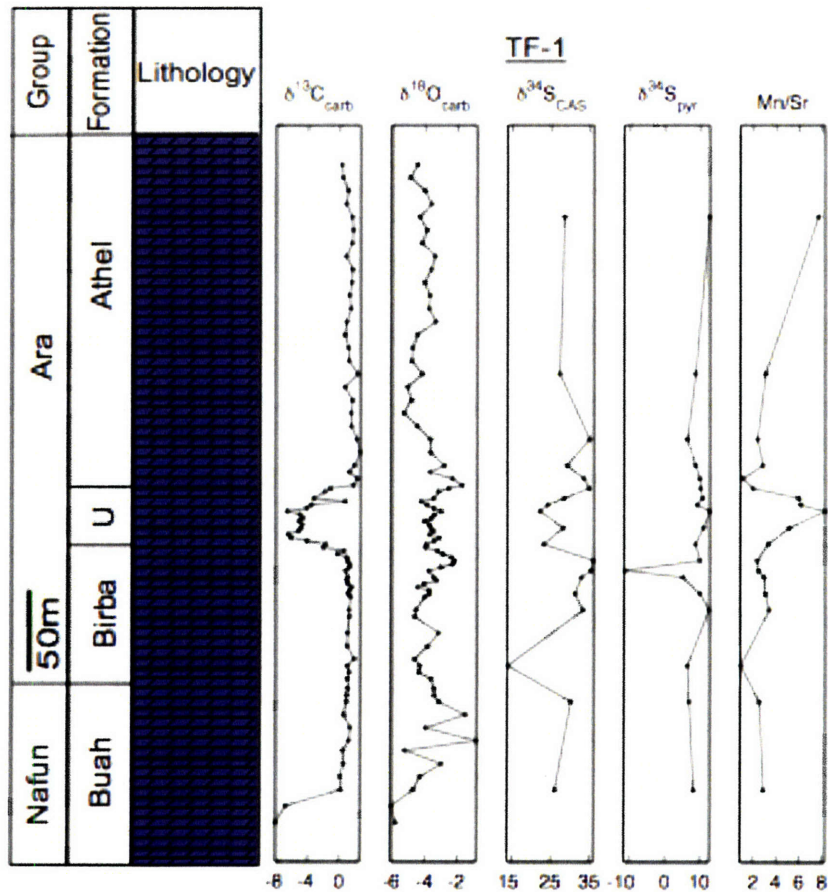
Figure 8: Geochemical and isotopic data from well TF-1. Lithology after Figure 2.

It is clear that the record of $\delta^{34}S_{CAS}$ in TF-1, particularly across the A4 unit, does not fit with the known $\delta^{34}S$ composition of Ara strata (Fike and Grotzinger, 2007a; Schröder et al., 2004) or other terminal Ediacaran-earliest Cambrian strata around the world (see summary in Fike and Grotzinger, 2007a). This could either reflect the fact that marine $\delta^{34}S_{SO4}$ was more spatially variable than previously thought or indicate that the $\delta^{34}S_{CAS}$ record in the TF-1 strata has been reset by diagenesis. Based on the inferred time of deposition for the A4 (~ 1 Myr), there is insufficient time (Kah et al., 2004) for marine $\delta^{34}S_{SO4}$ to change to the extent observed across the A4 unit (Figure 8). As such, the TF-1 $\delta^{34}S_{CAS}$ signal cannot reflect primary marine sulfate. It is still possible that TF-1 records the primary composition of a localized pool of sulfate in an isolated depositional environment. However, this is deemed unlikely for several reasons. First, the presence of the $\delta^{13}C_{carb}$ negative excursion across the A4 is evidence of connection to the open ocean (Amthor et al., 2003). Secondly, there is no parallel depletion in $\delta^{34}S_{pyr}$ as would be expected if the $\delta^{34}S_{CAS}$ depletion were primary. Finally, there is a correlation between $\delta^{34}S_{CAS}$ and both $\delta^{18}O_{carb}$ and Mn/Sr in TF-1 strata (Figure 9). Thus, it is inferred that the $\delta^{34}S_{CAS}$ record in these strata has been diagenetically altered by pyrite oxidation, followed by sulfate incorporation during carbonate recrystallization, and that this alteration occurred within the subsurface.
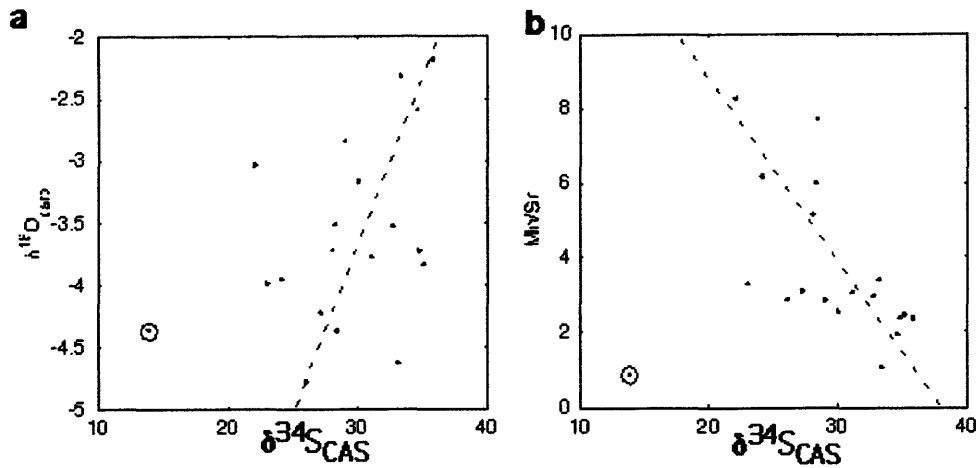
Figure 9: Geochemical assessment of diagenesis in TF-1 samples. a) Observed positive covariation between $\delta^{34}S_{CAS}$ and $\delta^{18}O_{carb}$. b) Observed negative correlation between $\delta^{34}S_{CAS}$ and Mn/Sr. The circled point has anomalously low $\delta^{34}S_{CAS}$ and likely reflects post-sampling pyrite oxidation in addition to subsurface diagenesis.

Well: SAR-2

The well SAR-2 was sampled across the transition between the upper Buah Formation and the basal (A0) Ara Group (Figure 10). Samples from SAR-2 are exclusively cuttings, which were collected for every 2m of stratigraphy. Analyzed samples have a coverage between 4-8 m. The lowermost strata of SAR-2 consists of ~50m of shaley carbonates overlain by a sharp contact and 250m of relatively pure carbonates assigned to the Buah Formation. Existing $\delta^{13}C_{carb}$ data from the Buah Formation are uniformly enriched (0 ± 1‰) relative to typical Buah profiles (COZZI et al., 2004a; COZZI et al., 2004b). As such, the current stratigraphic assignment is suspect. The 'Buah' carbonates are overlain by ~80m of shaley carbonates currently assigned to the basal Ara (A0) and overlain by several cycles of carbonate-evaporite deposition. We have examined $\delta^{13}C_{carb}$ and $\delta^{34}S_{CAS}$ composition across this pre-salt stratigraphy. $\delta^{13}C_{carb}$ is uniformly enriched, reaching values of +3 in the mid A0 before decreasing just under 0‰ in the uppermost A0. These strata record the progressive enrichment in $\delta^{34}S_{CAS}$ from

~ 34‰ at the base of SAR-2 to ~39‰ at the top of the A0. There is no significant scatter in $\delta^{34}S_{CAS}$, nor a correlation between $\delta^{34}S_{CAS}$ and $\delta^{13}C_{carb}$, $\delta^{18}O_{carb}$, or the carbonate content of these samples. As such, these data likely reflect a primary $\delta^{34}S_{CAS}$ signal that records the latter half of the rise in $\delta^{34}S_{SO4}$ from Nafun (~25‰) to Ara (~40‰) values. The enriched $\delta^{13}C_{carb}$ (~0-1‰) and elevated $\delta^{34}S_{CAS}$ (34-38‰) in the strata currently assigned to the Buah Formation (based on lithostratigraphy) do not fit within the existing chemostratigraphic framework (Burns and Matter, 1993; Cozzi et al., 2004b; Fike et al., 2006). It is likely that these strata reflect a generally unrecognized upper Buah member or basal Ara (A0) unit that is more extensive than previously appreciated.
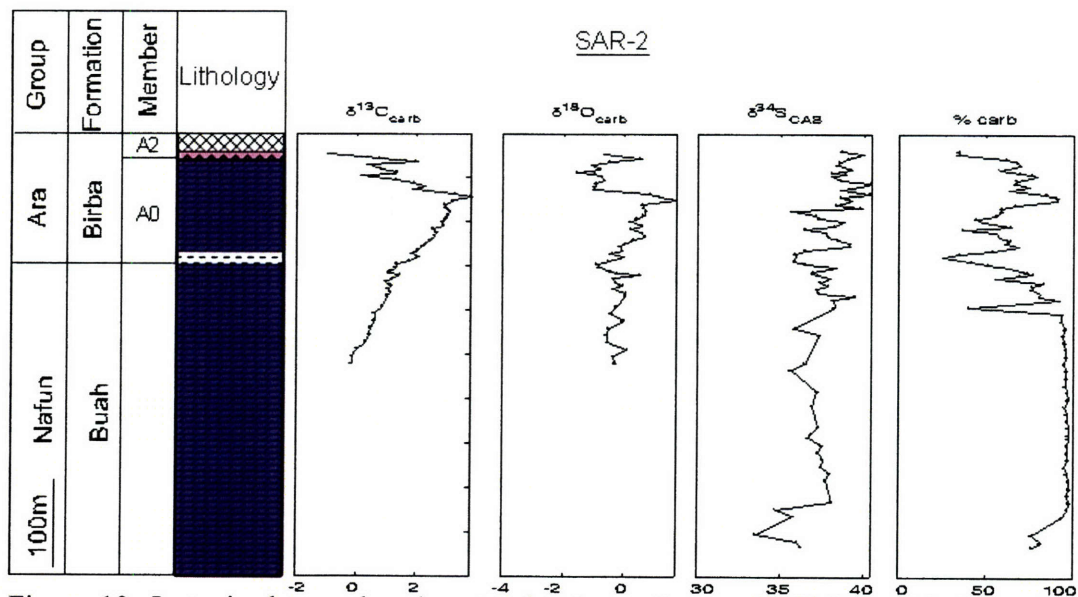
Figure 10: Isotopic data and carbonate abundance from well SAR-2. Lithology after Figure 2.

Well: SHM-1

The well SHM1 was sampled across the transition between the upper Buah Formation and the basal (A0) Ara Group as well as the A1, A2, A3, and A4 Ara units

(Figure 11). Samples from SHM-1 are the Buah-A0 interval are exclusively cuttings, while the samples from the A1-A4 carbonates were collected from drill core. Cuttings samples were collected every 2m. Analyzed samples have a coverage of 8 m in the A0, decreasing to 50m in the lowermost Buah strata. The stratigraphy of SHM-1 is divided into a pre-salt and an intra-salt component (Figure 11). The pre-salt stratigraphy comprises an approximately 750m package of calcareous and dolomitic shales grading up into mixed limestone/dolostone interbeds and an upper dolostone package of ~ 100m in thickness. The stratigraphic assignments of these units remains tentative, although it likely spans the transition from the upper Nafun Group into the basal Ara Group (A0/A1). Existing $\delta^{13}C_{carb}$ from the pre-salt component clusters between 0-2‰, making it likely that any Nafun stratigraphy is likely restricted to the uppermost Buah (COZZI et al., 2004a; COZZI et al., 2004b; FIKE et al., 2006), following the recovery from the Shuram excursion. The intra-salt component consist of three dolomitic packages from 50-100m in thickness, which are identified as the A2-A4 carbonates. This assignment is based on the presence of characteristic A4 signatures in the uppermost carbonate. The A4 unit is capped by halite and then unconformably overlain by the Haima clastics.

We look to the results of additional chemostratigraphic characterization of the lower strata of SHM-1 to shed some light on the proper stratigraphic assignments. The basal portion of the well records increasing $\delta^{13}C_{carb}$ from -1 to +1‰. There is no significant variability in $\delta^{18}O_{carb}$ and we note the values cluster around 0‰. Organic carbon $\delta^{13}C_{org}$ increases from -35‰ to -25‰ and the decreases back toward -33‰ with no coherent trend. $\delta^{34}S_{CAS}$ is enriched (36‰ – 41‰) relative to previous reports of Nafun $\delta^{34}S_{CAS}$ (FIKE et al., 2006), with an upsection trend to enriched $\delta^{34}S$.

The basal strata of SHM-1 appear analogous to those in SAR-2 and the Buah of TM-6, reflecting isotopically enriched $\delta^{13}C_{carb}$ and $\delta^{34}S_{CAS}$ relative to the existing chemostratrigraphic framework for the Nafun Group. As such, these strata resolve at least a portion of the poorly understood transition from the Nafun to Ara Groups with a stratigraphic assignment to a generally unrecognized upper Buah member or extensive basal Ara (A0) unit being the most likely.
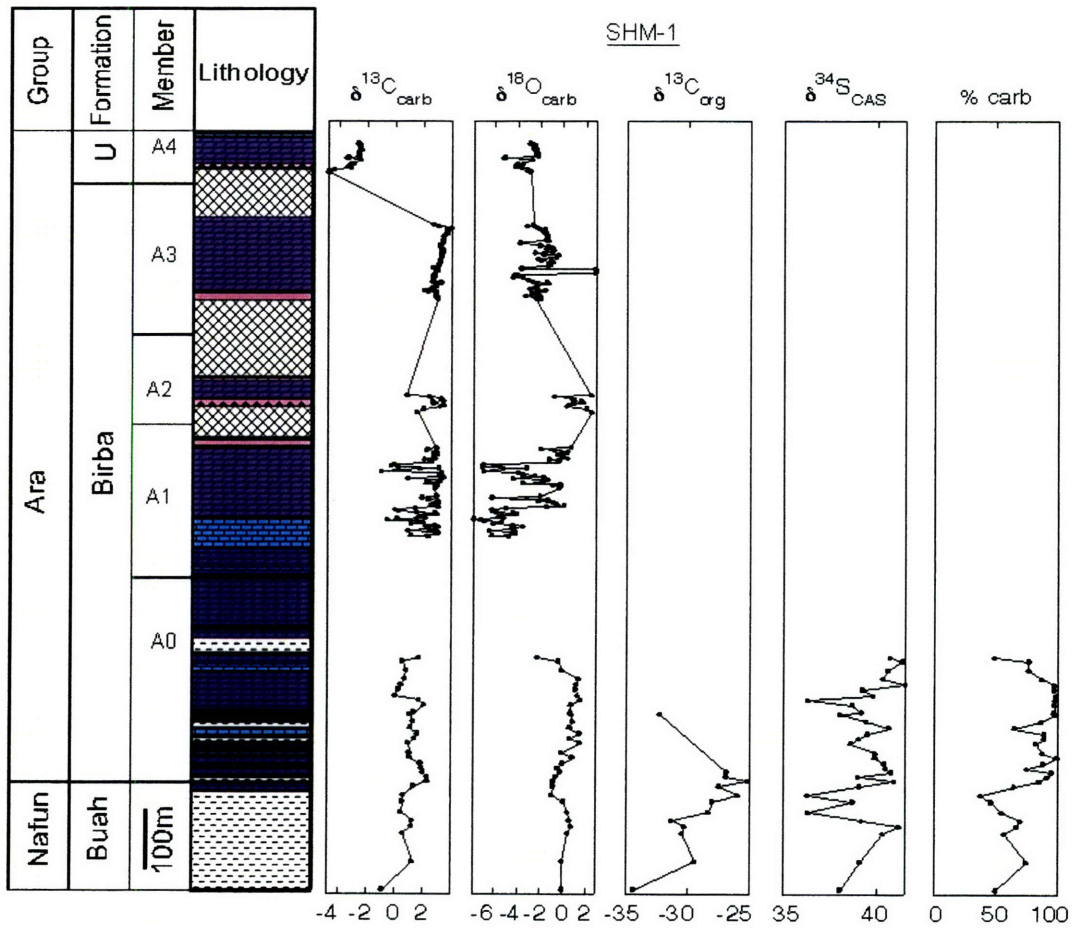
Figure 11: Isotopic data and carbonate abundance from well SHM-1. A3 and A4 $\delta^{13}C_{carb}$ have been reported previously (Chapter 4). Lithology after Figure 2.

Well: AAL-1

Samples from AAL-1 (Figure 12) come from units that have been traditionally assigned to the A0 and the immediately underlying strata of the Buah Formation. The A0 samples were taken from core, while the pre-A0 samples were collected from drill cuttings that were collected every 2m. The A0 unit is assigned to carbonates that are believed to overlie the Buah Formation and are not interbedded with evaporites. A volcanic ash from the A0 of AAL-1 has been dated to 546.7 ± 0.1 Ma (BOWRING et al., 2007). This is consistent with inferred ages of 550 and 548 for the mid and upper Buah Formations based on $\delta^{13}C_{carb}$ correlations to China (CONDON et al., 2005) and Namibia (GROTZINGER et al., 1995), respectively. AAL-1 $\delta^{34}S_{CAS}$ from the A0 ranges from 36 – 39‰. Further, $\delta^{34}S_{CAS}$ below the A0 unit, inferentially the Buah Formation, remains enriched (32 – 35‰). This enrichment is in contrast to the ~20–26‰ values reported from throughout the Buah in MQ-1 (FIKE et al., 2006) and the Buah outcrops in the Huqf and Oman Mountains (see below). As such, the Buah strata in AAL-1 likely reflect either the uppermost Buah Formation, not seen in MQ-1, or are a continuation of the overlying A0 carbonate unit.
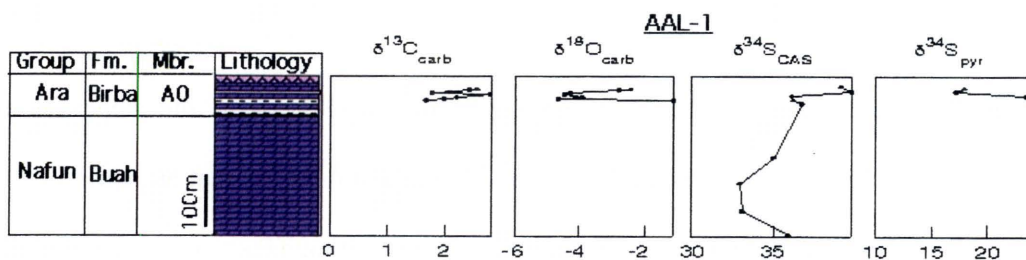
Figure 12: Isotopic data from well AAL-1. Lithology after Figure 2.

Well: MNH-1

The well MNH-1 (Figure 13) was sampled from the A1 to A3 units and overlying (unassigned) carbonates interbedded within the halite. The MNH-1 strata are evaporitic with anhydrite layers or anhydritic carbonates throughout. The A1 unit consists of interbedded dolostone and anhydrite. Samples taken from the A2 and A3 units were obtained from core, whereas the remainder were collected from drill cuttings, collected at a resolution of 2m. The middle of the A3 unit contained a volcanic ash that has been dated to 542.9 ± 0.1 Ma (BOWRING et al., 2007). There is no evidence in MNH-1 strata for the deposition of an A4 unit through a $\delta^{13}C_{carb}$ negative excursion, uranium enrichment, or the presence of the 541 Ma ash. This makes the assignment of the uppermost Huqf strata of MNH-1 tenuous.

Throughout MNH-1, $\delta^{13}C_{carb}$ is uniformly positive (with the exception of two isolated points from shale-rich intervals) at 2 ± 1‰, characteristic of the non-A4 Ara units. There is a record of progressive $\delta^{34}S_{CAS}$ enrichment from ~ 36 to 41‰ in the lower portion of MNH-1 analyzed and then relatively invariant $\delta^{34}S_{CAS}$ further upsection. There are abundant anhydrite layers throughout the MNH-1 stratigraphy, particularly the lower portion. The $\delta^{34}S_{anhyd}$ record nicely parallels with $\delta^{34}S_{CAS}$ record, showing an enrichment from 35‰ in the basal MNH-1 strata to ~41‰ in the upper strata investigated. There are small offsets between $\delta^{34}S_{CAS}$ and $\delta^{34}S_{anhyd}$ that are attributed to equilibrium fractionation and the effects of basin restriction (FIKE and GROTZINGER, 2007b). While sparsely sampled, the $\delta^{34}S_{pyr}$ record shows an increase that parallels that found in $\delta^{34}S_{CAS}/\delta^{34}S_{anhyd}$. There only evidence for diagenetic alteration comes from the two samples with anomalously low $\delta^{13}C_{carb}$, which are also strongly depleted in $\delta^{18}O_{carb}$

(Figure 13), providing confidence that they have undergone diagenetic alteration (Given and Lohmann, 1986; Kaufman et al., 1991). Taken together, the lower strata of MNH1 record the latter half of the rise in $\delta^{34}S_{SO4}$ that is observed elsewhere between the canonical Nafun and Ara Groups (see above).
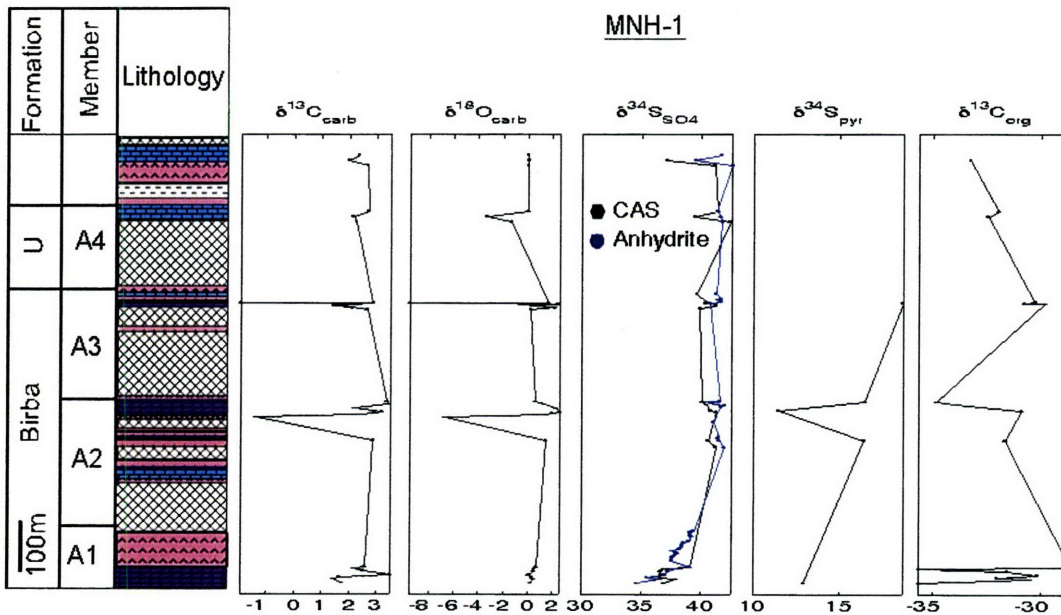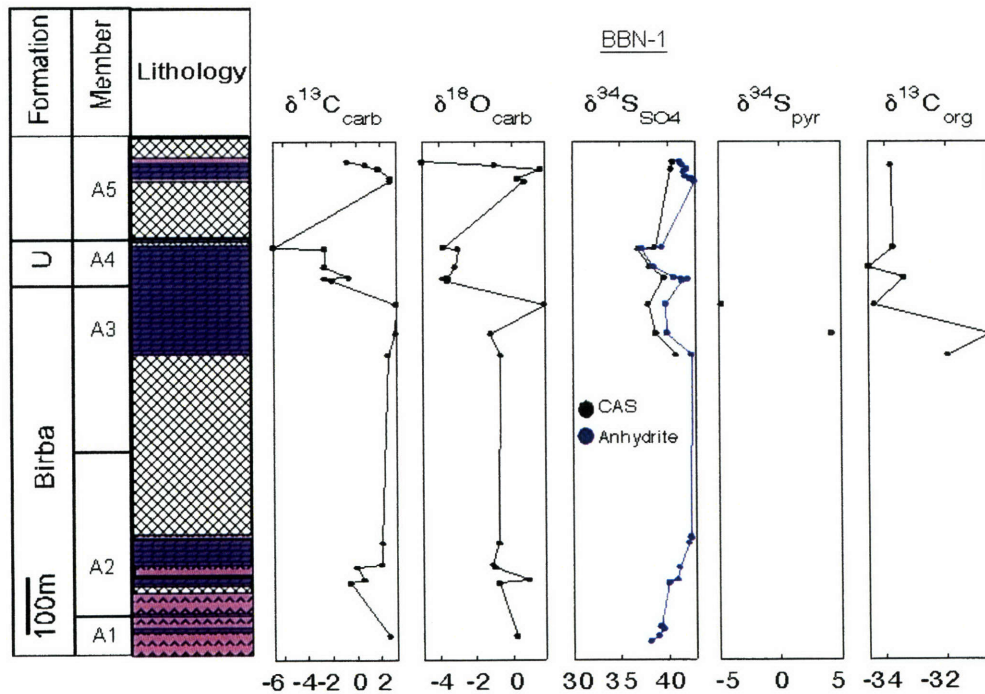

Figure 13: Isotopic data from well MNH-1. A3 $\delta^{13}C_{carb}$ has been reported previously (Chapter 4). Lithology after Figure 2.

Well: BBN-1

BBN-1 samples come exclusively from cuttings, with one sample collected for every 2m of stratigraphy (Figure 14). The basal stratigraphy examined in BBN-1 is an evaporitic A1 carbonate unit, capped by anhdyrite interspersed with halite, and the A2 carbonate, bounded by floor and roof anhydrites. This is overlain by halite and then a thick (~120m) A3 carbonate that lies unconformably under the A4 carbonate. The A4 designation is indicated by the presence of the U enrichment, $\delta^{13}C_{carb}$ negative excursion,

and a volcanic ash, all known to characterize the A4 throughout the Birba area (Schröder et al., 2003). There is a thin A5 carbonate in halite overlying the A4 carbonate. Strata other than the A4 are characterized by $\delta^{13}C_{carb}$ between 0 – 2‰, whereas A4 strata have $\delta^{13}C_{carb}$ between ~ -2‰ – -6‰. The $\delta^{34}S_{CAS}$ values range between 37 – 40‰ in the A3 – A5 units. Coexisting anhydrite from these units are 38 – 42‰ with an average enrichment relative to $\delta^{34}S_{CAS}$ of ~2‰, consistent with the fractionation associated with gypsum from seawater (RAAB and SPIRO, 1991). Anhydrite layers lower in the well (assigned to the A1 and 2 units) provide the opportunity to further calibrate the rise in $\delta^{34}S$. Here $\delta^{34}S_{anhyd}$ increases from 37‰ to 42‰ in the basal anhydrites of BBN-1. Enriched $\delta^{34}S_{pyr}$ values near 0‰ are consistent with known values for the Ara (FIKE and GROTZINGER, 2007a).

Figure 14: Isotopic data from well BBN-1. A3 $\delta^{13}C_{carb}$ has been reported previously (Chapter 4). Lithology after Figure 2.

The δ^{34}S data from BBN-1 are in agreement with previously measured sections through the Ara sGroup. In particular, the lower strata in BBN-1 provide another example of the rise in δ^{34}S$_{SO4}$ that occurs in the basal Ara (as seen in MNH-1, SAR-2, SHM-1, and AAL-1). Similarly, the δ^{34}S$_{SO4}$ values in the unambiguously identified A4 unit overlap with those observed in TM-6 and BB-4 (below).

Well: BB-4

The well BB-4 (Figure 15) penetrates the Ara A3 and A4 carbonate units. The A4 is identified by the U enrichment, volcanic ash bed, and the δ^{13}C$_{carb}$ negative excursion and the immediately underlying unit is inferentially assigned to the A3 unit. Samples from BB-4 were taken exclusively from core. The A3 δ^{13}C$_{carb}$ record is characterized by enriched values (+3‰), typical of the (non-A4) Ara. There is a sharp decrease in δ^{13}C$_{carb}$ in the A4 to -5‰, followed by a gradual recovery to -2‰. δ^{34}S$_{CAS}$ over this interval is uniformly enriched (~39‰), with a small but distinctive 1‰ negative excursion associated with the A4. There is an isolated depleted point at the base of the A4 that is attributed to syndepositional sulfide oxidation (FIKE and GROTZINGER, 2007b). The δ^{34}S$_{pyr}$ values over the Ara are characteristically enriched and average ~ 12‰ in BB-4 (FIKE and GROTZINGER, 2007a). The BB-4 δ^{34}S$_{CAS}$ record across the A4 is in agreement with that preserved in the SOSB strata of BBN-1 and in the non-evaporitic strata of the Eastern Flank (TM-6). This demonstrates the correlation potential of δ^{34}S$_{CAS}$ over one of the few unambiguously correlated sections of the Huqf stratigraphy.
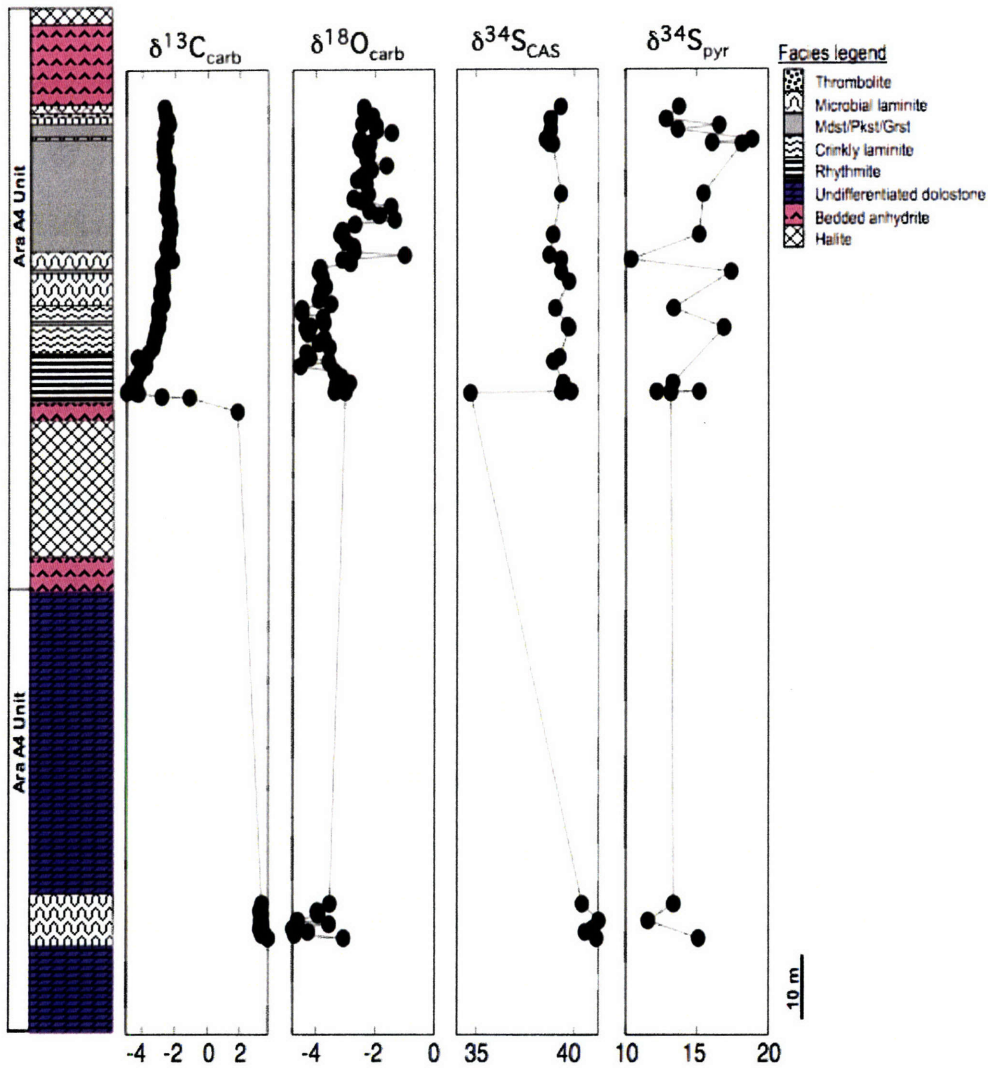
Figure 15: Isotopic data from well BB-4. Carbonate facies are predominantly dolomite. A3 and A4 $\delta^{13}C_{carb}$ has been reported previously (Chapter 4).

Outcrop data:

We have sampled and analyzed outcrop sections in both the Huqf area and in the Jabal Akhdar of the Oman Mountains (Figure 1). These sections have a paleoenvironmental range from shallow water facies (Huqf area) to deeper water facies (Jabal Akhdar). Known outcrop stratigraphy is limited to that of the Nafun Group, although possible Ara-equivalent strata were investigated in the 'post-Buah' carbonates

of the Huqf area (Nicholas, 1999). The existence of the Ara Group in outcrop would greatly improve our knowledge of the transition between Nafun and Ara Group deposition, as the basal Ara is poorly understood in the subsurface. The uniquely enriched $\delta^{34}S_{SO4}$ signature of the Ara strata makes sulfur isotopic analysis an excellent screening tool for possible Ara-equivalent outcrops. The discussion of the outcrop sections begins with those from the Huqf area and finishes with those in Jabal Akhdar. Within each area, the sections will be discussed in ascending stratigraphic order.

Huqf area

In the Huqf area, the Nafun Group stratigraphy of the Khufai, Shuram, and Buah Formations were sampled, as well as two sections through possible Ara-equivalent carbonates overlying the Buah Formation (Figure 1).

Khufai Formation (MDA/MDB)

The Khufai Fm. was studied at Mukhaizna Dome (sections MDA and MDB). MDA consisted of 50m of massive to laminated grey limestones. The base of MDA began at the contact with the uppermost shales of the underlying Masirah Bay Fm (Figure 16). There was a single, silificied, possibly tuffaceous bed in the middle of MDA; however, this layer did not contain any zircons (S. Bowring, pers. comm.). MDB (section MD-18 of (McCARRON, 2000)) consisted of ~ 160m of predominantly laminated grey limestones overlain by ~100m of dolomite that became increasingly silicified upsection. At MDB, the basal contact between the Masirah Bay and Khufai Formations was obscured by cover and the two sections were aligned by the existence of the silificied layer within the

lower Khufai limstones. $\delta^{13}C_{carb}$ over these sections are typically enriched at + 4‰, although there is a trend toward negative values in the uppermost 10m. In addition, there is a strong depletion in $\delta^{13}C_{carb}$ in both MDA and MDB associated with the silicified layer. Finally, there is a decrease in $\delta^{13}C_{carb}$ to ~ 0‰ in the upper Khufai dolostones of MDB as the dolostones become progressively more evaporitic. $\delta^{18}O_{carb}$ shows a general trend toward increasing values from -6‰ to ~0‰ upsection, although there is drop to - 4‰ in the uppermost 10m associated with the decrease in $\delta^{13}C_{carb}$. There is an anomalously depleted $\delta^{18}O_{carb}$ value associated with the silicified layer in MDA. $\delta^{34}S_{CAS}$ records an increase through the Khufai from ~ 18‰ to 28‰ at the uppermost Khufai, with a small decrease in the uppermost 10m associated with decreased $\delta^{13}C/\delta^{18}O$. Again, there is anomalously enriched $\delta^{34}S_{CAS}$ associated with the silicified layer.

In examining these data, we find no evidence for diagenetic alteration, except in the strata immediately surrounding the silificied zone within the lower Khufai limestones. The $\delta^{13}C_{carb}$ pattern observed here is in agreement with that found in the subsurface, including the drop to near 0‰ in the upper Khufai. There is a trend toward increasing $\delta^{18}O_{carb}$ through the Khufai that mirrors that seen in the wells MQ-1 and TM-6. supporting the interpretation of diagenetic alteration of these samples. Finally, the observed trends in $\delta^{34}S_{CAS}$ is remarkably similar to that observed in well MQ-1 (constant through most of the Khufai, becoming progressively more enriched toward the upper Khufai), although the absolute value is depleted by ~ 2‰ in outcrop relative to the subsurface. There is a decrease in $\delta^{13}C_{carb}/\delta^{18}O_{carb}/\delta^{34}S_{CAS}$ in the uppermost few meters of the Khufai in outcrop. It is unclear if this results from diagenetic alteration to strata immediately beneath the inferred unconformity (and subaerial exposure) that separates

the Khufai and Shuram Formations, or if these data are a primary record that captures the onset of the Shuram excursion.
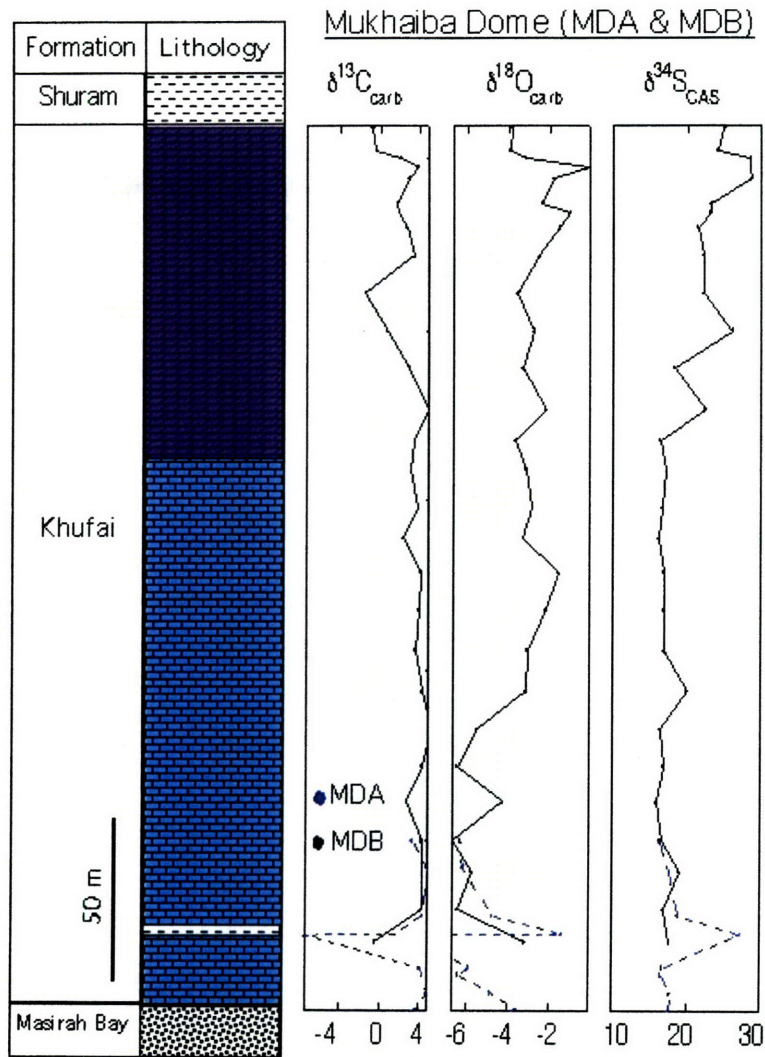
Figure 16: Isotopic data from Huqf area outcrop sections MDA and MDB. Lithology after Figure 2.

Shuram and Buah Formations (WA2)

The upper Shuram and lower Buah Formations (Figure 17) were studied in the Huqf at Wadi Aswad (WA2, section WA2 of (LE GUERROUE et al., 2006b)). The upper portion of the Shuram Formation consisted of a series of stacked siliciclastic to carbonate

parasequences that covered 55m, overlain by the 65m of lower Buah carbonates. These strata record the upper portion of the Shuram excursion ($\delta^{13}C_{carb}$ returning from -10‰ to ~0‰). Over this section $\delta^{34}S_{CAS}$ averages 17 ± 2‰ with a slight negative trend upsection. The contact between parasequences is often marked by depletions in $\delta^{34}S_{CAS}$ of a few permil.
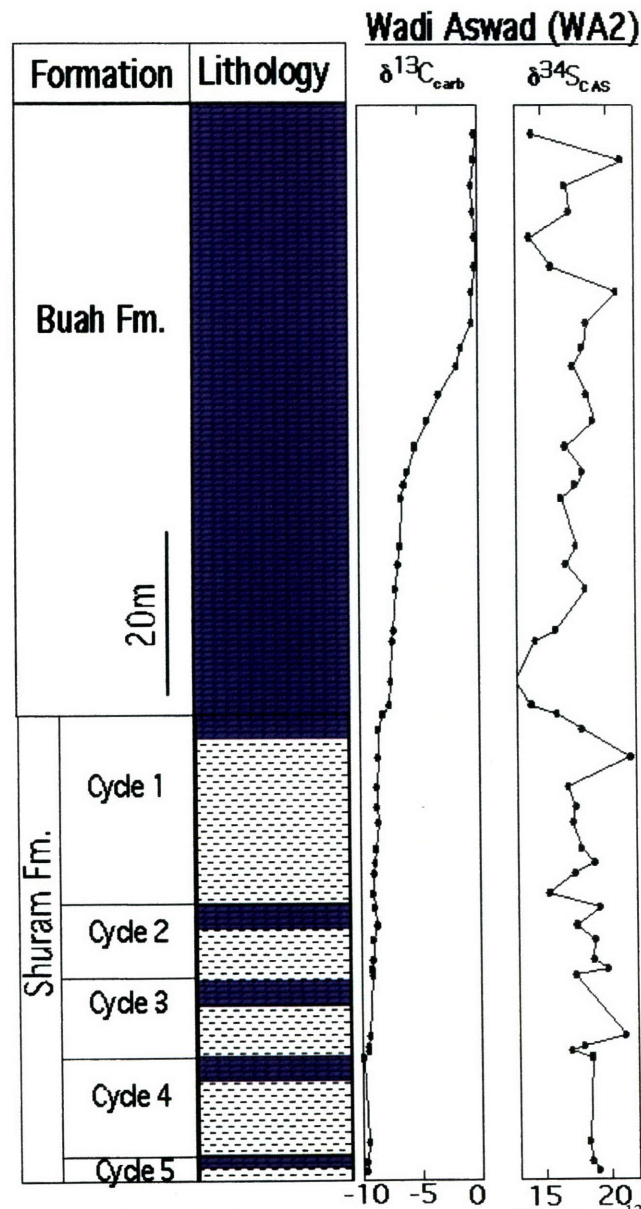
Figure 17: Isotopic data from Huqf area outcrop section WA2. $\delta^{13}C_{carb}$ data are from (Cozzi et al., 2004a; Le Guerroue et al., 2006b). Lithology after Figure 2.

The observed decreases in $\delta^{34}S_{CAS}$ in WA2 across the parasequence boundaries likely reflect syndepositional or early diagenetic oxidation of sulfides. There is no other clear indication of diagenesis in these strata. The observed trend in $\delta^{34}S_{CAS}$ (decreasing throughout the Shuram excursion) is the same as that observed in both MQ-1 and TM-6, although $\delta^{34}S_{CAS}$ from WA2 is depleted by ~3‰ relative to that observed in MQ-1 and m while similar to the TM-6 signal, this is believed to have been slightly altered (depleted) by diagenetic pyrite oxidation.

Post-Buah carbonates (YD1, MDC)

Post-Buah carbonates from two sections, one at Yiddah and the other in Mukhaibah Dome were examined. These strata are of unknown stratigraphic affinity, although they have been postulated to be Ara-equivalent (Nicholas, 1999). The existence of outcrops of the Ara would provide useful context for interpreting the subsurface Ara Group and, in particular, the poorly understood Buah-Ara transition.

YD1

The Yiddah section (YD1, section YD1 of (NICHOLAS, 1999)) spanned ~ 250m of dolomites and layers of gypsum that had been replaced by calcite (Figure 18). These replacement calcites were concentrated toward the bottom of the section and the upper ~100m was dominated by stromatolitic and thrombolitic dolomites, including m-scale conophyton stromatolites. The lower portion of the section (a combination of dolomitic grainstones, microbial laminites, and stromatolites interspersed with the replacement calcite) is characterized by a relatively invariant $\delta^{13}C_{carb}$ of ~ 0‰. There is an abrupt

increase to +8‰ at the base of the upper half of YD1 and the remainder of this section (stromatolitic/thrombolitic dolomite) has $\delta^{13}C_{carb}$ of ~ 3‰. $\delta^{18}O_{carb}$ increases over the section from ~ -5‰ to 0‰. The aberrant $\delta^{13}C_{carb}$ point (+8‰) also has a distinct 4‰ depletion in $\delta^{18}O_{carb}$. $\delta^{34}S_{CAS}$ over this interval is relatively invariant (mean: 20 ± 2‰) with no obvious trend.
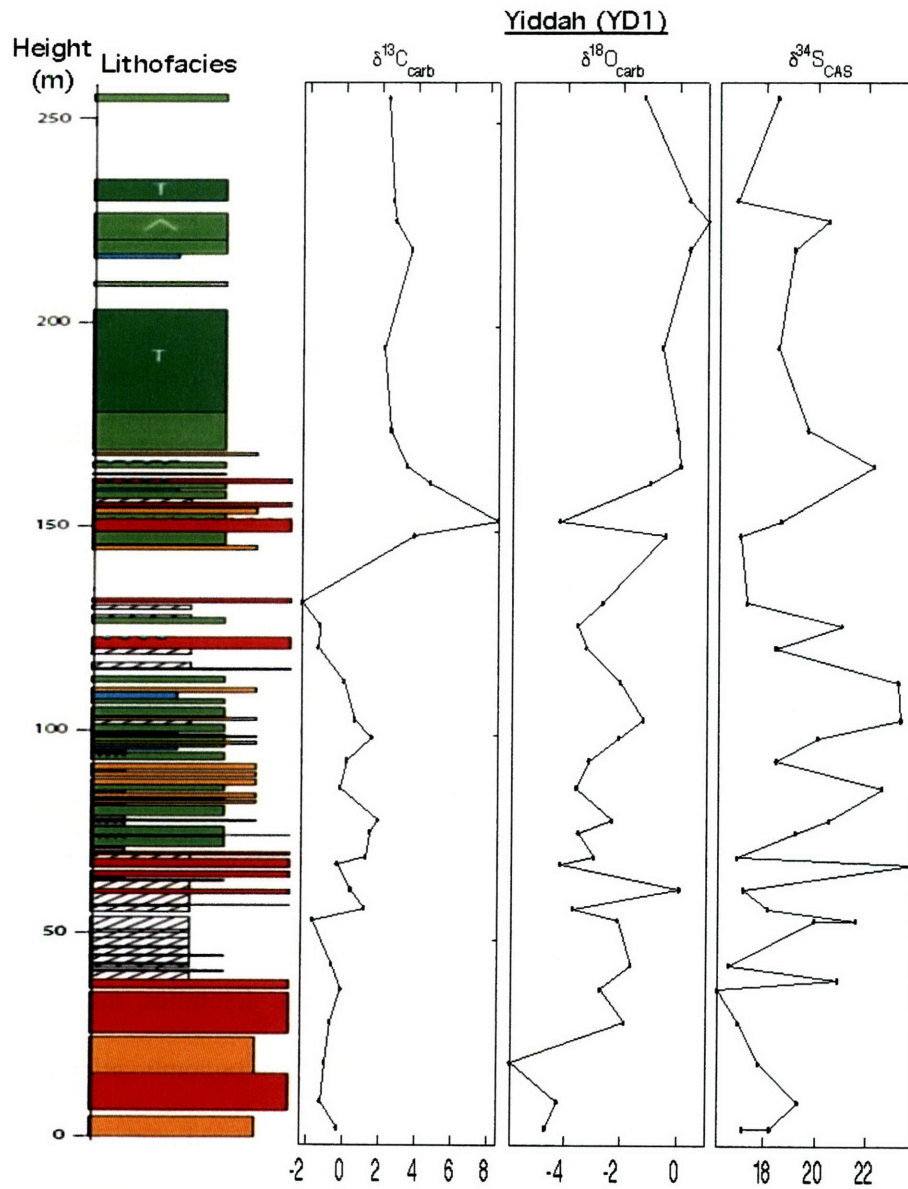
Figure 18: Isotopic data from the Huqf area outcrop section YD1 (post-Buah carbonates). See Figure 19 for lithofacies legend.

Overall, the $\delta^{34}S_{CAS}$ values do not resemble those obtained from any of the subsurface Ara samples and, if primary, are more inline with the upper Buah values of MQ-1, which would be consistent with the $\delta^{13}C_{carb}$ values. However, the variability is larger than expected (on a ‰/m-basis) and may indicate some diagenetic alterations. From analysis of $\delta^{13}C$-$\delta^{18}O$, the only obvious candidate for diagenetic alteration would be the enriched $\delta^{13}C_{carb}$ sample, which does not have a particularly unusual $\delta^{34}S_{CAS}$ value. However, the replacement of gypsum evaporites with calcite (NICHOLAS, 1999) indicates significant post-depositional remobilization of sulfate and thus these samples may not reflect their original $\delta^{34}S_{CAS}$ composition.

MDC

The Mukhaibah Dome section (MDC, section MK1 of (NICHOLAS, 1999)) spanned ~ 120m of dolomites, again interspersed with gypsum replaced by calcite (Figure 19). These calcites were concentrated toward the base of the section. In MDC, there was limited $\delta^{34}S_{SO4}$ variability (mean $\delta^{34}S = 21 \pm 2$‰) with a slight upsection trend toward increasing values. Again, while similar to YD1, the MDC $\delta^{34}S_{CAS}$ values do not resemble those obtained from any of the subsurface Ara samples. The presence of the replacement calcites and scatter within $\delta^{34}S_{CAS}$ probably indicate modest diagenetic alteration. As such, these samples may not reflect their original $\delta^{34}S_{CAS}$ composition.
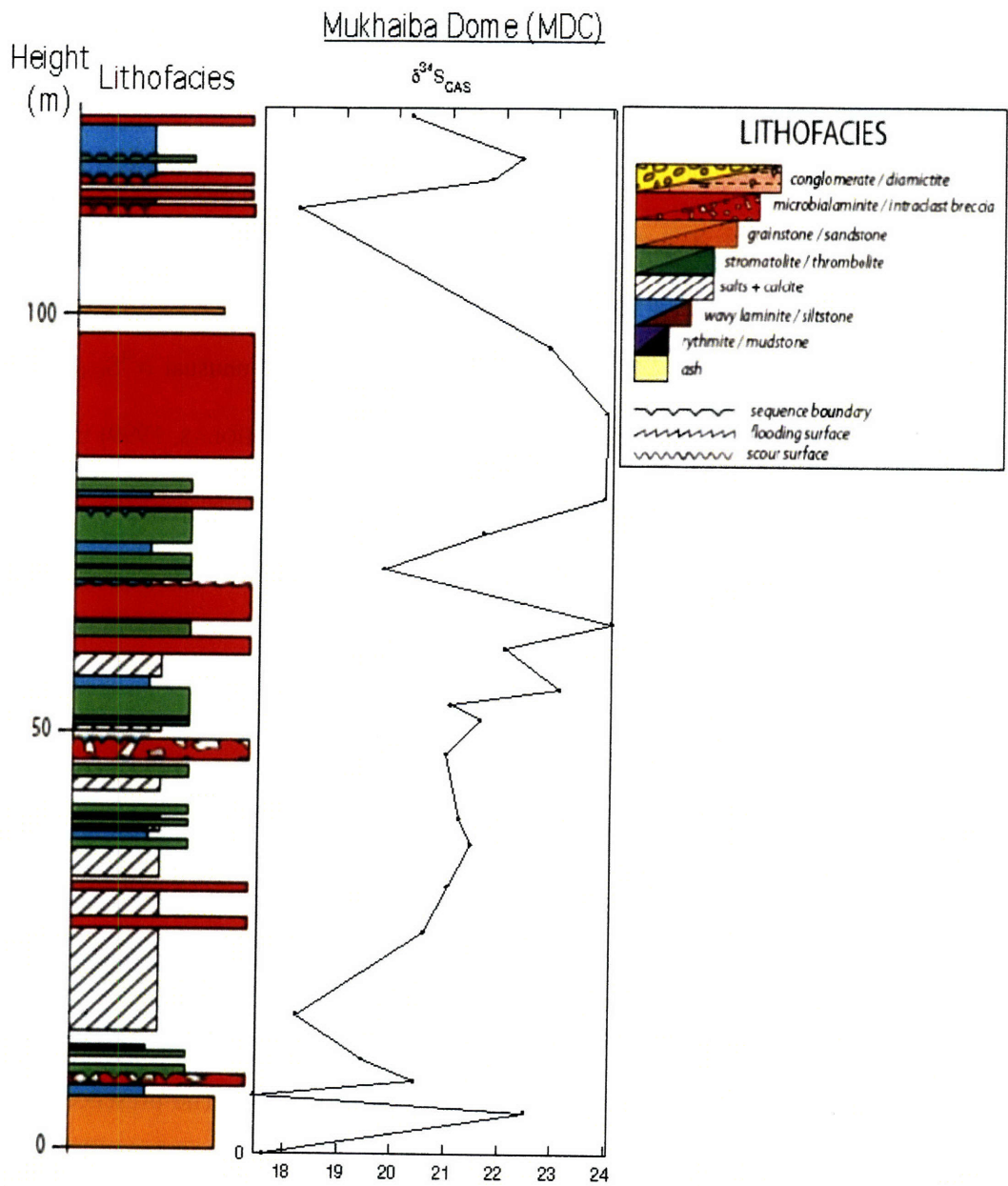
Figure 19: Isotopic data from the Huqf area outcrop section MDC (post-Buah carbonates).

JABAL AKHDAR, OMAN MOUNTAINS

Samples were also obtained from outcrops in the Jabal Akhdar region of the Oman Mountains (Figure 1). Sections were collected through the Hadash cap carbonate (H), the

transition from the Hadash to the lower Masirah Bay Formation (KG), the Khufai to basal Shuram Formations (KS), and the Buah Formation (WBA).

Hadash cap carbonate and the transition to lower Masirah Bay (H, KG)

The Hadash Formation (Marinoan-equivalent cap carbonate) was sampled from the type locality outside Hadash village (section H) in the Ghubrah Bowl of the Jabal Akhdar in the Oman Mountains. The Hadash Formation is known to have the characteristic Marinoan $\delta^{13}C_{carb}$ negative excursion (LEATHER et al., 2002). Here the cap is preserved as a 7-m thick sequence that is dolomitic for the lower 5m and transitions to limestone in the upper 2-m (similar to the lithologic transitions observed in other cap carbonates (HOFFMAN et al., 2007). $\delta^{34}S_{CAS}$ across the cap range from 12-19‰, similar for values reported for Hadash strata from the subsurface (FIKE et al., 2006) and in broad agreement with the open marine sections ($\delta^{34}S_{CAS} \sim$ 15-30‰) observed from the lower and middle members of the Marinoan cap carbonate in Namibia (HURTGEN et al., 2006). A nearby section in Khufai Gorge (KG) sampled the transition from the uppermost Hadash into the basal Masirah Bay Fms. The $\delta^{34}S_{CAS}$ over this interval (13 – 19‰) was in agreement with those from the Hadash locality and well MQ-1. We see no evidence in Oman for the increase in $\delta^{34}S_{CAS}$ to + 40‰ seen in the uppermost cap from Namibia (HURTGEN et al., 2006).

Khufai to basal Shuram Formations (KS)

The Khufai and basal Shuram Formations were sampled at location KS in the Jabal Akhdar of the Oman Mountains. The Khufai Formation at this location was ~ 80m thick

sequence of massive grey-black limestone with abundant quartz veins in the upper portion. It is overlain by an abrupt transition to interbedded ~ 1m thick layers of quartz sandstones and pale grey carbonates. Sulfate concentrations in these samples were low and only three samples (of fifteen) yielded enough sulfate for isotopic analyses. These samples were from the lower Khufai and had an average $\delta^{34}S_{CAS}$ of ~16‰ (range 13.6 – 17.1‰). These values are in broad agreement with those from the Khufai Formation in the subsurface (MQ-1 and TM-6) and in the Huqf outcrop area (sections MDA/MDB), although the low resolution prohibits further interpretation.

Buah Formation (WBA)

The Buah Formation was sampled from Wadi Bani Awf (WBA) in the Jabal Akhdar of the Oman Mountains. The WBA Buah Fm. extends for ~ 220m and has been previously characterized in terms of lithology and $\delta^{13}C_{carb}$ (COZZI et al., 2004a; COZZI et al., 2004b). CAS concentrations were low in these sediments and only six of the seventeen samples collected yielded sufficient sulfate for isotopic analysis. $\delta^{34}S_{CAS}$ in these samples ranged from 17 to 35‰ with a general trend toward more enriched values upsection. This suggests that the upper Buah strata here may record the transition from typical Nafun values (~ 20 – 30‰) to Ara values (~40‰); however, limited resolution prevents verification of this. Pyrite $\delta^{34}S$ was analyzed for these six samples to leverage our understanding of variations over this crucial interval. Here $\delta^{34}S_{pyr}$ shows a marked increase from -30‰ at the base to ~10‰ at the top of the WBA Buah Fm. This transition from depleted $\delta^{34}S_{pyr}$ (as observed in Nafun strata of MQ-1 and TM-6) to enriched $\delta^{34}S_{pyr}$

(as observed throughout Ara strata, including TM-6) marks WBA as a key section recording the increase in $\delta^{34}S_{CAS}$ and $\delta^{34}S_{pyr}$ from Nafun to Ara strata.

DISCUSSION and INTERPRETATION

Section alignment and subsurface – outcrop correlation

The data presented here have been placed into a correlation framework based on their paired $\delta^{13}C_{carb}$-$\delta^{34}S_{CAS}$ stratigraphy, supplemented by $\delta^{13}C_{org}$, $\delta^{34}S_{pyr}$, and trace element abundances where available (Figure 20). These multiple proxies demonstrate that $\delta^{34}S_{CAS}$ can be used to support existing correlations based on $\delta^{13}C_{carb}$ and/or lithostratigraphy. This is observed across the Hadash cap carbonate (wells MQ-1, TM-6, and Jabal Akhdar sections H, KG), the Khufai Formation (wells MQ-1, TM-6; Huqf outcrops MDA, MDB; and Jabal Akhdar section KS), the Shuram Formation (wells MQ-1, TM-6; and Huqf outcrop section WA2), and the A4 unit of the Ara Group (wells TM-6, SHM-1, BBN-1, and BB-4). In addition, our alignment suggests that $\delta^{34}S_{CAS}$ is useful in its own right for making correlations in the absence of distinctive $\delta^{13}C_{carb}$ or lithologic signatures. In particular, $\delta^{34}S_{CAS}$ and $\delta^{34}S_{anhyd}$ have the potential to resolve the poorly understood transition from the Nafun Group to the basal Ara carbonates and the relationship between the lower (pre-A4) Ara units that are variably grounded (due to salt withdrawal) directly on Nafun strata or encased in halite. Our data indicate that there is a transition from ~ 25‰ to 40‰ that occurs over the upper Nafun to pre-A4 Ara. In particular, that there is a rise to ~ 30-35‰ within the latest Buah Formation (WBA in the Oman Mountains and well TM-6), and that the basal Ara stratigraphy record a rise from ~ 35 – 40‰ (wells TM-6, SAR-2, SHM-1, AAL-1, MH-1, and BBN-1). This increase in

$\delta^{34}S_{CAS}$ fits into the global pattern for latest Ediacaran – Cambrian $\delta^{34}S_{SO4}$ (FIKE and GROTZINGER, 2007a). The first order structure of this increase is a monotonic rise in $\delta^{34}S_{SO4}$ and thus, $\delta^{34}S_{CAS}$ can be used to place strata of uncertain stratigraphic position (the uppermost Buah Formation or pre-A4 Ara Group) into the correct stratigraphic order. This re-ordering will be greatly aided by the abundant $\delta^{34}S_{anhyd}$ from the Ara Group evaporites, although care must be taken to factor in offsets (up to 4‰) in $\delta^{34}S_{anhyd}$ that arise during basin restriction and freshening (FIKE and GROTZINGER, 2007b).

In general, there was significant agreement between outcrop and subsurface sections. In particular, $\delta^{34}S_{CAS}$ from the Khufai Formation at the Mukhaibah Dome (Huqf outcrop region) tracked $\delta^{34}S_{CAS}$ in both wells MQ-1 and TM-6, although the outcrop section was depleted by ~ 2‰ relative to the subsurface sections. The Shuram section from Wadi Aswad (Huqf outcrop region) also mirrored the decrease in $\delta^{34}S_{CAS}$ observed in MQ-1 and TM-6 over the Shuram excursion, although the outcrop section was again depleted by ~ 2‰ relative to the subsurface sections. The clear exception to our expected correlations comes from the two 'Post-Buah' carbonate sections (YD1 and MDC) from the Huqf. These had previously been postulated to be outcrop equivalents of the Ara Group (NICHOLAS, 1999). As such, they would be predicted to have $\delta^{34}S_{CAS}$ values somewhere between upper Buah values of ~ 25 - 30‰ and typical Ara values (~40‰). However, both sections had $\delta^{34}S_{CAS}$ of ~ 18‰. Even given the apparent 2‰ offset associated with outcrops relative to the subsurface, this does not put these sections within the range expected of Ara-equivalent strata. As such, we do not feel that these outrcrops should be considered a part of the Ara Group as currently defined. Rather, they appear to correlate with MQ-1 strata of the uppermost Buah Formation ($\delta^{13}C_{carb}$ just rising to 0‰

after the Shuram excursion and $\delta^{34}S_{CAS}$ around 20‰), based on both $\delta^{13}C_{carb}$ and $\delta^{34}S_{CAS}$.

Thus, these sections are interpreted to be either strata that should be considered as an upper member in the Buah Formation, or a newly recognized unit that is younger than the Buah Formation, and older than the basal (A0) Ara Group. The A0 is poorly understood, known only from a few subsurface wells, and this result could indicate it is a substantial unit in its own. Alternatively, the $\delta^{34}S_{CAS}$ record of these sections could be interpreted as significantly altered by the diagenesis that accompanied sulfate mobilization during calcite replacement of gypsum.

Figure 20 (following page): Composite alignment of the wells and outcrop sections studied, showing lithology, $\delta^{13}C_{carb}$ and $\delta^{34}S_{CAS}$ (and $\delta^{34}S_{anhyd}$, where available). All sections are shown at the same scale. Sections from the Jabal Akhdar are not plotted due to insufficient stratigraphic coverage from the few samples that yielded sufficient CAS for isotopic analysis. Existing stratigraphic assignments are shown by a color-coded square adjacent to the stratigraphic column that marks the top surface of a given unit (see legend). Our proposed stratigraphic assignments are shown in similarly colored circles placed along the stratigraphic column, with the addition of our proposed uppermost Buah – basal Ara unit (termed 'Post-Buah') here (covering the range in $\delta^{34}S$ from 30-35‰.

Basin-wide (subsurface & outcrop) correlation of sulfur and carbon isotopes
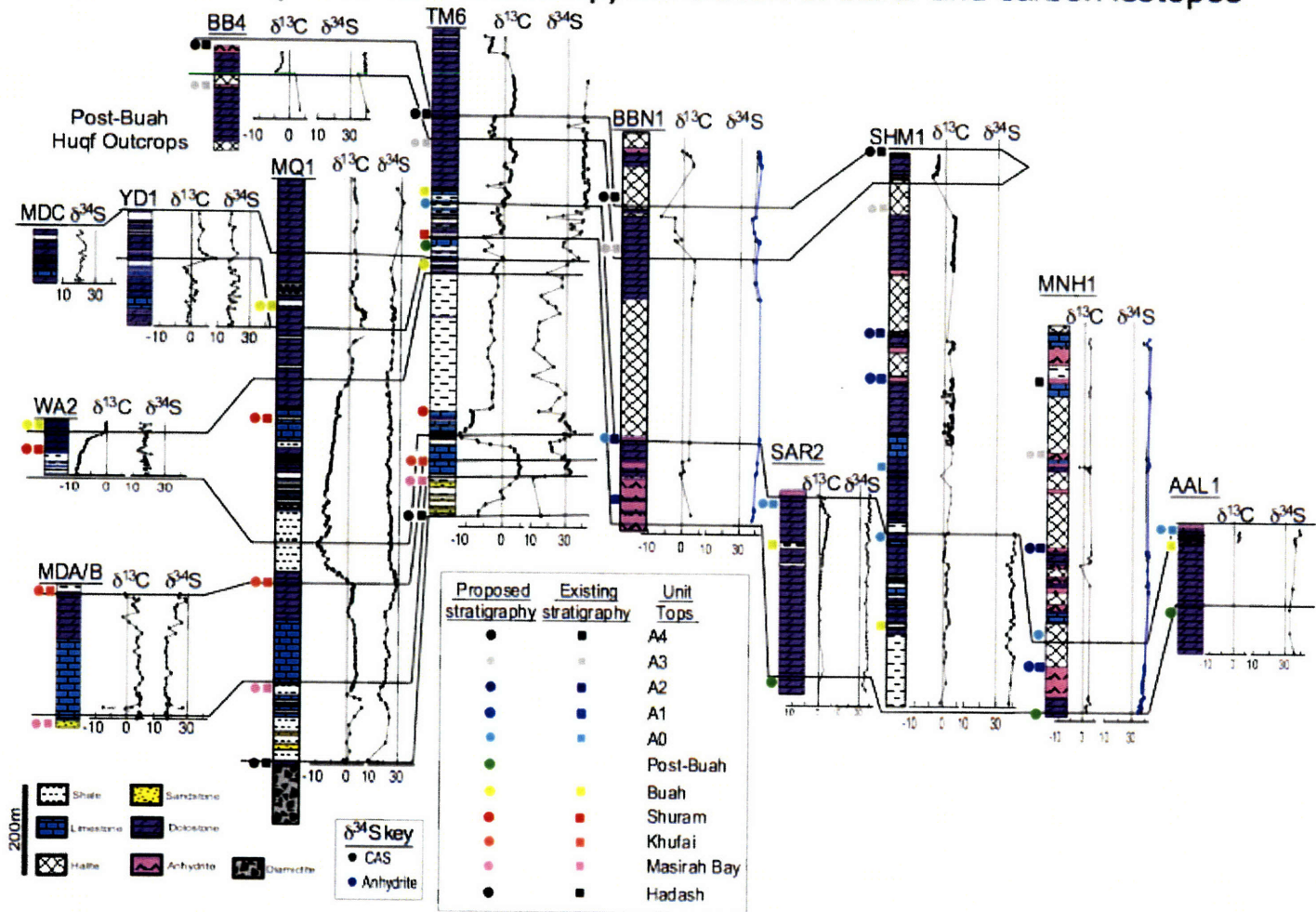
Discussion of diagenesis

In assigning interpretations to geochemical data preserved in the stratigraphic record it is essential to demonstrate that these samples reflect primary composition and are not compromised by post-depositional (diagenetic) alteration. This is especially important when dealing with Neoproterozoic strata as this time interval seems to record evidence for very unusual carbon, sulfur and strontium cycling (Burns et al., 1994; Burns and Matter, 1993; Calver, 1995; Fike and Grotzinger, 2007a; Fike et al., 2006; Halverson et al., 2007; Rothman et al., 2003; Shields and Veizer, 2002). Because of the unprecedented scale of the Shuram $\delta^{13}C_{carb}$ excursion (BURNS and MATTER, 1993; FIKE et al., 2006; LE GUERROUE et al., 2006a; LE GUERROUE et al., 2006c; McCARRON, 2000), it is important to consider the possibility of diagenetic alteration.

Unlike typical diagenetically altered carbonates, the $\delta^{13}C_{carb}$ across the Shuram excursion are not scattered, rather they reflect a large excursion that is more than 10 times larger than the largest point to point variability between samples. Examples of known diagenetic 'excursions' are typified by stratigraphically incoherent 'single-point' excursions or excursions with up to 10‰ over just a few meters. In addition being characterized by little isotopic scatter, the Shuram excursion also shows little spatial variability and has been reproduced in over 20 sections in Oman (BURNS and MATTER, 1993; LE GUERROUE et al., 2006a; McCARRON, 2000). These argue strongly against a diagenetic origin. The occurrence of putatively correlative sections around the world that all record an excursion of the same magnitude, typically through several hundred meters of strata, suggests that this excursion reflects a primary change in global carbon cycling

(Calver, 2000; Condon et al., 2005; Kaufman et al., 2007; Workman et al., 2002). If the Shuram excursion is diagenetic in origin, then it reflects an unprecedented regional to global coherence in what otherwise should be a highly local phenomenon. In comparing the Shuram strata to other intervals that have been identified as diagenetically altered (the Ara Group of both wells MQ-1 and TF-1), we find no evidence for a diagenetic origin for the Shuram excursion. Rather, we conclude it reflects the primary operation of the carbon cycle in mid Ediacaran time.

Conclusions

We have conducted parallel analyses of $\delta^{13}C_{carb}$, $\delta^{34}S_{CAS}$ in over 14 sections through Huqf Supergroup strata to evaluate the reproducibility of $\delta^{34}S_{CAS}$, relative to lithostratigraphy and $\delta^{13}C_{carb}$ chemostratigraphy, across more than 1,000 km. These data enable correlation of broad scale features in the $\delta^{34}S$ record, particularly the rise in $\delta^{34}S_{SO4}$ between Nafun (~25‰) and Ara (~40‰) strata. The $\delta^{34}S_{SO4}$ stratigraphy was able to verify existing correlations based on $\delta^{13}C_{carb}$ chemostratigraphy and lithostratigraphy (such as the onset of the Shuram excursion and A4 carbonate). In addition, $\delta^{34}S_{CAS}$ (and $\delta^{34}S_{anhyd}$) show clear potential for resolving the uncertain stratigraphic assignments associated with the transition from the upper Buah Formation to the basal Ara Group and among the lower Ara (A0-A3) units themselves. In general, outcrop sections have more variability and are depleted in $\delta^{34}S_{CAS}$ by ~ 2‰ relative to subsurface sections. This is attributed to pyrite oxidiation during surface weathering and recrystallization of carbonates. The increased variability is also a likely result of the decreased concentration of sulfate in the outcrop samples (particular in the Jabal Akhdar

of the Oman Mountains), which makes them more susceptible to diagenetic alteration.

This study clearly demonstrates the basin-wide reproducibility of $\delta^{34}S_{CAS}$ and its

applicability for chemostratigraphic correlations.

References

Allen, P.A., Grotzinger, J.P., Le Guerroue, E., Cozzi, A., al Siyabi, H., and Newall, M., 2005, Neoproterozoic Geology of the Jebel Akhdar and Core from Subsurface, Field Guide, IAS 2005: Muscat, Oman.

Amthor, J.E., Grotzinger, J.P., Schroder, S., Bowring, S.A., Ramezani, J., Martin, M.W., and Matter, A., 2003, Extinction of Cloudina and Namacalathus at the Precambrian-Cambrian boundary in Oman: Geology, v. 31, p. 431-434.

Arnold, G.L., Anbar, A.D., Barling, J., and Lyons, T.W., 2004, Molybdenum isotope evidence for widespread anoxia in mid-proterozoic oceans: Science, v. 304, p. 87-90.

Bowring, S.A., Grotzinger, J.P., Condon, D.J., Ramezani, J., and Newall, M., 2007, Geochronologic constraints on the chronostratigraphic framework of the Neoproterozoic Huqf Supergroup, Sultanate of Oman: American Journal of Science, v. (in press).

Brasier, M., McCarron, G., Tucker, R., Leather, J., Allen, P., and Shields, G., 2000, New U-Pb zircon dates for the Neoproterozoic Ghubrah glaciation and for the top of the Huqf Supergroup, Oman: Geology, v. 28, p. 175-178.

Burns, S.J., Haudenschild, U., and Matter, A., 1994, The Strontium Isotopic Composition of Carbonates from the Late Precambrian (Approximate-to-560-540 Ma) Huqf Group of Oman: Chemical Geology, v. 111, p. 269-282.

Burns, S.J., and Matter, A., 1993, Carbon isotopic record of the latest Proterozoic from Oman: Eclogae Geologicae Helvetiae, v. 86, p. 595-607.

Calver, C.R., 1995, Ediacaran isotope stratigraphy of Australia: PhD Thesis (Macquarie University).

—, 2000, Isotope stratigraphy of the Ediacarian (Neoproterozoic III) of the Adelaide Rift Complex, Australia, and the overprint of water column stratification: Precambrian Research, v. 100, p. 121-150.

Canfield, D.E., 2001, Biogeochemistry of sulfur isotopes: Reviews in Mineralogy & Geochemistry: Stable Isotope Geochemistry, v. 43, p. 607-636.

—, 2004, The evolution of the Earth surface sulfur reservoir: American Journal of Science, v. 304, p. 839-861.

Canfield, D.E., Lyons, T.W., and Raiswell, R., 1996, A model for iron deposition to euxinic Black Sea sediments: American Journal of Science, v. 296, p. 818-834.

Claypool, G.E., Holser, W.T., Kaplan, I.R., Sakai, H., and Zak, I., 1980, The age curves of sulfur and oxygen isotopes in marine sulfate and their mutual interpretation: Chemical Geology, v. 28, p. 199-260.

Condon, D., Zhu, M., Bowring, S., Wang, W., Yang, A., and Jin, Y., 2005, U-Pb Ages from the Neoproterozoic Doushantuo Formation, China: Science, v. 308, p. 95 - 98.

Cozzi, A., Allen, P.A., and Grotzinger, J.P., 2004a, Understanding carbonate ramp dynamics using delta C-13 profiles: examples from the Neoproterozoic Buah Formation of Oman: Terra Nova, v. 16, p. 62-67.

Cozzi, A., Grotzinger, J.P., and Allen, P.A., 2004b, Evolution of a terminal Neoproterozoic carbonate ramp system (Buah Formation, Sultanate of Oman): Effects of basement paleotopography: Geological Society of America Bulletin, v. 116, p. 1367 - 1384.

Farquhar, J., and Wing, B., 2003, Multiple sulfur isotopes and the evolution of the atmosphere: Earth and Planetary Science Letters, v. 213, p. 1 - 13.

Fike, D.A., and Grotzinger, J.P., 2007a, A paired sulfate-pyrite δ 34S approach to understanding the evolution of the Ediacaran-Cambrian sulfur cycle: Geochimica et Cosmochimica Acta, v. submitted.

—, 2007b, Detection of variable basin restriction using sulfate δ 34S in carbonate-evaporite strata: An example from the Ediacaran-Cambrian Ara Group, Sultanate of Oman: Geology, v. in prep.

Fike, D.A., Grotzinger, J.P., Love, G.D., and Summons, R.E., 2007, The Ediacaran-Cambrian boundary: a two-stage record of ecological and geochemical change: PNAS, v. in prep.

Fike, D.A., Grotzinger, J.P., Pratt, L.M., and Summons, R.E., 2006, Oxidation of the Ediacaran Ocean: Nature, v. 444, p. 744 - 747.

Given, R.K., and Lohmann, K.C., 1986, Isotopic evidence for the early meteoric diageness of the reef facies, Permian Reef Complex of West Texas and New Mexico: Journal of Sedimentary Petrology, v. 56, p. 183 - 193.

Grotzinger, J.P., Al-Siyabi, A.H., Al-Hashimi, R.A., and Cozzi, A., 2002, New model for tectonic evolution of Neoproterozoic-Cambrian Huqf Supergroup basins, Oman: GeoArabia, v. 7, p. 241.

Grotzinger, J.P., Bowring, S.A., Saylor, B.Z., and Kaufman, A.J., 1995, Biostratigraphic and Geochronological Constraints on Early Animal Evolution: Science, v. 270, p. 598-604.

Halverson, G.P., Dudas, F.O., Maloof, A.C., and Bowring, S.A., 2007, Evolution of the $^{87}Sr/^{86}Sr$ Composition of Neoproterozoic Seawater: Palaeogeography Palaeoclimatology Palaeoecology, v. in press.

Hayes, J.M., 1993, Factors controlling the 13C contents of sedimentary organic compounds: Principles and evidence: Marine Geology, v. 113.

—, 2001, Fractionation of carbon and hydrogen isotopes in biosynthetic processes, Stable Isotope Geochemistry, Volume 43: Reviews in Mineralogy & Geochemistry, p. 225-277.

Hayes, J.M., Strauss, H., and Kaufman, A.J., 1999, The abundance of C-13 in marine organic matter and isotopic fractionation in the global biogeochemical cycle of carbon during the past 800 Ma: Chemical Geology, v. 161, p. 103-125.

Hoffman, P.F., Halverson, G.P., Domack, E.W., Husson, J.M., Higgins, J.A., and Schrag, D.P., 2007, Are basal Ediacaran (635 Ma) post-glacial "cap dolostones" diachronous?: Earth and Planetary Science Letters, v. 258, p. 114-131.

Holser, W.T., 1977, Catastrophic Chemical Events in History of Ocean: Nature, v. 267, p. 403-408.

Hurtgen, M.T., 2006, Sulfur cycling in the aftermath of a Neoproterozoic (Marinoan) snowball glaciation: Evidence for a syn-glacial sulfidic deep ocean: Earth and Planetary Science Letters, v. 245, p. 551 - 570.

Hurtgen, M.T., Halverson, G.P., Arthur, M.A., and Hoffman, P.F., 2006, Sulfur cycling in the aftermath of a 635-Ma snowball glaciation: Evidence for a syn-glacial sulfidic deep ocean: Earth and Planetary Science Letters, v. 245, p. 551-570.

Kah, L.C., Lyons, T.W., and Frank, T.D., 2004, Low marine sulphate and protracted oxygenation of the proterozoic biosphere: Nature, v. 431, p. 834-838.

Kampschulte, A., and Strauss, H., 2004, The sulfur isotopic evolution of Phanerozoic seawater based on the analysis of structurally substituted sulfate in carbonates: Chemical Geology, v. 204, p. 255-286.

Kaufman, A.J., Corsetti, F.A., and Varni, M.A., 2007, The effect of rising atmospheric oxygen on carbon and sulfur isotope anomalies in the Neoproterozoic Johnnie Formation, Death Valley, USA: Chemical Geology, v. in press.

Kaufman, A.J., Hayes, J.M., Knoll, A.H., and Germs, G.J.B., 1991, Isotopic compositions of carbonates and organic-carbon from upper Proterozoic successions in Namibia - stratigraphic variation and the effects of diagenesis and metamorphism: Precambrian Research, v. 49, p. 301-327.

Laws, E.A., Popp, B.N., Bidigare, R.R., Kennicutt, M.C., and Macko, S.A., 1995, Dependence of phytoplankton carbon isotopic composition on growth-rate and [CO2](aq) - theoretical considerations and experimental resutls: Geochimica Et Cosmochimica Acta, v. 59, p. 1131-1138.

Le Guerroue, E., Allen, P.A., and Cozzi, A., 2006a, Chemostratigraphic and sedimentological framework of the largest negative carbon isotopic excursion in Earth history: The Neoproterozoic Shuram Formation (Nafun Group, Oman): Precambrian Research, v. 146, p. 68 - 92.

—, 2006b, Parasequence development in the Ediacaran Shuram Formation (Nafun Group,Oman): high-resolution stratigraphic test for primary origin of negative carbon isotopic ratios: Basin Research, v. 18, p. 205 - 219.

Le Guerroue, E., Allen, P.A., Cozzi, A., Etienne, J.L., and Fanning, M., 2006c, 50 million year duration negative carbon isotope excursion in the Ediacaran ocean: Terra Nova, v. 18, p. 147 - 153.

Leather, J., Allen, P.A., Brasier, M.D., and Cozzi, A., 2002, Neoproterozoic snowball earth under scrutiny: Evidence from the Fiq glaciation of Oman: Geology, v. 30, p. 891-894.

Marenco, P.J., Corsetti, F.A., Hammond, D.E., Kaufman, A.J., and Bottjer, D.J., 2007, Fidelity of the carbonate associated sulfate signal: Implications for geobiological studies, Southern California Geobiology Symposium: Pasadena, CA.

Mattes, B.W., and Conway-Morris, S., 1990, Carbonate/evaporite deposition in the Late Precambrian–Early Cambrian Ara Formation of southern Oman, in Robertson, A.H.F., Ed2, Ed3, Ed4, Ed5, and Ed6, eds., The geology and tectonics of the Oman region, Volume 69: Special Publication: London, Geological Society, p. 617 - 636.

McCarron, G., 2000, The sedimentology and chemostratigraphy of the Nafun Group, Huqf Supergroup,Oman: PhD Thesis (Oxford University), p. 175.

Nicholas, C., 1999, The Ara Group in outcrop, University of Oxford.

Popp, B.N., Parekh, P., Tilbrook, B., Bidigare, R.R., and Laws, E.A., 1997, Organic carbon delta C-13 variations in sedimentary rocks as chemostratigraphic and paleoenvironmental tools: Palaeogeography Palaeoclimatology Palaeoecology, v. 132, p. 119-132.

Raab, M., and Spiro, B., 1991, Sulfur isotopic variations during seawater evaporation with fractional crystallization: Chemical Geology, v. 86, p. 323 - 333.

Ripperdan, R.L., 1994, Global variations in carbon isotope composition during the latest Neoproterozoic and earliest Cambrian: Annual Reviews in Earth and Planetary Sciences, v. 22, p. 385 - 417.

—, 2001, Stratigraphic Variation in Marine Carbonate Carbon Isotope Ratios, in Valley, J.W., and Cole, D., eds., Stable Isotope Geochemistry, Volume 43: Reviews in Mineralogy & Geochemistry, p. 225-277.

Ross, G.M., Bloch, J.D., and Krouse, H.R., 1995, Neoproterozoic strata of the southern Canadian Cordillera and the isotopic evolution of seawater sulfate: Precambrian Research, v. 73 , p. 71 - 99.

Rothman, D.H., Hayes, J.M., and Summons, R.E., 2003, Dynamics of the Neoproterozoic carbon cycle: Proceedings of the National Academy of Sciences of the United States of America, v. 100, p. 8124-8129.

Saddiqi, O., Michard, A., Goffe, B., Poupeau, G., and Oberhaensli, R., 2006, Fission-track thermochronology of the Oman Mountains continental windows, and current problems of tectonic interpretation: Bulletin de la Societe Geologique de France, v. 177, p. 127 - 134.

Saylor, B.Z., Kaufman, A.J., Grotzinger, J.P., and Urban, F., 1998, A composite reference section for terminal Proterozoic strata of southern Namibia: Journal of Sedimentary Research, v. 68, p. 1223-1235.

Schröder, S., Schreiber, B.C., Amthor, J.E., and Matter, A., 2003, A depositional model for the terminal Neoproterozoic - Early Cambrian Ara Group evaporites in south Oman: Sedimentology, v. 50, p. 879-898.

—, 2004, Stratigraphy and environmental conditions of the terminal Neoproterozoic-Cambrian period in Oman: evidence from sulphur isotopes: Journal of the Geological Society, v. 161, p. 489-499.

Shields, G., and Veizer, J., 2002, Precambrian marine carbonate isotope database: Version 1.1: Geochemistry Geophysics Geosystems, v. 3.

Strauss, H., 1993, The Sulfur Isotopic Record of Precambrian Sulfates - New Data and a Critical-Evaluation of the Existing Record: Precambrian Research, v. 63, p. 225-246.

Thode, H.D., and Monster, J., 1965a, Sulfur-isotope geochemistry of petroleum, evaporites, and ancient seas, Fluids in Subsurfaces Environments, Memoir 4, Volume Memoir 4: Tulsa, OK, American Association of Petroleum Geologists, p. 367 - 77.

Thode, H.G., and Monster, J., 1965b, Sulfur-isotope geochemistry of petroleum, evaporites, and ancient seas, in Young, A., and Galley, J.E., eds., Fluids in subsurface environments, Volume 4: Memoirs: Tulsa, AAPG, p. 367 - 377.

Veizer, J., 1983, Chemical diagenesis of carbonates: Theory and application of trace element technique, in Arthur, M.A., Anderson, T.F., Kaplan, I.R., Veizer, J., and Land, L.S., eds., Stable isotopes in sedimentary geology, Volume 10, Society of Economic Paleontologists and Mineralogists Short Course No. 10, p. 3.1 - 3.100.

Veizer, J., Ala, D., Azmy, K., Bruckschen, P., Buhl, D., Bruhn, F., Carden, G.A.F., Diener, A., Ebneth, S., Godderis, Y., Jasper, T., Korte, G., Pawellek, F., Podlaha, O.G., and Strauss, H., 1999, $^{87}Sr/^{86}Sr$, $\delta^{13}C$, and $\delta^{18}O$ evolution of Phanerozoic seawater: Chemical Geology, v. 161, p. 59-88.

Workman, R.K., Grotzinger, J.P., and Hart, S.R., 2002, Constraints on Neoproterozoic ocean chemistry from delta (super 13) C and delta (super 11) B analyses of carbonates from the Witvlei and Nama Groups, Namibia: Geochimica Et Cosmochimica Acta, v. 66, p. 847.